# MODELLING THE IMPACT OF (NON-)PHARMACEUTICAL INTERVENTIONS DURING COVID-19

## DISSERTATION

zur Erlangung des Grades des Doktors der Naturwissenschaften der Naturwissenschaftlich-Technischen Fakultät der Universität des Saarlandes

von
Christiane Dings
Diplom Pharmazeut / Apotheker

Saarbrücken
2024

| | |
|---|---|
| **Tag des Kolloquiums:** | 06.02.2025 |
| **Dekan:** | Prof. Dr.-Ing. Dirk Bähre |
| **Berichterstatter:** | Prof. Dr. Thorsten Lehr |
| | Prof. Dr. Marc Schneider |
| **Vorsitz:** | Dr. Jessica Hoppstädter |
| **Akad. Mitarbeiter:** | Prof. Dr. Claus Jacob |

Die vorliegende Arbeit wurde von Dezember 2015 bis Oktober 2024 unter Anleitung von Herrn Professor Dr. Thorsten Lehr in der Fachrichtung Klinische Pharmazie der Naturwissenschaftlich-Technischen Fakultät der Universität des Saarlandes angefertigt.

*If you base medicine on science, you cure people.*
*If you base the design of planes on science, they fly.*
*If you base the design of rockets on science, they reach the moon.*
*It works... bitches.*

– Richard Dawkins

# INCLUDED PUBLICATIONS

## Project I - COVID-19 Hospitalizations and Deaths

**Model-based analysis of SARS-CoV-2 infections, hospitalization and outcome in Germany, the federal states and districts.**
Christiane Dings, Katharina Martha Götz, Katharina Och, Iryna Sihinevich, Quirin Werthner, Sigrun Smola, Marc Bliem, Felix Mahfoud, Thomas Volk, Sascha Kreuer, Jürgen Rissland, Dominik Selzer and Thorsten Lehr.
*Viruses* 2022; 14(10):2114. DOI: 10.3390/v14102114 [1]

## Project II - COVID-19 Spreading in Different Age Groups

**Effect of vaccinations and school restrictions on the spread of COVID-19 in different age groups in Germany.**
Christiane Dings, Dominik Selzer, Nicola Luigi Bragazzi, Eva Möhler, Markus Wenning, Thomas Gehrke, Ulf Richter, Alexandra Nonnenmacher, Folke Brinkmann, Tobias Rothoeft, Michael Zemlin, Thomas Lücke and Thorsten Lehr.
*Infectious Disease Modelling* 2024; 9(4):1250-1264. DOI: 10.1016/j.idm.2024.07.004 [2]

## Project III - Azelastine Effect on SARS-CoV-2 Viral Load

**Pharmacometric modeling of the impact of azelastine nasal spray on SARS-CoV-2 viral load and related symptoms in COVID-19 patients.**
Christiane Dings, Peter Meiser, Frank Holzer, Michael Flegel, Dominik Selzer, Eszter Nagy, Ralph Mösges, Jens Peter Klussmann and Thorsten Lehr.
*Pharmaceutics* 2022; 14(10):2059. DOI: 10.3390/pharmaceutics14102059 [3]

# CONTRIBUTION REPORT

The author wishes to clarify their contributions to the publications included in this thesis, complemented by the contributor roles taxonomy (CRediT) [4, 5].

### Project I - COVID-19 Hospitalizations and Deaths

Conceptualization, Data Curation, Formal Analysis, Methodology, Visualization, Writing — Original Draft, Writing — Review & Editing.

### Project II - COVID-19 Spreading in Different Age Groups

Methodology, Data Curation, Formal Analysis, Investigation, Writing — Original Draft, Writing — Review & Editing, Visualization.

### Project III - Azelastine Effect on SARS-CoV-2 Viral Load

Methodology, Validation, Formal Analysis, Investigation, Visualization, Writing — Original Draft, Writing — Review & Editing.

# ABSTRACT

During the onset of the COVID-19 pandemic, both pharmaceutical and non-pharmaceutical interventions (NPIs) were urgently required. However, assessing their impact proved challenging due to the variability in individual viral load and disease progression. Evaluating NPIs is even more complex as controlled studies are not feasible and the rapidly evolving landscape of the pandemic introduces numerous confounding factors. In such cases, mathematical modelling, including epidemiological and pharmacometric approaches, offers valuable means to simultaneously investigate multiple factors influencing these non-linear processes.

In this thesis, non-linear mixed-effects (NLME) modelling were employed to gain insights into the COVID-19 pandemic across Germany´s federal states. The Susceptible-Infected-Recovered model was adapted to assess the impact of age, sex, variant of concerns (VOCs) and testing strategy on disease severity. Additionally, the spread of SARS-CoV-2 among age groups was evaluated, considering the influence of school holidays, remote schooling, VOCs and vaccinations. Furthermore, a pharmacokinetic/pharmacodynamic model was developed to compare the effects of azelastine nasal spray to placebo on viral load and COVID-19 symptoms.

In conclusion, this thesis demonstrates how NLME modelling can effectively address complex processes like pandemic spreading and disease progression, offering valuable insights into the factors impacting these dynamics at both individual and population levels.

# ZUSAMMENFASSUNG

Die COVID-19 Pandemie erforderte die schnelle Erforschung effektiver Behandlungsmöglichkeiten und nicht-pharmazeutischer Interventionen (NPIs). Allerdings erschweren individuelle Schwankungen der Viruslast und Krankheitsschwere die Untersuchung potentieller Arzneistoffe. Noch komplexer gestaltet sich die Bewertung von NPIs, da keine kontrollierten Studien möglich sind und sich die Bedingungen, unter denen die Pandemie sich entwickelt, ständig ändern. Epidemiologische und pharmakometrische Modellierung ermöglicht die gleichzeitige Untersuchung multifaktorieller, nicht-linearer Prozesse und trägt so zur Klärung dieser Fragestellungen bei.

In dieser Arbeit wurde die COVID-19 Pandemie in den deutschen Bundesländern mittels nichtlinearer gemischte-Effekt (NLME) Modelle beschrieben. Das SIR Modell, das die Bevölkerung in Empfängliche, Infizierte und Genesene aufteilt, wurde um den Einfluss von Alter, Geschlecht, Virusvariante (VOC) und Teststrategie auf die Krankheitsschwere erweitert. Zudem wurde die Ausbreitung von SARS-CoV-2 zwischen Altersgruppen mit Fokus auf den Einfluss von Schule, VOC und Impfungen untersucht. Außerdem wurde mittels Pharmakokinetik/-Dynamik-Modell der Einfluss von Azelastin auf Viruslast und Symptomstärke von COVID-19 Patienten mit Placebo verglichen.

Diese Arbeit zeigt, wie NLME Modellierung komplexe Prozesse von Krankheitsausbreitung und -verlauf auf individueller und Populationsebene abbilden und dadurch wesentlich zur ihrer Aufklärung beitragen kann.

# GRAPHICAL ABSTRACT

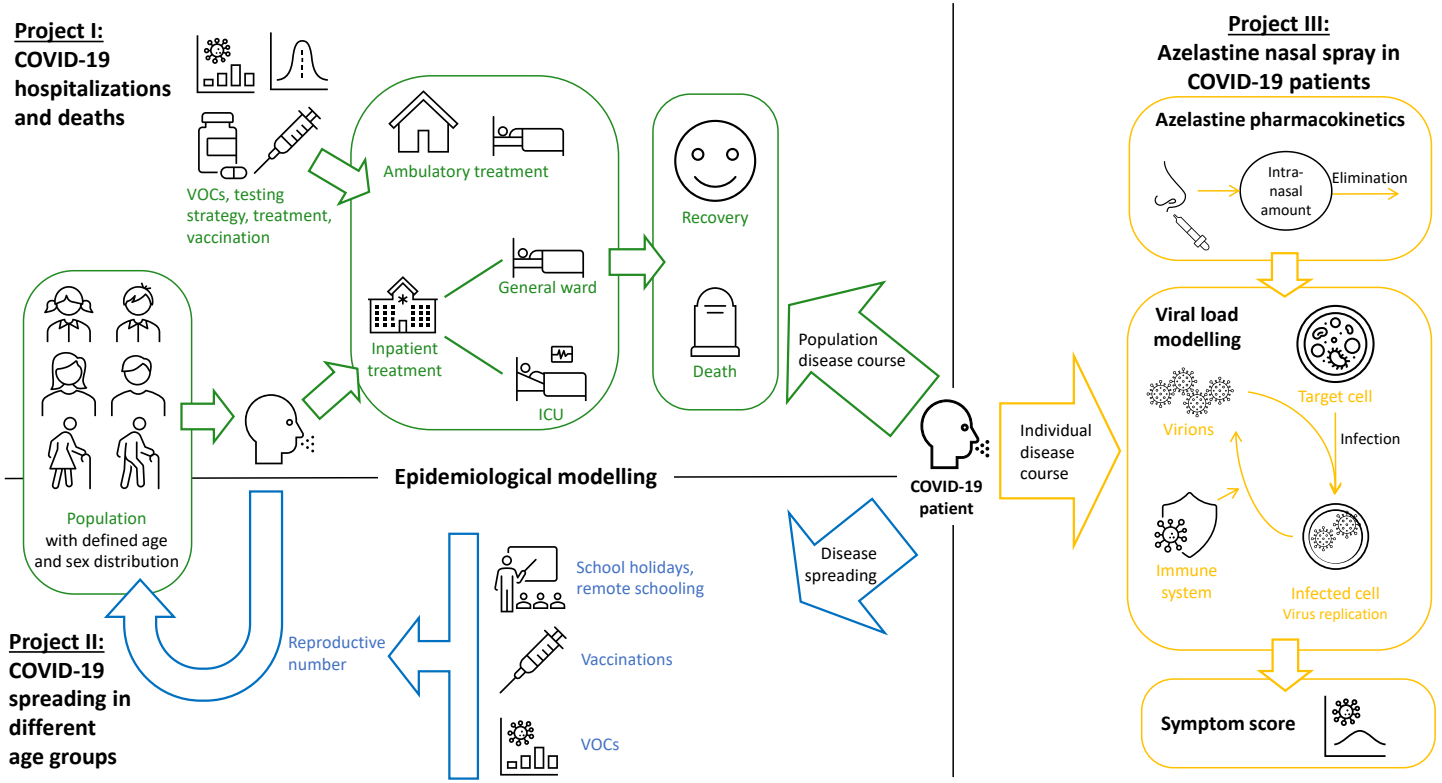


Figure 1: Graphical abstract. ICU: Intensive care unit, VOC: Variant of concern

# CONTENTS

# ABBREVIATIONS

| | |
|---|---|
| **COVID-19** | Coronavirus disease |
| **CFR** | Case-fatality rate |
| **CV** | Coefficient of variation |
| **ECMO** | Extracorporeal membrane oxygenation |
| **EMA** | European Medicines Agency |
| **FFP2** | Filtering face piece-2 |
| **ICU** | Intensive care unit |
| **IIV** | Inter-individual variability |
| **IOV** | Inter-occasion variability |
| **mAb** | Monoclonal antibody |
| **MID3** | Model-informed drug discovery and development |
| **NLME** | Non-linear mixed-effects |
| **NPI** | Non-pharmaceutical intervention |
| **ODE** | Ordinary differential equation |
| **PBPK** | Physiologically-based pharmacokinetics |
| **PCR** | Polymerase chain reaction |
| **PD** | Pharmacodynamic |
| **PK** | Pharmacokinetic |
| **PK/PD** | Pharmacokinetic/pharmacodynamic |
| **QSP** | Quantitative Systems Pharmacology |
| $\mathbf{R_0}$ | Basic reproductive number |
| **Rt** | Effective reproductive number |
| **SARS-CoV-2** | Severe acute respiratory syndrome coronavirus type 2 |
| **SEIR** | Susceptible-Exposed-Infected-Recovered |
| **SIR** | Susceptible-Infected-Recovered |
| **VOC** | Variant of concern |

# 1 INTRODUCTION

## 1.1 Motivation

Since the emergence of the new severe acute respiratory syndrome coronavirus type 2 (SARS-CoV-2) in December 2019, the virus rapidly spread worldwide, causing a pandemic with more than 770 million confirmed infections which resulted in more than 7 million deaths as of October 2024, according to the World Health Organization (WHO)[6]. SARS-CoV-2 is a highly transmissible ribonucleic acid (RNA) virus that belongs to the group of pathogenic coronaviruses[7]. While individuals of all ages are susceptible to infection, clinical manifestations of the coronavirus disease (COVID-19) vary by age with children and younger patients often experiencing asymptomatic infections or mild disease courses[7].

The most common COVID-19 symptoms, occurring in more than 25% of patients, include fever, cough, fatigue, dyspnoea, and the presence of sputum[8]. Patients with severe or critical symptoms suffer from low oxygen saturation due to lung damage, requiring intensive care treatment with oxygen supplementation, mechanical ventilation or extracorporeal membrane oxygenation (ECMO)[9].

SARS-CoV-2 spreads efficiently because the peak viral load coincides with the time of symptom onset, and infected individuals can transmit the virus during the presymptomatic stage[7,10]. This means that even if patients quarantine as soon as they experience COVID-19 symptoms, the disease can still spread efficiently. At the beginning of the pandemic, the basic reproduction number ($R_0$) of the SARS-CoV-2 wild type was estimated to be 2.87, indicating that each infected person, on average, spreads the disease to 2.87 more individuals, leading to an exponential growth of infections[11].

Conclusively, the emerging virus combined concerning characteristics: (i) a high reproductive number, (ii) causing severe disease with life-threatening complications and (iii) poor responsiveness to available treatments. This combination led hospitals to quickly reach their capacity limits, at times even necessitating the cancellation of elective surgeries to cope with the overwhelming influx of COVID-19 patients[11,12].

Therefore, gathering scientific knowledge to understand and contain the spread of SARS-CoV-2 was of critical importance. A thorough understanding of transmission mechanisms was essential for effective disease management. In particular, the recognition that SARS-CoV-2 spreads via airborne transmission of aerosols prompted the widespread use of filtering face piece-2 (FFP2) masks to disrupt infection chains[13,14]. Based on this evidence, the wearing of FFP2 masks in German public places soon became mandatory, significantly impacting the transmission of SARS-CoV-2[15].

In order to protect the population effectively, potential influencing factors affecting disease course and viral transmission needed to be investigated. Figure 1.1 provides an overview of the various factors, highlighting the challenges and research questions that arose with the emergence of SARS-CoV-2.

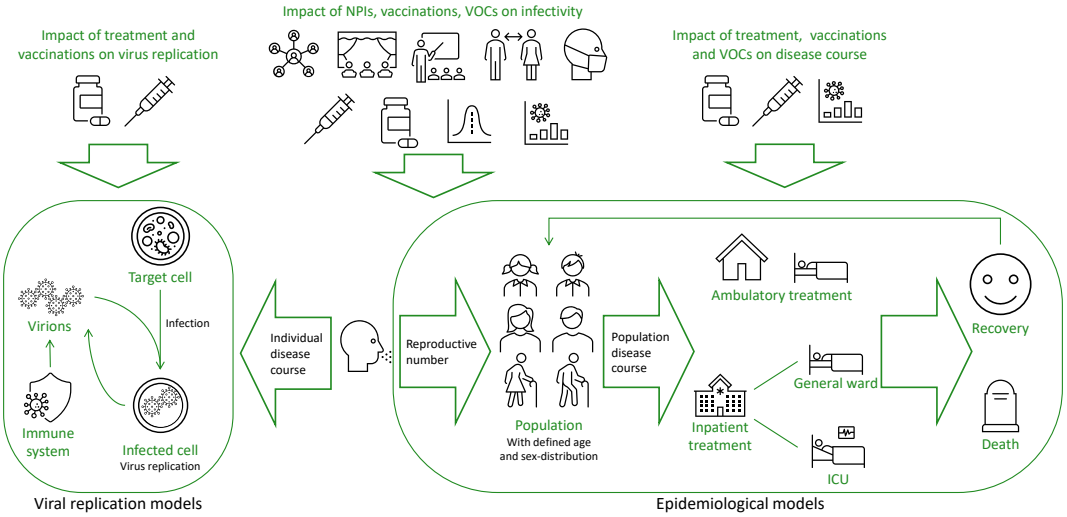


Figure 1.1: Visual representation of impacting variables during the pandemic and mathematical models used to answer arising research questions.

When investigating impact factors, mathematical modelling plays a crucial role, as it enables the simulation and prediction of complex biological systems and disease dynamics. For example, viral replication models (Figure 1.1, left side) can provide valuable insights into covariates modulating the individual disease course and are a powerful tool to evaluate the dose-exposure-response relationship of antiviral drugs[16]. As such, pharmacometric modelling provides a quantitative framework that has been successfully employed for decades and is appreciated by regulatory authorities[17,18].

In public health, epidemiological models are highly valuable for identifying factors that influence the transmission trajectories of pathogens[19]. While these models are broadly applicable to various infectious diseases, in our case, they were specifically employed to study the COVID-19 pandemic. Epidemiological modelling allows for the analysis and prediction of the pandemic's progression on a population scale (Figure 1.1, right side), which can help to optimize resource allocation[20]. Furthermore, these models enable simulations to predict future trajectories under different scenarios, significantly enhancing our understanding of pandemic dynamics – especially given the common human tendency to underestimate exponential growth[21]. Here, visualization of simulated trajectories can be crucial for effective science communication and to explain the need for precautionary measures to the general public[19].

## 1.2 COVID-19 Prevention

To prevent the spread of diseases, control strategies can be categorized into a 'high-risk' approach, which focuses on protecting individuals at high risk for severe disease, and the 'population' approach, which aims to decrease the overall incidence[22]. Both approaches were adopted in managing the SARS-CoV-2 pandemic in Germany. Especially during 2020, when vaccinations and rapid tests were not yet available, non-pharmaceutical interventions (NPIs) were of vital importance[23]. Initially, NPIs centred on limiting personal contacts, targeting both the high-risk elderly and medically vulnerable population with strict visitation restrictions in hospitals and retirement homes, as well as the general population through the closure of schools, remote teaching and the closure of leisure facilities such as restaurants or sports facilities. When it became evident that wearing face masks could reduce the risk of infection in spaces where close personal contact was unavoidable[24], NPIs were extended to include the mandatory wearing of FFP2 masks in enclosed public places, such as doctor's offices or public transportation.

With the availability of COVID-19 vaccinations and rapid testing, NPIs evolved into more complex rule systems, where access to various facilities was bound to the presentation of vaccination certificates or negative rapid test results.

The first vaccinations against COVID-19 were approved in August 2020: CoronaVac by Sinovac Biotech for military use in China[25] and Sputnik V for emergency use in Russia[26]. In Europe, BNT162b2, developed by BioNTech and Pfizer, was the first COVID-19 vaccine for which the European Medicines Agency (EMA) recommended conditional marketing authorisation[27]. The second approval of a COVID-19 vaccine in Europe soon followed with ChAdOx1nCov-19 by Oxford-AstraZeneca – authorized for individuals older than 18 years[28]. In Germany, the most used COVID-19 vaccines were BNT162b2, ChAdOx1nCov-19, mRNA-1273 by Moderna and Ad26.COV2-S by Janssen with 164.7, 37.7, 14.4 and 5.4 million doses administered as of April 2023, respectively[29].

Throughout the pandemic, mutations of the virus gave rise to various lineages, some of which were classified as variant of concerns (VOCs). Mutations occur naturally as the virus replicates, introducing genetic changes that can occasionally enhance transmissibility, immune evasion, or other viral properties. A mutation or lineage is usually defined as a VOC when it exhibits reduced neutralization by antibodies generated from a previous infection or vaccination, reduced efficacy of treatments or diagnostic tests, increased transmissibility, or increased disease severity[30]. For SARS-CoV-2, these attributes often arise when one or more mutations alter the spike protein, a surface glycoprotein critical for viral entry into host cells and the primary target of most COVID-19 vaccines[31,32].

Early mutations in the spike protein for VOCs Alpha, Beta, Gamma and Delta had a relatively small impact on the effectiveness of first-generation COVID-19 vaccines[33,34,35]. For the VOC Delta, vaccinations showed low efficacy against infection yet high efficacy

against severe disease, and booster vaccinations substantially increased overall efficacy[34]. However, with the arrival of Omicron – a VOC that contained 50 mutations, with at least 30 mutations affecting the spike protein[33], antibodies produced via first-generation vaccinations were more likely to be ineffective, necessitating the development of new, bivalent vaccinations against different subvariants of this VOC[36].

A general observation for all vaccinations was a time-dependent decrease in effectiveness, underscoring the need for regular booster vaccinations[37,38]. Furthermore, the decline in neutralizing antibodies over time significantly correlated with reduced effectiveness against symptomatic and severe COVID-19 after infection with various VOCs[38].

In summary, studying the impact of NPIs and vaccinations on the individual or population risk of infection is a complex task, as it is impossible to conduct studies in a controlled environment with a defined individual risk of infection[39]. Additionally, the population's perception of disease and infection risk plays a substantial role in behaviour change and adherence to NPIs[40]. Therefore, observed infection numbers are influenced not only by the general prevalence of infections at a given time but also by individual behaviors such as adherence to public health measures, and the emergence of new VOCs, which may exhibit altered transmissibility or immune evasion. These dynamic variables introduce significant uncertainty into predictive models of pandemic trajectories, particularly when multiple scenarios – such as varying levels of public health intervention, vaccine uptake, or the emergence of new variants – must be considered. As a result, accurate forecasting requires sophisticated models that account for these complex, interdependent factors.

## 1.3 COVID-19 Treatment

Treatment options for COVID-19 target either the virus through antiviral activity or antibody therapy, or the host's response to infection, including inflammation, thrombosis, acute respiratory distress syndrome (ARDS), and renin–angiotensin–aldosterone system (RAAS) activation[41].

Anti-inflammatory agents are beneficial for COVID-19 patients, as hyperinflammation processes play a critical role in the pathophysiology of severe cases[41]. Effective treatments include the glucocorticoid dexamethasone, the humanized monoclonal antibody tocilizumab, which targets the IL-6 receptor, and the Janus kinase (JAK) 1 and 2 inhibitor baricitinib[41,42].

Several antiviral drugs have shown efficacy against SARS-CoV-2, such as remdesivir and paxlovid. Remdesivir is a prodrug nucleoside analogue with antiviral activity against many RNA viruses[41]. Paxlovid is the combination of nirmatrelvir and ritonavir; nirmatrelvir inhibits the main protease of SARS-CoV-2 that cleaves polyproteins during viral replication, while ritonavir serves as a cytochrome P450 (CYP) 3A4 inhibitor, reducing

the metabolism of nirmatrelvir[41].

Other treatment options, such as the passive immunization with pathogen-specific monoclonal antibodys (mAbs), were evaluated for COVID-19 patients. However, while mAbs can be valuable for the treatment of infectious diseases particularly in immunocompromised patients[41], current studies show a lack of benefit of mAbs for COVID-19 patients[41].

Hypoxaemic respiratory failure is the leading cause of critical illness and death in COVID-19 patients[41]. Therefore, alongside pharmacological interventions, adequate oxygen delivery is crucial[41]. Patients with hypoxaemic respiratory insufficiency may require high flow nasal cannula, continuous positive airway pressure or non-invasive ventilation. Those with severe hyoxaemia require invasive mechanical ventilation[42]. In the most severe cases, ECMO may be considered the *ultima ratio*, serving as a life-saving intervention when all other treatments have failed[41].

### *1.3.1 Azelastine*

Given the multifactorial nature of COVID-19 treatment and the limited available options, the search for effective therapies extended to include drugs already approved for other diseases (drug repurposing). Azelastine emerged as a candidate in a retrospective study using data mining of electronic health records[43]. This study found a significantly lower rate of SARS-CoV-2 infections among patients older than 60 years with a history of therapy with azelastine in comparison with patients without previous azelastine treatment (odds ratio 0.41, p=0.001)[43].

Azelastine is a well-tolerated histamine-1 receptor antagonist[44]. Its anti-inflammatory effects are achieved through mast cell stabilization and the inhibition of leukotriene C4 and pro-inflammatory cytokine production[44,45]. It is primarily used to treat seasonal or perennial allergic rhinitis via nasal spray formulation at a concentration of 0.1% w/v and has been approved for this application for more than 30 years. Hence, its side effect profile, including headache, sleepiness, change in taste, and sore throat is well known[46].

Further *in vitro* studies found that azelastine inhibits the interaction between the SARS-CoV-2 spike protein and the ACE2-receptor[47], potentially blocking the virus's entry into cells. *In silico* studies also identified an interaction with the main protease of SARS-CoV-2[48,49], which was confirmed by a kinetic activity assay[48].

General antiviral activity *in vitro* was demonstrated using Vero E6 cells, with an $EC_{50}$ of approximately 6 µM[43,50]. An *in vitro* model of reconstituted human nasal tissue provided evidence for almost complete inhibition of viral replication within 72 hours after SARS-CoV-2 infection by treatment with a 0.02% w/v azelastine solution, which corresponds to a five-fold dilution of the commercially available nasal spray formulation[51].

Following these promising results, a study investigated the effect of azelastine in SARS-CoV-2 positive patients[45]. Patients received placebo, 0.02% or 0.1% azelastine

nasal spray for 11 days, during which the viral load was assessed using quantitative polymerase chain reaction (PCR). Moreover, COVID-19 related symptoms were documented using electronic diaries[45]. While the viral load was reduced in all groups after treatment ($p<0.0001$), this effect was more pronounced in the 0.1% group compared to placebo ($p=0.007$)[45]. Patients with an initial $Ct<25$ showed a significantly reduced viral load on day 4 in the 0.1% azelastine group compared to placebo ($p=0.005$)[45]. In both azelastine treated groups, PCR results were negative earlier and more frequently[45]. At the same time, no unexpected adverse events occurred in all treatment groups[45].

## 1.4 Model-Informed Drug Discovery and Development

In recent years, the term model-informed drug discovery and development (MID3) has been established to describe the implementation of a quantitative framework aimed at enhancing the decision-making quality during drug development[52]. MID3 integrates mathematical models that describe compound, mechanism, and disease-level data to generate knowledge and inform drug development decisions[52].

Within this framework, pharmacometrics plays a crucial role by developing and applying mathematical and statistical models to characterize, understand and predict the pharmacokinetics, pharmacodynamics and disease progression[53]. Pharmacometric modelling is a well-established tool for assessing treatment effectiveness and has been endorsed by public agencies such as the EMA in Europe as well as the Food and Drug Administration (FDA) in the US[54,55].

Pharmacokinetic/pharmacodynamic (PK/PD) modelling typically follows a dose-exposure-effect-efficacy approach. It describes drug concentration in relation to dosing and the drug´s absorption, distribution, metabolism, excretion (ADME) properties. The concentration is then linked to biomarkers or outcomes associated with clinical efficacy and/or safety. During pharmacokinetic (PK) model development, the biological system is divided into a series of well-stirred compartments. Each compartment represents a combination of tissues and/or organs that are pharmacokinetically distinct but assumed to be in rapid equilibrium regarding drug concentrations. The mass balance of the drug within each compartment is described by one or more ordinary differential equations (ODEs). These ODEs account for the rates of drug absorption, distribution, metabolism, and excretion between compartments, effectively modelling the dynamic changes in drug concentration over time.

In addition to modelling drug concentrations, PK/PD models incorporate pharmacodynamic responses to capture the relationship between drug concentration and its therapeutic or toxic effects. This is often achieved by linking the PK model to a pharmacodynamic (PD) model using additional ODEs or mathematical functions that describe the drug's effect on biological targets, such as receptors or enzymes. These

PD models can represent mechanisms like receptor binding, signal transduction, or gene expression, effectively modelling the dynamic changes in both drug concentration and physiological response over time.

PK/PD models aim to represent biological systems with varying levels of complexity, depending on their specific purpose, methodology and available data: Empirical models are primarily descriptive, based solely on observed concentrations rather than underlying physiological processes. Semi-mechanistic models, such as viral replication models, capture key biological processes but remain simplified in comparison to mechanistic models such as physiologically-based pharmacokinetics (PBPK) or Quantitative Systems Pharmacology (QSP) models. These aim to closely reflect biological systems and require extensive knowledge of the underlying physiological processes. PBPK modelling uses pre-existing knowledge regarding the constitutive physiology and drug-specific properties to simulate complex drug behaviour in the body, predicting drug concentration and distribution in various organs and tissues in the body over time[56]. By integrating disease biology and physiological systems with data on drug properties, QSP allows for simulation and prediction of drug behaviour in complex biological systems. It accounts for multiple factors influencing drug response, such as molecular interactions, cellular signalling pathways, and organ function[57].

## 1.5 Infectious Disease Modelling

Research questions raised during the COVID-19 pandemic can be addressed through infectious disease modelling on two levels: (i) between-host transmissions which includes population risks of severe disease and (ii) within-host disease dynamics, which covers viral replication and symptom occurrence[58]. With increasing knowledge, the link between within-host and between-host dynamics can be approximated by calculating transmission risks based on an individual´s viral load[59].

During epidemics and pandemics, modelling can serve several purposes. It can provide real-time estimates of disease severity at individual levels, help to predict the proportion of infections that will require intensive medical care, or offer risk assessments for individual patients to inform triage[60]. Additionally, modelling can offer insights into the expected size of epidemics and pandemics based on initial growth rates and the impact of both pharmaceutical and non-pharmaceutical interventions[60].

### *1.5.1 Epidemiologic Modelling*

In epidemiology, mathematical modelling is crucial for understanding and controlling the spread of infectious diseases and managing health resources[61]. Accordingly, the basic Susceptible-Infected-Recovered (SIR) model, which divides the population into susceptible, infected and recovered individuals, was already developed nearly 100 years ago

and to this day serves as the basis for many epidemiological model adaptations[60,62]. Epidemiologic models usually use basic assumptions, collected statistical data and information on the number of infections, vaccination effects, and the impact of NPIs[61]. These models estimate the effects of variables that are difficult to quantify otherwise and predict future infection patterns under varying assumptions[61].

Epidemiologic modelling is usually performed using either deterministic or stochastic models[61]. Deterministic models are suitable for large populations and are often depicted as compartmental models described by differential equations. In these models, the population is stratified into different stages of the infection-outcome cascade, such as susceptible, infected, recovered, or deceased. While individuals move through these stages, the model's input variables are static, meaning the disease course is assumed the same for every individual. Hence, deterministic models show how infections progress on average and work best for large populations[61].

Stochastic models, such as agent-based models, include random variables, focusing on the probability distributions of individual scenarios, such as the risk of exposure. For example, they can depict that the transition between stages can occur after a variable amount of time for each individual. Furthermore, as network-based models, they allow for the incorporation of specific individual traits, such as age-dependent contact patterns. Hence, each simulation yields a unique outcome due to stochastic fluctuations. Therefore, the calculation of median outcomes requires numerous simulations which renders this method computationally expensive. However, these simulations offer higher accuracy for smaller populations compared to deterministic models[63].

For large populations, the outcomes of many stochastic model simulations align with those of deterministic models. Stochastic models are thus employed when random variations are expected to have a significant impact on the outcome, which is common for smaller populations, localized outbreaks, and rare diseases. Here, simulating random fluctuations reduces the likelihood of local extinction during an outbreak[61].

During the COVID-19 pandemic, multi-level non-linear mixed-effects (NLME) approaches gained popularity in epidemiological modelling[64] as they allow to account for the complex interplay of variability between levels of interest and thereby provided a framework for more precise analyses and more fine-grained identification of the pandemic´s dynamics. For example, analysing the variability of the effective reproductive number (Rt) over time and comparing it to current NPIs and vaccination rates, which varied between federal states in Germany, resulted in more accurate estimates of their effectiveness.

### *1.5.2 Viral Load Modelling*

Mathematical models are powerful tools for analysing within-host disease dynamics of viral infections. They provide insights into viral pathogenesis at various scales: intracel-

lular interactions between viruses and host cells, extracellular interactions between the virus, infected and healthy cells, and the spread of viruses between organs or organisms[65].

For SARS-CoV-2 infections, viral load models on extracellular scales have proven particularly useful in linking viral load to disease severity and infection timing[66]. These models capture the non-linear dynamics of viral load over time within a host, accounting for viral count, infected and healthy cells, as well as the immune response. They can capture the key processes during viral infection, including host cell infection, virus replication and the death of infected cells. These basic models can be extended to various degrees, for example, to include the effects of the innate and adaptive immune systems.

Furthermore, viral load models can be used to estimate and describe the impact of anti-viral drugs based on their modes of action and their target of the virus replication cycle, such as cell entry or viral replication. By doing so, they support the evaluation of treatment options and the understanding of drug resistance[65].

# 2 OBJECTIVES

This thesis aimed to gain insights into the course of the COVID-19 pandemic in Germany and the impact of different prevention methods and treatments. For this purpose, mathematical models were developed and applied to study the trajectory of SARS-CoV-2 infections and the disease course in dependence of NPIs in Germany, followed by an in-depth analysis of the spread of the disease between different age groups with a focus on the effect of vaccinations. Finally, to gain more detailed insights into the individual course of the disease, the impact of azelastine nasal spray treatment on COVID-19 biomarkers and symptoms was evaluated.

## 2.1 Project I: COVID-19 Hospitalizations and Deaths

The aim of this work was to establish an epidemiologic model that depicts the trajectory of the COVID-19 pandemic in Germany. The model was developed to describe the number of SARS-CoV-2 infections and the resulting COVID-19 inpatients, intensive care unit (ICU) patients with and without the need for mechanical ventilation, recoveries, and fatalities for Germany's 16 federal states and validated using the case incidence data of the 400 districts. The model was established at the beginning of the pandemic with the aim to successively adapt it the changing pandemic landscape. Therefore, it considers the dynamics of infectiousness, the severity of the disease due to new VOCs, and advances in therapy options and vaccination programs. Furthermore, the impact of testing strategy, age, sex, and VOC emergence was evaluated as covariates on the fractions of hospitalized patients, ICU patients, and deaths.

## 2.2 Project II: COVID-19 Spreading in Different Age Groups

The aim of this work was to investigate the impact of NPIs, VOCs, and vaccinations on the spreading of SARS-CoV-2 within different age groups. The main objective of this work was to quantify the impact of NPIs which focuses on certain age groups, such as the closing of schools and remote schooling, in comparison to NPIs with an impact on the total population, such as travel restrictions. Furthermore, the impact of school closure during school holidays was compared to school closure with remote schooling. Finally, the impact of vaccinations was evaluated. The German vaccination program focused on protecting the older population first, as these are more susceptible to severe disease. Hence, by a time-dependent analysis, the impact of vaccinations could also be studied in dependence of the vaccination rates in each age group at each time point.

## 2.3 Project III: Azelastine Effect on SARS-CoV-2 Viral Load

The aim of this work was to first develop a PK model for azelastine which could then be used for the development of PK/PD models to compare the impact of placebo to azelastine on the individual SARS-CoV-2 viral load and COVID-19 disease course. Furthermore, the impact of the covariates on viral load, infectivity, and symptoms was explored. Finally, the model was used to simulate the impact of preventive treatment with azelastine on the transmission risk of SARS-CoV-2.

# 3 METHODS

## 3.1 Non-Linear Mixed-Effects Modelling

Non-linear mixed-effects (NLME) modelling techniques are a powerful tool to analyse pooled data from individual experimental units with multiple measurements[67]. In projects I and II of this work, the experimental units were German federal states and districts while the experimental unit in project III was individual patients, which is the standard experimental unit in population PK/PD modelling.

The "non-linear" aspect of NLME modelling refers to the description of patterns as changes of trends over time in a non-linear fashion[68,69]. The "mixed-effects" component comprises the combination of fixed and random effects. Fixed effects represent the overall population trends and are dependent on known factors such as the dose and time. Random effects, on the other hand, capture variability on different levels, including inter-individual (IIV), inter-occasion, and residual variability[68,69]. IIV accounts for differences between individuals, enabling the simultaneous investigation of patient- or study-specific characteristics[67]. By distinguishing between inter-individual and residual variability, NLME modelling allows the analysis of data measured with error. It enables the evaluation and quantification of the impact of covariates such as demographic characteristics, lab results, and co-medication[67]. This dual consideration of fixed and random effects allows for a nuanced understanding of the underlying data.

Therefore, NLME models typically consist of three submodels: The structural, the stochastic, and the covariate submodel, which are described in detail in sections 3.1.1 to 3.1.3. Figure 3.1 visualizes the role of each submodel in explaining the data.

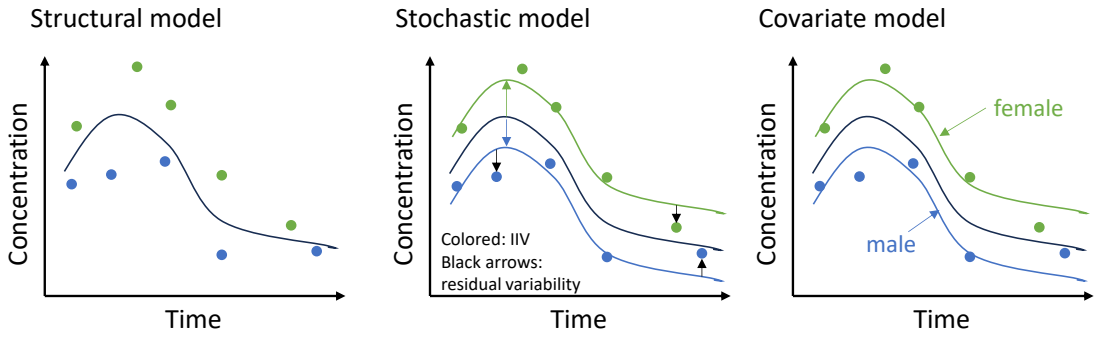


Figure 3.1: Visual representation of the concept behind the structural, stochastic, and covariate submodels for exemplary concentration-time profiles.

By evaluating data from all experimental units simultaneously, NLME modelling facilitates the analysis of data from studies with varying individual profiles and sampling times, accommodating unbalanced studies or datasets with missing data. Moreover, it supports the analysis of data from a few individuals with extensive sampling or many individuals with sparse sampling.

Therefore, NLME modelling provides a comprehensive framework for analysing complex datasets by incorporating variability at multiple levels and integrating covariate information[70]. This approach is particularly advantageous for population studies, as it enhances the understanding of how different factors influence the population and individual responses, but has been gaining growing popularity in epidemiological modelling during the COVID-19 pandemic[64].

### *3.1.1 Structural Model*

The structural submodel describes the relationship between dependent variables, such as plasma concentration or drug effect, and independent variables, such as time, as a function of the input such as the drug dose, and model parameters such as clearance and volume of distribution. These models can either be empirical or mechanistic models and are defined by fixed-effect parameters, denoted by the symbol $\theta$. For example, for the development of PK models, one-, two- and three-compartment models with linear or saturable elimination are usually evaluated.

### *3.1.2 Stochastic Model*

The stochastic submodel characterizes the variability in fixed-effects parameters and distinguishes between the inter-individual variability (IIV), inter-occasion variability (IOV), and residual error.

IIV refers to the variation in fixed-effects parameters among individuals. This variability of a fixed effects parameter k within the studied population is represented by $\eta_{k,i}$ values. These $\eta_{k,i}$ values are assumed to be symmetrically distributed with a mean of 0 and variance denoted by $\omega_k^2$[71]. For stochastic model building, the IIV can be implemented using different models as depicted in equations 3.1 - 3.3.

$$\text{Additive variability model:} \qquad k_i = \theta_k + \eta_{k,i} \tag{3.1}$$

$$\text{Proportional variability model:} \qquad k_i = \theta_k \times (1 + \eta_{k,i}) \tag{3.2}$$

$$\text{Exponential variability model:} \qquad k_i = \theta_k \times e^{\eta_{k,i}} \tag{3.3}$$

The exponential model is most commonly used. Unlike the additive model, the exponential model constrains the individual parameter $k_i$ to positive values. Compared to the proportional model, the exponential model assumes a log-normal distribution of the

individual parameters, which is often observed in parameters of biological systems with low to moderate variability (5-30 %Coefficient of variation (CV))[72,73].

IOV describes variation in fixed-effects parameters within an individual over different occasions. IOV is typically considered when there is a reasonable expectation for a PK or PD parameter to change over time within an individual.

The residual variability represents the deviation of measured values (obs) from the predicted value (ipred). It is a random effects parameter that accounts for the variability in the measured value due to imprecision. The random-effect parameter $\epsilon_{i,j}$ is also assumed to be symmetrically distributed with mean 0 and variance $\sigma^2$. The most commonly used stochastic models for the residual variability are the additive error model (equation 3.4), which assumes a homoscedastic error with constant variance var(Cobs-Cpred) and the proportional error model (equation 3.5), which poses a heteroscedastic error with a constant Coefficient of variation var((Cobs-Cpred)/Cpred). Often, a combined additive and proportional model is employed to account for both constant and, proportional errors in the data.

Additive error model: $$obs_{i,j} = ipred_{i,j} + \epsilon_{i,j} \tag{3.4}$$

Proportional error model: $$obs_{i,j} = ipred_{i,j} \times (1 + \epsilon_{i,j}) \tag{3.5}$$

### *3.1.3 Covariate Model*

The covariate submodel aims to explain the IIV and thereby reduce the unexplained IIV. Covariates typically include patient-specific or study-specific characteristics that influence model parameters. These characteristics encompass demographic information (e.g. age, sex, weight, and ethnic group), as well as clinical laboratory parameters (e.g. albumin, aspartate transaminase), organ functions (e.g. estimated glomerular filtration rate), genetics, disease stage, concomitant diseases, and medication. NLME modelling also allows for the investigation of time-varying covariates[74].

There are different procedures for covariate model building, all of which are based on the statistical level of significance[75,76]. Covariates can either be selected through regression analysis comparing the individual model empirical bayes estimates (EBEs) to the covariates or by stepwise inclusion of each potential covariate into the model[76]. When all identified covariates are included in the model, the covariate analysis is usually concluded by stepwise, univariate exclusion of covariates with a stricter level of significance[76].

By incorporating relevant covariates, the covariate submodel enhances the explanatory power of the NLME model, thereby providing a deeper understanding of the factors influencing variability in the population.

## 3.2 Infectious Disease Modelling

### *3.2.1 Epidemiologic Modelling*

#### *3.2.1.1 SIR models*

In projects I and II, the SIR model was adapted to describe the number of German inhabitants with confirmed SARS-CoV-2 infections. The SIR model divides the population into three consecutive groups: the susceptibles (S) who can be infected by the infectious (I) population, followed by the recovered (R) population which is no longer infectious and has gained immunity. This most simple case example is described by a system of three ODEs as depicted in Equations 3.6-3.8.

$$\text{Susceptible:} \quad d/dt(S) = -\beta \times I(t) \times S(t) \tag{3.6}$$

$$\text{Infected:} \quad d/dt(I) = \beta \times I(t) \times S(t) - \gamma \times I(t) \tag{3.7}$$

$$\text{Recovered:} \quad d/dt(R) = \gamma \times I(t) \tag{3.8}$$

Here, $\beta$ is the disease transmission rate and $1/\gamma$ represents the mean infectious period. Figure 3.2 visualizes the population transitioning through the three stages of the SIR model.

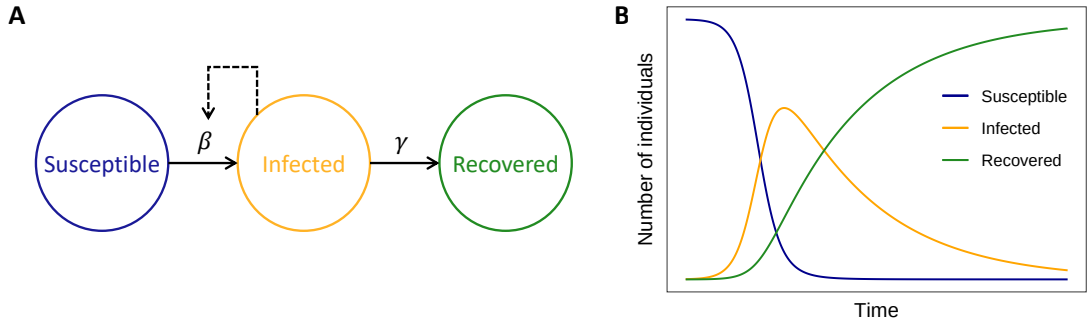


Figure 3.2: A: Schematic representation of the SIR model. B: Visual representation of the time course of a viral infection spreading through a population as described by the SIR model.

The SIR model can be expanded to include additional compartments as needed. One common augmentation is the Susceptible-Exposed-Infected-Recovered (SEIR) model, which additionally describes the exposed (E) population, which is infected but not yet infectious.

Other extensions of the SIR model include additional compartments such as quarantined individuals that are physiologically infective but physically separated from the susceptible population and thereby deprived of their potential to infect further indi-

viduals. Furthermore, recovered and vaccinated individuals can be described as less or not susceptible after their vaccination. Other expansions of the SIR model include the stratification by treatment setting (inpatient vs. outpatient) or outcome (fatalities vs. recoveries). The choice of stratification depends on the research question and data availability to support the stratification.

In Project I, the population was stratified into susceptibles, infected (and infectious) quarantined, and recovered individuals as well as fatalities. The quarantined population was furthermore subdivided to ambulatory patients, inpatients, ICU patients, and ventilated ICU patients. This deep stratification was enabled by the available data on the number of German patients at each stage and supported by information on individual inpatient disease courses.

In Project II, a less thorough stratification was used with respect to the individual disease course, as the main focus was the spreading of SARS-CoV-2 between individuals of different age groups. Therefore, the population was only stratified into susceptible, infected, and quarantined individuals, however each of these stages was stratified by age group.

#### *3.2.1.2 Reproductive Number*

When a system of SIR or SEIR differential equations is initialized by $S(0)=S_0$, $I(0)>0$, $I(0)\ll S(0)$ and $R(0)=0$, the basic reproductive number ($R_0$) is defined by Equation 3.9[77], with $S_0$ being the number of susceptible individuals in the population.

$$R_0 = \frac{\beta \times S_0}{\gamma} \tag{3.9}$$

The value of $R_0$ is defined as the number of secondary cases caused by one infected individual in a fully susceptible, unvaccinated, and non-immune population and thereby determines the outbreak dynamics: $R_0<1$ leads to a decline in infections to zero, while $R_0>1$ results in an epidemic, which eventually subsides as the number of susceptible individuals decreases. However, these conclusions are based on the assumptions that (i) there is no birth rate contributing to the susceptible population and (ii) recovered individuals have complete immunity against reinfection. Thereby, it poses a strong simplification for most diseases.

After the initial outbreak, when the population is no longer fully susceptible, the effective reproductive number (Rt) is used to describe the potential for disease spread at time t[78]. Rt usually deviates from $R_0$ and determines the potential for the spreading of the pandemic at time t[79]. Rt accounts for the decline of susceptibles and the impact of control measures such as public health interventions and vaccination. Regular re-evaluation of Rt is essential to assess the effectiveness of these measures.

Various methods are available to determine Rt, which can be broadly categorized into

mathematical and statistical approaches[80]. Mathematical methods, based on mechanistic transmission models as discussed above, rely on background information such as the latent period[81].

Statistical methods rely on the serial interval (the time between symptom onset in successive cases) and case notification data[80,81]. These methods calculate the likelihood of one case i being infected by case j given their time difference between symptom onset normalized for the likelihood of infection of case i by another case k[82]. The sum of these likelihoods at each time then results in Rt[82]. While statistical methods only require knowledge of the number of cases and the serial interval, they cannot implement outbreak-specific information like changes of infectiousness due to VOCs[80].

Both methods for determining Rt can be affected by underreporting of cases as well as variability in testing infrastructure (e.g. due to general medical practices being closed during weekends). To mitigate biases introduced by weekday fluctuations in case reporting of SARS-CoV-2, 7-day incidence rates were commonly reported. For example, the German public health institute Robert Koch-Institute (RKI) evaluated Rt over 4- and 7-day periods[83]. To circumvent the daily fluctuations between weekdays, in Projects I and II, NLME modelling techniques were used to describe the number of cases based on mechanistic models, estimating time periods during which a constant Rt could explain the number of cases.

### *3.2.2 Viral Load Modelling*

For the description of individual viral load-time profiles on a population scale, the target-cell limited model is the most extensively used model[65]. The minimal version of this model consists of three ODEs which are depicted in equations 3.10 - 3.12[65,84].

Target cells: $$d/dt(T) = \lambda - d \times T - \beta \times V \times T \quad (3.10)$$

Infected virus-producing cells: $$d/dt(I) = \beta \times V \times T - \delta \times I \quad (3.11)$$

Virus load: $$d/dt(V) = \pi \times I - \gamma \times V \quad (3.12)$$

In these equations, T represents the number of susceptible target cells, I represents the infected target cells, and V represents the viral load, which are described in dependence of the target cell death rate $d$, the target cell production rate $\lambda$, the infectivity rate $\beta$, the death rate $\delta$ of infected cells, the virus production rate $\pi$ and the virus elimination rate $\gamma$[65]. This model assumes that intracellular processes can be neglected and the infection is limited by the number of target cells. Figure 3.3 visualizes the time course of a virus infection as described by the target-cell limited model.

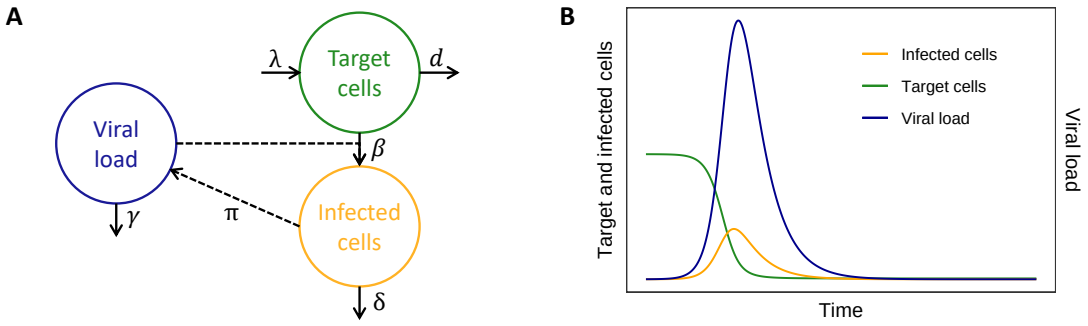


Figure 3.3: A: Schematic representation of the minimal target-cell limited model. B: Visual representation of the time course of a viral infection described by the minimal target-cell limited model.

The target-cell limited model is often extended by a latent (or 'eclipse') phase (E), in which cells are infected but not yet producing virions[85]. This phase can be necessary to represent the initial time frame of infections adequately; however, it was not identified as required for describing SARS-CoV-2 infections[85]. Other potential extensions of the model include the description of refractory cells, which are target cells protected from infection[65].

The target-cell limited model can be extended to include an immune-response model. In contrast to the target-cell limited model, immune-controlled models take into account the regulation of the viral load through the host's immune response. However, the target-cell limited model usually describes viral load data of virus infections adequately and has the advantage of a smaller number of model parameters which can be identified based on viral load-time profiles alone[84,86].

However, for an accurate description of the SARS-CoV-2 viral load over time, the extension for an immune-response model is required[85,87]. Ideally, the immune-response models differentiate between the innate and the adaptive immune responses[88]. The innate immune response is the immediate response mediated by macrophages, cytokines and chemokines and has a broad specificity. The adaptive immune response requires the development of naive T- and B-lymphocytes into more specific immune cells, such as CD8+ and plasma cells[88]. Due to its ability to generate an immunological memory, the adaptive immune response mechanisms are utilized in vaccinations. Numerous modelling approaches with varying degrees of complexity have been described for COVID-19[85,87,88,89].

In Project III, a viral load model developed for SARS-CoV-2 by Goyal et al.[87] was employed for the analysis of the SARS-CoV-2 viral load over time in dependence of the azelastine concentration. This model is an extension of the minimal target-cell limited model that includes the effect of an early, innate immune response and a late T cell

response, as depicted in equations 3.13 to 3.18:

Target cells: $$d/dt(T) = -\beta \times V \times T \tag{3.13}$$

Infected cells: $$d/dt(I) = \beta \times V \times T - \delta \times I \times I^k - m \times \frac{E^r}{E^r + \phi^r} \times I \tag{3.14}$$

Virus load: $$d/dt(V) = \pi \times I - \gamma \times V \tag{3.15}$$

Precursor T cells: $$d/dt(M_1) = \omega \times I \times M_1 - q \times M_1 \tag{3.16}$$

$$d/dt(M_2) = q \times (M_1 - M_2) \tag{3.17}$$

Effector T cells: $$d/dt(E) = q \times M_2 - \delta_E \times E \tag{3.18}$$

In this model, the early, innate immune response is represented by the term $\delta I^k$ and the acquired, late T cell response is described via the delayed production of effector cells (E) via the precursor cells $M_1$ and $M_2$. $k$ represents the dependency between the infected cell density and the first death rate. The late T cell response is defined by the proliferation rate $\omega$, the differentiation rate $q$, and the effector cell death rate $\delta_E$. The impact of the effector cells on the elimination of infected cells is described by a Hill function with maximum $m$, half-maximum effective effector cells $\phi$ and hill coefficient $r$.

The viral load models can be used to analyse the effect of antiviral drugs based on their mechanism of action. The effect of drugs that block the infection can be described via their impact on the infectivity rate $k$ (equations 3.10 and 3.11). Drugs affecting the production of viral particles would reduce the production rate $p$ (equation 3.12)[65].

In this context, the impact of a drug is usually implemented using Hill- or Emax-effect model as expressed in equation 3.19[90].

Hill effect model: $$Effect = \frac{Emax \times C(t)^n}{EC50^n + C(t)^n} \tag{3.19}$$

with *Emax* as the maximum drug effect, *EC50* as the drug concentration with half-maximum effect, *C(t)* the drug concentration at time t and $n$ as the hill coefficient, which renders the shape and steepness of the drug effect, resulting in a sigmoidal curve for n>1[90]. For n=1, the Hill effect model corresponds to the so-called Emax-effect model.

# 4 RESULTS

## 4.1 Project I: COVID-19 Hospitalizations and Deaths

### *4.1.1 Reference*

**Model-based analysis of SARS-CoV-2 infections, hospitalization and outcome in Germany, the federal states and districts.**
Christiane Dings, Katharina Martha Götz, Katharina Och, Iryna Sihinevich, Quirin Werthner, Sigrun Smola, Marc Bliem, Felix Mahfoud, Thomas Volk, Sascha Kreuer, Jürgen Rissland, Dominik Selzer and Thorsten Lehr.
*Viruses* 2022;14(10):2114. DOI: 10.3390/v14102114[1]

### *4.1.2 Author Contributions*

Author contributions according to the contributor roles taxonomy (CRediT)[4,5] were as following:

| | |
|---|---|
| Christiane Dings | See Contribution Report (page ii) |
| Katharina Martha Götz | Data curation, formal analysis |
| Katharina Och | Data curation, formal analysis |
| Iryna Sihinevich | Data curation |
| Quirin Werthner | Data curation |
| Sigrun Smola | Conceptualization, writing — review & editing |
| Marc Bliem | Conceptualization, data curation, writing — review & editing |
| Felix Mahfoud | Conceptualization, writing — review & editing |
| Thomas Volk | Conceptualization, writing — review & editing |
| Sascha Kreuer | Conceptualization, writing — review & editing |
| Jürgen Rissland | Conceptualization, formal analysis, writing — review & editing |
| Dominik Selzer | Conceptualization, formal analysis, methodology, Writing — original draft, writing — review & editing |
| Thorsten Lehr | Conceptualization, data curation, formal analysis, methodology, project administration, resources, supervision, writing — original draft, writing — review & editing |

### *4.1.3 Copyright*

*viruses*

MDPI

*Article*

# Model-Based Analysis of SARS-CoV-2 Infections, Hospitalization and Outcome in Germany, the Federal States and Districts

**Christiane Dings [1], Katharina Martha Götz [1], Katharina Och [1], Iryna Sihinevich [1], Quirin Werthner [1], Sigrun Smola [2,3], Marc Bliem [4], Felix Mahfoud [5,6], Thomas Volk [7], Sascha Kreuer [7], Jürgen Rissland [2], Dominik Selzer [1] and Thorsten Lehr [1,*]**

1 Department of Clinical Pharmacy, Saarland University, 66123 Saarbrücken, Germany
2 Institute of Virology, Saarland University Medical Center, 66421 Homburg, Germany
3 Helmholtz Institute for Pharmaceutical Research Saarland (HIPS), Helmholtz Centre for Infection Research (HZI), 66123 Saarbrücken, Germany
4 CompuGroup Medical (CGM), 56070 Koblenz, Germany
5 Department of Internal Medicine III (Cardiology, Angiology, Intensive Care Medicine), Saarland University Medical Center and Saarland University Faculty of Medicine, 66421 Homburg, Germany
6 Institute for Medical Engineering and Science, Massachusetts Institute of Technology, Cambridge, MA 02139, USA
7 Department of Anesthesiology, University Hospital of the Saarland, 66421 Homburg, Germany
* Correspondence: thorsten.lehr@mx.uni-saarland.de; Tel.: +49-681-302-70255

check for updates

**Citation:** Dings, C.; Götz, K.M.; Och, K.; Sihinevich, I.; Werthner, Q.; Smola, S.; Bliem, M.; Mahfoud, F.; Volk, T.; Kreuer, S.; et al. Model-Based Analysis of SARS-CoV-2 Infections, Hospitalization and Outcome in Germany, the Federal States and Districts. *Viruses* **2022**, *14*, 2114. https://doi.org/10.3390/v14102114

Academic Editors: Luis Martinez-Sobrido and Fernando Almazan Toral

Received: 11 August 2022
Accepted: 20 September 2022
Published: 24 September 2022

**Publisher's Note:** MDPI stays neutral with regard to jurisdictional claims in published maps and institutional affiliations.



**Abstract:** The coronavirus disease 2019 (COVID-19) pandemic challenged many national health care systems, with hospitals reaching capacity limits of intensive care units (ICU). Thus, the estimation of acute local burden of ICUs is critical for appropriate management of health care resources. In this work, we applied non-linear mixed effects modeling to develop an epidemiological SARS-CoV-2 infection model for Germany, with its 16 federal states and 400 districts, that describes infections as well as COVID-19 inpatients, ICU patients with and without mechanical ventilation, recoveries, and fatalities during the first two waves of the pandemic until April 2021. Based on model analyses, covariates influencing the relation between infections and outcomes were explored. Non-pharmaceutical interventions imposed by governments were found to have a major impact on the spreading of SARS-CoV-2. Patient age and sex, the spread of variant B.1.1.7, and the testing strategy (number of tests performed weekly, rate of positive tests) affected the severity and outcome of recorded cases and could reduce the observed unexplained variability between the states. Modeling could reasonably link the discrepancies between fine-grained model simulations of the 400 German districts and the reported number of available ICU beds to coarse-grained COVID-19 patient distribution patterns within German regions.

**Keywords:** coronavirus disease 2019 (COVID-19); SARS-CoV-2; mathematical model; age; sex; testing strategy; variant of concern (VOC); intensive care; non-pharmaceutical interventions

## 1. Introduction

Severe acute respiratory syndrome coronavirus-2 (SARS-CoV-2) was first identified in December 2019 in Wuhan, China [1], and caused a worldwide pandemic with more than 550,000,000 confirmed cases and 6,300,000 coronavirus disease (COVID-19)-related deaths as of 21 July 2022 [2]. COVID-19 patients with severe courses of disease challenged national health care systems, with hospitals reaching capacity limits of intensive care units (ICUs) [3,4].

Because only a few countries successfully implemented major suppression or local eradication strategies [5], for the vast majority of the world, staying ahead of the pandemic regarding case management with non-pharmaceutical interventions (NPIs), vaccination

programs, and health care resource management was and still is of vital importance [6]. The need for vigilance was particularly highlighted as new variants of concern (VOCs) such as lineage B.1.1.7 (Alpha) emerged and quickly spread globally due to a significant advantage in transmissibility compared to wild type [7]. Moreover, infections with some of the VOCs were associated with a higher risk of critical care admission and mortality [8].

The risk for severe courses of COVID-19 differs vastly between individuals, with previous studies identifying age and sex as strong predictors for severity and outcome [9–12]. As national testing capacities varied throughout the pandemic due to the availability of testing infrastructure [13], further longitudinal predictors might be needed to estimate the prospective number of expected hospitalized patients and fatalities from a number of confirmed SARS-CoV-2 infections. Here, mathematical modeling might be useful to analyze different predictors for COVID-19 hospitalizations and disease outcomes, connecting longitudinal data on confirmed infections and individual risk factors (such as age and sex) as well as systemic case-outcome-related factors (originating from, e.g., regional or national testing strategies) [14–17].

In this work, we developed a mathematical infectious disease model that describes the first two waves of the pandemic and the emergence of VOC B.1.1.7 in Germany until April 2021. The impact of covariates such as testing strategy, age, sex, and VOC emergence was evaluated to describe SARS-CoV-2 infections and the resulting number of COVID-19 inpatients, ICU patients with and without the need for mechanical ventilation, recoveries, and fatalities for Germany's 16 federal states and 400 districts. Moreover, the developed model should serve as a foundation which can be adapted to changes in the pandemic, such as the dynamics of infectiousness, the severity of the disease due to new variants, improved therapy options, and advances in vaccination programs.

## 2. Materials and Methods

### *2.1. Epidemiological Data*

The local ethics committee of the medical association of the Saarland granted ethical approval for this study (Ärztekammer des Saarlandes, Short title: "CoSim"; Bu 78/20). Data were gathered from several sources: Confirmed SARS-CoV-2 infections as well as COVID-19-related deaths and recoveries were collected at the federal state level from the database of the regional newspaper "Berliner Morgenpost", which has compiled information from the John Hopkins University CSSE, reports from German authorities, and data from the Robert Koch Institute (RKI) and federal state health authorities since 27 January 2020 [18]. Data on confirmed cases at the district level as well as age- and sex-stratified information on SARS-CoV-2 infections were available from the RKI (age groups 0–4, 5–14, 15–34, 35–59, 60–79, and >80 years) [19].

If information was available, the dataset included the number of current COVID-19 inpatients and daily new inpatients as reported by the health ministries of the 16 federal states [20–32]. The number of occupied ICU beds with and without mechanical ventilation was available from the German Intensive Care Register DIVI and the RKI [33,34]. A detailed listing of epidemiological data sources can be found in Supplementary Table S1.

The model was informed by prior information on clinical outcomes obtained from the hospital financial information system MetaKIS (CompuGroup Medical (CGM), Koblenz, Germany). This database included a representative cohort of about 10% of all confirmed SARS-CoV-2 cases in German hospitals and provided information about diagnosis (ICD-10 coding), age, sex, and duration of treatment at various hospital wards, as well as duration of mechanical ventilation and outcome on a patient-specific level. In total, the database contained data of 30,723 patients admitted to hospitals between 23 March 2020 and 1 March 2021 with a positive test for infection with SARS-CoV-2 (ICD-10 Code U07.1: COVID-19, virus identified) and released from the hospital as recovered or perished (N = 23,810 and N = 6913, respectively). Recovered inpatients with an unusually short hospital stay of less than a day were excluded from the analysis (N = 1876). Patients with a record of ICU stay for less than one hour were handled as inpatients that only required treatment in the

general ward. The analysis of data from the resulting 28,847 COVID-19 patients provided information about hospital admissions per confirmed case, admissions to the ICU, the need for mechanical ventilation, length of stay, and rates of in-hospital death differentiated by general ward, ICU, and need for mechanical ventilation. COVID-19 admission rates and mortality were stratified by sex and age via post hoc analysis, with age groups following the schema of the RKI (0–4, 5–14, 15–34, 35–59, 60–79, and >80 years). The duration of stay was stratified by clinical ward and outcome.

### *2.2. Model Development*

Non-linear mixed-effects modeling was applied for the stepwise parametrization and development of a compartmental model consisting of three submodels for (I) infections, (II) hospitalization, and (III) outcomes of SARS-CoV-2 infections. The model was developed for Germany on a federal state level and subsequently applied to describe and analyze the pandemic in the 400 German districts.

Non-linear mixed-effects modeling was performed using the software NONMEM (7.4.3., ICON Development Solutions, Ellicott City, MD, USA). The statistical programming language R 3.6.3 (The R Foundation for Statistical Computing, Vienna, Austria) was used for dataset generation, statistical analysis, and visualization.

Model development was performed in two steps: First, the number of daily infections was described, with dependence on NPIs and other influences causing changes in infectiousness over time. Second, estimated parameters describing daily infections were fixed, and the numbers of daily inpatients, ICU patients, ventilated patients, and fatalities were described. A detailed description of submodel development is provided in the following sections.

### *2.3. Infections*

The number of daily infections was described using the classical epidemiological compartment model [35], where the population is transferred through the stages susceptible (S) and infected (I) before counting as a confirmed case (C), as depicted in Equations (1)–(3)

$$\frac{dS}{dt} = -\beta(t) * \frac{S(t)}{N} * I(t) \quad (1)$$

$$\frac{dI}{dt} = \beta(t) * \frac{S(t)}{N} * I(t) - \gamma * I(t) \quad (2)$$

$$\frac{dC}{dt} = y * I(t) \quad (3)$$

with N being the number of inhabitants. The transmission rate $\gamma$ from the infectious stage to confirmed cases was fixed to an infectious period of 7 days, with $\gamma = 1/7$ based on 6 days of mean incubation time plus 1 day of lag between showing symptoms and registering a positive test result [36]. The transmission rate $\beta(t)$ for the transfer from the susceptible to the infectious stage is related to $\gamma$ and the infectiousness ($R_\alpha$) as depicted in Equation (4):

$$\beta(t) = R_\alpha(t) * \gamma \quad (4)$$

The infectiousness was described depending on intrinsic local changes implemented at discrete points in time. Furthermore, when VOC B.1.1.7. started to emerge in Germany in the winter of 2020/2021, VOC infections were set to have a 35% increase in infectiousness compared to wild type, as estimated by Graham et al. [7].

### *2.4. Hospitalization and Outcome of COVID-19 Patients in Germany*

To describe the number of hospitalized patients and ICU patients with and without mechanical ventilation, the modeled confirmed infections were then split into the four scenarios of interest: patients requiring no inpatient treatment (Q), patients requiring inpatient treatment without treatment at ICU (H), patients requiring ICU treatment without

mechanical ventilation (ICU), and patients requiring mechanical ventilation (V). Each group was further split into the outcomes recovery and death. For each scenario and outcome, the mean times until discharge were derived from the clinical database and used as the mean transit time (MTT) for the transition of the population through the respective stages. Here, transit rates were defined as $(n+1)/\mathrm{MTT}$, with n being the number of additional transit compartments [37]. For this, models with one and two transit compartments and different structural models were tested, resulting in $8 * (n+1)$ differential equations describing the SARS-CoV-2-positive population transitioning through the disease stages. To compute the total number of hospital inpatients at a certain time point, the numbers of patients in the transit compartments for each ward and outcome were calculated as described in Appendix A Equation (A54).

The covariates age, sex, fraction of cases infected with VOC B.1.1.7, testing strategy, and the number of daily and weekly infections per 100,000 inhabitants were tested for their impact on different model parameters. Model parameters for hospital ward admission and death rates were stratified by age and sex according to rates derived for each age group from the clinical database.

For example, to obtain the fraction of SARS-CoV-2-positive patients requiring inpatient treatment at time t, the fraction of cases with a certain age and sex $p(a,s,t)$, as reported with the number of cases by the RKI, was multiplied by the age- and sex-stratified risk for hospitalization according to the clinical database $fh(a,s)$, resulting in the fraction of new cases requiring hospitalization $h(t)$ at a certain timepoint (Equation (5)).

$$h(t) = \sum_{s=\mathrm{Male}}^{s=\mathrm{Female}} \sum_{a=\mathrm{Age}\ 0-5}^{a=\mathrm{Age}\ 80+} fh(a,s) * p(a,s,t) \tag{5}$$

ICU, ventilation, and fatality rates were calculated accordingly, as described in Appendix A, Equations (A28), (A29), (A31), (A33) and (A35).

For other covariates, different linear, exponential, and sigmoid Emax models were tested to describe the impact of the covariates on different model parameters [38]. If the analysis of the clinical data and model goodness-of-fit plots revealed the need for rate changes at distinct time points that could not be explained by the previously discussed covariates, rate changes were included in the model with time-dependent sigmoid Emax models.

### *2.5. Model Parametrization and Mixed-Effects Modeling*

If possible, model parameters were informed by literature or metrics derived from the clinical database. Missing parameters were estimated using first-order conditional estimation with interaction (FOCEI) [39] implemented in NONMEM. The objective function value ($-2$ log-likelihood; OFV), precision of parameter estimates reported as relative standard errors (RSE) [38], as well as visual inspection of the goodness-of-fit plots [40] were used as evaluation criteria for model selection.

Model parameters that could not be informed by literature or database analysis were estimated using fixed effects and random effects. For this, unknown changepoints in infectiousness and all hospitalization and outcome model parameters were estimated as fixed effects. Random effects were estimated for local infectiousness for every changepoint and the error models. Here, combined residual error models with additional and proportional errors were used for each modeled outcome (hospital, ICU, ventilated, deaths) except for the cumulative cases, where a combined additional and exponential error was assumed.

For the model describing the number of cases, the changepoints of infectiousness were either fixed to dates of reported changes in federal or local policy regarding NPIs, or they were estimated as fixed effects (see Supplementary Table S3). For the implementation of changepoints, the NONMEM model event time parameter (MTIME) was used. A random effect model was used to describe the differences in change of infectiousness between federal states or districts, assuming a log-normal distribution with a prior of 30% CV.

The development of the infectiousness model was initiated at the beginning of the pandemic in Germany and was updated weekly. Here, previously estimated changepoints

and infectiousness were fixed, and only the latest three changepoints and $R(t)s$ were estimated every week. If the implementation of a new infectiousness changepoint led to a significant improvement in the description of the data ($p < 0.01$, dOFV > 11.345 for 3 degrees of freedom), it was retained in the model. Changepoint starting values were set to be at least 5 days apart from the previous changepoint. For the estimation process, $R(t)$ values were clamped to a range between 0 and 3. For the simulation of infection trajectories for every state and district, maximum a posteriori estimation was used to estimate individual model parameters. The simulation of infections within the whole German population was accomplished using the population estimates.

For the hospitalization and outcome models, the estimated individual parameters from the infectiousness model were fixed. For the hospitalization and outcome models' parametrization, only fixed effects were used (see Appendix B Table A1). Here, starting values were set to assure that parameters ranged within reasonable boundaries (e.g., the fraction of patients requiring inpatient treatment would not exceed 1).

## 3. Results

### *3.1. Clinical Database*

The clinical database covered approximately 10% of all German COVID-19 inpatients from 139 hospitals and included a total of 28,847 COVID-19 inpatients (53% males) with a median age of 73 years (interquartile range of 57–83 years). A comprehensive summary of the data can be found in Supplementary Table S2. During the study period, 18% (N = 5235) of inpatients required ICU treatment, and 67% (N = 3508) of ICU inpatients required mechanical ventilation. Overall, 24% (N = 6913) of inpatients died. The average time until discharge and time spent on each ward were stratified by outcome (Table 1). The mean time until discharge (recovery or death) was 2.1-fold longer for recovered patients who needed ICU treatment compared with patients treated in the general ward. Patients dying had a shorter duration of inpatient treatment in comparison to recovering inpatients. In particular, patients requiring mechanical ventilation showed a 46% shorter hospital stay compared with recovered patients. On average, inpatients required mechanical ventilation for 28% of their stay until recovery (8 days), whereas patients dying were ventilated for 63% of their hospital stay (9.8 days). Moreover, patients requiring ventilation spent on average 43% (12.7 days) or 68% (10.5 days) of their time as inpatients in the ICU if the outcome was recovery or death, respectively. Patients without the need for mechanical ventilation spent 29% (5.9 days) or 44% (8.8 days) of their hospital stay at the ICU when recovering or dying, respectively.

**Table 1.** Mean time until discharge, proportion of time on ICU and on a mechanical ventilator as well as standard deviations (sd) derived from the clinical database as used in the model for patients in the general ward, ICU inpatients, and ICU inpatients who needed mechanical ventilation as well as outcomes recovery and death.

| Ward (Fraction of Patients) | Outcome (Fraction of Patients by Ward) | Total Duration until Discharge [Days] (sd) | Proportion of Time in ICU [%] (sd) | Proportion of Time Ventilated [%] (sd) |
|---|---|---|---|---|
| General ward only (81.8%) | Recovery (82.2%) | 11.5 (11.4) | | |
| | Death (17.8%) | 10.6 (11.2) | | |
| ICU without ventilation (6.0%) | Recovery (76.1%) | 20.4 (17.1) | 29 (96) | |
| | Death (23.9%) | 20.0 (20.5) | 44 (33) | |
| ICU with ventilation (12.2%) | Recovery (34.5%) | 28.6 (18.3) | 43 (39) | 28 (21) |
| | Death (65.5%) | 15.5 (12.6) | 68 (31) | 63 (34) |

### *3.2. Model Structure*

The course of the COVID-19 pandemic in the 16 federal states and 400 districts of Germany from the beginning of the pandemic (25 February 2020, first verified SARS-CoV-2

infection in Germany leading to an outbreak with untraceable chains of infection) until the beginning of the third wave (1 April 2021) was analyzed using a comprehensive epidemiological compartment model. The model consists of 29 ordinary differential equations (ODEs) that describe the population transitioning through seven infection and disease-relevant stages. Figure 1 illustrates a simplified representation with submodels for infections, hospitalizations, and outcomes. Figure 2 shows a comprehensive overview of all model compartments and references to the ODEs listed in Appendix A. The NONMEM model files (infection-only and full model) can be found in the Supplementary Materials.

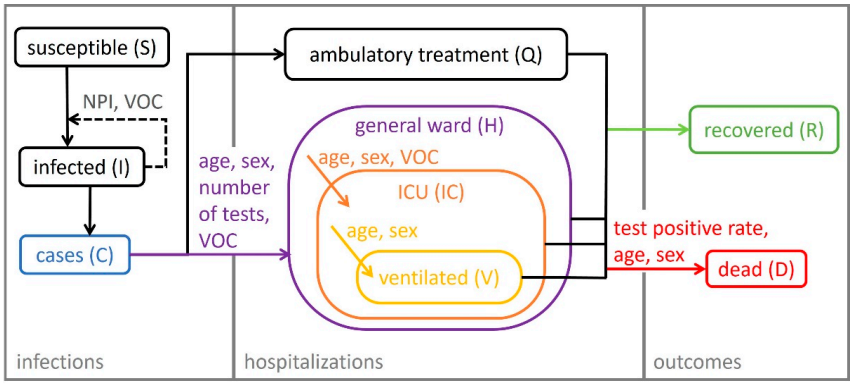


**Figure 1.** Schematic representation of the epidemiological compartment model. Solid arrows indicate the flow of individuals between compartments during the infection/disease process. Covariates influencing the flow rates are assigned to the respective arrows. Dashed arrows indicate the influence of a compartment value on the rates. NPI: non-pharmaceutical interventions, VOC: fraction of cases infected with the variant of concern B.1.1.7, number of tests: number of weekly performed PCR tests in Germany.

As in classical epidemiological SIR compartment models [35], the population is assigned to one of the three stages: susceptible (S), infected (I), and recovered (R). In the presented model, three new stages were implemented: quarantined patients in an ambulatory setting (Q), inpatients, and disease-related fatalities (D). Inpatients were divided into patients in a general ward (H), ICU patients (IC), and patients who need mechanical ventilation during any period of their ICU stay (V). Moreover, inpatients could recover or die at each of these stages. Age, sex, the fraction of patients infected with VOC B.1.1.7, the number of weekly PCR tests, and test positivity rate were identified as significant covariates influencing the rate and distribution of new inpatients as well as outcomes. Model parameters which were not informed by metrics derived from the clinical database but estimated as fixed effects can be found in Table A1 of Appendix B. The model described the number of hospitalizations (stratified by hospital ward and need for mechanical ventilation), recoveries, and COVID-19-related deaths for Germany and the 16 federal states very well. Figure 3 shows the time courses of all relevant observations and model predictions for Germany and three selected federal states, and Supplementary Figure S1 shows all federal states. Further details on the submodel structures are described in the following sections.

### *3.3. Infectiousness*

Cases were described by a stepwise estimation of the infectiousness depending on NPIs, estimated infectiousness changepoints, and the fraction of cases infected with VOC B.1.1.7. In total, 24 significant infectiousness changepoints could be observed or estimated over the 48 weeks of investigation, with a mean period of 15.5 days between changes (minimum 6 days, maximum 30 days), as depicted in Figure 4.

*Viruses* **2022**, *14*, 2114 

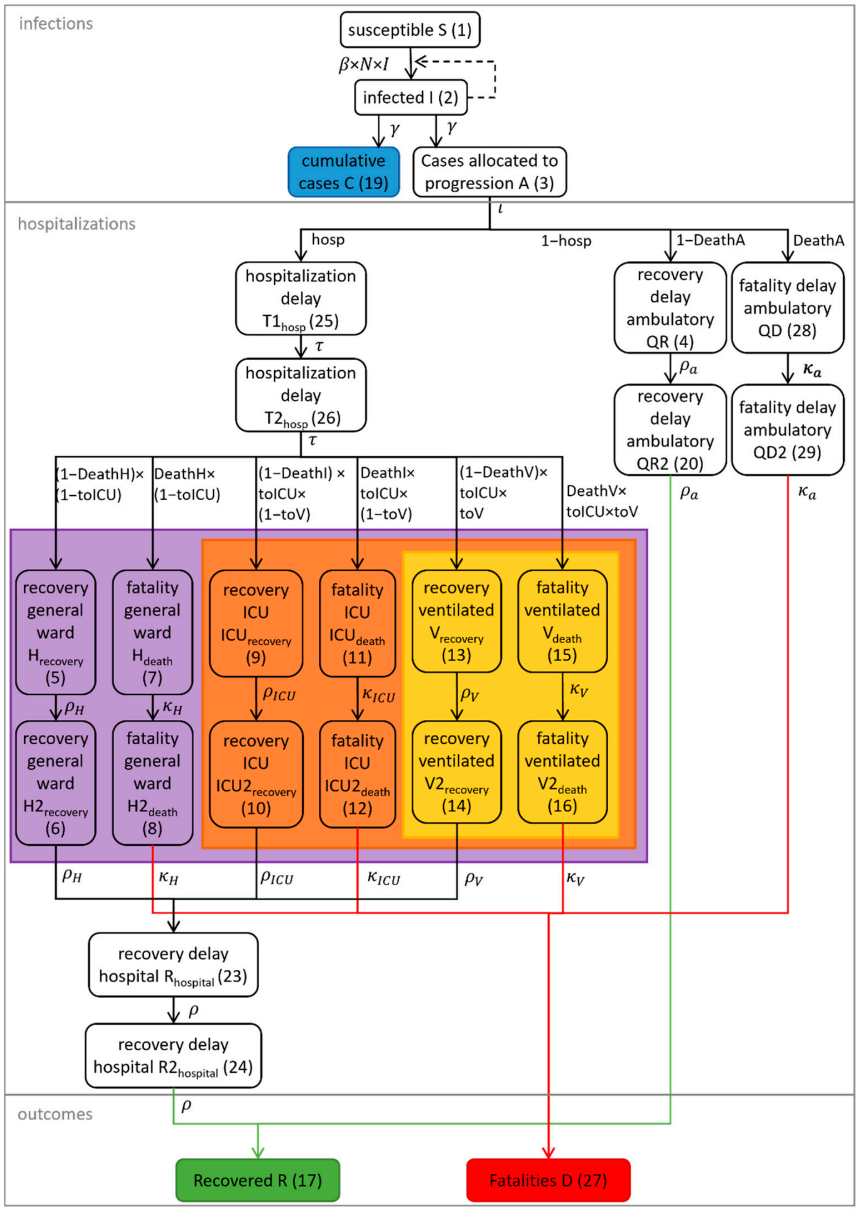


**Figure 2.** Detailed depiction of the compartmental model including flow rate constants. Numbers represent the compartment numbers used in the NONMEM model file. Not depicted are compartment numbers 18, 21, and 22, which were used for the computation of daily deaths, daily hospitalizations, and cumulative ICU patients. The violet, orange, and yellow areas represent the compartments used for the calculation of inpatients, ICU patients, and ventilated patients, respectively, according to Equations (A52)–(A54) (see Appendix A).

*Viruses* **2022**, *14*, 2114 

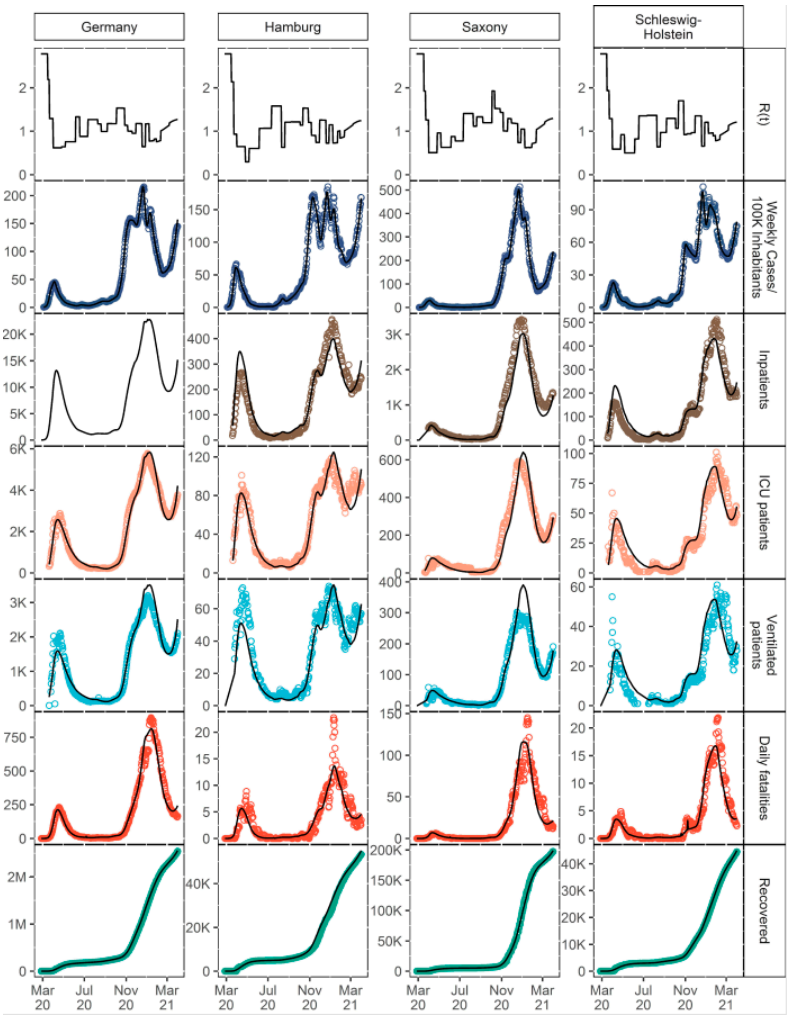


**Figure 3.** Descriptive performance plots for Germany and three selected federal states. Points: observations, lines: individual model predictions. Information about the total number of inpatients was not available for Germany in total.

For 15 out of 24 changepoints, variation in infectiousness could be attributed to changes in NPI policies (e.g., inception or lifting of mandates by the federal or state governments). Seven changepoints could be linked to other causes, such as local superspreading events during periods with low daily confirmed cases or raised awareness and voluntary contact reductions within the population at the beginning of the pandemic. For two changepoints (4 October 2020 and 30 November 2020), no exogenous cause for the significant increase in infectiousness could be identified. In our estimations, school closures at the beginning of the pandemic led to an average reduction of infectiousness of approximately 31%. Furthermore, curfew or contact-restraining orders that were reinforced on average 5 days after school closure led to a further reduction of infectiousness by 42%. With the resolution of the nationwide so-called "lockdown light" on 28 October 2020 (including the shutdown of restaurants, bars, and leisure and sports facilities, as well as limitations for retail stores and contact restrictions), the infectiousness was reduced on average by 28%.

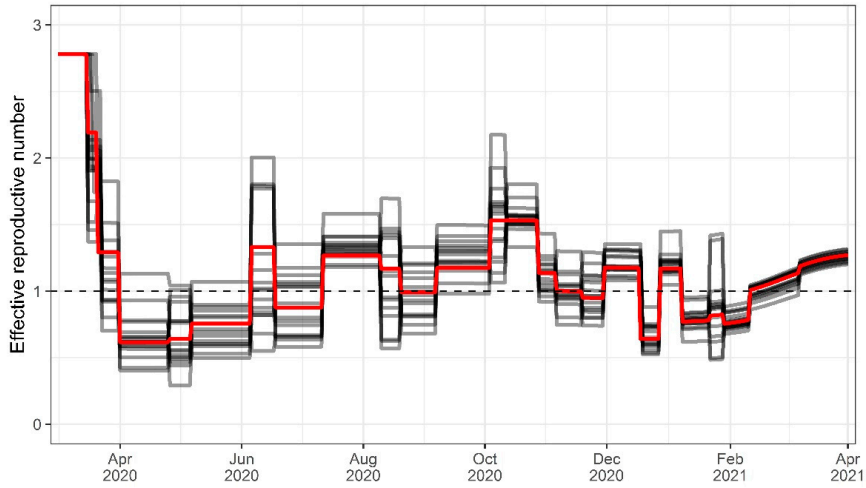


**Figure 4.** Changes in effective reproductive number over time for Germany (red line) and the federal states (grey lines).

The coefficient of variation (CV) of the infectiousness between the states was on average 17.7% (range 3.9–40.6%). When NPIs were reinforced by federal state governments, the average CV was 23.2% (6.9–40.6%). After the reinforcement of nationwide NPIs, the average inter-state variability was lower (11.2%, range 3.9–29%). All infectiousness changepoints, the resulting effective reproductive numbers (R(t)), and associated events, such as changes in NPI policies, are listed in Supplementary Table S3.

### *3.4. Hospitalization and Outcome of COVID-19 Patients in Germany*

In the presented model, infected individuals were allocated to two different paths: (i) a quarantine path for patients in home quarantine (Q) and (ii) a hospital path for inpatients (T). Analysis of our clinical database and modeling outcomes revealed that the hospitalization rate $hosp(t)$ (Appendix A Equation (A8)) was dependent on the age and sex of the infected individuals, the number of PCR tests ($NT$) performed weekly in Germany, and the fraction of infections with VOC B.1.1.7. Furthermore, a changepoint could be observed with a noticeable shift in the hospitalization rate. All effects are presented in detail in the following sections.

Inpatients were split into three groups depending on severity of illness: patients only treated in a general ward, patients in an ICU without ventilation, and patients being ventilated. Furthermore, all three groups were stratified per outcome (recovery or death). Hence, for inpatients, six groups of wards and outcomes were defined, with specific times until discharge for each group. All patients recovering enter recovery transit compartments (Appendix A Equations (A48) and (A49)) after their stay in the respective hospital ward before they are counted as recovered (R) to adjust recovery time to the RKI definition (14 days after discharge). In contrast to the recovered patients, inpatient fatalities (D) were counted without delay. The model works under the simplification that recovered patients are immune to reinfection with SARS-CoV-2 wild type and VOC B.1.1.7 [41].

### *3.5. Age and Sex*

Age and sex were significant covariates impacting the severity of disease and outcome ($p < 0.001$). We calculated the fractions of confirmed SARS-CoV-2 cases receiving inpatient treatment by age and sex based on the clinical database and the reported cases from RKI. The fractions of inpatients receiving treatment at the ICU and mechanical ventilation as well as fatality rates stratified by age and sex were calculated based on the clinical database. An

*Viruses* **2022**, *14*, 2114 

overview of the fractions is depicted in Figure 5 and listed in Supplementary Table S4. The risk of hospitalization and death was highest in elderly male patients (50.3% for patients > 80 years), and the risk of inpatients needing intensive care treatment increased with age and was highest for patients aged 60 to 80 (54.1% for male patients). For most age groups, female confirmed SARS-CoV-2 cases had a lower risk of hospitalization compared to male cases (24% to 41% risk ratio). However, for female cases age 15 to 34, a higher risk of hospitalization (females 2.38% vs. males 1.54%, 55% risk ratio) could be observed. Figure 6 depicts the demographic changes of the confirmed cases over time and the resulting changes in fractions of confirmed cases hospitalized, treated in an ICU, and ventilated, as well as death rates.


**Figure 5.** Fractions of confirmed cases hospitalized, treated in an ICU, and ventilated and death rates stratified by age and sex as extracted from the clinical database and data from RKI.

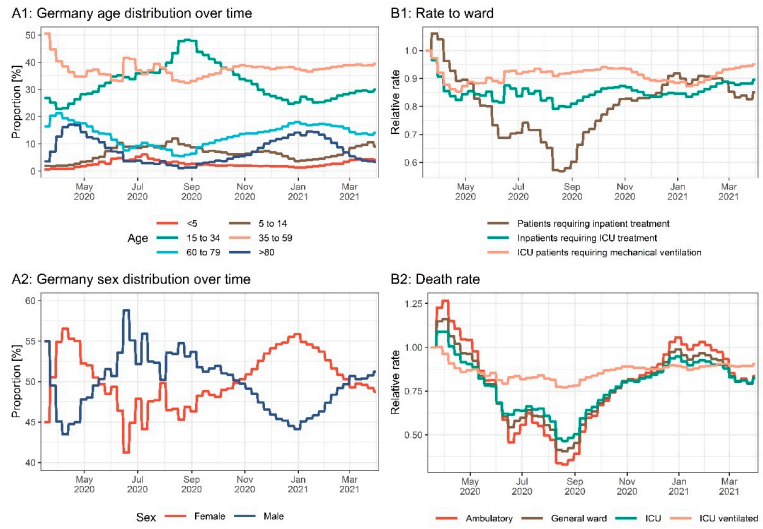


**Figure 6.** Age (**A1**) and sex (**A2**) distribution of confirmed cases over time. Relative changes in fractions of confirmed cases hospitalized, treated in an ICU, and ventilated (**B1**) as well as death rates (**B2**) resulting from changes in the age and sex distributions of the confirmed cases over time.

*Viruses* **2022**, *14*, 2114 

### *3.6. Variants of Concern*

In winter 2020/2021, VOC B.1.1.7. started to emerge in Germany. In our model, the fraction of infections with VOC B.1.1.7 ($VOC(t)$) was estimated using an exponential growth function (Equation (6)) with a growth rate k = 0.072 and an initial fraction of infections with VOC B.1.1.7 ($F_{init}t$) of 0.2% according to Volz et al. [42]. The initial time ($t_{init}$) was estimated to fit the model to the fractions reported by the RKI at 17 February 2021 for the preceding 6 weeks [43]:

$$\mathrm{VOC(t)} = 1/(1 + \frac{1 - \mathrm{F_{init}}}{\mathrm{F_{init}}} * \mathrm{e}^{-\mathrm{k} * (\mathrm{t} - \mathrm{t_{init}})}). \quad (6)$$

VOC B.1.1.7. was first detected on 24 December 2020 in Germany [44]. However, retrospective analysis showed that it had already emerged in November 2020 [25]. Our model estimated 0.02% of infections with VOC B.1.1.7 as of 3 December 2020.

Variant spreading and variant-associated infectiousness were fixed in our model to be 35% higher in comparison to wild type as reported by Graham et al. [7] (Figure 7). The stepwise change of infectiousness due to NPIs was estimated for the infectiousness of the wild type $R_{\alpha WT}$, with $R_\alpha(t) = R_{\alpha WT}(t)$ before the emergence of B.1.1.7 at $t_{init}$ with:

$$R_\alpha(t) = R_{\alpha WT}(t) * (1 + 0.35 * VOC(t)). \quad (7)$$

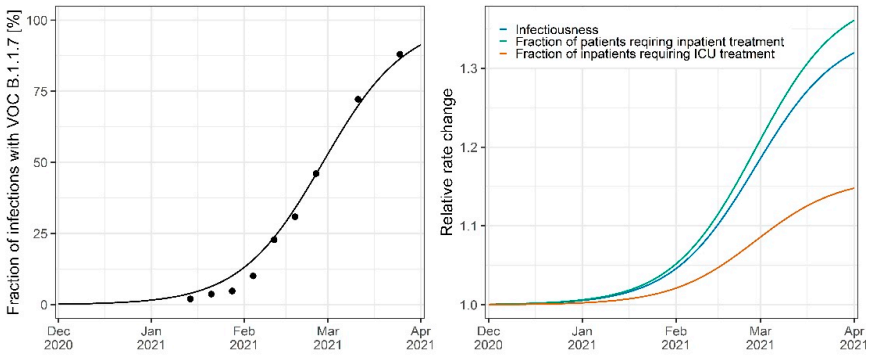


**Figure 7.** Fraction of infections with VOC B.1.1.7 in Germany (**left**) and impact of VOC B.1.1.7 on the infectiousness, fraction of patients requiring inpatient treatment, and fraction of inpatients requiring ICU treatment (**right**). Points indicate observed fraction of infections in Germany. Lines indicate the model-predicted fraction or rate changes.

The impact of VOC B.1.1.7 on disease severity was estimated by fitting VOC-dependent changes in various model rates to the observed inpatient and fatality data from the federal states. As depicted in Figure 7, the fraction of patients requiring inpatient treatment increased by 39.5% (RSE 14.1%, $p < 0.001$), and the fraction of inpatients requiring intensive care treatment increased by 16.2% (RSE 33.1%, $p < 0.001$) for patients infected with VOC B.1.1.7 in comparison to infections with the wild type. An additional change in inpatient death rates due to VOC B.1.1.7 was not significant in our analysis.

### *3.7. Testing Strategy*

The number of weekly performed PCR tests had a significant impact ($p < 0.001$) on the fraction of hospitalized confirmed cases (more performed tests were positively correlated with fewer hospitalizations, see Figure 8A). Moreover, the fraction of positive tests had a significant effect ($p < 0.001$) on the fatality rate of outpatients and patients in a general ward (higher positive ratios were associated with a higher fatality rate, see Figure 8B).

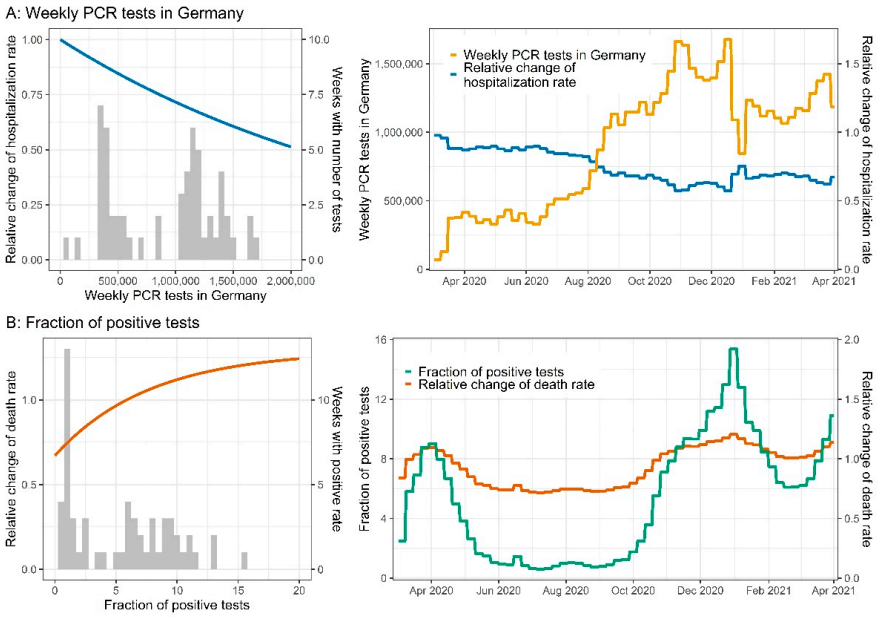


**Figure 8.** (**A**) Weekly PCR tests in Germany. Blue lines indicate the change in the hospitalization rate vs. the number of tests performed (**left plot**) and time (**right plot**). The histogram represents the number of weeks with the respective number of weekly tests. The yellow line represents the weekly tests vs. time. (**B**) Fraction of positive tests. Orange lines indicate the change in the death rate vs. the number of tests (**left plot**) and time (**right plot**). The histogram represents the number of weeks with the respective fraction of positive tests. The green line represents the fraction of positive tests vs. time.

### *3.8. Hospitalization Rates and Time Effects*

Investigation of inpatient data and model changepoint analysis revealed shifts in disease stage transitions and outcome dynamics that could not solely be explained by the already included covariates. The time until discharge of mechanically ventilated patients decreased noticeably during the summer of 2020, and a changepoint was estimated by the model on 10 June 2020, with a significant reduction of the time until discharge by 65% (from 47.3 days to 16.7 days, $p < 0.001$).

Furthermore, comparing data from our clinical database and newly confirmed cases over time, a drop in the fraction of patients requiring inpatient treatment could be observed in September 2020, and the model estimated a significant decrease in the fraction requiring inpatient treatment of 49.6% on 9 September 2020 (RSE 1.6%, $p < 0.001$). Simultaneously, the rate of inpatients requiring ICU treatment increased ($p < 0.001$). This increase was significantly higher in seven (Bavaria, Berlin, Bremen, Hamburg, Hesse, North Rhine-Westphalia, and Saarland) of the 16 federal states (29.0% [RSE 4.2%] vs. 9.4% [RSE 10.2%]). However, the overall fraction of confirmed cases requiring ICU treatment still declined by 33.7–43.8%. The rate of modeled outpatient deaths increased to 23% for male patients older than 79 years during the second wave around 15 December 2020 and decreased again to 0% around 11 March 2021 ($p < 0.001$).

Figure 9 depicts the model flow rates that result from the incorporation of all previously described covariates and time effects.

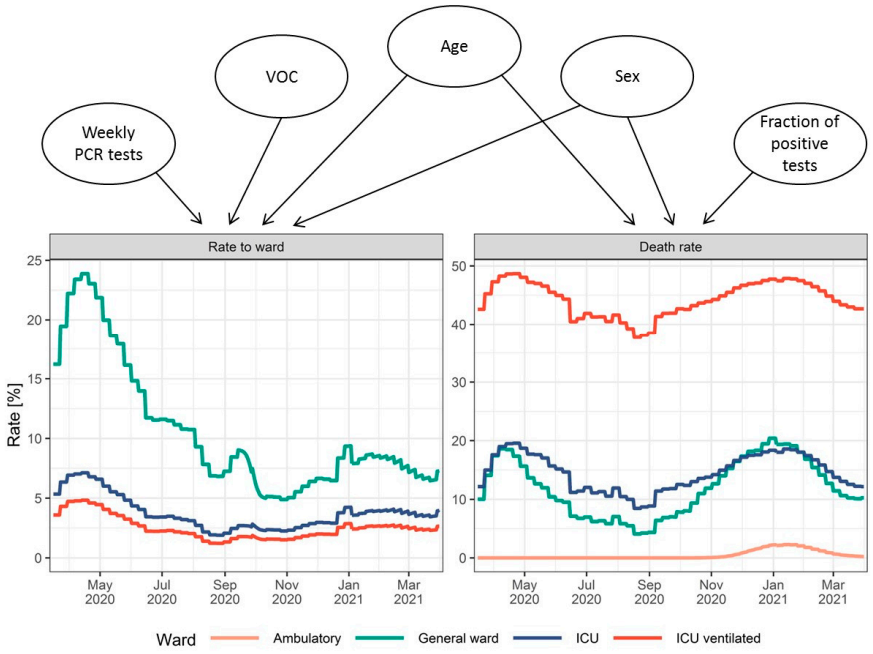


**Figure 9.** Covariate impacts on the modeled fraction of cases requiring treatment in different wards (**left**) and fatality rates differentiated by ward (**right**) resulting from covariate changes over time in Germany.

### *3.9. German Districts*

The model parameterized for Germany and the 16 federal states was subsequently applied to the pandemic in the 400 German districts. The number of weekly cases in each district was described very well using the estimated federal state model changepoints for infectiousness with a district-specific random-effect estimation of the infectiousness (see Supplementary Figure S2). Moreover, the number of ICU patients was calculated based on the estimated number of local cases and the respective age and sex distributions. Figure 10 and Supplementary Figure S2 show that predictions of ICU patients and ventilated ICU patients are in reasonable agreement with the observed number of patients for many, but not all districts. To investigate which districts were not described well, we calculated the mean residuals of ICU predictions per 100,000 inhabitants for each district. Here, for 101 districts (25.3%) predictions were in good agreement with the observed data (residuals between $-0.5$ and 0.5), whereas for 113 districts (28.3%), larger underpredictions (residuals $< -0.5$) were seen, and for 182 districts (45.5%), sizable overpredictions (residuals $> 0.5$) could be observed. For four rural districts (1%), no information regarding the number of ICU inpatients was available. Discrepancies between observed and predicted ICU inpatient numbers were consistent in both total ICU occupancy and ICU patients receiving mechanical ventilation, with a Pearson correlation coefficient of the residuals (ICU inpatients and mechanically ventilated inpatients) of $R^2 = 0.81$ ($p < 0.001$). It could be observed that the number of available ICU beds per inhabitant was significantly higher in urban districts (German "Stadtkreise", SK) compared to rural districts (German "Landkreise", LK; median 5.44 vs. 1.87 beds/1,000,000 inhabitants for SK and LK, respectively, $p < 0.001$). Further investigations revealed a correlation between the mean discrepancies and the number of ICU beds available per inhabitant ($R^2 = 0.62$, $p < 0.001$). This relationship is also demonstrated via a closer investigation of an exemplary region in the Midwest of Germany (Figure 10C,D). The urban district Münster, which maintains a large academic hospital, hosts more ICU patients than predicted based on the cases of this district, whereas the surrounding rural districts host fewer patients than expected, especially at peak times of the pandemic.

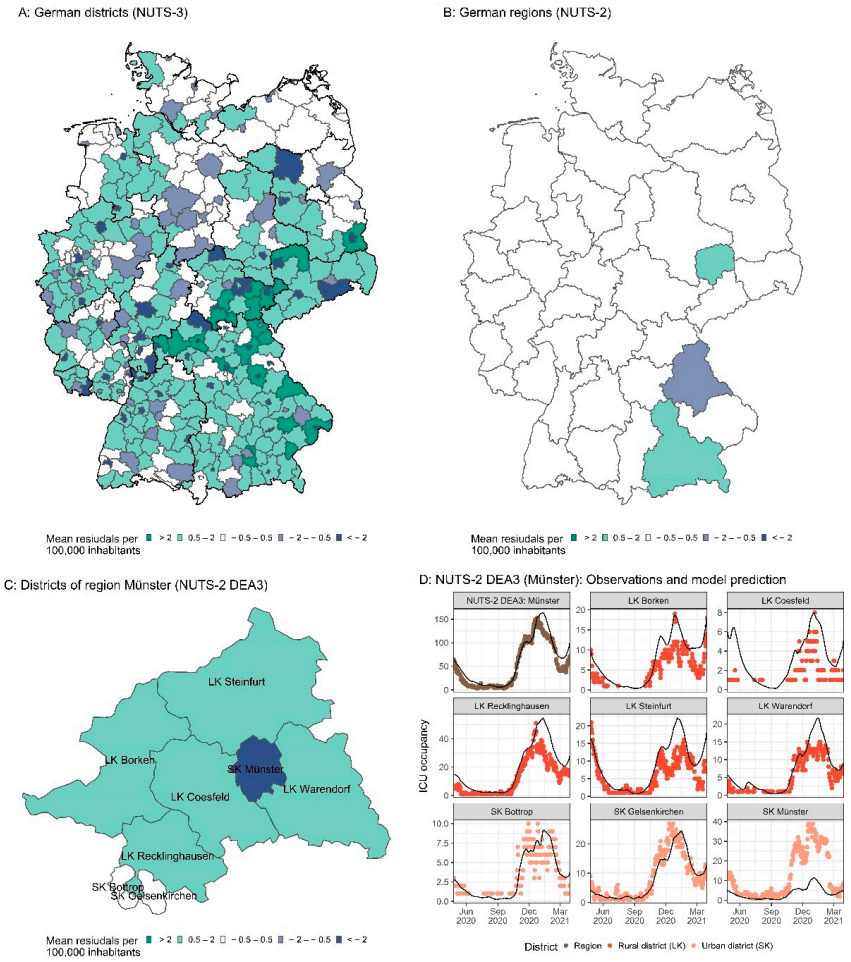


**Figure 10.** ICU prediction on the district level, (**A**): Mean residuals of ICU predictions per 100,000 inhabitants per district (NUTS-3). (**B**): Mean residuals of ICU predictions per 100,000 inhabitants per government region (NUTS-2). (**C**): Mean residuals of ICU predictions in counties per 100,000 inhabitants in exemplary government region DEA3. (**D**): Observations and model predictions of ICU occupancy for the full exemplary government region DEA3 and its districts. Points indicate observations, and lines indicate model predictions. LK refers to "Landkreis" (rural district). SK refers to "Stadtkreis" (urban district).

We also investigated the predictive performance at the regional level (NUTS-2). NUTS (Nomenclature of Territorial Units for Statistics) is a European standard for the subdivision of countries into units of approximately the same population size while favoring administrative units [45]. NUTS-2 aggregates the districts (NUTS-3) into regions with 0.8 to 3 million inhabitants, most of which are smaller than the federal states (NUTS-1). In Germany, 38 NUTS-2 regions exist which correspond to governmental regions known as "Regierungsbezirke" in Germany. Predictions on the NUTS-2 level showed that occupied ICU beds were well predicted (Figure 10D), and over- or underprediction could be eliminated for 92% (35 of 38) of the regions (Figure 10B).

**4. Discussion**

In the presented work we developed a comprehensive mathematical model that describes the number of SARS-CoV-2 infections, inpatients, ICU patients with and without mechanical ventilation, recoveries, and fatalities for the first two waves of the SARS-CoV-2 pandemic in Germany, its 16 federal states, and its 400 districts. Here, the description of hospitalized patients and fatalities was based solely on the number of infections and on the age and sex of the patients, variant of concern B.1.1.7, and the testing strategy (number of tests performed weekly, test positive rate) as covariates.

To describe the number of infections, the change in infectiousness was estimated at discrete changepoints considering inter-state and inter-district variability over time. The use of changepoints allowed us to accurately describe the number of infections without a daily infectiousness reevaluation and to only incorporate and analyze significant epidemiological changes in the infection dynamics. Still, the average estimated infectiousness was similar to the infectiousness estimated using continuous (daily) variations [46].

Over the 48 weeks of investigation, 24 significant changepoints of infectiousness could be observed or estimated, with a mean period of 15.5 days between consecutive changepoints. During the winter months (October until February), the period between changepoints was smaller (mean 18.3 days, range 7–30 days and mean 11.8 days, range 6.2–18.4 days in summer and winter, respectively), which can be attributed to the faster spread of SARS-CoV-2 due to seasonality and the consequential high frequency of changes in NPIs. When the German government initiated nationwide measures to control the pandemic in October 2020 [47], the inter-state variability in R(t) decreased in comparison to the beginning of the pandemic, when federal state governments enacted individual measures that were only effective locally (23.2% CV and 11.2% CV before and after October 2020, respectively).

A total of 21 of the 24 changepoints of infectiousness could be attributed to changes in NPI policies. The closing of schools in the spring of 2020, for example, led to an average decrease in infectiousness of 31%, which is in line with several other studies where a decrease between 0% and 60% was documented [48]. Contact restrictions at the beginning of the pandemic reduced infectiousness by 42%. However, because other NPIs were stacked and nested during these times, the results regarding the extent of these effects are likely biased. The reopening and closure of schools during the summer and fall of 2020 were subject to different local regulations and were implemented at different points in time, which rendered evaluation of the effects of school reopening and closure on $R(t)$ impossible for the summer and fall of 2020.

The numbers of inpatients, ICU patients, ventilated patients, recoveries, and fatalities were well described based on the predicted number of infections and the age and sex of the infected patients, VOC B.1.1.7, the number of weekly performed PCR tests, and the test positivity rate. Here, the analysis of metrics derived from the clinical database MetaKIS allowed the analysis of the typical hospital stay of inpatients with COVID-19, including the time until discharge and time spent in the ICU and with mechanical ventilation. With a mean length of hospital and ICU stay of 12.7 and 9.3 days, respectively, our analysis of individual inpatient data was in line with observations from Berger et al. [49], which were obtained by dividing the respective current number of patients by the respective cumulative number of patients (length of hospital and ICU stay of 14.3 and 12.8 days, respectively).

Moreover, our analysis is in line with other studies showing that the risk of hospitalization and death increases exponentially with increasing age [9–11,14,15,50]. The risk of ICU treatment among hospitalized patients was highest in the age group 60–80, which is in agreement with results from Switzerland and the United States, where patients aged 55–74 had the highest risk of ICU treatment [15,50]. The higher risk of more severe outcomes in older patients (such as the need for inpatient treatment, need for ICU treatment, and fatality) might be driven by two main factors: (i) older patients often have more comorbidities such as obesity, hypertension, diabetes, cardiovascular diseases, and chronic respiratory diseases which impose a higher risk of severe disease [51]; and (ii) the ageing immune

system results in hyperinflammatory, pathological innate responses as well as ineffective T cell response and diminished antibody maturation [50,51]. Differences in the immune response might also explain the higher risk of severe disease in male patients [52]. Herein, the highest risk was observed among elderly male patients, which is in line with previous findings [50].

The length of hospital stay and duration of ICU treatment or mechanical ventilation were also explored and stratified by the age and sex of the patients. The mean length of stay was similar for females and males (12.3 and 13.1 days, respectively), which is in line with findings from the United States by Ohsfeldt et al. [53] of 8.5 and 9.6 days for females and males, respectively. The difference between female and male patients was even smaller when analyzed by ward, as more male patients received ICU treatment, which is associated with a longer stay. For patients staying in a general ward only, both male and female patients had an average length of stay of 11.2 days; for ICU patients, the average length of stay was 19.6 days for females and 19.7 days for males.

Older patients stayed in the hospital for a longer period (e.g., 7.4 days and 13.1 days for patients < 35 and $\geq$35 years, respectively). However, this difference was smaller when considering the higher fraction of older patients requiring ICU treatment: Patients not requiring ICU treatment stayed on average 6.7 and 11.5 days, for ages < 35 and $\geq$35 years, respectively. ICU patients had an average stay of 16.5 and 19.8 days for ages <35 and $\geq$35 years, respectively. Furthermore, patients younger than 35 years old only represented 6.5% of all inpatients. Hence, the impact of correcting the duration of stay for the age of the patients was very small in comparison to the added level of complexity to the model.

VOC B.1.1.7 has been shown to have increased ACE2 binding and cell infectivity due to a mutation on the spike protein which results in an advantage in transmissibility and an increase in disease severity compared to the wild type. By assessment of the proportion of B.1.1.7 cases and the number of reinfections, Graham et al. estimated the increase in the effective reproduction number to be 35% based on data from the United Kingdom [7], which we used to describe the number of cases in our model, resulting in a good correlation between the increase of cases and the appearance of VOC B.1.1.7.

At the time of model development, the impact of VOC B.1.1.7 on the severity of disease was not clear. A study from Denmark reported a relative risk of hospital admission of 1.42 [54], and a study from the United Kingdom reported a mortality hazard ratio of 1.64 in comparison to the wild type [55]. Both studies adjusted for confounding patient characteristics such as age and sex. Using our multivariate approach, we differentiated between the increase in the fraction of patients hospitalized (39.5%) and the fraction treated in an ICU (16.2%) in Germany while also considering other model covariates, such as age, sex, and testing strategy. The increase in hospitalization was similar to the increase found in Denmark [54]. In our model, no significant rise in death rates in the respective hospital wards could be observed. However, due to the increase in the fractions hospitalized and treated in an ICU, which are both linked to higher fatality rates, the apparent case fatality rate increased.

A comprehensive testing strategy was anticipated to result in a lower dark figure of cases and consequently a lower fraction of severe cases, as the fraction of detected asymptomatic infections would increase accordingly. This hypothesis was confirmed by our model, as the number of weekly tests was associated with a decrease in the fraction of hospitalized patients, and the test positivity rate was correlated with an increase in death rates. Here, both covariates improved the model performance significantly. The impact of the testing strategy has been previously discussed by Modi et al., who estimated infection rates based on the number of fatalities in Italy [56]. Liang et al. observed a similar link between mortality and the number of tests per 100 inhabitants in a dataset comprising 169 countries [57].

The combination of information from the clinical dataset and mathematical modeling allowed us to identify and quantify changes in the dynamics of the pandemic, which could not solely be explained by changes in the age and sex distribution of the infected

population over time or other covariates. A significant decrease in the time until discharge for recovering of ventilated patients of 64.8% could be discovered in the summer of 2020. The date of change (8 August 2020) corresponded well to the time at which dexamethasone treatment for severe COVID-19 cases was first discussed and clinical guidelines were revised [58]. The model-estimated decrease of the time until discharge is in line with the work of Tomazini et al., who observed in 299 patients with COVID-19–associated acute respiratory distress syndrome that treatment with dexamethasone increased the number of ventilator-free days in recovered patients by 65.0% without decreasing mortality [59].

During the second wave of the pandemic in September 2020, the fraction of confirmed cases requiring inpatient and ICU treatment decreased. This trend was observed in the clinical database and confirmed by our model, with an estimated decrease in the hospitalization rate of 49.6% and of the patients requiring ICU treatment of 41.9% on 28 September 2020. While the underlying causes remain unknown, these changes might have been driven by an increased awareness of the disease and higher acceptance of comprehensive testing. Subsequently, the number of detected asymptomatic cases might have increased. For seven states, a significantly higher fraction of inpatients treated in an ICU could be observed (29% vs. 9%, $p < 0.01$). However, no explicit cause for the difference between these states was found.

Daily fatalities during the second wave could not be explained by the model's covariates, nor could an increase in death rates be observed for hospitalized patients recorded in the clinical database. To describe excess fatalities, we assumed that this increase might have occurred for the death rate of outpatients, for which no explicit data were available in Germany. This assumption is in line with press reports that covered the high fatality rates in nursing homes and press critiques regarding nursing home residents not receiving adequate inpatient treatment during the time of unexplainable excess deaths [60].

In contrast to previously published epidemiological modeling approaches [14,15,61], the presented model was developed using data from the federal states (NUTS-1 level) and was successfully applied to describe the number of ICU patients in the whole country (NUTS-0 level), regions (NUTS-2 level), and districts (NUTS-3 level). The prediction of the district ICU and ventilated patient numbers underlines the importance of the covariate effects (age and sex) for the cases. However, for some districts, discrepancies between observations and model predictions could be observed. This was more pronounced for districts neighboring each other and correlated with the number of available ICU beds per inhabitant in the respective districts. Districts with overpredicted ICU occupancies were mostly rural districts with smaller or less specialized hospitals. Districts reporting higher ICU occupancies than predicted were often urban districts with larger hospitals (some of which are university hospitals) and higher ICU capacities. Hence, it seems plausible that small hospitals in districts with fewer ICU beds available tended to transfer patients to neighboring districts with larger hospitals and higher ICU capacities. Despite the observed discrepancies for some districts (NUTS-3 level), the model provided valuable information for the management of regional ICU capacities (NUTS-2 level).

Epidemiological ODE models describing the SARS-CoV-2 pandemic in other countries that were published previously used only stratification of infected patients by age [14,15,61] and ignored stratification by sex. However, some models used a more comprehensive stratification for age groups [15,61]. Here, our analysis was limited to the seven age groups for which the RKI provided the number of daily cases. Further limitations of our analysis originate from restricted access to information concerning the number of German COVID-19 inpatients, the background of fatalities, and further demographic information of all patients. For VOC B.1.1.7, only data for the nationwide average spread were available. Additionally, anonymization of the clinical database patient data prevented the tracking of transferred patients. Hence, the exclusion of patients with unknown outcomes from the analysis might have introduced bias regarding the estimation of inpatient outcome rates and duration of stay.

*Viruses* **2022**, *14*, 2114 

## 5. Conclusions

The presented mathematical model is an accurate tool for describing and analyzing the COVID-19 pandemic in Germany. It provides valuable insights into the expected number of inpatients and allows the simulation of different scenarios not only considering different levels of infectiousness but also the investigated covariates. Thereby, the model displayed the high effectiveness of NPIs to reduce the number of cases. Furthermore, the model could successfully be applied to describe the number of cases and ICU patients at the regional level (NUTS-2), highlighting the sufficiency of the covariates and the generalizable character of the model. Hence, the model might be applicable to other countries with similar health care systems. Furthermore, through the modeling process and when analyzing the patient data from the clinical database, changes in the course of the pandemic due to VOC B.1.1.7 and improved treatment modalities could be implemented successfully, demonstrating the flexibility of the model in adapting to further dynamic changes. The adaption to other VOCs and vaccinations has been ongoing over the past year, and the resulting model is available as a publicly accessible online simulation tool at https://covid-simulator.com/ (accessed on 1 September 2022).

**Supplementary Materials:** The following supporting information can be downloaded at: https://www.mdpi.com/article/10.3390/v14102114/s1, Figure S1: Descriptive performance plots for Germany and all federal states; Figure S2: Descriptive performance plots for German counties (NUTS-3); Model file S1: NONMEM model file of the infectiousness model; Model file S2: NONMEM model file of the full model; Table S1: Data Sources; Table S2: Summary of MetaKIS data. Age is summarized as median and interquartile range; Table S3: Changes in infectiousness according to NPIs and model-estimated changepoints; Table S4: Fractions of confirmed cases hospitalized, treated in an ICU, and ventilated and death rates as functions of age and sex as extracted from the MetaKIS database.

**Author Contributions:** Conceptualization, C.D., S.S., M.B., F.M., T.V., S.K., J.R., D.S. and T.L.; data curation, C.D., K.M.G., K.O., I.S., Q.W., M.B. and T.L.; formal analysis, C.D., K.M.G., K.O., J.R., D.S. and T.L.; methodology, C.D., D.S. and T.L.; project administration, T.L.; resources, T.L.; supervision, T.L.; visualization, C.D.; writing—original draft, C.D., D.S. and T.L.; writing—review and editing, C.D., S.S., M.B., F.M., T.V., S.K., J.R., D.S. and T.L. All authors have read and agreed to the published version of the manuscript.

**Funding:** No funding was received for the development of this project. S.S. received funding from the Saarland Staatskanzlei and the Dr. Rolf M. Schwiete Stiftung. F.M. is supported by Deutsche Gesellschaft für Kardiologie (DGK), Deutsche Forschungsgemeinschaft (SFB TRR219), and Deutsche Herzstiftung. He has received scientific support from Medronic and ReCor Medical and speaker honoraria from Astra-Zeneca, Bayer, Boehringer Ingelheim, Inari, Medtronic, Merck, and ReCor Medical.

**Institutional Review Board Statement:** The study was conducted in accordance with the Declaration of Helsinki and approved by the local ethics committee of the medical association of the Saarland (Ärztekammer des Saarlandes, Bu 78/20).

**Informed Consent Statement:** Not applicable.

**Data Availability Statement:** Data can be made available upon request.

**Conflicts of Interest:** The authors declare no conflict of interest.

## Appendix A

The differential equations depicting the transfer of COVID-19 patients through different disease stages are shown below.

$$\frac{dS}{dt} = -\beta(t) * \frac{S(t)}{N} * I(t) \tag{A1}$$

$$\frac{dI}{dt} = \beta(t) * \frac{S(t)}{N} * I(t) - \gamma * I(t) \tag{A2}$$

$$\frac{dC}{dt} = y * I(t) \tag{A3}$$

with N being the number of inhabitants. The transmission rate $\gamma$ from the infectious stage (I) to confirmed cases (C) was fixed to an infectious period of 7 days, with $\gamma = 1/7$ based on 6 days of mean incubation time plus 1 day of lag between showing symptoms and registering a positive test result [36]. $B(t)$ is defined as the transmission rate from the susceptible (S) to the infectious stage by contact with an infected subject and is related to $\gamma$ and the infectiousness ($R_\alpha$) as depicted in Equation (A4):

$$\beta(t) = R_\alpha(t) * \gamma \tag{A4}$$

The effective reproduction number $R(t)$ was defined as

$$R(t) = R_\alpha(t) * \frac{S(t)}{N} \tag{A5}$$

The transmission rate $\iota$ from the allocator compartment (A) to the quarantine or hospital pathway was fixed to a high value (100 $day^{-1}$) to model a short time lag.

$$\frac{dA}{dt} = \gamma * I(t) - \iota * A(t) \tag{A6}$$

The age- and sex-specific fraction of hospitalized COVID-19 patients ($fh(a,s)$) was derived from the number of hospitalized COVID-19 patients recorded in the clinical database and the number of cases according to RKI data as shown in Supplementary Table S4. The fraction hospitalized was corrected by an estimated fixed effect factor (Hosp), as the clinical database only included information on approximately 10% of German COVID-19 inpatients. The age-, sex-, and time-dependent hospitalization rate h(t) was calculated as the sum of each age- and sex-specific rate ($fh(a,s)$) multiplied by the fraction of newly infected patients assigned to the respective age group at each time ($p(a,s,t)$):

$$h(t) = \sum_{s=\text{Male}}^{s=\text{Female}} \sum_{a=\text{Age }0-5}^{a=\text{Age }80+} fh(a,s) * p(a,s,t) \tag{A7}$$

For the influence of the numbers of weekly performed PCR tests in Germany, an exponential effect model with factor $Fntest_{Hosp}$, normalized for the average number of 1,000,000 tests per week, described the data best. The effect ($fH_{VOC}$) of the fraction of VOC B.1.1.7 infections on the hospitalization rate was estimated using a linear effect model. Furthermore, a decrease in the hospitalization rate was observed both in the clinical database as well as in the number of occupied hospital beds. This decrease was implemented using a time-dependent hill equation, with fKH as the relative decrease in hospitalization rate and CPHosp as the timepoint at which the half-maximum change occurred. Hence, the final hospitalization rate $hosp(t)$ considering all covariates can be depicted as:

$$hosp(t) = h(t) * Ch(t) \tag{A8}$$

$$Ch(t) = e^{-Fntest_{Hosp} * \frac{NT(t)}{1{,}000{,}000}} * (1 + VOC(t) * fH_{VOC}) * \left(1 - \frac{fKH * t^{hill}}{CPHosp^{hill} + t^{hill}}\right) \tag{A9}$$

The average delay between a positive test result and the deterioration of COVID-19 patients leading to hospitalization was implemented via two transit compartments ($T1_{hosp}$, $T2_{hosp}$) and the transit rate $\tau$.

$$\frac{dT1_{hosp}}{dt} = hosp(t) * \iota * A(t) - \tau * T1_{hosp}(t) \tag{A10}$$

$$\frac{dT2_{hosp}}{dt} = \tau * T1_{hosp}(t) - \tau * T2_{hosp}(t) \tag{A11}$$

Quarantined individuals in an ambulatory setting ($QR$) were counted as recovered patients after 14 days, per the RKI definition of recovered cases; thus, the transit rate through the recovery compartments was defined as $\rho_a$ = 2/14 day$^{-1}$. The fraction of death among the outpatients (fa(t)) was estimated as dependent on age and sex (similar to calculations of the hospitalization rate, with $\mathrm{fda}(a, s)$ as age- and sex-specific death rate) and multiplied by the fraction of outpatients of each age group:

$$\mathrm{fa}(t) = \sum_{s=\mathrm{Male}}^{s=\mathrm{Female}} \sum_{a=\mathrm{Age\ 0-5}}^{a=\mathrm{Age\ 80+}} \mathrm{fda}(a,s) \ * \ (1 - \mathrm{fh}(a,s,t) * \mathrm{Ch}(t)) * \mathrm{p}(a,s,t) \quad \text{(A12)}$$

Due to the lack of information regarding the course of COVID-19 in outpatients, it was assumed to be similar to the course of inpatients in a general ward. Hence, the average time to death for outpatients ($TD_{H,D}$) was set to the average time to death observed in inpatients in a general ward; the transit rate $\kappa_a \kappa_a = 2/TD_{H,D}$ for outpatients with outcome death was calculated as $\kappa_a = 2/TD_{H,D}$. Due to the lack of data on outpatient deaths in Germany, this death rate was estimated as a fixed effect.

Over time, several changes in death rates could be observed. Data from the clinical database showed a clear correlation between the death rate in general wards and the number of new infections as well as the positivity rate of PCR tests for SARS-CoV-2 (PR). Hence, both parameters were tested as covariates using different empirical effect models. The influence of PR on the death rate of general ward patients as well as outpatients improved the model performance significantly and was implemented using an exponential function with the estimated fixed effects $PQ_{max}$, $PQ_{min}$, and $PQ_{rate}$:

$$\mathrm{PQ_{Death}}(t) = \ \mathrm{PQ_{max}} \ * \ \left(1 - \mathrm{PQ_{min}} * \mathrm{e}^{-\mathrm{PR}(t) \ * \ \mathrm{PQ_{rate}}}\right) \quad \text{(A13)}$$

Initially, the model included only inpatient fatalities. All ambulatory patients recovered. However, at the beginning of the year 2021, we noticed an underestimation of COVID-19-related deaths by the model. At that time, reports about COVID-19-related deaths in German nursing homes accumulated [60]. Therefore, different rate changes in the death rate in an ambulatory setting were tested during this period. A model with an increase at the beginning of November 2020 followed by a decrease in February 2021 described the data best. These changes were implemented using empirical time-dependent hill functions with fixed effects regarding the extent ($D_{OUT}$), the slope ($hill_D$), and the timepoints ($CP_{D1}$, $CP_{D2}$) of the rate change:

$$\mathrm{DeathA}(t) = \ \mathrm{fa}(t) \ * \ \frac{\mathrm{D_{OUT}} * t^{\mathrm{hill_D}}}{{\mathrm{CP}_{D1}}^{\mathrm{hill_D}} + t^{\mathrm{hill_D}}} \ * \ \left(1 - \frac{t^{\mathrm{hill_D}}}{{\mathrm{CP}_{D2}}^{\mathrm{hill_D}} + t^{\mathrm{hill_D}}}\right) * \mathrm{PQ_{Death}}(t) \quad \text{(A14)}$$

Equations (A15)–(A18) describe the transit of patients in an ambulatory setting until they count as recovered (Equations (A15) and (A16)) or dead (Equations (A17) and (A18)).

$$\frac{\mathrm{dQ_R}}{\mathrm{dt}} = (1 - \mathrm{DeathA}(t)) \ * \ (1 - \mathrm{hosp}(t)) * \iota \ * \ \mathrm{A}(t) - \rho_a * \mathrm{Q_R}(t) \quad \text{(A15)}$$

$$\frac{\mathrm{dQ_{R2}}}{\mathrm{dt}} = \rho_a * \mathrm{Q_R}(t) - \rho_a * \mathrm{Q_{R2}}(t) \quad \text{(A16)}$$

$$\frac{\mathrm{dQ}_D}{\mathrm{dt}} = \mathrm{DeathA}(t) \ * \ (1 - \mathrm{hosp}(t)) * \iota \ * \ \mathrm{A}(t) - \kappa_a * \mathrm{Q}_D(t) \quad \text{(A17)}$$

$$\frac{\mathrm{dQ}_{D2}}{\mathrm{dt}} = \kappa_a * \mathrm{Q}_D(t) - \kappa_a * \mathrm{Q}_{D2}(t) \quad \text{(A18)}$$

Transit rates for each ward were calculated by dividing the number of transit compartments by the time until discharge, with $\kappa$ depicting the rates for dying patients, $\rho$ for

recovering patients, and suffixes H, ICU, and V for patients in a general ward, in an ICU, and receiving mechanical ventilation, respectively.

$$\kappa_H = \frac{2}{TD_{H,D}} \tag{A19}$$

$$\rho_H = \frac{2}{TD_{H,R}} \tag{A20}$$

$$\kappa_{ICU} = \frac{2}{TD_{I,D}} \tag{A21}$$

$$\rho_{ICU} = \frac{2}{TD_{I,R}} \tag{A22}$$

$$\kappa_V = \frac{2}{TD_{V,D}} \tag{A23}$$

$$\rho_V(t) = \frac{2}{TD_{V,R}(t)} \tag{A24}$$

Observational data from the clinical database showed a change in the time until discharge of recovering ventilated patients. This change was implemented into the model using a hill equation with estimated fixed effects $f_{Vent1}$, $f_{Vent2}$, $CP_{Vent}$, and hill:

$$TD_{V,R}(t) = TD_{V,R,base} * f_{Vent1} * \left(1 + \frac{f_{Vent2} * t^{hill}}{CP_{Vent}{}^{hill} + t^{hill}}\right) \tag{A25}$$

To describe the number of patients requiring treatment in an ICU, the rate had to be adapted with estimated fixed effects toICU1 and toICU2 at the timepoint $CP_{Hosp}$ at which the change in the hospitalization rate occurred. Furthermore, including an effect of $VOC(t)$ improved the description of occupied ICU beds significantly. Therefore, the fraction of patients requiring ICU treatment was calculated from the age- and sex-specific fraction $I(t)$ and the covariate effects $Ci(t)$:

$$toICU(t) = I(t) * Ci(t) \tag{A26}$$

$$Ci(t) = toICU1 * \left(1 + \frac{toICU2 * t^{hill}}{CP_{Hosp}{}^{hill} + t^{hill}}\right) * (1 + VOC(t) * fICU_{VOC}) \tag{A27}$$

$$I(t) = \sum_{s=Male}^{s=Female} \sum_{a=Age\ 0-5}^{a=Age\ 80+} fh(a,s) * Ch(t) * fi(a,s) * p(a,s,t) \tag{A28}$$

The fraction of patients requiring mechanical ventilation was dependent on the age and sex of the patients in an ICU:

$$toV(t) = \sum_{s=Male}^{s=Female} \sum_{a=Age\ 0-5}^{a=Age\ 80+} \begin{array}{l} h(a,s) * Ch(t) * fi(a,s) * \\ Ci(t) * fv(a,s) * p(a,s,t) \end{array} \tag{A29}$$

As described previously, the death rate in general wards ($Death_H$) was dependent on the age and sex of the patients $hd(t)$ and changed with the rate of positive tests:

$$Death_H(t) = hd(t) * PQ_{Death}(t) \tag{A30}$$

$$hd(t) = \sum_{s=Male}^{s=Female} \sum_{a=Age\ 0-5}^{a=Age\ 80+} fh(a,s) * Ch(t) * fdh(a,s) * p(a,s,t) \tag{A31}$$

To assure a stable relation between the median death rates in each ward, the death rates for ICU $id(t)$ and ventilated patients $vd(t)$ extracted from the clinical database were corrected for the implantation of the covariate *PR* on the death rate in general wards by multiplying them with the influence of the median observed PR of 3.12% during the time

of the investigation. The resulting death rates for ICU patients ($\text{Death}_\text{I}$) and ventilated patients ($\text{Death}_\text{V}$) are depicted in Equations (A32) and (A34).

$$\text{Death}_\text{I}(t) = \text{id}(t) * \text{PQ}_\text{max} * \left(1 - \text{PQ}_\text{min} * e^{-3.12 * \text{PQ}_\text{rate}}\right) \tag{A32}$$

$$\text{id}(t) = \sum_{s=\text{Male}}^{s=\text{Female}} \sum_{a=\text{Age 0-5}}^{a=\text{Age 80+}} \begin{matrix} \text{fh}(a,s) * \text{Ch}(t) * \text{fi}(a,s) * \\ \text{Ci}(t) * \text{fdi}(a,s) * \text{p}(a,s,t) \end{matrix} \tag{A33}$$

$$\text{Death}_\text{V}(t) = \text{vd}(t) * \text{PQ}_\text{max} * \left(1 - \text{PQ}_\text{min} * e^{-3.12 * \text{PQ}_\text{rate}}\right) \tag{A34}$$

$$\text{vd}(t) = \sum_{s=\text{Male}}^{s=\text{Female}} \sum_{a=\text{Age 0-5}}^{a=\text{Age 80+}} \begin{matrix} \text{fh}(a,s) * \text{Ch}(t) * \text{fi}(a,s) * \text{Ci}(t) * \\ \text{fv}(a,s) * \text{fdv}(a,s) * \text{p}(a,s,t) \end{matrix} \tag{A35}$$

The following ODE system was used for the description of COVID-19 inpatients, with H depicting patients in a general ward only, ICU depicting patients in an ICU during any portion of their stay, and *V* depicting patients requiring mechanical ventilation during their stay, with the suffixes death and recovery for the outcome of the patients:

$$\frac{\text{dH}_\text{death}}{\text{dt}} = \text{Death}_\text{H}(t) * \tau * (1 - \text{toICU}(t)) * \text{T2}_\text{hosp}(t) - \kappa_\text{H} * \text{H}_\text{death}(t) \tag{A36}$$

$$\frac{\text{dH2}_\text{death}}{\text{dt}} = \kappa_\text{H} * \text{H}_\text{death}(t) - \kappa_\text{H} * \text{H2}_\text{death}(t) \tag{A37}$$

$$\frac{\text{dICU}_\text{death}}{\text{dt}} = \text{Death}_I(t) * \tau * \text{toICU}(t) * (1 - \text{toV}(t)) * \text{T2}_\text{hosp}(t) - \kappa_\text{ICU} * \text{ICU}_\text{death}(t) \tag{A38}$$

$$\frac{\text{dICU2}_\text{death}}{\text{dt}} = \kappa_\text{ICU} * \text{ICU}_\text{death}(t) - \kappa_\text{ICU} * \text{ICU2}_\text{death}(t) \tag{A39}$$

$$\frac{\text{dV}_\text{death}}{\text{dt}} = \text{Death}_V(t) * \tau * \text{toICU}(t) * \text{toV}(t) * \text{T2}_\text{hosp}(t) - \kappa_\text{V} * \text{V}_\text{death}(t) \tag{A40}$$

$$\frac{\text{dV2}_\text{death}}{\text{dt}} = \kappa_\text{V} * \text{V}_\text{death}(t) - \kappa_\text{V} * \text{V2}_\text{death}(t) \tag{A41}$$

$$\frac{\text{dH}_\text{recovery}}{\text{dt}} = (1 - \text{Death}_\text{H}(t)) * \tau * (1 - \text{toICU}(t)) * \text{T2}_\text{hosp}(t) - \rho_\text{H} * \text{H}_\text{recovery}(t) \tag{A42}$$

$$\frac{\text{dH2}_\text{recovery}}{\text{dt}} = \rho_\text{H} * \text{H}_\text{recovery}(t) - \rho_\text{H} * \text{H2}_\text{recovery}(t) \tag{A43}$$

$$\frac{\text{dICU}_\text{recovery}}{\text{dt}} = (1 - \text{Death}_I(t)) * \tau * \text{toICU}(t) * (1 - \text{toV}(t)) * \text{T2}_\text{hosp}(t) - \rho_\text{ICU} * \text{ICU}_\text{recovery}(t) \tag{A44}$$

$$\frac{\text{dICU2}_\text{recovery}}{\text{dt}} = \rho_\text{ICU} * \text{ICU}_\text{recovery}(t) - \rho_\text{ICU} * \text{ICU2}_\text{recovery}(t) \tag{A45}$$

$$\frac{\text{dV}_\text{recovery}}{\text{dt}} = (1 - \text{Death}_V(t)) * \tau * \text{toICU}(t) * \text{toV}(t) * \text{T2}_\text{hosp}(t) - \rho_\text{V}(t) * \text{V}_\text{recovery}(t) \tag{A46}$$

$$\frac{\text{dV2}_\text{alive}}{\text{dt}} = \rho_\text{V}(t) * \text{V}_\text{recovery}(t) - \rho_\text{V}(t) * \text{V2}_\text{recovery}(t) \tag{A47}$$

All patients recovering enter the recovery transit compartments (Equations (A48) and (A49)) after their stay in their respective hospital wards before they are counted as recovered (R) to adjust recovery time to the RKI definition (14 days), with the transit rate $\rho = 2/14$.

$$\frac{\text{dR}_\text{hospital}}{\text{dt}} = \rho_\text{H} * \text{H2}_\text{recovery}(t) + \rho_\text{ICU} * \text{ICU2}_\text{recovery}(t) + \rho_\text{V} * \text{V2}_\text{recovery}(t) - \rho * \text{R}_\text{hospital}(t)t) \tag{A48}$$

$$\frac{\text{dR2}_\text{hospital}}{dt} = \rho * \text{R}_\text{hospital}(t) - \rho * \text{R2}_\text{hospital}(t) \tag{A49}$$

The total number of recovered patients is calculated by Equation (A50):

$$\frac{dR}{dt} = \rho_a * QR2(t) + \rho * R_{hospital}(t) \tag{A50}$$

In contrast to the recovered patients, fatalities ($D$) in hospitals were counted without delay.

$$\frac{dD}{dt} = \kappa_H * H2_{death}(t) + \kappa_{ICU} * ICU2_{death}(t) + \kappa_V * V2_{death}(t) + \kappa_a * QD2(t) \tag{A51}$$

For all federal states, the number of patients currently in an ICU and being ventilated was multiplied by the fraction of time the patients stayed in the respective wards (Equations (A54)–(A56)). The ministries of the city-states of Berlin, Hamburg, and Bremen explicitly commented that a notable fraction of COVID-19 inpatients were not registered residents of the respective cities and hence did not contribute to the respective case counts. To account for this bias, correcting factors for Berlin, Bremen, and Hamburg were calculated: The number of resident inpatients in each city and the total number of inpatients (city residents and non-city residents) were available from 17 December 2020 to 7 January 2021. The factors $fBL_{Berlin}$, $fBL_{Bremen}$, and $fBL_{Hamburg}$ were calculated as the mean ratio of total inpatients to resident inpatients. Furthermore, for the federal state Hesse, the only inpatient data available consisted of the sum of confirmed and suspected COVID-19 cases in hospitals. Hence, the factor for Hesse inpatients $fBL_{Hesse}$ was calculated as the mean ratio of confirmed COVID-19 patients to the sum of suspected and confirmed cases.

The number of currently ventilated patients (Ventilated$(t)$, Equation (A52)), current ICU patients (ICU$(t)$, Equation (A53)), and currently hospitalized patients (Hospitalized$(t)$, Equation (A54)) can be calculated by multiplying the number of patients in the ODE system (as depicted by Equations (A36)–(A47)) at time t with the time fractions spent in each ward as depicted in Table 1, with:

$$\text{Ventilated}(t) = \begin{pmatrix} PVent_{V,R} * (V_{alive}(t) + V2_{alive}(t)) + \\ PVent_{V,D} * (V_{death}(t) + V2_{death}(t)) \end{pmatrix} * fBL_{State} \tag{A52}$$

$$\text{ICU}(t) = \begin{pmatrix} PICU_{I,R} * (ICU_{alive}(t) + ICU2_{alive}(t)) + \\ PICU_{I,D} * (ICU_{death}(t) + ICU2_{death}(t)) + \\ PICU_{V,R} * (V_{alive}(t) + V2_{alive}(t)) + \\ PICU_{V,D} * (V_{death}(t) + V2_{death}(t)) \end{pmatrix} * fBL_{State} \tag{A53}$$

$$\text{Hospitalized}(t) = \begin{pmatrix} H_{alive}(t) + H2_{alive}(t) + \\ H_{death}(t) + H2_{death}(t) + \\ ICU_{alive}(t) + ICU2_{alive}(t) + \\ ICU_{death}(t) + ICU2_{death}(t) + \\ V_{alive}(t) + V2_{alive}(t) + \\ V_{death}(t) + V2_{death}(t) \end{pmatrix} * fBL_{State} \tag{A54}$$

## Appendix B

**Table A1.** Model parameter estimates for the hospitalization and outcome model.

| Model Parameter | Unit | Population Estimate | RSE [%] | Parameter Description |
|---|---|---|---|---|
| **Population Parameters (Fixed Effects)** | | | | |
| Hosp | - | 0.99 | - | Factor on the age-specific hospitalization rates |
| fKH | - | −0.496 | 1.6 | Relative change in hospitalization rate at $CP_{Hosp}$ |
| $CP_{Hosp}$ | Day * | 281 | 0.2 | Time of hospitalization rate change |
| hill | - | 100 | - | Hill factor of time-dependent hospitalization and ICU rate change |

**Table A1.** *Cont.*

| Model Parameter | Unit | Population Estimate | RSE [%] | Parameter Description |
|---|---|---|---|---|
| $\text{Fntest}_{Hosp}$ | $10^6$/Tests | 0.344 | 3.7 | Slope of death rate change per 1,000,000 PCR tests performed |
| $f_{\text{Vent1}}$ | - | 1.69 | 0.9 | Factor time to discharge of recovering ventilated patients |
| $f_{\text{Vent2}}$ | - | −0.648 | 1.6 | Relative change in fBEAT1 at $CP_{Vent}$ |
| $CP_{Vent}$ | Day * | 228 | 0.5 | Time of change in fVent1 |
| toICU1 | - | 0.476 | 0.9 | Factor on the age-specific ICU rates |
| $\text{toICU2}_{\alpha}$ | - | 0.29 | 4.2 | Relative change of toICU for some states ** at $CP_{Hosp}$ |
| $\text{toICU2}_{\beta}$ | - | 0.0904 | 10.2 | Relative change of toICU for the states other than ** at $CP_{Hosp}$ |
| $\text{toICU2}_{\gamma}$ | - | 0.153 | 0.0 | Relative change of toICU Germany at $CP_{Hosp}$ |
| $PQ_{max}$ | - | 1.05 | 2.1 | Maximum death rate change depending on the test positivity rate |
| $PQ_{min}$ | - | 0.48 | 2.7 | Minimum death rate change depending on the test positivity rate |
| $PQ_{rate}$ | 1/% | 0.129 | 9.9 | Slope of death rate change depending on the test positivity rate |
| $D_{\text{OUT}}$ | $\text{day}^{-1}$ | 0.226 | 5.4 | Death rate of outpatients between $CP_{D1}$ and $CP_{D2}$ |
| $CP_{D1}$ | Day * | 348 | 0.6 | Time of change in $D_{\text{OUT}}$ |
| $CP_{D2}$ | Day * | 446 | 0.8 | Time of change in $D_{\text{OUT}}$ |
| $hill_D$ | - | 27 | 10.6 | Hill factor of time-dependent death rate changes |
| $\text{fH}_{\text{VOC}}$ | - | 0.395 | 14.1 | Relative hospitalization rate change for VOC B.1.1.7 |
| $\text{fICU}_{\text{VOC}}$ | - | 0.162 | 33.1 | Relative rate change to ICU for VOC B.1.1.7 |
| $\tau$ | - | 100 | - | Transit rate from confirmed case to inpatient |
| **Residual Errors** | | | | |
| $E_{cases}$ | %CV | 0.55 | 3 | Exponential error cases |
| $A_{cases}$ | SD | 32.6 | 4.6 | Additive error cases |
| $P_{ICU}$ | %CV | 23.3 | 2.8 | Proportional error ICU |
| $A_{ICU}$ | SD | 4.56 | 5 | Additive error ICU |
| $P_{death}$ | %CV | 9.78 | 2.9 | Proportional error fatalities |
| $A_{death}$ | SD | 11.8 | 6.8 | Additive error fatalities |
| $P_{hosp}$ | %CV | 35.2 | 3.5 | Proportional error hospitalizations |
| $A_{hosp}$ | SD | 11.8 | 13 | Additive error hospitalizations |
| $P_{vent}$ | %CV | 29.7 | 2.6 | Proportional error ventilated patients |
| $A_{vent}$ | SD | 1.48 | 9.3 | Additive error ventilated patients |
| $P_{dailydeath}$ | %CV | 80.4 | 2.7 | Proportional error daily fatalities |
| $A_{dailydeath}$ | SD | 0.36 | 6.4 | Additive error daily fatalities |
| $P_{dailyhosp}$ | %CV | 261 | 3.5 | Proportional error daily fatalities and hospitalizations |
| $A_{dailyhosp}$ | SD | 1.46 | 17 | Additive error daily fatalities and hospitalizations |

* as days since 22 December 2019; ** Bavaria, Berlin, Bremen, Hamburg, Hesse, North Rhine-Westphalia, and Saarland.

## References


1. Wu, F.; Zhao, S.; Yu, B.; Chen, Y.M.; Wang, W.; Song, Z.G.; Hu, Y.; Tao, Z.W.; Tian, J.H.; Pei, Y.Y.; et al. A New Coronavirus Associated with Human Respiratory Disease in China. *Nature* **2020**, *579*, 265–269. [CrossRef] [PubMed]
2. World Health Organization Coronavirus Disease (COVID-19) Dashboard. Available online: https://covid19.who.int/ (accessed on 21 July 2022).
3. Taylor, L. COVID-19: Brazil's Hospitals Close to Collapse as Cases Reach Record High. *BMJ* **2021**, *372*, n800. [CrossRef] [PubMed]
4. Ellen Ehni, C.M. ARD-DeutschlandTREND Januar 2021. Available online: https://www.tagesschau.de/inland/deutschlandtrend-2471.pdf (accessed on 19 January 2021).
5. Cousins, S. New Zealand Eliminates COVID-19. *Lancet* **2020**, *395*, 1474. [CrossRef]

6. Ferguson, N.; Laydon, D.; Nedjati Gilani, G.; Imai, N.; Ainslie, K.; Baguelin, M.; Bhatia, S.; Boonyasiri, A.; Cucunuba Perez, Z.; Cuomo-Dannenburg, G.; et al. *Report 9: Impact of Non-Pharmaceutical Interventions (NPIs) to Reduce COVID19 Mortality and Healthcare Demand*; Imperial College London: London, UK, 2020. [CrossRef]
7. Graham, M.S.; Sudre, C.H.; May, A.; Antonelli, M.; Murray, B.; Varsavsky, T.; Kläser, K.; Canas, L.S.; Molteni, E.; Modat, M.; et al. Changes in Symptomatology, Reinfection, and Transmissibility Associated with the SARS-CoV-2 Variant B.1.1.7: An Ecological Study. *Lancet Public Health* **2021**, *6*, e335–e345. [CrossRef]
8. Martina Patone, A.; Thomas, K.; Hatch, R.; San Tan, P.; Coupland, C.; Liao, W.; Mouncey, P.; Harrison, D.; Rowan, K.; Horby, P.; et al. Analysis of Severe Outcomes Associated with the SARS-CoV-2 Variant of Concern 202012/01 in England Using ICNARC Case Mix Programme and QResearch Databases. *medRxiv* **2021**. [CrossRef]
9. Petrilli, C.M.; Jones, S.A.; Yang, J.; Rajagopalan, H.; O'Donnell, L.; Chernyak, Y.; Tobin, K.A.; Cerfolio, R.J.; Francois, F.; Horwitz, L.I. Factors Associated with Hospitalization and Critical Illness among 4,103 Patients with COVID-19 Disease in New York City. *medRxiv* **2020**. [CrossRef]
10. Killerby, M.E.; Link-gelles, R.; Haight, S.C.; Schrodt, C.A.; England, L. Characteristics Associated with Hospitalization among Patients. *MMWR Morb. Mortal. Wkly. Rep.* **2020**, *69*, 790–794. [CrossRef]
11. Gallo Marin, B.; Aghagoli, G.; Lavine, K.; Yang, L.; Siff, E.J.; Chiang, S.S.; Salazar-Mather, T.P.; Dumenco, L.; Savaria, M.C.; Aung, S.N.; et al. Predictors of COVID-19 Severity: A Literature Review. *Rev. Med. Virol.* **2021**, *31*, 1–10. [CrossRef]
12. Garg, S.; Kim, L.; Whitaker, M.; O'Halloran, A.; Cummings, C.; Holstein, R.; Prill, M.; Chai, S.; Kirley, P.; Alden, N.; et al. Hospitalization Rates and Characteristics of Patients Hospitalized with Laboratory-Confirmed Coronavirus Disease 2019—COVID-NET, 14 States, March 1–30, 2020. *Morb. Mortal. Wkly. Rep.* **2020**, *69*, 458–464. [CrossRef]
13. Bundesministerium für Gesundheit. Robert Koch-Institut Aktualisierung Der Nationalen Teststrategie Und Neuverkündung Der Verordnung Zum Anspruch Auf Testung in Bezug Auf Einen Direkten Erreger- Nachweis Des Coronavirus SARS-CoV-2 (Coronavirus- Testverordnung–TestV). *Epidemiol. Bull.* **2020**, *43*, 3–6. [CrossRef]
14. Bentout, S.; Tridane, A.; Djilali, S.; Touaoula, T.M. Age-Structured Modeling of COVID-19 Epidemic in the USA, UAE and Algeria. *Alex. Eng. J.* **2020**, *60*, 401–411. [CrossRef]
15. Balabdaoui, F.; Mohr, D. Age-Stratified Discrete Compartment Model of the COVID-19 Epidemic with Application to Switzerland. *Sci. Rep.* **2020**, *10*, 21306. [CrossRef] [PubMed]
16. Kuhl, E. Data-Driven Modeling of COVID-19—Lessons Learned. *Extrem. Mech. Lett.* **2020**, *40*, 100921. [CrossRef] [PubMed]
17. Wells, C.R.; Townsend, J.P.; Pandey, A.; Moghadas, S.M.; Krieger, G.; Singer, B.; McDonald, R.H.; Fitzpatrick, M.C.; Galvani, A.P. Optimal COVID-19 Quarantine and Testing Strategies. *Nat. Commun.* **2021**, *12*, 356. [CrossRef]
18. Corona Zahlen Aktuell: Karte Für Deutschland + Weltweit. Available online: https://interaktiv.morgenpost.de/corona-virus-karte-infektionen-deutschland-weltweit/ (accessed on 4 August 2022).
19. SurvStat@RKI 2.0. Available online: https://survstat.rki.de/Content/Query/Create.aspx (accessed on 4 August 2022).
20. Informationen Zu Corona: Häufige Fragen-Bayerisches Staatsministerium Des Innern, Für Sport Und Integration. Available online: https://www.stmi.bayern.de/miniwebs/coronavirus/lage/index.php (accessed on 4 August 2022).
21. COVID-19 Berlin. Available online: https://www.berlin.de/corona/lagebericht/desktop/corona.html#stationäre-behandlung (accessed on 4 August 2022).
22. Pressemitteilungen | Ministerium Für Soziales, Gesundheit, Integration Und Verbraucherschutz. Available online: https://msgiv.brandenburg.de/msgiv/de/presse/pressemitteilungen/ (accessed on 4 August 2022).
23. Corona-Fallzahlen-Die Senatorin Für Gesundheit, Frauen Und Verbraucherschutz. Available online: https://www.gesundheit.bremen.de/corona/zahlen/corona-fallzahlen-37649 (accessed on 4 August 2022).
24. Corona: Zahlen, Fälle, Statistik von COVID-19-Hamburg.De. Available online: https://www.hamburg.de/corona-zahlen/ (accessed on 4 August 2022).
25. Presseinformationen | Nds. Ministerium Für Soziales, Gesundheit Und Gleichstellung. Available online: https://www.ms.niedersachsen.de/startseite/service_kontakt/presseinformationen/ (accessed on 4 August 2022).
26. Daten Zur Corona-Pandemie-LAGuS. Available online: https://www.lagus.mv-regierung.de/Gesundheit/InfektionsschutzPraevention/Daten-Corona-Pandemie (accessed on 4 August 2022).
27. NRW-Dashboard Zur Corona-Pandemie. Available online: https://www.giscloud.nrw.de/corona-dashboard.html (accessed on 4 August 2022).
28. Coronavirus SARS-CoV-2: Aktuelle Fallzahlen Für Rheinland-Pfalz. Available online: https://lua.rlp.de/de/presse/detail/news/News/detail/coronavirus-sars-cov-2-aktuelle-fallzahlen-fuer-rheinland-pfalz/ (accessed on 4 August 2022).
29. Infektionsfälle in Sachsen-Coronavirus in Sachsen-Sachsen.De. Available online: https://www.coronavirus.sachsen.de/infektionsfaelle-in-sachsen-4151.html (accessed on 4 August 2022).
30. Pressemitteilungen. Available online: https://ms.sachsen-anhalt.de/presse/pressemitteilungen/ (accessed on 4 August 2022).
31. COVID-19—Institut Für Infektionsmedizin. Available online: https://www.infmed.uni-kiel.de/de/epidemiologie/covid-19 (accessed on 4 August 2022).
32. TMASGFF: Infektionslage. Available online: https://www.tmasgff.de/covid-19/fallzahlen (accessed on 4 August 2022).
33. DIVI Intensivregister. Available online: https://www.intensivregister.de/#/aktuelle-lage/laendertabelle (accessed on 4 August 2022).
34. Tagesdaten-CSV Aus Dem DIVI-Intensivregister. Available online: https://edoc.rki.de/ (accessed on 4 August 2022).

35. Hethcote, H.W. The Mathematics of Infectious Diseases. *SIAM Rev.* **2000**, *42*, 599–653. [CrossRef]
36. World Health Organization. Coronavirus disease 2019 (COVID-19): Situation report, 73. *World Health Organization.* 2020. Available online: https://apps.who.int/iris/handle/10665/331686 (accessed on 5 January 2021).
37. Savic, R.M.; Jonker, D.M.; Kerbusch, T.; Karlsson, M.O. Implementation of a Transit Compartment Model for Describing Drug Absorption in Pharmacokinetic Studies. *J. Pharmacokinet. Pharmacodyn.* **2007**, *34*, 711–726. [CrossRef]
38. Upton, R.N.; Mould, D.R. Basic Concepts in Population Modeling, Simulation, and Model-Based Drug Development: Part 3-Introduction to Pharmacodynamic Modeling Methods. *CPT Pharmacomet. Syst. Pharmacol.* **2014**, *3*, e88. [CrossRef]
39. Wang, Y. Derivation of Various NONMEM Estimation Methods. *J. Pharmacokinet. Pharmacodyn.* **2007**, *34*, 575–593. [CrossRef]
40. Karlsson, M.O.; Savic, R.M. Diagnosing Model Diagnostics. *Clin. Pharmacol. Ther.* **2007**, *82*, 17–20. [CrossRef]
41. Helfand, M.; Fiordalisi, C.; Wiedrick, J.; Ramsey, K.L.; Armstrong, C.; Gean, E.; Winchell, K.; Arkhipova-Jenkins, I. Risk for Reinfection After SARS-CoV-2: A Living, Rapid Review for American College of Physicians Practice Points on the Role of the Antibody Response in Conferring Immunity Following SARS-CoV-2 Infection. *Ann. Intern. Med.* **2022**, *175*, 547–555. [CrossRef]
42. Volz, E.; Mishra, S.; Chand, M.; Barrett, J.C.; Johnson, R.; Hopkins, S.; Gandy, A.; Rambaut, A.; Ferguson, N.M. Transmission of SARS-CoV-2 Lineage B.1.1.7 in England: Insights from Linking Epidemiological and Genetic Data. *medRxiv* **2021**. [CrossRef]
43. Robert Koch-Institut. 2. Bericht Zu Virusvarianten von SARS-CoV-2 in Deutschland, Insbesondere Zur Variant of Concern (VOC) B.1.1.7. Available online: https://www.rki.de/DE/Content/InfAZ/N/Neuartiges_Coronavirus/DESH/Bericht_VOC_2021-02-17.pdf?__blob=publicationFile (accessed on 18 February 2021).
44. RKI-Navigation-Besorgniserregende SARS-CoV-2-Virusvarianten (VOC). Available online: https://www.rki.de/DE/Content/InfAZ/N/Neuartiges_Coronavirus/Virusvariante.html;jsessionid=47C4433E4DE091FA86315701A0870406.internet081?nn=2444038 (accessed on 4 August 2022).
45. Eurostat; European Commission. *Statistical Regions in the European Union and Partner Countries: NUTS and Statistical Regions 2021: 2020 Edition*; Publications Office of the European Union: Luxembourg, 2020.
46. an der Heiden, M. *SARS-CoV-2-Nowcasting Und -R-Schaetzung*; Zenodo: Berlin, Germany, 2022.
47. Videokonferenz Der Bundeskanzlerin Mit Den Regierungschefinnen Und Regierungschefs Der Länder Am 28. Oktober 2020. Available online: https://www.bundesregierung.de/breg-de/suche/videokonferenz-der-bundeskanzlerin-mit-den-regierungschefinnen-und-regierungschefs-der-laender-am-28-oktober-2020-1805248 (accessed on 4 August 2022).
48. Walsh, S.; Chowdhury, A.; Braithwaite, V.; Russell, S.; Birch, J.M.; Ward, J.L.; Waddington, C.; Brayne, C.; Bonell, C.; Viner, R.M.; et al. Do School Closures and School Reopenings Affect Community Transmission of COVID-19? A Systematic Review of Observational Studies. *BMJ Open* **2021**, *11*, e053371. [CrossRef] [PubMed]
49. Elke, B.; Juliane, W.; Helene, E.; Ulrike, N.; Dimitra, P.; Christoph, R.; Tanja, R.; Reinhard, B. A Country-Level Analysis Comparing Hospital Capacity and Utilisation during the First COVID-19 Wave across Europe. *Health Policy* **2022**, *126*, 373–381. [CrossRef]
50. Jun, T.; Nirenberg, S.; Weinberger, T.; Sharma, N.; Pujadas, E.; Cordon-Cardo, C.; Kovatch, P.; Huang, K. Analysis of Sex-Specific Risk Factors and Clinical Outcomes in COVID-19. *Commun. Med. 2021 11* **2021**, *1*, 3. [CrossRef] [PubMed]
51. Starke, K.R.; Petereit-Haack, G.; Schubert, M.; Kämpf, D.; Schliebner, A.; Hegewald, J.; Seidler, A. The Age-Related Risk of Severe Outcomes Due to COVID-19 Infection: A Rapid Review, Meta-Analysis, and Meta-Regression. *Int. J. Environ. Res. Public Health* **2020**, *17*, 5974. [CrossRef]
52. Ciarambino, T.; Para, O.; Giordano, M. Immune System and COVID-19 by Sex Differences and Age. *Women's Health* **2021**, *17*, 1–6. [CrossRef]
53. Ohsfeldt, R.L.; Choong, C.K.C.; Mc Collam, P.L.; Abedtash, H.; Kelton, K.A.; Burge, R. Inpatient Hospital Costs for COVID-19 Patients in the United States. *Adv. Ther.* **2021**, *38*, 5557–5595. [CrossRef]
54. Bager, P.; Wohlfahrt, J.; Fonager, J.; Rasmussen, M.; Albertsen, M.; Michaelsen, T.Y.; Møller, C.H.; Ethelberg, S.; Legarth, R.; Button, M.S.F.; et al. Risk of Hospitalisation Associated with Infection with SARS-CoV-2 Lineage B.1.1.7 in Denmark: An Observational Cohort Study. *Lancet Infect. Dis.* **2021**, *21*, 1507–1517. [CrossRef]
55. Challen, R.; Brooks-Pollock, E.; Read, J.M.; Dyson, L.; Tsaneva-Atanasova, K.; Danon, L. Risk of Mortality in Patients Infected with SARS-CoV-2 Variant of Concern 202012/1: Matched Cohort Study. *BMJ* **2021**, *372*, n579. [CrossRef]
56. Modi, C.; Böhm, V.; Ferraro, S.; Stein, G.; Seljak, U. Estimating COVID-19 Mortality in Italy Early in the COVID-19 Pandemic. *Nat. Commun.* **2021**, *12*, 2729. [CrossRef]
57. Liang, L.L.; Tseng, C.H.; Ho, H.J.; Wu, C.Y. COVID-19 Mortality Is Negatively Associated with Test Number and Government Effectiveness. *Sci. Rep.* **2020**, *10*, 12567. [CrossRef] [PubMed]
58. Johnson, R.M.; Vinetz, J.M. Dexamethasone in the Management of COVID-19. *BMJ* **2020**, *370*, m2648. [CrossRef] [PubMed]
59. Tomazini, B.M.; Maia, I.S.; Cavalcanti, A.B.; Berwanger, O.; Rosa, R.G.; Veiga, V.C.; Avezum, A.; Lopes, R.D.; Bueno, F.R.; Silva, M.V.A.O.; et al. Effect of Dexamethasone on Days Alive and Ventilator-Free in Patients With Moderate or Severe Acute Respiratory Distress Syndrome and COVID-19: The CoDEX Randomized Clinical Trial. *JAMA* **2020**, *324*, 1307–1316. [CrossRef] [PubMed]
60. Versteckte Triage?: Das Sterben Der Alten Menschen-ZDFheute. Available online: https://www.zdf.de/nachrichten/panorama/corona-triage-pflegeheime-100.html (accessed on 4 August 2022).
61. Booton, R.D.; MacGregor, L.; Vass, L.; Looker, K.J.; Hyams, C.; Bright, P.D.; Harding, I.; Lazarus, R.; Hamilton, F.; Lawson, D.; et al. Estimating the COVID-19 Epidemic Trajectory and Hospital Capacity Requirements in South West England: A Mathematical Modelling Framework. *BMJ Open* **2021**, *11*, 41536. [CrossRef]

## 4.2 Project II: COVID-19 Spreading in Different Age Groups

### *4.2.1 Reference*

**Effect of vaccinations and school restrictions on the spread of COVID-19 in different age groups in Germany.**
Christiane Dings, Dominik Selzer, Nicola Luigi Bragazzi, Eva Möhler, Markus Wenning, Thomas Gehrke, Ulf Richter, Alexandra Nonnenmacher, Folke Brinkmann, Tobias Rothoeft, Michael Zemlin, Thomas Lücke and Thorsten Lehr.
*Infectious Disease Modelling* 2024; 9(4):1250-1264. DOI: 10.1016/j.idm.2024.07.004 [2]

### *4.2.2 Author Contributions*

Author contributions according to the contributor roles taxonomy (CRediT)[4,5] were as following:

| | |
|---|---|
| Christiane Dings | See Contribution Report (page ii) |
| Dominik Selzer | Conceptualization, Methodology, Writing — Review & Editing, Supervision |
| Nicola Luigi Bragazzi | Formal analysis, Writing - Review & Editing |
| Eva Möhler | Writing — Review & Editing |
| Markus Wenning | Writing — Review & Editing |
| Thomas Gehrke | Writing — Review & Editing |
| Ulf Richter | Writing — Review & Editing |
| Alexandra Nonnenmacher | Writing — Review & Editing |
| Folke Brinkmann | Writing — Review & Editing |
| Tobias Rothoeft | Writing — Review & Editing |
| Michael Zemlin | Writing — Review & Editing |
| Thomas Lücke | Writing — Review & Editing |
| Thorsten Lehr | Conceptualization, Methodology, Writing — Review & Editing, Supervision, Project administration |

### *4.2.3 Copyright*

Infectious Disease Modelling 9 (2024) 1250–1264

Contents lists available at ScienceDirect

Infectious Disease Modelling

journal homepage: www.keaipublishing.com/idm

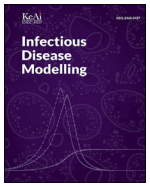


# Effect of vaccinations and school restrictions on the spread of COVID-19 in different age groups in Germany

Christiane Dings [a], Dominik Selzer [a], Nicola Luigi Bragazzi [a], Eva Möhler [b], Markus Wenning [c], Thomas Gehrke [c], Ulf Richter [d], Alexandra Nonnenmacher [d], Folke Brinkmann [e, f], Tobias Rothoeft [e], Michael Zemlin [g], Thomas Lücke [c, e], Thorsten Lehr [a, *]

[a] Department of Clinical Pharmacy, Saarland University, 66123, Saarbrücken, Germany
[b] Department of Child and Adolescent Psychiatry, Saarland University Hospital, 66421, Homburg, Germany
[c] Medical Association, Westfalen-Lippe, 48151, Münster, Germany
[d] School of Education and Psychology, Siegen University, 57072, Siegen, Germany
[e] University Children's Hospital, Ruhr University, 44791, Bochum, Germany
[f] University Children's Hospital, Airway Research Center North (ARCN), German Center for Lung Research (DZL), Lübeck, Germany
[g] Department of General Pediatrics and Neonatology, Saarland University Hospital, 66421, Homburg, Germany

ARTICLE INFO

*Article history:*
Received 1 April 2024
Received in revised form 20 July 2024
Accepted 23 July 2024
Available online 24 July 2024
Handling Editor: Dr Yiming Shao

*Keywords:*
COVID-19
Vaccination
Non-pharmaceutical interventions
Age
Mathematical modeling

ABSTRACT

With the emergence of SARS-CoV-2, various non-pharmaceutical interventions were adopted to control virus transmission, including school closures. Subsequently, the introduction of vaccines mitigated not only disease severity but also the spread of SARS-CoV-2. This study leveraged an adapted SIR model and non-linear mixed-effects modeling to quantify the impact of remote learning, school holidays, the emergence of Variants of Concern (VOCs), and the role of vaccinations in controlling SARS-CoV-2 spread across 16 German federal states with an age-stratified approach. Findings highlight a significant inverse correlation (Spearman's $\rho = -0.92$, $p < 0.001$) between vaccination rates and peak incidence rates across all age groups. Model-parameter estimation using the observed number of cases stratified by federal state and age allowed to assess the effects of school closure and holidays, considering adjustments for vaccinations and spread of VOCs over time. Here, modeling revealed significant ($p < 0.001$) differences in the virus's spread among pre-school children (0–4), children (5–11), adolescents (12–17), adults (18–59), and the elderly (60+). The transition to remote learning emerged as a critical measure in significantly reducing infection rates among children and adolescents ($p < 0.001$), whereas an increased infection risk was noted among the elderly during these periods, suggesting a shift in infection networks due to altered caregiving roles. Conversely, during school holiday periods, infection rates among adolescents mirrored those observed when schools were open. Simulation exercises based on the model provided evidence that COVID-19 vaccinations might serve a dual purpose: they protect the vaccinated individuals and contribute to the broader community's safety.



* Corresponding author. Department of Clinical Pharmacy, Saarland University, 66123, Campus C4 3, Saarbrücken, Germany
*E-mail address:* thorsten.lehr@mx.uni-saarland.de (T. Lehr).
Peer review under responsibility of KeAi Communications Co., Ltd.

https://doi.org/10.1016/j.idm.2024.07.004

**Abbreviations**

| | |
|---|---|
| Alpha (B.1.1.7) | The Alpha variant of SARS-CoV-2, first identified in the United Kingdom |
| Delta (B.1.617.2) | The Delta variant of SARS-CoV-2, initially identified in India |
| EMA | European Medicines Agency |
| NLME | Non-linear Mixed-effects (modeling) |
| NPI | Non-pharmaceutical Intervention |
| Omicron BA.1 | A subvariant of the Omicron variant of SARS-CoV-2 |
| Omicron BA.2 | A subvariant of the Omicron variant of SARS-CoV-2 |
| Omicron BA.4/BA.5 | Further subvariants of the Omicron variant of SARS-CoV-2, grouped together due to their close genetic relationship and similar epidemiological impact |
| PCR | Polymerase Chain Reaction |
| RKI | Robert Koch Institute |
| RSE | Relative Standard Error |
| SIR | Susceptible, Infectious, Recovered (model) |
| STIKO | German Standing Committee on Vaccination |
| VOC | Variant of Concern |
| WT | Wild Type |

## 1. Introduction

In 2020, the emergence of SARS-CoV-2 resulted in a global pandemic of coronavirus disease (COVID-19), posing a critical challenge to healthcare systems worldwide and demanding effective strategies for the control of the spreading of infections (Ellen Ehni, 2021; Taylor, 2021). Prior to the approval of COVID-19 vaccines, non-pharmaceutical interventions (NPIs) —including school closures, restrictions on public spaces such as restaurants and leisure facilities, as well as mandatory FFP2 mask waring —were key strategies to mitigate virus spreading (Lionello et al., 2022). The efficacy and impact of these NPIs, especially in the pandemic's early stages, were subjects of considerable debate (Talic et al., 2021). School closures, in particular, presented notable logistical challenges, necessitating remote learning infrastructure and imposing substantial burdens on parents and children alike (Freundl et al., 2021). These closures not only disrupted education but also considerably impacted children's social development and well-being (Hume et al., 2023; Hussong et al., 2022; Paulus et al., 2022; Ravens-Sieberer et al., 2020). Considering the typically milder COVID-19 symptoms in children (Yuki et al., 2020) and their hypothesized lower contribution to virus transmission (Ludvigsson, 2020), the necessity of such measures was repeatedly questioned.

With the approval of COVID-19 vaccines, vaccinations emerged as a pivotal tool in reducing infection rates and disease severity (Pritchard et al., 2021). In Germany, however, the initial scarcity of vaccines sparked debates over prioritization strategies. At the end of 2020, the foremost aim of the German Standing Committee on Vaccination (STIKO) COVID-19 vaccination guideline has been to avert critical health incidents, such as hospital admissions and fatalities linked to COVID-19, alongside shielding healthcare workers and individuals in other susceptible professions from SARS-CoV-2 contagions, impeding the spread of the virus, ensuring safety in areas with numerous vulnerable persons and a pronounced likelihood of outbreaks, and upholding vital governmental operations and societal activities (Vygen-Bonnet et al., 2020). Hence, the vaccination rollout initially targeted and prioritized older individuals and workers in professions with a high risk of infection (Steiger et al., 2021). Moreover, the STIKO initially recommended vaccination primarily for adolescents at high risk of severe disease or in high-risk occupations, citing limited data on adverse reactions and estimated minimal impact on transmission rates in younger demographics (Robert Koch-Institut, 2021). This stance evolved over time, with STIKO later advocating for broader vaccination coverage among adolescents (Presse- und Informationsamt der Bundesregierung, 2021a).

The increase in Germany's vaccination efforts in early 2021 coincided with the second wave of infections (week 40 2020—week 08 2021), which, at that juncture, was the most critical wave, primarily impacting the elderly population (Dings et al., 2022). The subsequent third wave (week 09 2021—week 23 2021) saw a shift, with the younger population being more affected, suggesting a protective effect of vaccinations against infection among the older, vaccinated population. Yet, the extent of this protection across different age groups remained a matter of ongoing investigation (Bar-On et al., 2021; Chemaitelly et al., 2022; Sadarangani et al., 2021).

This evolving landscape of the pandemic (Markov et al., 2023; Roemer et al., 2023), marked by fluctuating incidence rates and the emergence of viral strains with increased transmissibility and virulence, potentially undermined the effectiveness of public health measures. The novel strains defined as variants of concern (VOC) added layers of complexity to the unfolding of the pandemic, characterized by variable disease severity, differences in immune status, and altered responses to interventions across age groups. All this underscored the necessity for a more nuanced understanding of the dynamics of SARS-CoV-2 transmissions (Nunes et al., 2024). Hence, it became increasingly important to examine how various factors, including

vaccination status and the implementation of NPIs, influenced the course of the pandemic across different segments of the population. To address this, we adapted and extended a Susceptible-Infectious-Recovered (SIR) model to describe the progression of infections over time across German federal states, stratified by age groups. We estimated the unknown model parameters using non-linear mixed effects (NLME) modeling. This statistical approach enables the analysis of data with both fixed and random effects which allowed us to analyze the differential impacts of fixed effects variables such as vaccination coverage, NPIs, including school closures with remote learning and school holidays, and the emergence of VOCs on SARS-CoV-2 incidence across various age groups over time, while providing a stochastic framework accounting for variability between geographical regions via random effects. Moreover, model simulations were conducted to explore the potential impact of prioritizing vaccinations for the younger population on the spread of SARS-CoV-2.

## 2. Methods

### 2.1. Dataset

Our study made use of an extensive dataset gathered from various sources, with the primary data coming from the Robert Koch Institute (RKI). A detailed list of all data sources can be found in Table 1.

For the period between December 21, 2020 and August 08, 2022, we collected detailed data from Germany including both the number of weekly and cumulative confirmed SARS-CoV-2 infections (Robert Koch-Institut, 2024) and vaccination records (Robert Koch-Institut, 2022), stratified by age groups and German federal states. To ensure analytical consistency, we standardized the age categories of the infection data to match those used in the vaccination dataset: 0–4, 5–11, 12–17, 18–59, and over 60 years. Additionally, we obtained the weekly fraction of confirmed cases infected with each VOC (Robert Koch-Institut, 2023). The dataset further encompasses dates of school holidays, school closures with remote learning and periods of mandatory mask wearing in school settings.

### 2.2. Model development

Our analysis involved an adaptation of the classical SIR compartmental model, specifically designed to estimate both the weekly new and total cumulative confirmed infections across the age groups and federal states in Germany. In this model, the population progresses through the stages of 'susceptible', 'infected', and 'confirmed cases'. Individuals in the 'infected' stage are considered as infected and capable of transmitting the virus. Those classified in the 'confirmed cases' category are assumed to be quarantined, which prevents further transmissions. A notable aspect of our model is the inclusion of immunity dynamics. It is assumed that individuals previously infected with wildtype (WT) or pre-Omicron VOCs are immune to reinfection with these strains for the period of investigation. However, these individuals remain susceptible to the Omicron variant (Arabi et al., 2023).

The transition dynamics for each stage and age group were modeled using a system of ordinary differential equations (ODEs). Parameters were sourced from existing literature along with unknown parameters estimated within our NLME framework. Fig. 1 presents a schematical representation of the used data and parameter identification processes, which are described in detail in sections 2.2.1–2.2.4. Random effects were used to allow the effective reproductive number (Rt) to vary across German federal states. Error models for both cumulative and daily data were considered using proportional and additive error structures. A full list of informed model parameters and fixed effects estimates is presented in Table 2 of the Results section.

The model was implemented in NONMEM® (7.4.3., ICON Development Solutions, Ellicott City, MD, USA). Here, the underlying set of ODEs was numerically solved via LSODA (Hindmarsh & Petzold, 2005). Model parameters were estimated via First Order Conditional Estimation with Interaction (FOCEI) (Wang, 2007). A significant ($p \leq 0.05$; chi-squared test) improvement of the objective function value (−2 log-likelihood), precision of parameter estimates reported as relative standard errors (RSE) (Mould & Upton, 2012), as well as visual inspection of the goodness-of-fit plots (Karlsson & Savic, 2007) were used as criteria for model selection.

**Table 1**
Overview of data sources and characteristics for model information and training.

| Data | Time resolution | Stratification | Source |
|---|---|---|---|
| Cumulative confirmed infections | Weekly | Age group, federal state | Robert Koch-Institut (2024) |
| Vaccinations | Daily | Age group, federal state, vaccination details (primary or booster vaccination) | Robert Koch-Institut (2022) |
| Fraction of confirmed cases infected with a specific VOC | Weekly | VOC | Robert Koch-Institut (2023) |
| School closure, school holidays, mask mandates | Daily | Federal state | Government websites, federal press reports |
| R(t) changepoints and between-state variability | Daily | – | Dings et al. (2022) |

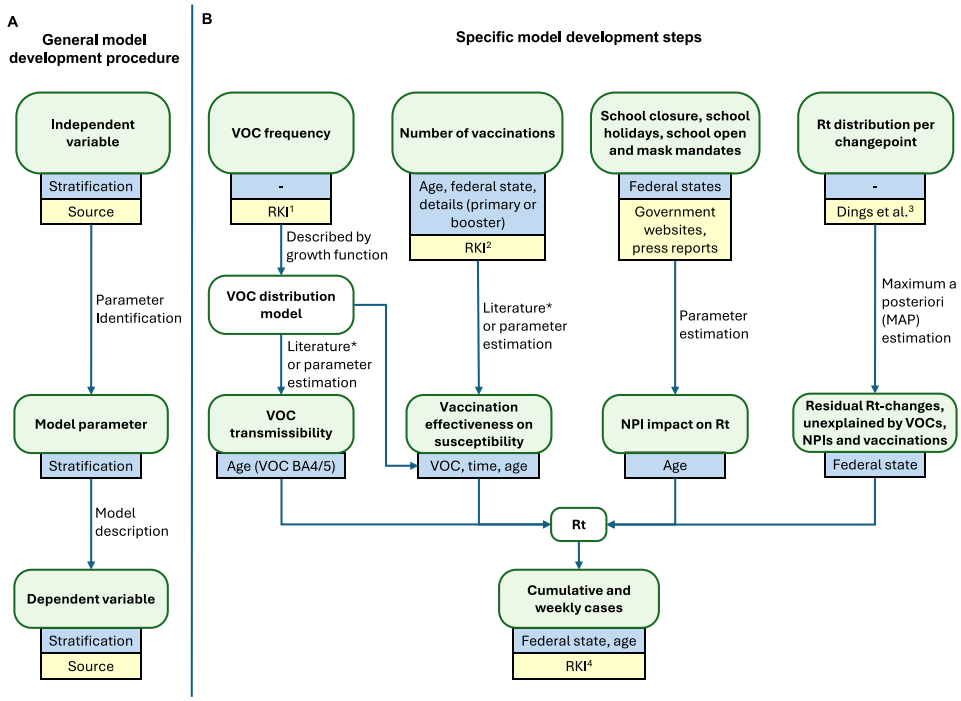


**Fig. 1.** (A) general model development procedure, (B) specific model development steps for the investigated variables. Sources: [1] (Robert Koch-Institut, 2023), [2] (Robert Koch-Institut, 2022), [3] (Dings et al., 2022), [4] (Robert Koch-Institut, 2024), * Sources for model parameters are listed in Table 1 and Supplementary Table 1.

The statistical programming language R 3.6.3 (The R Foundation for Statistical Computing, Vienna, Austria) was employed for dataset generation, statistical analysis, and generation of plots. With the final model, we conducted simulations to project the impact of varying vaccine coverage levels on prospective incidence rates of different age cohorts.

### 2.2.1. Variants of concern

We obtained information on the proportion of individuals infected with key virus VOCs over time — Alpha (B.1.1.7), Delta (B.1.617.2), and Omicron subvariants BA.1, BA.2 and BA.4/BA.5 — from the RKI (Robert Koch-Institut, 2023).

A specific growth function (Dings et al., 2022) was used to integrate the emergence of these VOCs in the model. This function (see Equation (1)) captures the exponential increase or logistic growth of VOCs within the population over time, thereby enabling dynamic adjustments to the model based on the evolving prevalence of these variants.

$$VOC_{\text{variant}}(t) = F_{\max} \Big/ \left(1 + \frac{1 - F_{\text{init}}}{F_{\text{init}}} * e^{-k * (t - t_{\text{init}})}\right) \tag{1}$$

Here, k is a VOC-specific growth rate, $F_{init}$ is the initial fraction of infections with a specific VOC (fixed to 0.2% to estimate a corresponding initial time), $t_{init}$ being the initial time and $F_{max}$ is the maximum distribution. This function was fitted via least-squares to the fraction of cases infected with a specific VOC or WT reported by the RKI. Point estimates for parameters regarding VOCs Alpha, Delta, Omicron BA.1, BA.2 as well as BA.4/BA.5 are presented in Supplementary Table 1. The fraction of infected individuals over time with a specific VOC plotted in Supplementary Fig. 1.

In dependence of the fraction described by the growth function, changes in the effective reproductive number attributable to the emergence of the respective VOCs were implemented in the model according to transmissibility changes obtained from literature or derived from the slope of the growth function (see Supplementary Table 1). For VOC BA4/5, observed patterns of age-stratified infections significantly ($p < 0.001$) deviated from the overall population trends. Therefore, the change in transmissibility due to VOC BA4/5 was subsequently refined by stratifying data by age group to achieve enhanced precision.

### 2.2.2. Vaccinations

We sourced the number of individuals vaccinated in each German federal state over time from the RKI's GitHub repository (Robert Koch-Institut, 2022). This data was broken down by age group, vaccine and the specific dose of the administered vaccine (primary or booster vaccination). Throughout our study period, a range of mono- and bivalent COVID-19 vaccines

received approval and became available in Germany. The analysis did not differentiate between vaccine technologies or manufacturers due to the predominance of the BNT162b2 vaccine (BioNTech/Pfizer, Mainz, Germany/New York, United States), representing 73% of administered COVID-19 vaccines by the end of the study period (Robert Koch-Institut, 2022).

In our analysis, we defined 'fully vaccinated' individuals as those who had received, in accordance with the label of the vaccine, one or two doses, with a two-week interval following the final dose. This definition was based on the recognition that the efficacy of most COVID-19 vaccines is limited immediately after the dose. Consequently, in our model, only individuals meeting these criteria were considered 'vaccinated'.

The effectiveness of full vaccinations and booster treatment against infections was implemented for WT/Alpha and VOC Delta via parametrization gathered from literature (see Table 2). For VOC Omicron, the effects of vaccinations were estimated via model fitting (see Table 2 for estimated vaccine effectiveness against infection). Given the known decline in vaccine effectiveness against infections over time, our analysis estimated a specific change point in the effectiveness for individuals aged 18 years and older.

*2.2.3. Non-pharmaceutical interventions*

We gathered data on periods with COVID-19 related school closures, school holidays and mask mandates for each federal state as well as nursery school attendance rules from diverse public sources, including official government websites and media and press reports.

The influence of these NPIs on the infection dynamics of each age was quantified via model parameter estimation. For this purpose, the largest age group (ages 18–59 years) was set as a reference group, and factors expressing increased or decreased virus transmission were estimated for each setting and age group.

*2.2.4. Rt changepoints and residual variability in Rt*

Temporal changes in the effective reproductive number not attributable to VOCs, vaccinations and the previously discussed NPIs were described using specific time points where shifts occurred. These time points and the corresponding median reproduction numbers (Rt's, see Table 2 of the Supplementary Materials) were anchored to values derived from the model previously developed by Dings et al. (Dings et al., 2022), which detailed cumulative cases in German federal states on a daily basis. In numerous instances, the timing of the changepoints could be attributed to modifications in NPI policies (Dings et al., 2022), as presented in Supplementary Table 2.

*2.3. Model equations*

For the structural model, equations (2)–(13) depict key model equations used to describe the number of confirmed cases over time per age group.

$$\frac{dS_{age}}{dt} = -\beta_{age}(t)*\frac{S_{age}(t)}{N_{age}}*I(t)*Nrel_{age} \tag{2}$$

$$\frac{dI_{age}}{dt} = \beta_{age}(t)*\frac{S_{age}(t) + VOC_{Omicron}(t)*SO_{age}(t)}{N_{age}}*I(t)*Nrel_{age} - \gamma*I_{age}(t) \tag{3}$$

$$\frac{dC_{age}}{dt} = \gamma*I_{age}(t) \tag{4}$$

$$\frac{dSO_{age}}{dt} = (1 - VOC_{Omicron}(t))*\gamma*I_{age}(t) - VOC_{Omicron}(t)*\beta_{age}(t)*\frac{SO_{age}(t)}{N_{age}}*I(t)*Nrel_{age} \tag{5}$$

$$\beta_{age}(t) = R(t)*\gamma \tag{6}$$

$$R(t) = \left\{ \begin{array}{c} R_0*\log\,(u_{o,j}) \text{ for } t_0 \le t \le t_1 \\ R_1*\log(u_{1,j}) \text{for } t_1 \le t \le t_2 \\ \vdots \\ R_n*\log\,(u_{n,j}) \text{ for } t_n \le t \le t_{n+1} \\ R_{n+1}*\log(u_{n+1,j}) \text{for } t \ge t_{n+1} \end{array} \right\} *VOC(t, age)*Veff_{age}(t)*NPI(t, age) \tag{7}$$

$$\mathrm{VOC(t,age)} = \sum_{i=WT}^{n\in\{Alpha,Delta,BA.1,BA.2,BA.4/5\}} \varepsilon_i * \alpha_{i,age} * \begin{cases} frac_i(t) - frac_{i+1}(t), \text{for i} < \text{n} \\ frac_i(t), \text{for i} = \text{n} \end{cases} \quad (8)$$

$$\mathrm{Veff_{age}(t) = UVacc_{age}(t) + FVacc_{age}(t)*FI_{age}(t) + FBoost_{age}(t)*FI_{Booster}(t)} \quad (9)$$

$$\mathrm{FI_{age}(t) = fs_{age,WT/Alpha}(1-VOC_{Delta}(t)) + fs_{age,Delta}(t)(VOC_{Delta}(t) - VOC_{Omicron}(t)) + fs_{age,Omicron}VOC_{Omicron}(t)} \quad (10)$$

$$\mathrm{FI_{Booster}(t) = fsb_{WT}(1-VOC_{Delta}(t)) + fsb_{Delta}(VOC_{Delta}(t) - VOC_{Omicron}(t)) + fsb_{Omicron}VOC_{Omicron}(t)} \quad (11)$$

$$\mathrm{NPI(t,age) = f_{dist}(t,age)*f_{school}(t,age)*f_{holiday}(t,age)*f_{nurs}(t,age)} \quad (12)$$

$$\mathrm{f_x(t,age)} = \begin{cases} \mathrm{f_{x,age}} \text{ for times of remote learning (x = dist), school open (x = school),} \\ \text{school holidays (x = holiday), nursery school attendance rules (x = nurs)} \\ \text{1 otherwise} \end{cases} \quad (13)$$

with $S_{age}$, $C_{age}$, $I_{age}$ and $SO_{age}$ being the number of susceptibles, infected individuals, PCR-confirmed (and quarantined) cases and susceptibles for VOC Omicron, respectively, for each age group. Compartment I represents the sum of infected individuals through all age groups. The total population of the age group is given by $N_{age}$, and $Nrel_{age}$ is the relative proportion of that age group within the total population. The infection rate $\beta_{age}(t)$ depends on change points in the effective reproduction number R(t) (see Supplementary Table 2 and Supplementary Fig. 2), modulation of transmissibility due to emergence of VOCs denoted by VOC(t) (Equation (8)), the effectiveness of vaccinations against the VOCs (Equations (9)–(11)), and age-stratified effects of NPIs (Equations (12) and (13)).

Spontaneous changes in the effective reproduction number (Equation (7)) were estimated for previously derived change points via random effects $u_{i,j}$ for change point i and federal state j with population fixed effects $R_i$ adopted from previous work (Dings et al., 2022). Rt-modulators $f_x(t,age)$ for NPIs were estimated via fixed effects and set to 1 at time NPI-free time periods. The effect of VOCs on change in transmissibility over time VOC(t, age) per age group was calculated based on the fraction of the specific VOC i ($frac_i(t)$ at time t). Here, $frac_i(t)$ was computed via Equation (1). Moreover, $\varepsilon_i$ is the relative increase in transmissibility for VOC i as presented in Table 1 of the Supplementary Materials and $\alpha_{i,age}$ being the age-specific relative change in transmissibility for VOC i (see Table 2 in the results section). For this, $\alpha_{i,age}$ was not estimated (fixed to 1) for WT and VOCs pre-BA.4/BA.5. $FI_{age}(t)$ represents the fraction of vaccinated individuals prone to infection and was fixed to data available in existing literature or, if no data was available, estimated for each age group over time taking the age-specific vaccine effectiveness (*fs*, see Table 2) into account. In comparison, $FI_{Booster}(t)$ is defined as the fraction of individuals vaccinated by boosters, but still prone to infection based on the booster effectiveness (*fsb*, see Table 2). As a result of these, $Veff_{age}$ describes the decrease of the effective reproductive number due to vaccinations with $UVacc_{age}$, the fraction of the population not vaccinated, $FVacc_{age}$ the fraction of the vaccinated but not boostered population and $FBoost_{age}$ the fraction of the population that received at least one booster vaccination.

## 3. Results

### 3.1. Data exploration

The data collection period extended from December 21, 2020 to August 08, 2022, coinciding with the initiation of the COVID-19 vaccination campaign in Germany. The first administration of a COVID-19 vaccine occurred on December 26, 2020. Fig. 2 illustrates the vaccination program's progression and impact in Germany comparing the vaccinated fraction of the population stratified by age to the relative incidence. The relative incidence was calculated as the weekly incidence/100 000 inhabitants of the respective age group divided by the weekly incidence/100 000 inhabitants of the total population.

During our study, we observed the prioritization and progression of COVID-19 vaccinations across different age groups in Germany. Initially, individuals aged over 80 years were assigned the highest priority for vaccination, due to their increased risk of severe disease outcomes. This was followed by vaccinations for younger adults who either had a high risk of severe disease or were employed in professions involving contact with high-risk patients. A notable shift in the pandemic's trajectory was observed in May 2021, marking a period when the vaccination campaign had predominantly targeted the elderly population (age 60+). Correspondingly, there was a substantial decline in the relative incidence rate within this age group. The expansion of the vaccination campaign to younger populations was shaped by key regulatory approvals. The European Medicines Agency (EMA) authorized the use of BNT162b2 for adolescents aged 12–17 on May 28, 2021, and later for children aged 5–11 on November 25, 2021 (European Medicines Agency, 2021a; 2021b). Following these approvals, Germany began offering vaccinations to adolescents from June 7, 2021 (Presse- und Informationsamt der Bundesregierung, 2021b). During the summer months of 2021, the relative incidence rates among the age groups 5–11 and 12–17 were observed to be similar

**Table 2**
Model parameter estimates or parameters derived from literature for base model, NPIs, age groups, vaccine effects and VOCs.

| Parameter | Description | Estimate (RSE) or literature value (source) |
|---|---|---|
| **Initialization of the model** | | |
| R(0) | Population Rt value at study initialization (December 21, 2020) | 1.41 (30.9%) |
| $\gamma$ | Rate of exposed individual becoming a PCR-confirmed case [days$^{-1}$] | 1/7 (Dings et al., 2022) |
| C(0) | Number of exposed individuals per 100.000 individuals at study initialization (December 21, 2020) | 106 (60.1%) |
| **Rt factor during school opening for each age group in comparison to reference group** | | |
| $f_{school,0}$ | Rt factor age 0–4 | 0.378 (8.4%) |
| $f_{school,5}$ | Rt factor age 5–11 | 0.445 (9.5%) |
| $f_{school,12}$ | Rt factor age 12–17 | 0.555 (8.6%) |
| $f_{school,18}$ | Rt factor age 18–59 (reference group) | 1.09 (1.9%) |
| $f_{school,60}$ | Rt factor age >60 | 1.05 (3.4%) |
| **Rt factor during school closure with remote learning for each age group in comparison to reference group** | | |
| $f_{dist,0}$ | Relative Rt age 0–4 | 0.811 (5.8%) |
| $f_{dist,5}$ | Relative Rt age 5–11 | 1.13 (4.2%) |
| $f_{dist,12}$ | Relative Rt age 12–17 | 1.48 (2.4%) |
| $f_{dist,18}$ | Relative Rt age 18–59 (reference group) | $f_{school,18}$ |
| $f_{dist,60}$ | Relative Rt age >60 | 0.528 (3.1%) |
| **Rt factor during school holiday for each age group in comparison to reference group** | | |
| $f_{holiday,0}$ | Relative Rt age 0–4 | 0.511 (13.4%) |
| $f_{holiday,5}$ | Relative Rt age 5–11 | 0.963 (5%) |
| $f_{holiday,12}$ | Relative Rt age 12–17 | 1.48 (4.8%) |
| $f_{holiday,18}$ | Relative Rt age 18–59 (reference group) | $f_{school,18}$ |
| $f_{holiday,60}$ | Relative Rt age >60 | 0.524 (7.9%) |
| **Rt changepoint and factor for nursery school children** | | |
| $CP_{NURS}$ | Approximated change date for nursery school attendance rules [days] | 616 (1.3%) = 2021/08/29 |
| $f_{nurs,0}$ | Rt factor after $CP_{NURS}$ age 0–4 | 0.464 (3.6%) |
| $f_{nurs,\neq 0}$ | Rt factor after $CP_{NURS}$ age $\neq$ 0–4 | 1 (fixed) |
| **Rt factor for infections with VOC BA4/5 in comparison to reference group** | | |
| $\alpha_{BA5/5,0}$ | Relative Rt change for infections with VOC BA4/5 age 0–4 | 0.306 (12.1%) |
| $\alpha_{BA5/5,5}$ | Relative Rt change for infections with VOC BA4/5 age 5–11 | 0.232 (11.1%) |
| $\alpha_{BA5/5,12}$ | Relative Rt change for infections with VOC BA4/5 age 12–17 | 0.518 (9.6%) |
| $\alpha_{BA5/5,18}$ | Relative Rt change for infections with VOC BA4/5 age 18–59 (reference) | 1(fixed) |
| $\alpha_{BA5/5,60}$ | Relative Rt change for infections with VOC BA4/5 age > 60 | 1.27 (8.8%) |
| **Vaccination effectiveness** | | |
| $fs_{WT/Alpha}$ | Fraction susceptible for WT or VOC Alpha after full vaccination | 0.08 (Dagan et al., 2021) |
| $fs_{0,Delta}$ | Fraction susceptible for VOC Delta age 0–17 after full vaccination | 0.1 (Lopez Bernal et al., 2021; Sheikh et al., 2021) |
| $fs_{18,Delta}$ | Fraction susceptible for VOC Delta age ≥18 after full vaccination | 0.2 (Lopez Bernal et al., 2021; Sheikh et al., 2021) |
| $fsb_{Delta}$ | Fraction susceptible for VOC Delta after booster vaccination | 0.1 (Fabiani et al., 2022) |
| $fs_{18,Delta}$ | Fraction susceptible for VOC Delta age ≥18 after full vaccination after change date $CP_{Vacc18}$ | 0.3 (Fabiani et al., 2022) |
| $CP_{Vacc18}$ | Change point for vaccination effectiveness $fi_{18,Delta}$ [days] | 636 (0.3%) = 2021/08/18 |
| $fs_{Omicron}$ | Fraction susceptible for VOC Omicron after full vaccination | 0.68 (10.6%) |
| $fsb_{Omicron}$ | Fraction susceptible for VOC Omicron after booster vaccination | 0.338 (10.1%) |

* WT = wild type, VOC = variant of concern, RSE = relative standard error.

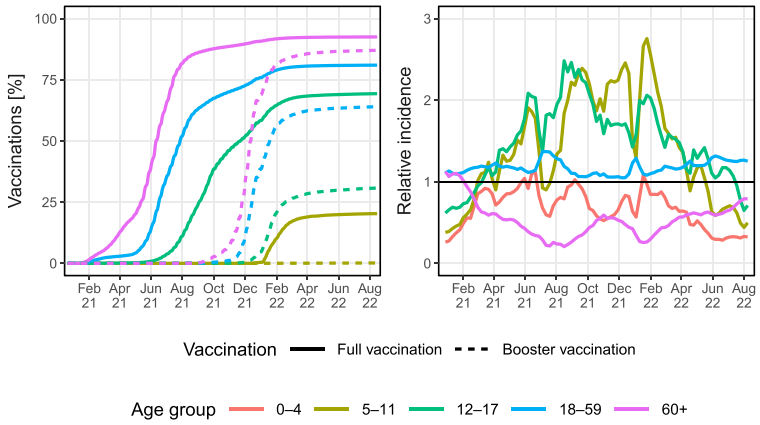


**Fig. 2.** Vaccinations per inhabitants [%] and relative incidences by age group. The relative incidence represents the incidence in the respective age group divided by the incidence across all age groups. Full vaccination: Individual received either one or two vaccinations depending on the respective vaccines' label. Booster vaccination: Individual received at least one additional vaccination after being fully vaccinated.

(Fig. 2). However, a distinct change occurred from October 2021 onwards. The age group of 12–17year-olds began to show a decrease in infection rates, a trend attributed to the rising number of vaccinations within this demographic (Fig. 2).

At the outset of 2022, following the authorization of COVID-19 vaccinations for children aged 5–11 years, Germany experienced its fifth wave of SARS-CoV-2 infections (week 52 2021 – week 21 2022). This wave was notable for recording the highest number of confirmed infections in the country to date. During this period, there were substantial differences in vaccination coverage across different age groups. Our analysis, as illustrated in Fig. 3, revealed a strong inverse correlation (Spearman's $\rho = -0.92$ (95%CI -0.95 to −0.86) for full vaccinations and $\rho = -0.93$, (95%CI -0.95 to −0.88) for booster vaccinations, with $p < 0.001$) between the proportion of the vaccinated population and the maximum incidence rate observed in each age group and federal state, emphasizing the vaccination's effectiveness in preventing infections.

### 3.2. Mathematical modeling

We adapted an SIR model to represent three primary stages: Susceptible individuals, infected individuals capable of transmitting the virus, and confirmed cases. The confirmed cases stage includes individuals who tested positive for SARS-CoV-2 via PCR and were recorded in the RKI register. A key element of our model is its focus on the dynamics of VOC transmission. It incorporates the critical understanding that individuals previously infected with the original strain or earlier VOCs may retain susceptibility to emergent variants, exemplified by the Omicron variant. To illustrate the structure of our model, Fig. 4 provides a schematic diagram that visually represents the progression of the population through these stages, with each circle in the diagram corresponding to an ODE.

The foundational framework depicted in Fig. 4 was initially developed for the entire population. Here, it was adapted and applied to each age group. This adaptation allowed a nuanced examination of virus transmission dynamics within distinct age groups. A critical component of our analysis involved assessing the contribution of the infected population to the transmission level of each age group. This assessment was conducted by aggregating the counts of infected individuals across age groups and applying weights proportional to the population size of each age group. Such weighting was crucial to accurately reflect the varying degrees of exposure and transmission risk across different age groups.

The effective reproductive number was determined for each age group and observed to undergo changes with the emergence of the BA4.5 variant. Additionally, significant changes in Rt were identified for NPIs implemented by federal states, comprising school holiday schedules, COVID-19 related school closures accompanied by remote learning as well as restrictions for nursing school attendance (all $p < 0.001$). The influence of these factors was assessed for each age group, highlighting the impacts of public health measures on different segments of the population. A changepoint of the effective

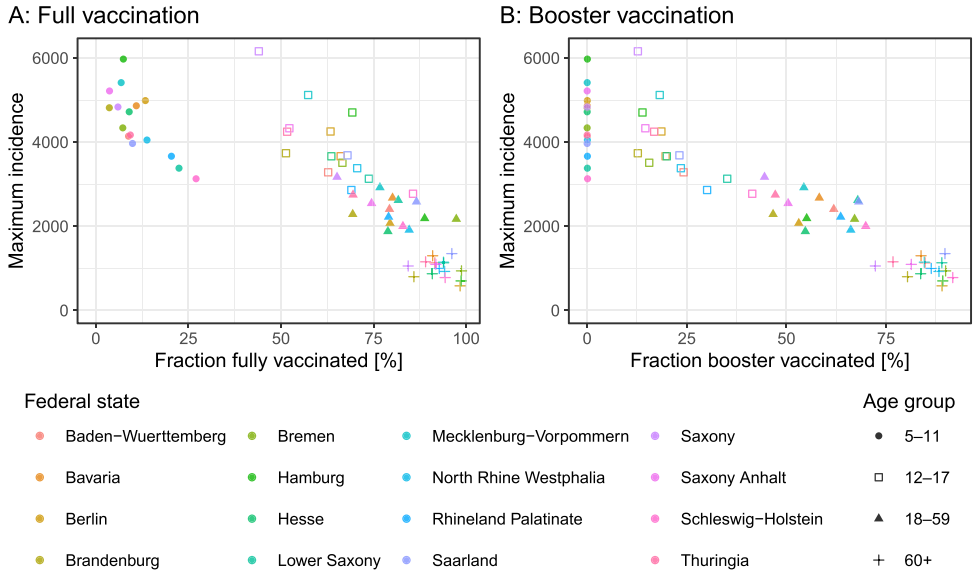


**Fig. 3.** Maximum weekly incidence/100 000 inhabitants from September 1, 2021 to August 8, 2022 vs vaccination rates for full vaccinations (A; Spearman's $\rho = -0.92$ with $p < 0.001$) and booster vaccinations (B; Spearman's $\rho = -0.93$ with $p < 0.001$) at the respective time point stratified by age group and federal state.

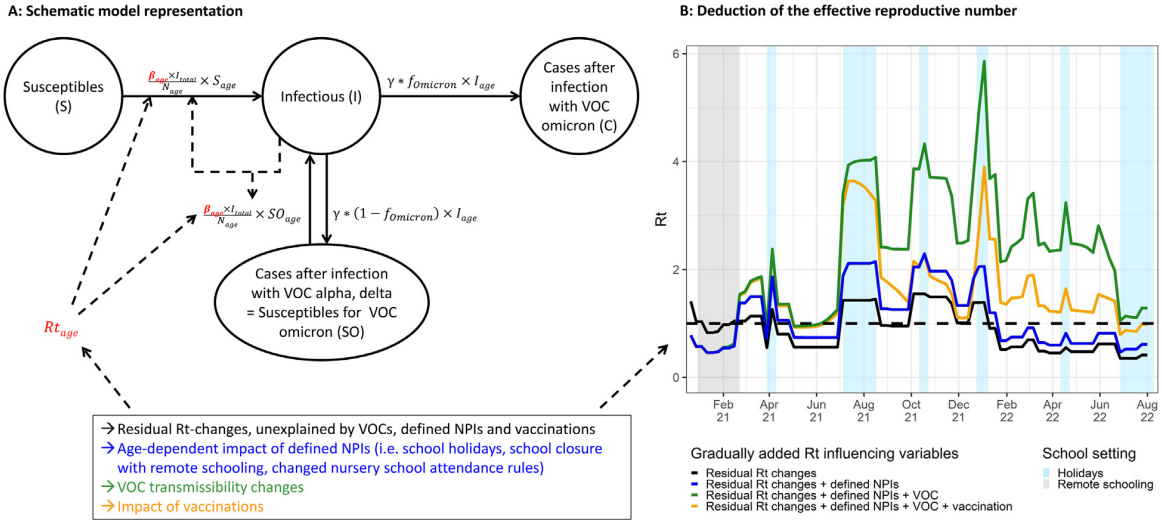


**Fig. 4.** A: Schematic representation of the model. Each full circle represents one ODE. Each of the age groups is represented by one of such systems of ODEs. Full arrows indicate the flow of individuals between compartments during the infection process. Dashed arrows indicate the influential processes. B: Effective reproductive number (Rt) vs time for exemplary state North Rhine Westphalia and age group 12–17 years, including the gradual adding of the impact of defined NPIs, VOCs and vaccinations on Rt. NPI: non-pharmaceutical intervention; VOC: variant of concern.

reproductive number was estimated for small children (age 0–4) on August 29, 2021, which coincided with altered attendance rules for sick children in nursing schools.

All fixed effect parameter estimates and model parameters derived from the literature are presented in Table 2.

For model stability and as a reference point, an average deviation from the median Rt obtained from the previously developed model (Dings et al., 2022) was estimated for the largest age group (ages 18–59 years, $\varepsilon_{18}$ in Table 2) and not corrected for implemented NPIs. For all other age groups, the deviations of Rt ($\varepsilon_{age}$ in Table 2) were estimated and corrected for effects of school-related NPIs ($f_{NPI,age}$ in Table 2). These parameter estimates express the relative difference of Rt between different age groups. Fig. 5 visually contrasts the resulting Rt-ratios, calculated by dividing the Rt of each age group or setting by that of the reference group, across the age groups under various settings. It reveals that during periods of school closure with enforced remote learning, the number of SARS-CoV-2 infections among the younger age groups (0–4, 5–11, and 12–17 years) was markedly reduced compared to periods of in-person schooling. Interestingly, the reduction in transmission was less pronounced during school holiday periods. Notably, among adolescents (12–17 years), the rate of infection was observed to increase during school holidays compared to regular school attendance periods.

Furthermore, a drop in virus transmission among infants aged 0–4 was observed towards the end of summer school holidays 2021 (estimated changepoint on August 29, 2021). This drop occurred at a time when many nursing schools tightened attendance rules for sick children with symptoms that can be related to SARS-CoV-2 infections. A significant change ($p < 0.001$) in vaccine effectiveness of full vaccination against VOC Delta (10%) was estimated for individuals 18 years and older on August 18, 2021 ($CP_{Vacc18}$) due to vaccine waning. At this time, the vast majority of vaccinees 18 years and older were already vaccinated, as displayed in Fig. 2. For the newly emerging VOC Omicron, the effectiveness of the vaccination $VE_{Omicron}$ was lower than the effectiveness of the booster vaccination ($VBE_{Omicron}$). This is in line with the waning effect of the vaccination against VOC Delta, as most vaccinees have been vaccinated for a long time at the emerge of VOC Omicron.

With the emergence of VOC BA4/5, a shift in transmissibility across age groups has been observed, as indicated by the discrepancies between model predictions and the reported infection numbers in Germany. The absence of other plausible explanations for this shift suggests a change in age-dependent susceptibility to VOC BA4/5 as the primary cause (Miyahara et al., 2023; Wiedenmann et al., 2023). Accordingly, new transmissibility factors for each age group ($\alpha_{BA5/5,age}$) were estimated to reflect this change.

We observed moderate variability in Rt across different states, with a coefficient of variation (CV) ranging from 4.4% to 50.3% (see Supplementary Materials Table 2 and Fig. 2). This variability highlighted the differences in transmission dynamics between states. A comprehensive set of Goodness-of-Fit (GoF) plots for all German federal states, highlighting variations in incidence trends across states and age groups, is detailed in Fig. 3 of the Supplementary Materials. Fig. 6, in the main text, exemplifies the model's accurate representation of data for selected federal states. The data clearly demonstrate that the temporal patterns of incidence vary not only among the federal states but also across different age groups.

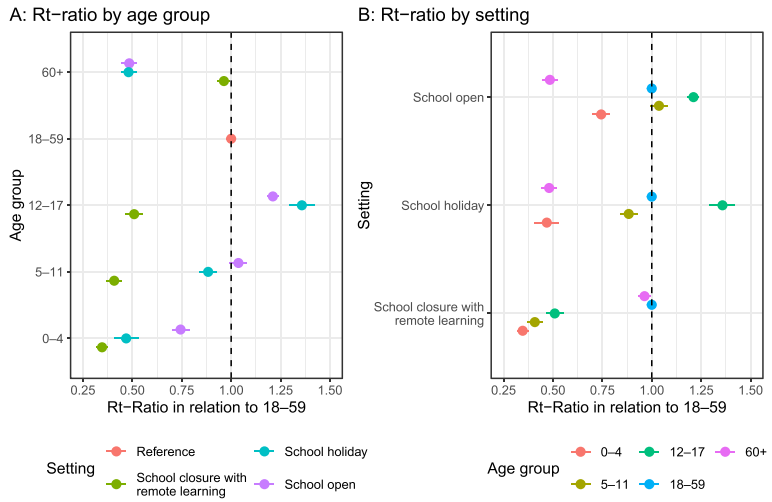


**Fig. 5.** Relative differences in Rt between age group under various NPIs in Germany. The reference category is the predominant age group (18–59 years). Data points represent the estimated Rt ratios, calculated by dividing the Rt of each age group or setting by that of the reference group. Error bars indicate the standard errors associated with these estimates.

Fig. 4 in the Supplementary Materials provides GOF plots that illustrate the model predictions of cumulative confirmed cases and incidence rates, segmented by age groups. Additionally, the figure includes plots of conditional weighted residuals for the predicted incidence rates.

Simulations were conducted to explore the potential impact of prioritizing vaccinations for the younger population (ages 5–17) on the spread of SARS-CoV-2. These simulations utilized vaccination rates for the adult and elderly populations (ages 18–59 and 60+, respectively) based on data from the German Federal Ministry of Health as of January 2023 (Bundesministerium für Gesundheit, 2023): 66% of the 18–59 age group and 85% of the 60+ age group had received booster vaccinations, while full vaccination rates stood at 17% and 5% for these groups, respectively. The vaccination scenarios for the younger population were categorized into three groups: no vaccinations; actual vaccination rates as of January 2023; and a high vaccination scenario, matching the booster rates of the 18–59 age group. The outcomes, illustrated in Fig. 7, indicate that vaccinating younger populations not only curtails the spread of infections among them but also offers indirect protection to the older age groups.

## 4. Discussion

This study utilized an adapted SIR model combined with NLME modeling techniques to analyze the spread of SARS-CoV-2 in Germany, stratified by age groups and federal states. Our findings reveal significant differences ($p < 0.001$) in the virus' spread among pre-school children (age 0–4), children (age 5–11), adolescents (age 12–17), adults (age 18–59), and the elderly (age 60+). Notably, the differential impact of NPIs, emergence of VOCs, and vaccination rates across these age groups provided insights into the dynamics of pandemic control and management.

In our analysis, the transition to remote learning has been instrumental in safeguarding children and adolescents from SARS-CoV-2 infections. This measure effectively decreased exposure risks in these younger age groups. Nonetheless, this protective strategy for the youth has coincided with an increased infection risk among the elderly, particularly those over 60 years of age, who are at the highest risk for severe outcomes from SARS-CoV-2 infections. This observation marks a deviation from the patterns observed during school holidays and periods when schools were operational, where the elderly were less frequently infected relative to the general population, benefiting from focused protective measures. The paradoxical increase in the elderly's infection risk during remote schooling periods could be attributed to the shift in caregiving roles, with grandparents more frequently stepping in to care for children while parents were occupied with work. This scenario likely facilitated greater virus transmission to the elderly. Evidence of this effect can be found in several studies (Chung et al., 2023; de Leeuw et al., 2023; Gilligan et al., 2020; Plagg et al., 2021; Stokes & Patterson, 2020).

To accurately assess the impact of school holidays on infection rates, analyzing data from the German federal states offered a unique advantage due to the staggered timing of school holidays across different states (von Bismarck-Osten et al., 2022). This variability allowed for a clearer distinction between the effects of school holidays and the overall trends in virus transmission. Specifically, among adolescents (age 12–17), the risk of infection remained notably high during school holidays. This sustained risk may be attributed to increased travel during these periods, as suggested by some studies (Plümper &

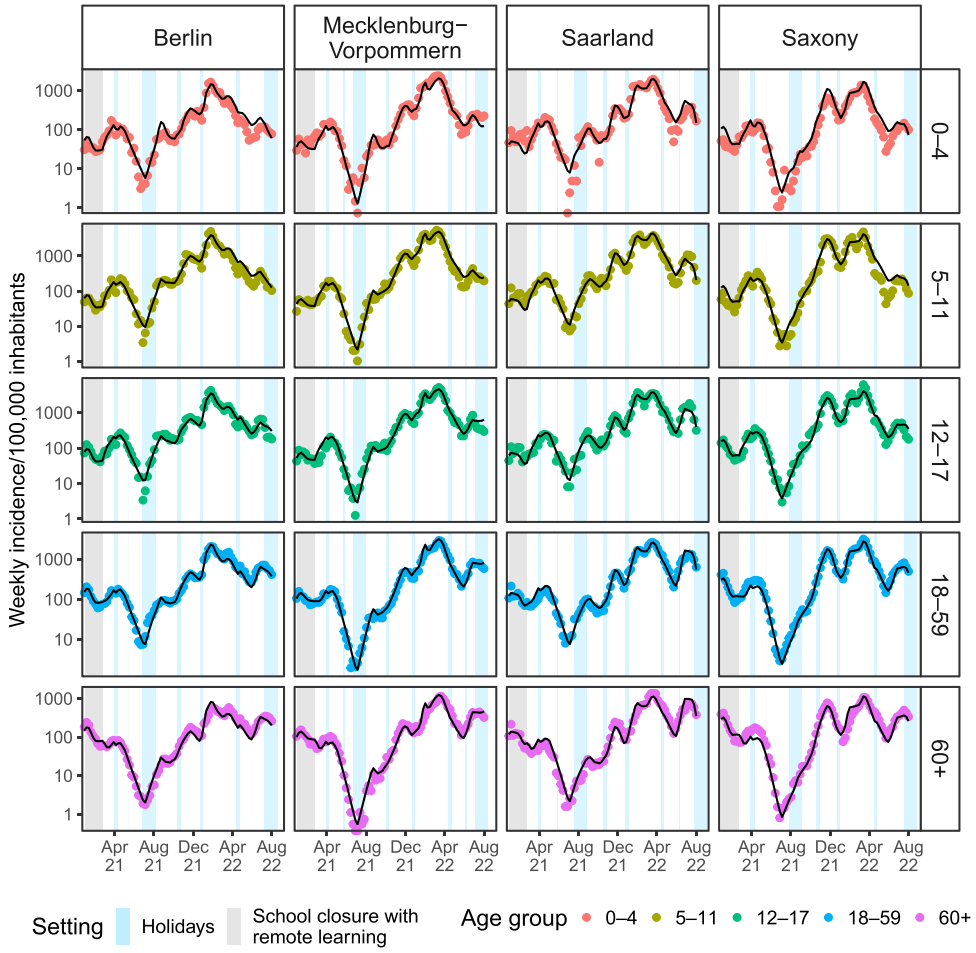


**Fig. 6.** Observed and model predicted weekly incidence/100 000 inhabitants by age group for four exemplary states. Points represent observations. Lines represent model predictions. Grey shaded areas indicate school closure with remote learning. Blue shaded areas indicate school holidays. While areas represent open schools. The full panel presenting all German states is shown in Fig. 4 of the Supplementary Materials.

Neumayer, 2021). Supporting evidence from a study conducted in the summer of 2021 highlighted that for adolescents, the opportunity to travel was among the least influential factors in their decision to get vaccinated (Rothoeft et al., 2023). This suggests adolescents did not perceive their holiday activities to be notably constrained by the pandemic. Generally, the risk of infection for adolescents when schools were operational were higher compared to younger children, likely due to factors such as larger class sizes (Goldstein et al., 2021).

The existing literature on the effectiveness of school closures as NPI presents mixed results (Walsh et al., 2021). While aligning with some studies (Mendez-Brito et al., 2021), the findings of the present simulations, showing that the shift to remote learning proved to be a crucial step in notably lowering infection rates among children and adolescents, differ from the results of a quasi-experimental study conducted in Germany that indicated that neither the summer nor the fall school closures significantly contained the spread of the virus among children or older generations (von Bismarck-Osten et al., 2022). Additionally, Bismarck-Osten and coworkers found no evidence that the return to full-capacity schooling after summer holidays increased infections among children or adults and the number of infections among children was found to increase during the last weeks of the summer holiday and decrease in the first weeks after schools reopened, attributed to travel returnees. While the authors did not explore the effects of VOCs, our analysis expands on this by offering a more detailed examination that includes the impacts of vaccinations and specific VOCs.

In particular, the model-based exploratory analysis comparing age-stratified incidence rates across German federal states with the progression of the 2021 vaccination campaign revealed insightful trends. Following the spring 2021 prioritization of vaccinations for the elderly (60+), a notable decrease in infection rates was observed in this age group during the summer, aligning with the vaccination strategy. In contrast, school-aged children and adolescents (5–11 and 12–17 years old)

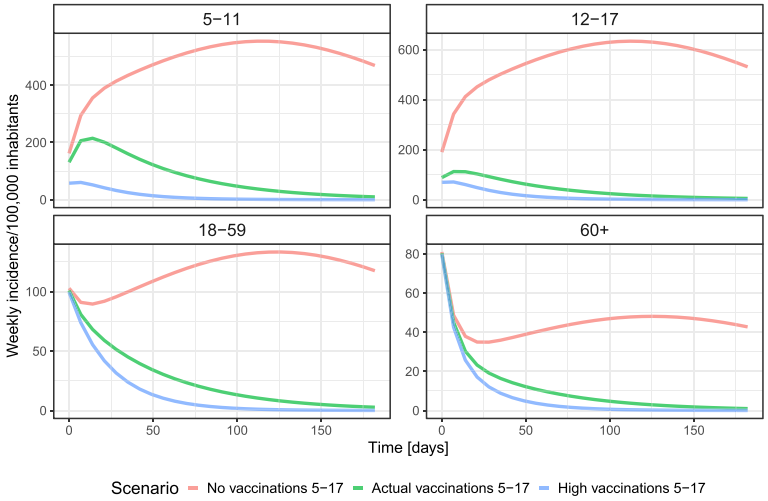


**Fig. 7.** Simulations comparing vaccination rates among younger populations (ages 5–11 and 12–17) under three distinct scenarios. Red lines depict the baseline scenario where the younger cohorts are unvaccinated. Green lines represent the real-world scenario, reflecting the vaccination uptake among these age groups as observed in January 2023. Blue lines illustrate a hypothetical scenario where young individuals are vaccinated at rates comparable to those seen in the 18–50 age group as of January 2023. In all scenarios, vaccination rates among older groups (aged 18–59 and 60+ years) are held constant.

experienced the highest incidence rates during the summer of 2021. However, from October 2021, a reduction in infections among adolescents (age 12–17) could be observed, correlating with the expansion of vaccination efforts to this age group. This temporal association suggests a potential impact of vaccination efforts on reducing infection rates. The relationship between vaccination campaigns and infection dynamics is further explored by analyzing the peak weekly infection numbers in conjunction with vaccination rates across various age groups and federal states. In this context, a robust and statistically significant correlation could be identified between the proportion of the population that received full vaccination, those administered booster doses, and the observed peak incidence rates (both $p < 0.001$ and Spearman's $\rho < -0.9$).

Incorporation of vaccination effects into the model allowed adjusting the infectivity for each age group in proportion to the corresponding vaccination coverage within that group. Differing degrees of immunity conferred by full vaccination and booster doses were modeled to reflect variations in protection levels across the population. The efficacy of vaccines against infections caused by the SARS-CoV-2 WT, as well as the Alpha and Delta VOCs, was parameterized based on efficacy data derived from the literature (Dagan et al., 2021; Lopez Bernal et al., 2021; Sheikh et al., 2021), which also accounted for the waning of vaccine-induced immunity over time (Fabiani et al., 2022). For the Omicron VOC, in the absence of specific studies addressing vaccine efficacy at the time of model development, efficacy rates for full and booster vaccination were estimated at 32% and 66.2%, respectively. These estimates align with the observed reduced vaccine effectiveness against the Omicron variant reported in subsequent research (Chenchula et al., 2022; Jacobsen et al., 2022; Khoury et al., 2021; Zou et al., 2022). In Germany, vaccines were initially offered to the elderly and those in high-risk jobs. The outcomes of our simulations support the effectiveness of this strategy and further reveal the added benefit of vaccinating younger groups, which indirectly safeguards the broader community.

Our study adds to the existing body of scholarly literature on the effectiveness of school closure on the spread of SARS-CoV-2. However, while most studies on this topic are susceptible to confounding due to the simultaneous implementation of other NPIs, vaccinations and the emerge of VOCs (Walsh et al., 2021), our study integrated comprehensive age- and federal state-stratified data coupled with an analysis approach exploiting fixed and random effects. Thereby, our study provides a more contextual insight into the spread of SARS-CoV-2 across different age groups and federal states in Germany, highlighting the interplay between NPIs, vaccinations, and VOCs.

On the other hand, this study encounters several limitations that must be acknowledged. A primary limitation arises from the method of recording vaccination data, which is based on the site of vaccination rather than the individual's place of residency. In contrast to this, confirmed cases were reported based on the individual's place of residency. This discrepancy introduces a potential source of error in estimating the vaccinated population fraction, particularly in federal states with smaller populations where cross-state vaccinations are more impactful. This discrepancy was notably observed in the city states Bremen and Hamburg which reached vaccination coverages of 99.0% and 99.3%, respectively, in the age group of 60+ when vaccination numbers are compared to the number of inhabitants. Additionally, the stratification of vaccination data into specific age groups was constrained by data availability, leading to non-uniform age group distributions. This limitation restricts the precision of our model, especially in accurately incorporating infection patterns across different age groups, as it prevented the use of contact matrices to model the age-specific transmission of infections.

A major limitation arises from the availability of data regarding the number of infections. Our analysis relies on confirmed SARS-CoV-2 infection counts which necessitates the assumption of a consistent ratio of undisclosed or unconfirmed cases across all age groups and over time. Various attempts have been made to estimate the number of undetected infections by leveraging case-fatality ratios, test-positive rates or data from seroprevalence studies (Barbarossa et al., 2020; Rocchetti et al., 2020; Schneble et al., 2021; Staerk et al., 2021). However, these attempts were mostly limited to describing the situation in Germany in the year 2020. Since the beginning of 2021, seroprevalence studies contained less informative value, as seropositivity could be obtained via infection and vaccination. Additionally, a shift in the age-dependent case-fatality ratio was already discussed to occur during the second wave of infections (Schneble et al., 2021) and even before the emergence of the first VOC. Hence, leveraging case-fatality ratios for the estimation of undetected cases is an intractable challenge with the emergence of VOCs and vaccinations. Moreover, due to the lack of individual-level vaccination data in Germany, it was not possible to implement a time-dependent decline in vaccine efficacy. Instead, a reduced efficacy against the VOC Delta variant was modeled using a change point as described in the Methods section. Lastly, one should account for variability in testing strategies, which could affect the accuracy of estimated model parameters (Nunes et al., 2024). However, the test positivity rate was not available stratified by age group, which rendered its informational content less valuable for our purpose. Amidst the unknown proportion of undetected cases, the implementation of routine screening among children through Point-of-Care antigen tests in schools, contrasted with the selective testing of adults, introduces a bias that may overestimate or underestimate the actual infection rates within these groups, respectively. Particularly, the shift to remote schooling and the consequent reduction in routine testing among children could obscure the true rate of asymptomatic infections, potentially overstating the impact of school closures on infection rates in this age group. The study acknowledges the challenge of capturing the varied implementation of NPIs across federal states yet offers insights into their diverse impacts. Given the complexity and varied nature of NPIs, coupled with the constraints in age stratification, our study focused selectively on key NPIs that directly affected younger age groups, notably policies regarding the operation and closure of schools. This selective consideration may not fully capture the comprehensive impact of NPIs on virus transmission dynamics across all demographics and settings.

## 5. Conclusions

In this study, we employed mathematical modeling to dissect the interplay between NPIs, vaccination strategies, and the dynamics of SARS-CoV-2 spread across different age groups within the German population. Our findings underscore the differential impact of school closures and vaccination efforts on modulating infection rates among children, adolescents, and the elderly. Key insights reveal that remote schooling effectively reduced viral spread among the youth, whereas vacation periods saw elevated transmission rates among adolescents, suggesting a nuanced role of behavioral factors in infection dynamics. Notably, the initial prioritization of vaccinations for the elderly and high-risk occupations, followed by extended coverage to younger demographics, demonstrated a discernible reduction in infection rates across all age groups, corroborated by a significant correlation ($p < 0.001$) between vaccination rates and lowered incidence peaks.

## Conflict of interest

The authors declare that they have no known competing financial interests or personal relationships that could have appeared to influence the work reported in this paper.

## CRediT authorship contribution statement

**Christiane Dings:** Writing – review & editing, Writing – original draft, Visualization, Methodology, Investigation, Formal analysis, Data curation. **Dominik Selzer:** Writing – review & editing, Supervision, Methodology, Conceptualization. **Nicola Luigi Bragazzi:** Formal analysis, Writing – review & editing. **Eva Möhler:** Writing – review & editing. **Markus Wenning:** Writing – review & editing. **Thomas Gehrke:** Writing – review & editing. **Ulf Richter:** Writing – review & editing. **Alexandra Nonnenmacher:** Writing – review & editing. **Folke Brinkmann:** Writing – review & editing. **Tobias Rothoeft:** Writing – review & editing. **Michael Zemlin:** Writing – review & editing. **Thomas Lücke:** Writing – review & editing. **Thorsten Lehr:** Writing – review & editing, Supervision, Project administration, Methodology, Conceptualization.

## Declaration of competing interest

The authors declare that they have no known competing financial interests or personal relationships that could have appeared to influence the work reported in this paper.

## Acknowledgements

Thorsten Lehr was funded by the European Union Horizon 2021 EUVABECO (grant 101132545). Views and opinions expressed are however those of the author(s) only and do not necessarily reflect those of the European Union. Neither the European Union nor the granting authority can be held responsible for them.

## Appendix A. Supplementary data

Supplementary data to this article can be found online at https://doi.org/10.1016/j.idm.2024.07.004.

## References


Arabi, M., Al-Najjar, Y., Sharma, O., Kamal, I., Javed, A., Gohil, H. S., Paul, P., Al-Khalifa, A. M., Laws, S., & Zakaria, D. (2023). Role of previous infection with SARS-CoV-2 in protecting against omicron reinfections and severe complications of COVID-19 compared to pre-omicron variants: A systematic review. *BMC Infectious Diseases, 23*(1), 432. https://doi.org/10.1186/s12879-023-08328-3

Bar-On, Y. M., Goldberg, Y., Mandel, M., Bodenheimer, O., Freedman, L., Alroy-Preis, S., Ash, N., Huppert, A., & Milo, R. (2021). Protection against covid-19 by BNT162b2 booster across age groups. *New England Journal of Medicine, 385*(26), 2421–2430. https://doi.org/10.1056/NEJMoa2115926

Barbarossa, M. V., Fuhrmann, J., Meinke, J. H., Krieg, S., Varma, H. V., Castelletti, N., & Lippert, T. (2020). Modeling the spread of COVID-19 in Germany: Early assessment and possible scenarios. *PLoS One, 15*(9), Article e0238559. https://doi.org/10.1371/journal.pone.0238559

Bundesministerium für Gesundheit. (2023). COVID-19 impfdashboard. https://impfdashboard.de/.

Chemaitelly, H., AlMukdad, S., Ayoub, H. H., Altarawneh, H. N., Coyle, P., Tang, P., Yassine, H. M., Al-Khatib, H. A., Smatti, M. K., Hasan, M. R., Al-Kanaani, Z., Al-Kuwari, E., Jeremijenko, A., Kaleeckal, A. H., Latif, A. N., Shaik, R. M., Abdul-Rahim, H. F., Nasrallah, G. K., Al-Kuwari, M. G., … Abu-Raddad, L. J. (2022). Covid-19 vaccine protection among children and adolescents in Qatar. *New England Journal of Medicine, 387*(20), 1865–1876. https://doi.org/10.1056/NEJMoa2210058

Chenchula, S., Karunakaran, P., Sharma, S., & Chavan, M. (2022). Current evidence on efficacy of COVID-19 booster dose vaccination against the omicron variant: A systematic review. *Journal of Medical Virology, 94*(7), 2969–2976. https://doi.org/10.1002/jmv.27697

Chung, P.-C., Chen, K. J., Chang, H.-M., & Chan, T.-C. (2023). Evaluating the effectiveness of school closure in {COVID-19-related} syndromes from community-based syndromic surveillance: Longitudinal observational study. *Interact. J. Med. Res., 12*, Article e44606.

Dagan, N., Barda, N., Kepten, E., Miron, O., Perchik, S., Katz, M. A., Hernán, M. A., Lipsitch, M., Reis, B., & Balicer, R. D. (2021). BNT162b2 mRNA covid-19 vaccine in a nationwide mass vaccination setting. *New England Journal of Medicine, 384*(15), 1412–1423. https://doi.org/10.1056/NEJMoa2101765

de Leeuw, S., Haelermans, C., Jacobs, M., van der Velden, R., van Vugt, L., & van Wetten, S. (2023). The role of family composition in students' learning growth during the COVID-19 pandemic. *Journal of Marriage and Family, 85*(3), 807–828. https://doi.org/10.1111/jomf.12912

Dings, C., Götz, K. M., Och, K., Sihinevich, I., Werthner, Q., Smola, S., Bliem, M., Mahfoud, F., Volk, T., Kreuer, S., Rissland, J., Selzer, D., & Lehr, T. (2022). Model-based analysis of SARS-CoV-2 infections, hospitalization and outcome in Germany, the federal states and districts. *Viruses, 14*(10), 2114. https://doi.org/10.3390/v14102114

Ellen Ehni, C. M. (2021). *ARD-DeutschlandTREND januar 2021.* https://www.tagesschau.de/inland/deutschlandtrend-2471.pdf.

European Medicines Agency. (2021a). Comirnaty COVID-19 vaccine: EMA recommends approval for children aged 5 to 11. https://www.ema.europa.eu/en/news/comirnaty-covid-19-vaccine-ema-recommends-approval-children-aged-5-11.

European Medicines Agency. (2021b). First COVID-19 vaccine approved for children aged 12 to 15 in EU. https://www.ema.europa.eu/en/news/first-covid-19-vaccine-approved-children-aged-12-15-eu.

Fabiani, M., Puopolo, M., Morciano, C., Spuri, M., Spila Alegiani, S., Filia, A., D'Ancona, F., Del Manso, M., Riccardo, F., Tallon, M., Proietti, V., Sacco, C., Massari, M., Da Cas, R., Mateo-Urdiales, A., Siddu, A., Battilomo, S., Bella, A., Palamara, A. T., … Pezzotti, P. (2022). Effectiveness of mRNA vaccines and waning of protection against SARS-CoV-2 infection and severe covid-19 during predominant circulation of the delta variant in Italy: Retrospective cohort study. *BMJ, 376*, Article e069052. https://doi.org/10.1136/bmj-2021-069052

Freundl, V., Lergetporer, P., & Zierow, L. (2021). Germany's education policy during the COVID-19 crisis. *Zeitschrift für Politikwissenschaft, 31*(1), 109–116. https://doi.org/10.1007/s41358-021-00262-7

Gilligan, M., Suitor, J. J., Rurka, M., & Silverstein, M. (2020). Multigenerational social support in the face of the COVID-19 pandemic. *Journal of Family Theory & Review, 12*(4), 431–447. https://doi.org/10.1111/jftr.12397

Goldstein, E., Lipsitch, M., & Cevik, M. (2021). On the effect of age on the transmission of SARS-CoV-2 in households, schools, and the community. *The Journal of Infectious Diseases, 223*(3), 362–369. https://doi.org/10.1093/INFDIS/JIAA691

Hindmarsh, A. C., & Petzold, L. R. (2005). LSODA, ordinary differential equation solver for stiff or non-stiff system. https://inis.iaea.org/search/search.aspx?orig_q=RN:41086668.

Hume, S., Brown, S. R., & Mahtani, K. R. (2023). School closures during {COVID-19}: An overview of systematic reviews. *BMJ Evid. Based Med., 28*(3), 164–174.

Hussong, J., Möhler, E., Kühn, A., Wenning, M., Gehrke, T., Burckhart, H., Richter, U., Nonnenmacher, A., Zemlin, M., Lücke, T., Brinkmann, F., Rothoeft, T., & Lehr, T. (2022). Mental health and health-related quality of life in German adolescents after the third wave of the COVID-19 pandemic. *Children, 9*(6), 780. https://doi.org/10.3390/children9060780

Jacobsen, H., Strengert, M., Maaß, H., Ynga Durand, M. A., Katzmarzyk, M., Kessel, B., Harries, M., Rand, U., Abassi, L., Kim, Y., Lüddecke, T., Metzdorf, K., Hernandez, P., Ortmann, J., Heise, J. K., Castell, S., Gornyk, D., Glöckner, S., Melhorn, V., … Cicin-Sain, L. (2022). Diminished neutralization responses towards SARS-CoV-2 Omicron VoC after mRNA or vector-based COVID-19 vaccinations. *Scientific Reports 2022, 12*(1), 1–11. https://doi.org/10.1038/s41598-022-22552-y, 12(1).

Karlsson, M. O., & Savic, R. M. (2007). Diagnosing model diagnostics. *Clinical Pharmacology & Therapeutics, 82*(1), 17–20. https://doi.org/10.1038/sj.clpt.2007.6100241

Khoury, D. S., Steain, M., Triccas, J. A., Sigal, A., Davenport, M. P., & Cromer, D. (2021). A meta-analysis of early results to predict vaccine efficacy against omicron. *medRxiv*. https://doi.org/10.1101/2021.12.13.21267748, 2021.12.13.21267748.

Lionello, L., Stranges, D., Karki, T., Wiltshire, E., Proietti, C., Annunziato, A., Jansa, J., & Severi, E. (2022). Non-pharmaceutical interventions in response to the COVID-19 pandemic in 30 European countries: The ECDC–JRC response measures database. *Euro Surveillance, 27*(41). https://doi.org/10.2807/1560-7917.ES.2022.27.41.2101190

Lopez Bernal, J., Andrews, N., Gower, C., Gallagher, E., Simmons, R., Thelwall, S., Stowe, J., Tessier, E., Groves, N., Dabrera, G., Myers, R., Campbell, C. N. J., Amirthalingam, G., Edmunds, M., Zambon, M., Brown, K. E., Hopkins, S., Chand, M., & Ramsay, M. (2021). Effectiveness of covid-19 vaccines against the B. 1.617.2 (delta) variant. *New England Journal of Medicine, 385*(7), 585–594. https://doi.org/10.1056/NEJMOA2108891/SUPPL_FILE/NEJMOA2108891_DISCLOSURES.PDF

Ludvigsson, J. F. (2020). Children are unlikely to be the main drivers of the COVID-19 pandemic – a systematic review. *Acta Paediatrica, International Journal of Paediatrics, 109*(8), 1525–1530. https://doi.org/10.1111/apa.15371

Markov, P. V., Ghafari, M., Beer, M., Lythgoe, K., Simmonds, P., Stilianakis, N. I., & Katzourakis, A. (2023). The evolution of {SARS-CoV-2. *Nature Reviews Microbiology, 21*(6), 361–379.

Mendez-Brito, A., El Bcheraoui, C., & Pozo-Martin, F. (2021). Systematic review of empirical studies comparing the effectiveness of non-pharmaceutical interventions against {COVID-19. *Journal of Infection, 83*(3), 281–293.

Miyahara, R., Tamura, K., Kato, T., Nakazaki, M., Otani, K., Ko, Y. K., Kamigaki, T., Arima, Y., Tani, H., Oishi, K., & Suzuki, M. (2023). SARS-CoV-2 variants and age-dependent infection rates among household and nonhousehold contacts. *Emerging Infectious Diseases, 29*(8), 1648–1650. https://doi.org/10.3201/eid2908.221582

Mould, D. R., & Upton, R. N. (2012). Basic concepts in population modeling, simulation, and model-based drug development. *CPT: Pharmacometrics & Systems Pharmacology, 1*(1), 1–14. https://doi.org/10.1038/psp.2012.4

Nunes, M. C., Thommes, E., Fröhlich, H., Flahault, A., Arino, J., Baguelin, M., Biggerstaff, M., Bizel-Bizellot, G., Borchering, R., Cacciapaglia, G., Cauchemez, S., Barbier–Chebbah, A., Claussen, C., Choirat, C., Cojocaru, M., Commaille-Chapus, C., Hon, C., Kong, J., Lambert, N., … Coudeville, L. (2024). Redefining

pandemic preparedness: Multidisciplinary insights from the CERP modelling workshop in infectious diseases, workshop report. *Infectious Disease Modelling, 9*(2), 501–518. https://doi.org/10.1016/j.idm.2024.02.008
Paulus, F. W., Joas, J., Gerstner, I., Kühn, A., Wenning, M., Gehrke, T., Burckhart, H., Richter, U., Nonnenmacher, A., Zemlin, M., Lücke, T., Brinkmann, F., Rothoeft, T., Lehr, T., & Möhler, E. (2022). Problematic internet use among adolescents 18 Months after the onset of the COVID-19 pandemic. *Children, 9*(11), 1724. https://doi.org/10.3390/children9111724
Plagg, B., Flarer, H., Conca, A., Wiedermann, C. J., Engl, A., Piccoliori, G., Mairhofer, S., Barbieri, V., & Eisendle, K. (2021). Who is watching the children? A quantitative analysis of strategies for reconciling work and parenting during lockdown in northern Italy. *International Journal of Environmental Research and Public Health, 18*(21), Article 11174. https://doi.org/10.3390/IJERPH182111174/S1
Plümper, T., & Neumayer, E. (2021). Fueling the covid-19 pandemic: Summer school holidays and incidence rates in German districts. *Journal of Public Health, 43*(3), e415–e422. https://doi.org/10.1093/PUBMED/FDAB080
Presse- und Informationsamt der Bundesregierung. (2021a). *Impfangebot für alle über 12 Jahre*. https://www.bundesregierung.de/breg-de/themen/coronavirus/impfangebot-12-jahre-1947904.
Presse- und Informationsamt der Bundesregierung. (2021b). Zulassung für Kinder ab 12 Jahre durch EU-Kommission. https://www.bundesregierung.de/breg-de/service/archiv/biontech-zulassung-jugendliche-1919360.
Pritchard, E., Matthews, P. C., Stoesser, N., Eyre, D. W., Gethings, O., Vihta, K.-D., Jones, J., House, T., VanSteenHouse, H., Bell, I., Bell, J. I., Newton, J. N., Farrar, J., Diamond, I., Rourke, E., Studley, R., Crook, D., Peto, T. E. A., Walker, A. S., & Pouwels, K. B. (2021). Impact of vaccination on new SARS-CoV-2 infections in the United Kingdom. *Nature Medicine, 27*(8), 1370–1378. https://doi.org/10.1038/s41591-021-01410-w
Ravens-Sieberer, U., Otto, C., Kaman, A., Adedeji, A., Devine, J., Napp, A.-K., Erhart, M., Becker, M., Blanck-Stellmacher, U., Löffler, C., Schlack, R., & Hurrelmann, K. (2020). Mental health and quality of life in children and adolescents during the COVID-19 pandemic. *Deutsches Ärzteblatt International, 117*(48), 828. https://doi.org/10.3238/arztebl.2020.0828
Robert Koch-Institut. (2021). RKI - Empfehlungen der STIKO - Mitteilung der STIKO zur Aktualisierung der COVID-19-Impfempfehlung für Kinder und Jugendliche. https://www.rki.de/DE/Content/Kommissionen/STIKO/Empfehlungen/PM_2021-08-16.html. (Accessed 16 August 2021).
Robert Koch-Institut. (2022). COVID-19-Impfungen in deutschland. https://doi.org/10.5281/zenodo.7408098.
Robert Koch-Institut. (2023). SARS-CoV-2 Sequenzdaten aus Deutschland. https://doi.org/10.5281/zenodo.8431311.
Robert Koch-Institut. (2024). SurvStat@RKI 2.0. https://survstat.rki.de/.
Rocchetti, I., Böhning, D., Holling, H., & Maruotti, A. (2020). Estimating the size of undetected cases of the COVID-19 outbreak in europe: An upper bound estimator. *Epidemiologic Methods, 9*(s1). https://doi.org/10.1515/em-2020-0024
Roemer, C., Sheward, D. J., Hisner, R., Gueli, F., Sakaguchi, H., Frohberg, N., Schoenmakers, J., Sato, K., O'Toole, Á., Rambaut, A., Pybus, O. G., Ruis, C., Murrell, B., & Peacock, T. P. (2023). {SARS-CoV-2} evolution in the Omicron era. *Nat. Microbiol., 8*(11), 1952–1959.
Rothoeft, T., Brinkmann, F., Maier, C., Selzer, D., Dings, C., Kuehn, A., Möhler, E., Grote, H., Nonnenmacher, A., Wenning, M., Zemlin, M., Richter, U., Lehr, T., & Lücke, T. (2023). Motivations for adolescent COVID-19 vaccination: A comparative study of adolescent and caregiver perspectives in Germany. *Children, 10*(12), 1890. https://doi.org/10.3390/children10121890
Sadarangani, M., Abu Raya, B., Conway, J. M., Iyaniwura, S. A., Falcao, R. C., Colijn, C., Coombs, D., & Gantt, S. (2021). Importance of COVID-19 vaccine efficacy in older age groups. *Vaccine, 39*(15), 2020–2023. https://doi.org/10.1016/j.vaccine.2021.03.020
Schneble, M., De Nicola, G., Kauermann, G., & Berger, U. (2021). A statistical model for the dynamics of COVID-19 infections and their case detection ratio in 2020. *Biometrical Journal, 63*(8), 1623–1632. https://doi.org/10.1002/bimj.202100125
Sheikh, A., McMenamin, J., Taylor, B., & Robertson, C. (2021). SARS-CoV-2 delta VOC in scotland: Demographics, risk of hospital admission, and vaccine effectiveness. *The Lancet, 397*(10293), 2461–2462. https://doi.org/10.1016/S0140-6736(21)01358-1
Staerk, C., Wistuba, T., & Mayr, A. (2021). Estimating effective infection fatality rates during the course of the COVID-19 pandemic in Germany. *BMC Public Health, 21*(1), 1073. https://doi.org/10.1186/s12889-021-11127-7
Steiger, E., Rass, S., Seidel, A., Kroll, L., & Czihal, T. (2021). COVID-19 vaccination in medical practices in Germany. *Deutsches Ärzteblatt International, 118*(44), 756–757. https://doi.org/10.3238/arztebl.m2021.0354
Stokes, J. E., & Patterson, S. E. (2020). Intergenerational relationships, family caregiving policy, and COVID-19 in the United States. *Journal of Aging & Social Policy, 32*(4–5), 416–424. https://doi.org/10.1080/08959420.2020.1770031
Talic, S., Shah, S., Wild, H., Gasevic, D., Maharaj, A., Ademi, Z., Li, X., Xu, W., Mesa-Eguiagaray, I., Rostron, J., Theodoratou, E., Zhang, X., Motee, A., Liew, D., & Ilic, D. (2021). Effectiveness of public health measures in reducing the incidence of covid-19, SARS-CoV-2 transmission, and covid-19 mortality: Systematic review and meta-analysis. *BMJ, 375*, Article e068302. https://doi.org/10.1136/bmj-2021-068302
Taylor, L. (2021). Covid-19: Brazil's hospitals close to collapse as cases reach record high. *BMJ, n800*. https://doi.org/10.1136/bmj.n800
von Bismarck-Osten, C., Borusyak, K., & Schönberg, U. (2022). The role of schools in transmission of the {SARS-CoV-2} virus: Quasi-experimental evidence from Germany. *Economic Policy, 37*(109), 87–130.
Vygen-Bonnet, S., Koch, J., Bogdan, C., Harder, T., Heininger, U., Kling, K., Littmann, M., Meerpohl, J., Meyer, H., Mertens, T., Schmid-Küpke, N., Scholz, S., Terhardt, M., Treskova-Schwarzbach, M., Überla, K., van der Sande, M., Wichmann, O., Wicker, S., Wiedermann, U., … von Kries, R. (2020). *Beschluss und Wissenschaftliche Begründung der Ständigen Impfkommission (STIKO) für die COVID-19-Impfempfehlung* (Vol. 2, pp. 3–63). https://doi.org/10.25646/7755
Walsh, S., Chowdhury, A., Braithwaite, V., Russell, S., Birch, J. M., Ward, J. L., Waddington, C., Brayne, C., Bonell, C., Viner, R. M., & Mytton, O. T. (2021). Do school closures and school reopenings affect community transmission of {COVID-19}? A systematic review of observational studies. *BMJ Open, 11*(8), Article e053371.
Wang, Y. (2007). Derivation of various NONMEM estimation methods. *Journal of Pharmacokinetics and Pharmacodynamics, 34*(5), 575–593. https://doi.org/10.1007/s10928-007-9060-6
Wiedenmann, M., Ipekci, A. M., Araujo-Chaveron, L., Prajapati, N., Lam, Y. T., Alam, M. I., L'Huillier, A. G., Zhelyazkov, I., Heron, L., Low, N., & Goutaki, M. (2023). SARS-CoV-2 variants of concern in children and adolescents with COVID-19: A systematic review. *BMJ Open, 13*(10), Article e072280. https://doi.org/10.1136/bmjopen-2023-072280
Yuki, K., Fujiogi, M., & Koutsogiannaki, S. (2020). COVID-19 pathophysiology: A review. *Clinical Immunology, 215*, Article 108427. https://doi.org/10.1016/j.clim.2020.108427
Zou, Y., Huang, D., Jiang, Q., Guo, Y., & Chen, C. (2022). The vaccine efficacy against the SARS-CoV-2 omicron: A systemic review and meta-analysis. *Frontiers in Public Health, 10*. https://doi.org/10.3389/fpubh.2022.940956

## 4.3 Project III: Azelastine Effect on SARS-CoV-2 Viral Load

### *4.3.1 Reference*

**Pharmacometric modeling of the impact of azelastine nasal spray on SARS-CoV-2 viral load and related symptoms in COVID-19 patients.**
Christiane Dings, Peter Meiser, Frank Holzer, Michael Flegel, Dominik Selzer, Eszter Nagy, Ralph Mösges, Jens Peter Klussmann and Thorsten Lehr.
*Pharmaceutics* 2022;14(10):2059. DOI: 10.3390/pharmaceutics14102059[3]

### *4.3.2 Author Contributions*

Author contributions according to the contributor roles taxonomy (CRediT)[4,5] were as following:

| | |
|---|---|
| Christiane Dings | See Contribution Report (page ii) |
| Peter Meiser | Conceptualization, investigation, resources, data curation, writing — review & editing, supervision, funding acquisition |
| Frank Holzer | Conceptualization, resources, writing — review & editing |
| Michael Flegel | Writing — review & editing |
| Dominik Selzer | Writing — original draft preparation |
| Eszter Nagy | Writing — review & editing |
| Ralph Mösges | Conceptualization, resources, writing — review & editing |
| Jens Peter Klussmann | Writing — review & editing |
| Thorsten Lehr | Conceptualization, methodology, investigation, resources, writing — original draft preparation, writing — review & editing, supervision, project administration |

### *4.3.3 Copyright*

*pharmaceutics*

MDPI

*Article*

# Pharmacometric Modeling of the Impact of Azelastine Nasal Spray on SARS-CoV-2 Viral Load and Related Symptoms in COVID-19 Patients

**Christiane Dings [1,2], Peter Meiser [3], Frank Holzer [3], Michael Flegel [3], Dominik Selzer [1], Eszter Nagy [4], Ralph Mösges [5], Jens Peter Klussmann [6,7] and Thorsten Lehr [1,2,*]**

1 Department of Clinical Pharmacy, Saarland University, 66123 Saarbrücken, Germany
2 Saarmetrics GmbH, Starterzentrum 1, Universität des Saarlandes, 66123 Saarbrücken, Germany
3 URSAPHARM Arzneimittel GmbH, Industriestraße 35, 66129 Saarbrücken, Germany
4 CEBINA GmbH, Karl-Farkas-Gasse 22, 1030 Vienna, Austria
5 Faculty of Medicine, Institute of Medical Statistics and Computational Biology (IMSB), University of Cologne, Kerpener Str. 62, 50937 Cologne, Germany
6 Faculty of Medicine, Center for Molecular Medicine Cologne (CMMC), University of Cologne, Robert-Koch-Str. 21, 50931 Cologne, Germany
7 Department of Otorhinolaryngology, Faculty of Medicine and University Hospital Cologne, University of Cologne, Kerpener Str. 62, 50937 Cologne, Germany
* Correspondence: thorsten.lehr@mx.uni-saarland.de; Tel.: +49-681-302-70255

**Abstract:** The histamine-1 receptor antagonist azelastine was recently found to impact SARS-CoV-2 viral kinetics in a Phase 2 clinical trial (CARVIN). Thus, we investigated the relationship between intranasal azelastine administrations and viral load, as well as symptom severity in COVID-19 patients and analyzed the impact of covariates using non-linear mixed-effects modeling. For this, we developed a pharmacokinetic (PK) model for the oral and intranasal administration of azelastine. A one-compartment model with parallel absorption after intranasal administration described the PK best, covering both the intranasal and the gastro-intestinal absorption pathways. For virus kinetic and symptoms modeling, viral load and symptom records were gathered from the CARVIN study that included data of 82 COVID-19 patients receiving placebo or intranasal azelastine. The effect of azelastine on viral load was described by a dose–effect model targeting the virus elimination rate. An extension of the model revealed a relationship between COVID-19 symptoms severity and the number of infected cells. The analysis revealed that the intranasal administration of azelastine led to a faster decline in viral load and symptoms severity compared to placebo. Moreover, older patients showed a slower decline in viral load compared to younger patients and male patients experienced higher peak viral loads than females.

**Keywords:** COVID-19; SARS-CoV-2; azelastine; PK model; virus kinetic model



**Citation:** Dings, C.; Meiser, P.; Holzer, F.; Flegel, M.; Selzer, D.; Nagy, E.; Mösges, R.; Klussmann, J.P.; Lehr, T. Pharmacometric Modeling of the Impact of Azelastine Nasal Spray on SARS-CoV-2 Viral Load and Related Symptoms in COVID-19 Patients. *Pharmaceutics* **2022**, *14*, 2059. https://doi.org/10.3390/pharmaceutics14102059

Academic Editors: Victor Mangas Sanjuán and Inaki F. Troconiz

Received: 29 August 2022
Accepted: 20 September 2022
Published: 27 September 2022



## 1. Introduction

Since the emergence of SARS-CoV-2 in December 2019, treatment options for coronavirus disease (COVID-19) have been scarce. Hence, many previously approved compounds have been reassessed for drug repositioning regarding the treatment of acute COVID-19. Several potential candidates could be found in a retrospective study that used data mining of electronic health records and could associate the usage of several common antihistamines with lower incidence of SARS-CoV-2 infections [1]. One of the identified compounds was the histamine-1 receptor antagonist azelastine hydrochloride. Azelastine has been approved for the treatment of seasonal or perennial allergic rhinitis for more than 30 years. An azelastine nasal spray formulation is currently available at a concentration of 0.1% $w/v$ that is known to be well-tolerated, with bitter taste and somnolence being the most common side effects [2]. Patients older than 60 years with a history of previous

azelastine use showed a significantly lower rate of SARS-CoV-2 infections compared to patients without previous azelastine treatment (odds ratio 0.41, 95% CI 0.25–0.68) [1].

Independently, in vitro studies have shown that azelastine inhibits the interaction of the SARS-CoV-2 spike protein with the ACE2-receptor (EC50 = 3.834 µM) in a pseudovirus infection assay [3]. Tested for its direct antiviral activity on the infection of Vero E6 cells with SARS-CoV-2 isolate USA-UF-1/2020, azelastine was effective with an EC50 of 2.24 µg/mL [1]. Furthermore, daily 20 min treatment with 0.02% azelastine solution in assays with reconstituted human nasal tissue showed antiviral activity by reducing the viral particle numbers by >99.9% 48 h post infection [4].

Recently, the CARVIN study was performed to evaluate the effect of azelastine nasal spray on the SARS-CoV-2 viral load and infection-related symptoms in SARS-CoV-2 positive patients with mild symptoms who do not require inpatient treatment [5]. In this double-blind study, patients received either placebo, 0.02 or 0.1% azelastine nasal spray three times daily for 11 days of treatment. COVID-19 related symptoms were reported daily, and SARS-CoV-2 viral load was assessed from nasal swabs on seven occasions throughout the study. Here, after treatment, virus load was reduced in all groups ($p < 0.0001$) but was greater in the 0.1% group compared to placebo ($p = 0.007$). In a subset of patients (initial Ct < 25) viral load was strongly reduced on day 4 in the 0.1% group compared to placebo ($p = 0.005$). Negative PCR results appeared earlier and more frequently in the azelastine treated groups: being 18.5 and 21.4% in the 0.1 and 0.02% groups, respectively, compared to 0% for placebo on day 8 [5].

However, analyses of the underlying mechanisms and dose-effect relationships considering individual infection characteristics were missing. Here, mathematical mixed-effects modelling can be beneficial as variability between patients, such as different baseline viral loads, can be considered. Furthermore, the relationship between the local drug concentration, drug effect, viral replication and the occurrence of virus-related symptoms is complex and driven by non-linear time-dependent processes. Hence, mathematical modelling using non-linear mixed-effects techniques can provide meaningful insights regarding the underlying mechanisms.

This work has aimed to use non-linear mixed-effects modelling for (i) developing a pharmacokinetic (PK) model for azelastine, (ii) describing the effect of azelastine on viral load and symptoms of SARS-CoV-2 positive patients from the CARVIN study and (iii) exploring the impact of the covariates on viral load, infectivity, and symptoms.

## 2. Materials and Methods

### *2.1. Studies Included in the Analysis*

A PK model for azelastine was developed based on digitized literature data from 5 studies including data after nasal and oral application of azelastine [6–10] since no azelastine plasma concentrations were measured in the CARVIN study. The study was registered in the German Clinical Trial Register (DRKS-ID: DRKS00024520; Date of Registration in DRKS: 12/02/2021) and the EU Clinical Trials Register (EudraCT number: 2020-005544-34). For data digitalization, GetData Graph Digitizer (http://getdata-graph-digitizer.com, accessed on 28 August 2020, version 2.26.0.20) was used according to best practices proposed by Wojtyniak and coworkers [11].

To analyze the impact of azelastine on viral load and COVID-19 symptoms, clinical data from the double-blind CARVIN study were used [5]. Here, 90 COVID-19 patients were included that were recently tested positive for SARS-CoV-2 not requiring hospitalization nor being at risk for severe disease. Patients were randomized into one of three treatment groups: 1 mg/mL nasal spray (0.1% azelastine), 0.2 mg/mL nasal spray (0.02% azelastine) or placebo nasal spray. Treatment was applied as one puff per nostril three times a day.

For the assessment of viral load, daily quantitative PCR (qPCR) was performed from nasopharyngeal sampling swabs on days 1 to 5 and on days 8 and 11. For our analysis, patients were excluded when SARS-CoV-2 qPCR test results were negative for $\geq$5 of 7 measurements ($n = 8$). Single viral load measurements were excluded if the gene copy

numbers of the two measured genes (E and ORF1a/b gene) differed by more than two orders of magnitude. Our modeling analysis was performed using the measurements of the ORF1a/b gene.

During the study, patients had to document the severity of twenty COVID-19 related symptoms (anosmia, ageusia, cough, sore throat, shortness of breath, coryza, general weakness, headache, aching limb, loss of appetite, pneumonia, nausea, abdominal pain, vomiting, diarrhea, conjunctivitis, rash, lymph node swelling, apathy, somnolence) daily from day 1 to 11 on a scale from 1 (very weak) to 5 (very strong). For an individual score of the disease severity, the sum of symptom scores was used as the outcome measure (symptom sum score). Further details of the study are published elsewhere [5].

### *2.2. Data Analysis*

Model development and simulations were performed using non-linear mixed-effects modeling implemented in the software NONMEM (version 7.4.3, ICON Development Solutions, Ellicott City, MD, USA). The objective function value (OFV; −2 log likelihood), the precision of parameter estimates assessing the respective relative standard errors (RSE) [12], as well as visual inspection of the goodness-of-fit plots and conditional weighted residuals (CWRES) vs. time [12], were used as evaluation criteria for model selection. A new model was accepted if the addition of one parameter led to a reduction of the OFV by at least 3.841 (chi-square distribution with 1 degree of freedom, $\alpha$-level 0.05). Dataset generation and graphical visualization of NONMEM results were performed using R (version 3.6.3, The R Foundation for Statistical Computing, Vienna, Austria).

### *2.3. Model Development*

First, a PK model describing the plasma concentration-time profiles for azelastine after intranasal and oral application was developed (PK model A) based on literature data from 5 clinical studies [6–10]. Here, one-, two-, and three-compartment models were tested. To describe the absorption process, zero- and first-order processes as well as delayed and parallel absorption were evaluated. For the elimination processes, first-order as well as saturable processes were tested. Since it was anticipated that the local, intranasal azelastine amount is of importance for the description of the effect on the viral load determined by nasal swabs, a second PK model (PK model B) was established to simulate the local intranasal azelastine amount based on prior knowledge about the kinetics of intranasally applied drugs from the literature.

For the description of the change of individual SARS-CoV-2 viral load over time, several known virus kinetic models were evaluated [13–16]. The influence of estimated azelastine plasma concentrations (PK model A) and estimated intranasal azelastine (PK model B) on different parameters of the virus replication model was evaluated using linear, Emax and hill effect models.

For the description of the symptom sum score, linear and turnover models were tested and linked to the PK-virus kinetic model. Since the symptom sum score comprises 20 symptoms and individual scores ranged between 1 (very weak) and 5 (very strong), a symptom sum score of 20 was defined as the absence of any symptoms. Hence, the model predicted symptom sum score was calculated with an offset of the minimal score of 20.

Covariate analyses were performed for the virus kinetic model and the symptom score model. For this, age, weight, height, BMI, sex, baseline copy number, baseline outcome level and date of initial positive SARS-CoV-2 test were evaluated as covariates. The covariate analysis was performed using forward inclusion ($p < 0.05$) and backward elimination ($p < 0.001$) with each covariate being evaluated univariately (one-by-one) [17].

### *2.4. Simulations*

Using the final covariate model, simulations were performed to illustrate the effects of different azelastine treatment schedules and the influence of the covariates age and sex. Here, an average patient was assumed (male, 32 years, treatment with 3 × 0.1% azelastine)

and one covariate was varied at a time. For age, simulations were performed for the median, 5th and 95th percentile of the study population (32, 19 and 57 years). Next to the study treatments (placebo, 3 × 0.02% azelastine, and 3 × 0.1% azelastine) 5 × 0.1% azelastine was simulated to explore the benefits of a more frequent application of azelastine.

Furthermore, the impact of preventive treatment with azelastine was explored by simulating the viral load with azelastine therapy starting before the time of infection using 3× and 5× daily application of 0.1% azelastine. With the equation proposed by Goyal et al. [18], the transmission risk T was approximated as a function of the viral load V as

$$T = (V^{\alpha}/(V^{\alpha} + \lambda^{\alpha}))^2, \quad (1)$$

with λ representing the viral load at which the transmission risk is 25% ($\lambda = 10^7$ cp/mL) and α representing the slope (α = 0.8), as described by Goyal et al. [18]. To evaluate the impact of the changed transmission risk by azelastine treatment, the difference of the area under the curve (AUC) of T until the time of diagnosis (and presumably isolation of the infected person) was calculated. This difference in the AUC of the transmission risk was used to estimate the spread of SARS-CoV-2 infections based on one index case. For this, the R(t) of a susceptible-infected-removed (SIR) infectious model was decreased by the respective, estimated AUC decrease in the transmission risk. For treatment with placebo, an R(t) of 1.2 was assumed, which represents the reported median R(t) value in Germany for the first two years of the pandemic (2 March 2020–2 March 2022) whenever R(t) was >1 according to the RKI nowcasting [19].

## 3. Results

### *3.1. Pharmacokinetic Model*

The digitized PK dataset included 8 mean plasma concentration-time profiles after intranasal application of 0.28, 0.548, 0.55 and 0.822 mg azelastine [6–9] and 2 profiles after oral application of 2 mg azelastine [10] from five different studies. A summary about characteristics of the study populations is presented in Appendix A Table A1. In total, the dataset contained 130 azelastine observations after 10 dosing events.

The azelastine plasma concentrations were described best by a one-compartment model with parallel absorption via a fast and a slow absorption arm after nasal application of high volumes of spray (i.e., two puffs per nostril, 140 µL/puff, PK model A, Appendix A Figure A1). For small volumes (one puff per nostril, 140 µL/puff), the fraction absorbed via the fast absorption arm was estimated to be approximately 100% and, thus, was finally fixed to 100%. The absorption rate for the fast arm was estimated very high and fixed to 100 $h^{-1}$. The relative bioavailability of intranasal absorption was estimated to be 36.8% compared to the oral bioavailability. Parameter estimates of the final PK model A are listed in Appendix A Table A2. Model predictions versus time and goodness-of-fit plots are presented in Appendix A Figures A2 and A3. Except for very low concentrations, all data points were randomly spread around the line of identity indicating good descriptive performance.

The second PK model (B) was established based on literature knowledge about the kinetics of intranasally applied drugs to simulate the local intranasal azelastine amount. In this model, the amount of azelastine in the respective spraying formulations was administered as a bolus amount and cleared with an elimination half-life of 20 min ($t_{1/2}$ = 0.0138 days corresponding to an elimination rate $k_{el}$ of 49.9 $day^{-1}$, Figure 1) as described by Schipper et al. [20].

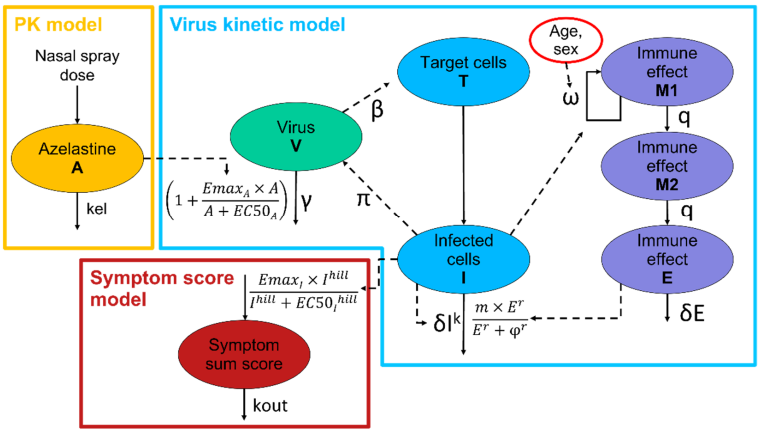


**Figure 1.** Schematic representation of the final PK-virus kinetic-symptom score model. The PK model is represented in yellow. Different parts of the virus kinetic model are represented in green, blue and violet. The symptom score model is represented in red.

### *3.2. PK-Virus Kinetic Model*

From the 90 patients included in the CARVIN study, 8 patients were excluded due to negative SARS-CoV-2 PCRs on ≥5 of 7 measurements, resulting in the final virus kinetic dataset of the CARVIN study containing 565 viral load qPCR measurements from 82 patients. Subjects included in this analysis were on average 32 years old (range 19–60 years) and weighed 72 kg (range 50–129 kg). Forty-two patients (51%) were female. One patient reported fever at baseline, one patient has been previously infected with SARS-CoV-2 and three patients had previously been vaccinated. The median delay between positive PCR test result and study inclusion was 1.44 days. Table 1 shows that the treatment groups had comparable demographic characteristics.

**Table 1.** Summary of the study population used for model development of the PK-virus kinetic and symptom score models. Age and weight are summarized as medians and standard deviations (sd). Patients' sex is summarized as the percentage and number of male patients.

| Group | *n* | Age [Years] (sd) | Weight [kg] (sd) | Sex [% male] (*n*) |
|---|---|---|---|---|
| Placebo | 27 | 33 (13.6) | 70 (16.3) | 48.1 (13) |
| 0.02% azelastine | 28 | 28 (12.8) | 70.5 (15.7) | 53.6 (15) |
| 0.1% azelastine | 27 | 35 (13.1) | 75 (15.7) | 44.4 (12) |
| All | 82 | 32 (13.1) | 71.5 (15.8) | 48.8 (40) |

Regarding the azelastine nasal-spray application in the CARVIN study, no exact dosing times were recorded. The study protocol suggested two puffs (one puff per nostril) three times a day (after waking up in the morning, around lunchtime and in the evening), preferentially every 6–8 h. Adherence concerning morning, midday and evening doses was self-reported by the patients together with the symptom questionnaire. For our analysis, the applications were assumed to be administered at 08:00 (morning), 14:00 (midday) and 20:00 (evening) if the patient self-reported the application of the respective dose.

The semi-mechanistic model by Goyal et al. [14] (Figure 1) described the viral load data best in comparison to the tested approaches. Here, target cells (T) can become infected by free virus turning them into infected cells (I). Infected cells produce virus (V) and be eliminated by an immune response. The model includes a fast immune response with a direct effect on the elimination of infected cells and a late T-cell immune response, depicted via transit compartments that describe the delay between infection and T-cell immune response (Figure 1, shown in purple).

Most virus kinetic model parameters were fixed to values reported by Goyal et al. [14] (see Table 2). Viral infectivity ($\beta$ = 8.89 $\times$ $10^{-9}$ virion$^{-1}$day$^{-1}$), virus elimination rate ($\gamma$ = 1.92 day$^{-1}$) and the time between infection and diagnosis (ALAG = 6.51 days) were estimated for our study. A moderate IIV of 54 %CV was identified for the time between infection and diagnosis ALAG. All model parameters are shown in Table 2.

**Table 2.** Model parameters of the final PK, PK-virus kinetic- and outcome model. No interindividual and residual variability was estimated for the PK model due to lack of PK data.

| Parameter | Value (RSE [1]/Shrinkage) * | Unit | Source | Parameter Description |
|---|---|---|---|---|
| **PK model** | | | | |
| $k_{el}$ | 49.9 | day$^{-1}$ | [20] | Azelastine elimination rate |
| **PK-virus kinetic model** | | | | |
| ALAG | 6.51 (3.2%) | days | estimated | Time between infection and diagnosis |
| $\beta$ | 8.89 $\times$ $10^{-9}$ (1.2%) | virion$^{-1}$day$^{-1}$ | estimated | Viral infectivity |
| $\gamma$ | 1.92 (6.7%) | day$^{-1}$ | estimated | Virus elimination rate |
| $\delta$ | 3.1 | day$^{-1}$cells$^{k}$ | [14] | Elimination rate of infected cells |
| $\omega$ | 2.75 $\times$ $10^{-5}$ | day$^{-1}$cells$^{-1}$ | [14] | Extend of T-cell response |
| $\pi$ | 398 | day$^{-1}$ | [14] | Virus production rate |
| k | 0.08 | - | [14] | Fast immune response |
| q | 2.4 $\times$ $10^{-5}$ | day$^{-1}$ | [14] | Differentiation rate of T-cells |
| $\delta$E | 1 | day$^{-1}$ | [14] | Elimination rate of T-cell response |
| m | 3 | day$^{-1}$cells$^{-1}$ | [14] | Maximum T-cell response |
| r | 10 | - | [14] | Hill coefficient of T-cell response |
| $\phi$ | 100 | cells | [14] | Half maximum effective effector cell level |
| I0 | 1 | cells | [14] | Baseline number of infected cells |
| M0 | 1 | cells | [14] | Baseline number of T-cells effect cells |
| T0 | $10^7$ | cells | [14] | Baseline number of target cells |
| $Emax_A$ | 0.37 (2.9%) | - | estimated | Maximum azelastine effect |
| $EC50_A$ | 0.0629 (5.1%) | µg | estimated | Half maximum effective azelastine amount |
| Sex—$\omega$ | 1.95 (9.8%) | - | estimated | Covariate effect of sex on $\omega$ |
| Age—$\omega$ | −0.287 (2.9%) | - | estimated | Covariate effect of age on $\omega$ |
| IIV ALAG | 58.0 (16.1%/9%) | %CV | estimated | Interindividual variability on ALAG |
| AE | 1.2 (0.8%) | SD, log cp/mL | estimated | Additive residual error viral load |
| **Symptom score model** | | | | |
| Kout | 0.37 (5.9%) | day$^{-1}$ | estimated | Output rate |
| $Emax_I$ | 15 (8.3%) | - | estimated | Maximum input rate |
| $EC50_I$ | 5.01 $\times$ $10^5$ (9%) | cells | estimated | Half maximal effective infected cells |
| hill | 0.298 (5.9%) | - | estimated | Hill coefficient |
| IIV Emax | 78.7 (9%/3%) | %CV | estimated | Interindividual variability on Emax |
| PE | 10–9 (2.6%) | %CV | estimated | Proportional residual error symptom sum score |

[1] RSE: Relative standard error, * applicable for model parameter estimates.

The two PK models (A and B) were tested for the impact of azelastine exposure on the virus kinetics. Here, PK model A depicted the plasma concentration after oral and intranasal dosing of azelastine. PK model B was developed to describe the intranasal azelastine amount. Both models were linked with the virus kinetic model and described the azelastine drug effect equally well using Emax effect models with a statistically significant ($p < 0.05$) influence on the virus elimination. However, PK model B was favored due to the principle of parsimony and the local mode of action for azelastine as well as the higher precision of parameter estimates. At maximum effect, azelastine increased the virus clearance by 32.2%.

Age and sex could be identified as covariates influencing the virus kinetics. Older patients showed a reduced late T-cell response to SARS-CoV-2 infected cells with an estimated exponent of −0.287. Female patients had a 95% increased late T-cell response compared to male patients (see Table 2).

The goodness-of-fit plot for the final model (Figure 2, left) shows that the viral load was well described throughout all treatment groups with observations vs. model predictions randomly scattered around the line of identity. Furthermore, Figure 2 (right) shows the good agreement between observed and model-predicted individual viral load-time profiles for two exemplary patients from each treatment group.

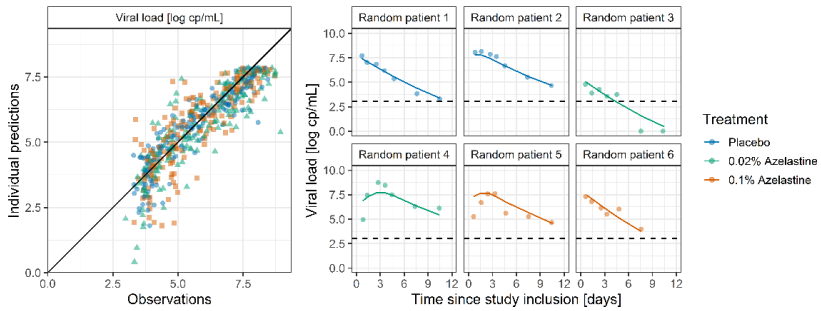


**Figure 2.** Goodness-of-fit plots for the PK-virus kinetic model (**left**) showing individual predictions vs. observations excluding negative test results (84.1% of which were predicted to be below the lower limit of quantification of 3.02). The black line indicates the line of identity. Exemplary plots (**right**) for two randomly drawn patients per study arm. Points indicate observations. Lines indicate individual model predictions. Observations below the LLOQ were set to 0 log cp/mL. Dashed lines indicate the LLOQ.

### *3.3. Symptom Score Model*

The dataset for the symptom score model included 859 observations of the symptom sum score for the 82 patients with viral load data described in Section 3.2. The median symptom sum score at study inclusion was 35. After 11 days, symptoms were considerably reduced with a median score of 23.

For the symptom score model, the parameters estimated for the PK-virus kinetic model were fixed, including the individually estimated values for the lag time between infection and diagnosis. The symptom sum score was described best by a turnover model (Figure 1, red part). An increase in the symptom score was triggered by the number of infected cells implemented by a hill effect model with an EC50 of 5.01 $\times$ $10^5$ infected cells and a hill coefficient of 0.298. The estimated elimination half-life of the infected cells was 1.87 days. A high IIV (78.7 %CV) was identified on the maximal impact of the infected cells on the outcomes (Emax). No significant impact of covariates on symptom sum score could be found.

The goodness-of-fit plot of the final symptom score model (Figure 3, left) shows that the symptom sum score was well described for all treatment groups with all points randomly scattered around the line of identity, even for extreme values with scores of >50. Furthermore, Figure 3 (right) shows the good agreement between observed and model predicted individual symptom sum scores for two exemplary patients from each treatment group.

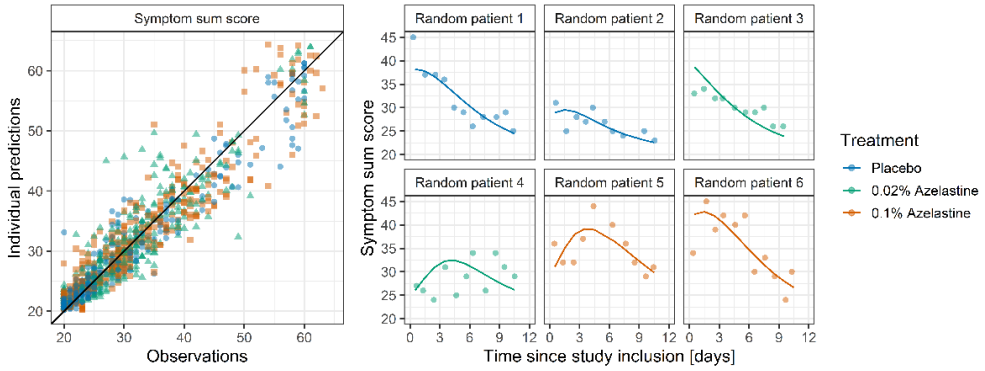


**Figure 3.** Goodness-of-fit plots for the symptom score model (**left**) showing individual predictions vs. observations. The black line indicates the line of identity. Exemplary plots (**right**) for two randomly drawn patients per study arm. Points indicate observations. Lines indicate individual model predictions.

### *3.4. Simulations*

To illustrate the effect of the covariates and different azelastine doses and treatment schedules, simulations were performed with the final PK-viral load-symptom score model. Scenarios for an average patient were tested (male, 32 years, treatment with 3 × 0.1% azelastine) and respective covariates were varied.

Results of the simulations are shown in Figure 4. Patients treated with azelastine showed a faster decrease in the SARS-CoV-2 viral load and symptom sum score compared to patients receiving placebo (Figure 4A): The time until the viral load drops below the lower limit of quantification (LLOQ) was reduced in patients receiving azelastine. Here, the effect size was dependent on dose and frequency of azelastine administration (10.6 days, 9.0 days, 8.7 days and 8.4 days after study inclusion with placebo, 3 × 0.02%, 3 × 0.1% and 5 × 0.1% azelastine, respectively). The time until the symptom score drops below 25 (corresponding to 15 very weak and 5 weak symptoms) was longest for patients treated with placebo (10.1 days) and drops with azelastine treatment to 9.6, 9.4 and 9.3 days for 3 × 0.02%, 3 × 0.1% and 5 × 0.1%, respectively. Figure 4B illustrates the slower decline in viral load and symptom score in older patients: Patients aged 57 years did not reach a viral load below the LLOQ after 11 days. Patients aged 19 and 32 years reach the LLOQ after 9.5 and 9.6 days, respectively. The time until symptom score of 25 was much shorter for younger patients (9 vs. 12 days for patients aged 19 and 32 vs. patients aged 65, Figure 4B). Male patients experienced higher peak symptoms (maximum symptom sum score 38.4 vs. 37.8 for male and female patients, Figure 4C). However, in the terminal phase of the disease after 7 days, male patients showed a faster decline in viral load and symptoms.

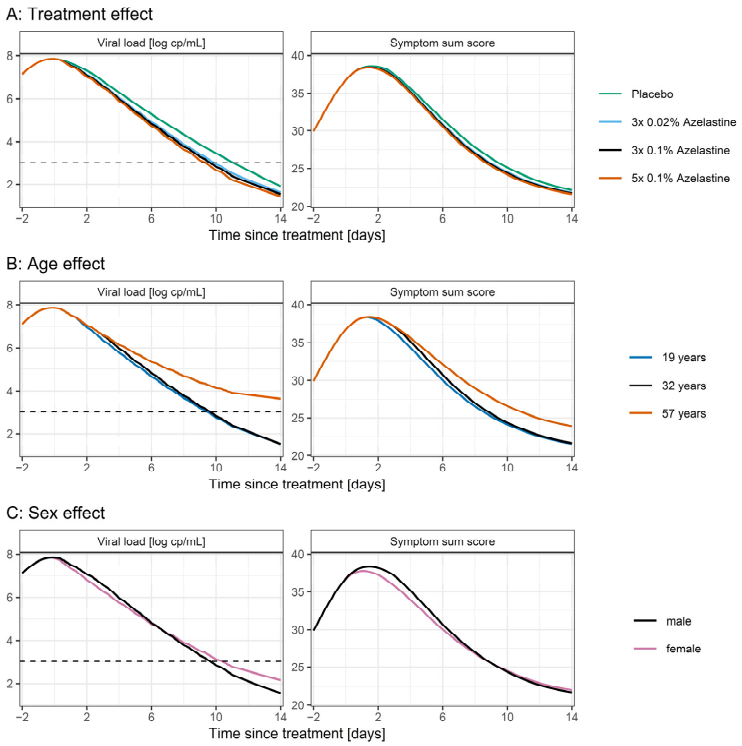


**Figure 4.** Scenario simulations of the viral load and symptom sum score dependent on univariate changes in treatment (**A**) or the covariates age (**B**) and sex (**C**). Black lines represent the standard patient (32 years, male) receiving 3 × 0.1% azelastine treatment. Colored lines indicate the univariate change of the respective covariates. Dashed lines indicate the LLOQ of the viral load.

*Pharmaceutics* **2022**, *14*, 2059 

To explore the possible impact of preventive treatment with azelastine, scenario simulations were performed assuming treatment with three- and five-times daily applications versus placebo before the time of infection. Here, slower increase and lower peak viral load upon azelastine treatment were predicted (Figure 5A). Next, the transmission risk was calculated based on the viral load. For patients receiving three times and five times daily azelastine, the AUC of transmission risk until the time of diagnosis was reduced by 11% and 15%, respectively, in comparison to patients receiving placebo (Figure 5B). For a subsequent scenario, this decrease in transmission risk was used to estimate the spread of SARS-CoV-2 infections based on one index case. Here, with a baseline R(t) of 1.2 for patients treated with placebo, one index case leads to 28 infections after 60 days (Figure 5C). For treatment with azelastine, 11 (R(t) = 1.07) and 7 (R(t) = 1.02) cases could be estimated for treatment with three and five times daily azelastine, respectively.

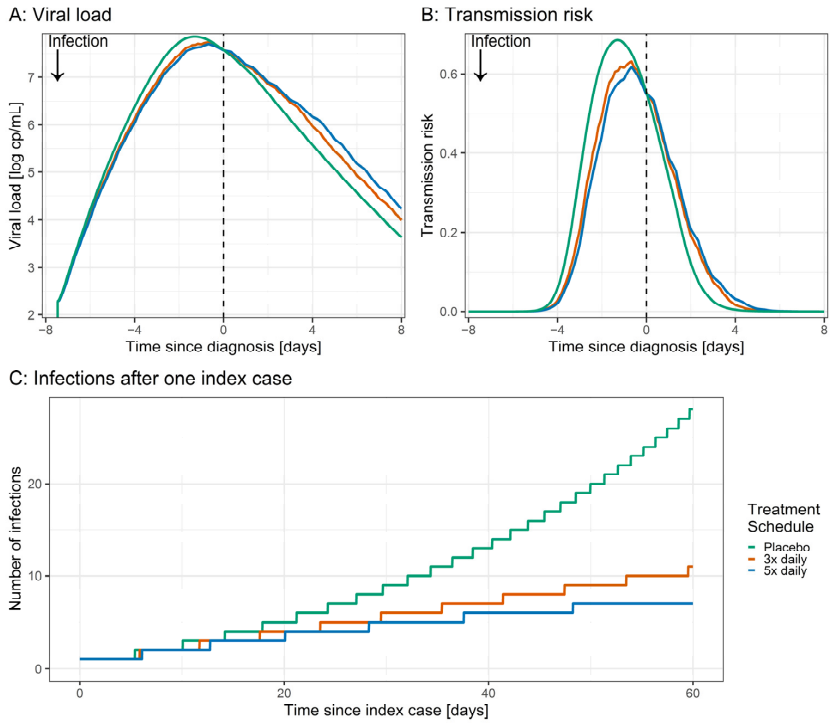


**Figure 5.** Scenario simulations of SARS-CoV-2 viral load (**A**), transmission risk (**B**) and subsequent infections (**C**) after placebo (green) vs. preventive administration of 3 × 0.1% azelastine (red), 5 × 0.1% azelastine (blue). Simulated preventive treatment started 11 days before infection and was continued until the end of simulations. (**A**) Viral load after infection with SARS-CoV-2. (**B**) Transmission risk associated with the respective viral load. (**C**) Number of infections resulting from the detection of one index case assuming modest contact restriction measures (baseline placebo R(t) = 1.2).

## 4. Discussion

In this work, pharmacometric modeling was applied to (i) describe the PK of azelastine after intranasal and oral dosing, (ii) adopt a virus kinetic model describing the SARS-CoV-2 viral load and (iii) develop a model describing the symptom severity of COVID-19 patients treated with placebo or azelastine nasal spray.

A one-compartment model with parallel absorption for the intranasal application described the PK of azelastine in plasma best (PK model A). Parallel absorption models have been previously suggested for other drugs after intranasal application [21,22], assuming that part of the dose is swallowed and absorbed via the gastrointestinal tract. In our

analysis, the effect of parallel absorption was only observed for the application of two sprays per nostril. With one spray per nostril, the fraction absorbed via the fast and presumably intranasal absorption pathway was estimated to be 100%. This effect might be due to the difference in the total volume of applied spray, where parts of the larger volume of two puffs are swallowed. Overall, PK model A described the data very well with the tendency of slightly underpredicting low concentrations in the final elimination phase. However, as the data were obtained by digitalization of published concentration-time curves, data points might be subject to inaccuracies due to known digitalization limitations in linear scale plots [11]. Nonetheless, the estimated azelastine bioavailability of 36.8% of the nasal spray application and an elimination half-life of 18.6 h are in line with previous non-compartmental analyses reporting 40% bioavailability and a half-life of 22 h [2].

A second PK model was developed describing the intranasal amount of azelastine (PK model B) in comparison to the plasma concentrations of PK model A. In PK model B, the elimination rate was set to correspond to the nasal mucociliary clearance of 20 min as reported by Schipper et al. [20]. The bioavailability was assumed to be 100% following the modeling results from PK model A for which no swallowing of the dose was assumed applying of one spray per nostril. For the description of the effect of azelastine on the viral load, measured by nasal swabbing, PK model B was favored as the descriptive performance of both models was comparable, but model B had a simpler structure with a more plausible local mode of action.

For the description of the virus kinetics in the CARVIN study, a previously published virus replication model was utilized. Here, only two population parameters had to be adapted and estimated for an accurate description of the data. For this, the viral infectivity ($\beta$) and virus clearance ($\gamma$) parameters were estimated about 85% lower compared to Goyal et al. [14]. This renders the within-host infectivity, which is correlated to the fraction $\beta/\gamma$ [23], 18% higher in comparison to Goyal et al. [14]. Furthermore, this change leads to a longer disease duration and a higher peak viral load. Both effects might be attributed to the difference in infectivity and severity between SARS-CoV-2 variants (VOCs) since the model developed by Goyal et al. was based on only data with wild-type SARS-CoV-2. In the CARVIN study, information regarding VOC infections was available for 59 patients (66%) with 92% of these carrying the VOC alpha (B.1.1.7). At the time of data collection (3 March–28 April 2021), VOC Alpha increased from 54.6% (4 March 2021) to 93.9% (29 April 2021) in Germany [24]. Hence, it is reasonable to assume that most study patients (including those with missing VOC infection status) were infected with VOC Alpha and differences in model parameters are due to substantial differences in virus replication kinetics between wild-type and VOC Alpha. Importantly, azelastine's anti-viral effect was found to be comparable against the D614G variant (one amino acid exchange in the Spike protein relative to the wild-type virus) and Alpha variant in in vitro infection models [4].

The intranasal amount of azelastine had a significant impact on the virus elimination rate with a maximum acceleration by 37% ($p = 0.0044$), as simulated by PK model B. The estimated EC50 of 0.848 µg azelastine corresponds to 0.28 mL of a 7.24 µM formulation. In previous in vitro studies, azelastine inhibited the virus entry into the cell by blocking the binding site of the SARS-CoV-2 spike protein with an EC50 of 3.834 µM [3] and EC50 of 2.2 to 3.7 µM in pre-infection and 4 to 6.5 µM in post-infection treatment settings in infection assays with different variants [4], which is in line with our findings.

The model was used to simulate the study treatment (placebo, 3 × 0.02% azelastine and 3 × 0.1% azelastine) as well as treatment with 5 × 0.1% azelastine. Analysis of the simulation results revealed a beneficial effect of all applied doses vs. the application of placebo with the largest effect being observed at 5× daily application of 0.1% azelastine.

As the analysis of PK model A revealed a higher systemic bioavailability after oral compared to intranasal applications, a dedicated investigation of potential (systemic) treatment benefits of oral administrations in COVID-19 patients could be reasonable. However, this analysis was only based on data after intranasal application and viral load measurement from nasal swabs. Hence, it was not possible to differentiate between local effects

and potential systemic effects. Furthermore, it might be unreasonable to assume that oral administration of azelastine, concentrations in the target sites of SARS-CoV-2 would be large enough to observe a treatment effect.

Age and sex could be identified as covariates on the extent of the late T-cell immune response of the virus kinetic model, which leads to male and older patients experiencing higher maximum viral loads and symptoms. This is in line with previous findings where female patients and younger patients showed a more robust T-cell immune response to the infection with SARS-CoV-2 [25]. Furthermore, older patients showed a slower decline in the viral load, which can be explained by the ageing of the immune system resulting in diminished antibody maturation and more hyperinflammatory and pathological innate responses to SARS-CoV-2 [26,27].

The symptom sum score was described best by a turnover model induced via hill effect to the number of infected cells estimated by the virus kinetic model. The combination of hill effect and turnover model causes the time of the maximum symptom score to be delayed by 1.7 days in comparison to the maximum viral load and by 2.2 days in comparison to the maximum number of infected cells. The IIV of symptoms between patients was very high (58 %CV) and could not be explained by any of the tested covariates. Effects of age, sex and applied azelastine dose on the symptom score were driven by the difference in infected cells estimated by the virus kinetic model. As expected by the mode of action, no additional effect of azelastine on the symptom score could be observed.

Azelastine nasal spray 0.1% has been approved for the treatment of seasonal allergic rhinitis and nonallergic vasomotor rhinitis for more than 30 years. Moreover, since then, its safety and tolerability have been proven in various clinical studies [2]. The most common reported adverse effect of the nasal spray formulation is bitter taste, which can be reduced by improving the dosing technique [8]. Further reported adverse effects were transient and of mild-to-moderate severity including somnolence, nasal burning, and headache [2]. Due to the favorable safety profile and the positive results from retrospective studies on the mined electronic health records [1], an investigation of the use of azelastine nasal spray for the prevention of infection with SARS-CoV-2 is reasonable. Hence, the developed virus kinetic model was applied to simulate the impact of azelastine intranasal application at the time of infection on the spread of the virus. Here, azelastine lowered the peak viral load from $7.08 \times 10^7$ (placebo) to $5.37 \times 10^7$ and $5.13 \times 10^7$ cp/mL for applications of $3 \times 0.1\%$ and $5 \times 0.1\%$ azelastine, respectively. Assuming the timepoint of diagnosis remained unchanged despite the lower viral load, the transmission risk until diagnosis was mitigated by preventive administration of azelastine, which substantially lowered the number of infected subjects by more than 50% in our scenario (28 vs. 11 vs. 7 after 60 days without, with $3 \times 0.1\%$ and $5 \times 0.1\%$ preventive azelastine applications, respectively). However, these calculations are based on some strong assumptions. For one, the simulation of the preventive effect of azelastine is based on model extrapolations outside of the data domain. Furthermore, it is unclear whether the time of diagnosis might be altered with lower viral loads. Additionally, the only preventive effect included in the simulation was the lower transmission risk from the infected person to a susceptible individual. However, previous studies also found a lower risk of infection for susceptible individuals taking azelastine [1]. Hence, further clinical studies would be needed to evaluate the preventive potential of azelastine nasal spray. For the treatment of acute disease, a higher frequency of application ($5 \times 0.1\%$ vs. $3 \times 0.1\%$ azelastine) shortened both the time until symptoms resolved (symptom sum score) as well as the time until viral load dropped below the LLOQ. In the preventive treatment scenario, model simulations of both dosage regimens also favored a higher azelastine dosage frequency to minimize transmission risk.

## 5. Conclusions

Mathematical models were developed to describe the PK of azelastine and the effect of azelastine vs. placebo nasal spray on SARS-CoV-2 viral load as well as COVID-19 symptoms. The PK of azelastine after an intranasal application was best described using a

parallel absorption model if two sprays per nostril were applied, implying that parts of the larger applied volume of the formulation (2 puffs) are swallowed. Furthermore, modeling revealed that the intranasal azelastine amount has a significant impact on the viral load measured by nasal swabbing in patients with mild disease. In our analysis, the number of infected cells triggered the disease symptoms with the peak of symptoms being delayed by 1.7 days in comparison to the peak viral load. The impact of azelastine on the viral load also translated to a significantly lower symptom score in patients treated with azelastine in comparison to patients receiving placebo nasal spray. Furthermore, the age and sex of the patients had a significant impact on the viral load with older patients showing a slower decrease in viral load in comparison to younger individuals and male patients experiencing higher peak viral loads compared to females.

**Author Contributions:** Conceptualization, P.M., R.M., F.H. and T.L.; methodology, T.L. and C.D.; validation, C.D.; formal analysis, C.D.; investigation, C.D., T.L. and P.M.; resources, P.M., F.H., R.M. and T.L.; data curation, P.M.; writing—original draft preparation, C.D., D.S. and T.L.; writing—review and editing, C.D., P.M., F.H., M.F., E.N., J.P.K., R.M., D.S. and T.L.; visualization, C.D.; supervision, T.L. and P.M.; project administration, T.L.; funding acquisition, P.M. All authors have read and agreed to the published version of the manuscript.

**Funding:** This research was funded by URSAPHARM Arzneimittel GmbH, Industriestraße 35, 66129 Saarbrücken, Germany. The preparation of the manuscript was not funded.

**Institutional Review Board Statement:** The study was conducted in accordance with the Declaration of Helsinki and approved by the Ethics Committee of the Faculty of Medicine of Cologne University on the 10 February 2021. Approval of the study by the German Federal Institute for Drugs and Medical Devices (BfArM) was given on 3 February 2021.

**Informed Consent Statement:** Informed consent was obtained from all subjects involved in the study.

**Data Availability Statement:** The data presented in this study are available on request from the corresponding author upon reasonable request and with permission of URSAPHARM Arzneimittel GmbH. The data are not publicly available due to use under license for the current study.

**Conflicts of Interest:** T.L. and C.D. have received funding from the sponsor URSAPHARM Arzneimittel GmbH for performing this analysis. P.M. and M.F. are employees at URSAPHARM Arzneimittel GmbH. F.H. is the CEO of URSAPHARM Arzneimittel GmbH. E.N. is shareholder in CEBINA GmbH and inventor on related patent applications. R.M. is the CEO of ClinCompetence Cologne, the CRO which organized the trial.

## Appendix A

**Table A1.** Summary of the studies used for model development of the PK models. Age and BMI are summarized as medians and range if available. Patients' sex is summarized as the percentage and number of male patients.

| Study | Administration | Doses [mg] | *n* | Age [Years] (Range) | BMI [kg/m$^2$] | Sex [% Male] (*n*) |
|---|---|---|---|---|---|---|
| Du 2014 [6] | Intranasal | 0.280 | 22 | 37.4 (21–55) | 24.57 | 54.5 (12) |
| Berger 2009 [7] | Intranasal | 0.548 | 36 | (18–50) | na | 100 (36) |
| Bernstein 2007 [8] | Intranasal | 0.550 | na | na | na | 100 |
| ClinPharmReview [9] | Intranasal | 0.548, 0.822 | 18 | (18–50) | na | 100 (18) |
| Park 2010 [10] | po | 2 | 23 | 23.0 (19–27) | na | 100 (23) |

na = not available.

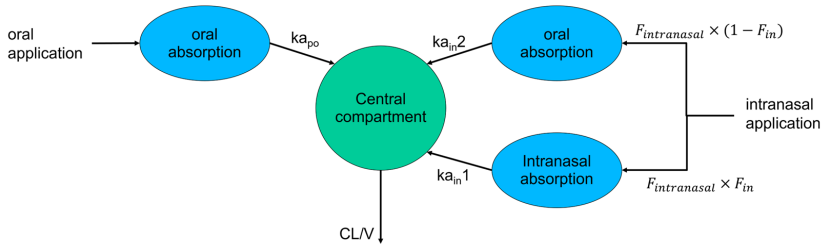


**Figure A1.** Schematic representation of the azelastine PK model A describing the plasma concentration-time profiles after oral and intranasal applications.

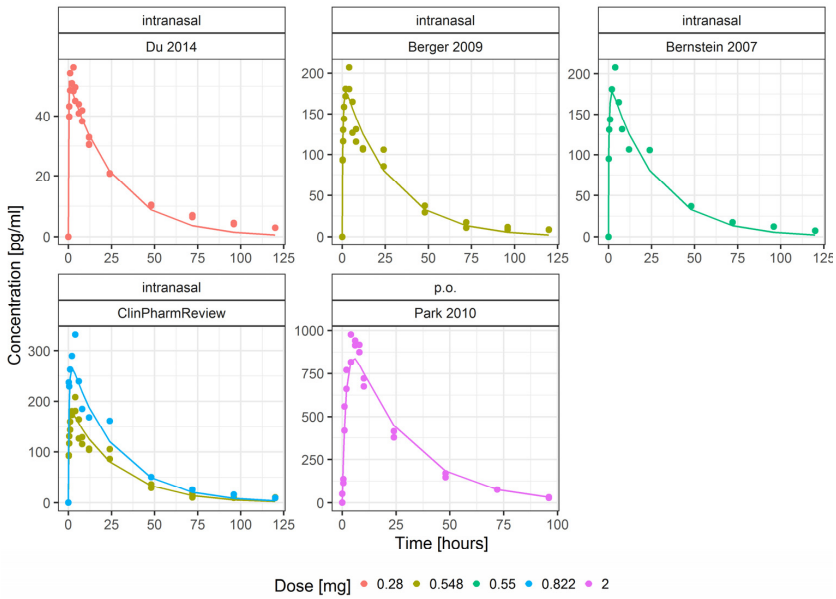


**Figure A2.** Azelastine plasma concentration-time profiles after intranasal or oral application of various amounts. Points represent observations from 5 different studies [6–10] and lines represent model predictions of the PK model A. Colors indicate dose amounts.

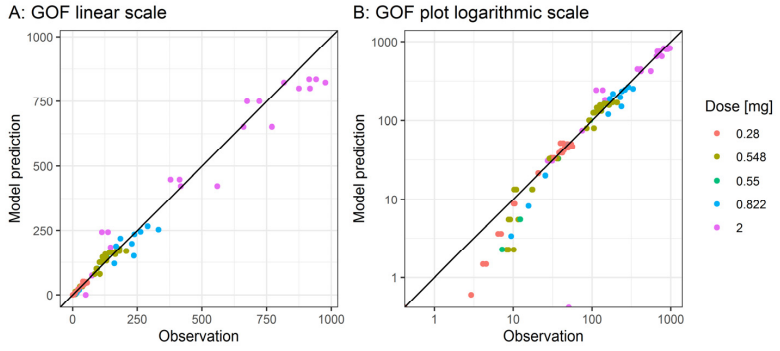


**Figure A3.** Goodness-of-fit (GOF) plots for PK model A showing predicted vs. observed azelastine plasma concentrations on linear scale (**A**) and log-log scale (**B**). Black lines indicate the lines of identity.

**Table A2.** Parameter estimates of the azelastine PK model A. No inter-individual variability (IIV) was estimated, as the mean curves of azelastine plasma concentrations could be described accurately without additional IIV.

| Parameter | Parameter Description | Unit | Estimate | RSE [1] |
|---|---|---|---|---|
| **Fixed effects** | | | | |
| V1/F | Volume of distribution | L | 1960 | 3.6% |
| CL/F | Clearance rate | L/h | 72.9 | 3.3% |
| $Ka_{po}$ | po absorption rate | 1/h | 0.55 | 8.7% |
| $F_{intranasal}$ | Intranasal relative bioavailability | - | 0.368 | 4.3% |
| $Ka_{in}1$ | Intranasal fast absorption rate | 1/h | 100 | FIX |
| $Ka_{in}2$ | Intranasal slow absorption rate | 1/h | 1.75 | 20.9% |
| $F_{in}$ (1 spray) | Intranasal fraction absorbed fast (1 spray) | - | 1 | FIX |
| $F_{in}$ (2 sprays) | Intranasal fraction absorbed fast (2 sprays) | - | 0.492 | 6.8% |
| **Residual error** | | | | |
| Prop. error | Proportional error | %CV | 15.0 | 16.6 |
| Add. error | Additive error | SD; pg/mL | 11.0 | 59.8 |

[1] RSE: Relative standard error.

## References


1. Reznikov, L.R.; Norris, M.H.; Vashisht, R.; Bluhm, A.P.; Li, D.; Liao, Y.-S.J.; Brown, A.; Butte, A.J.; Ostrov, D.A. Identification of Antiviral Antihistamines for COVID-19 Repurposing. *Biochem. Biophys. Res. Commun.* **2021**, *538*, 173–179. [CrossRef] [PubMed]
2. Lee, C.; Corren, J. Review of Azelastine Nasal Spray in the Treatment of Allergic and Non-Allergic Rhinitis. *Expert Opin. Pharmacother.* **2007**, *8*, 701–709. [CrossRef] [PubMed]
3. Ge, S.; Lu, J.; Hou, Y.; Lv, Y.; Wang, C.; He, H. Azelastine Inhibits Viropexis of SARS-CoV-2 Spike Pseudovirus by Binding to SARS-CoV-2 Entry Receptor ACE2. *Virology* **2021**, *560*, 110–115. [CrossRef] [PubMed]
4. Konrat, R.; Papp, H.; Kimpel, J.; Rössler, A.; Szijártó, V.; Nagy, G.; Madai, M.; Zeghbib, S.; Kuczmog, A.; Lanszki, Z.; et al. The Anti-Histamine Azelastine, Identified by Computational Drug Repurposing, Inhibits Infection by Major Variants of SARS-CoV-2 in Cell Cultures and Reconstituted Human Nasal Tissue. *Front. Pharmacol.* **2022**, *13*, 861295. [CrossRef]
5. Klussmann, J.; Grosheva, M.; Meiser, P.; Lehmann, C.; Szijártó, V.; Nagy, G.; Konrat, R.; Flegel, M.; Holzer, F.; Groß, D.; et al. COVID-19: Azelastine Nasal Spray Reduces Virus-Load in Nasal Swabs (CARVIN) Early Intervention with Azelastine Nasal Spray May Reduce Viral Load in SARS-CoV-2 Infected Patients—Results from a Randomized, Double-Blind, Placebo-Controlled Phase II Clinical Trial; PREPRINT (Version 1). 2022. Available online: https://www.researchsquare.com/article/rs-1893502/v1 (accessed on 19 September 2022).
6. Du, D.; Targett, D.; Stolberg, E.; Canali, A. A Clinical Pharmacokinetic Study Comparing Two Azelastine Hydrochloride Nasal Formulations in a Single-Dose Design. *Eur. J. Drug Metab. Pharmacokinet.* **2014**, *39*, 69–75. [CrossRef]
7. Berger, W.E. Pharmacokinetic Characteristics and Safety and Tolerability of a Reformulated Azelastine Hydrochloride Nasal Spray in Patients with Chronic Rhinitis. *Expert Opin. Drug Metab. Toxicol.* **2009**, *5*, 91–102. [CrossRef]
8. Bernstein, J.A. Azelastine Hydrochloride: A Review of Pharmacology, Pharmacokinetics, Clinical Efficacy and Tolerability. *Curr. Med. Res. Opin.* **2007**, *23*, 2442–2452. [CrossRef]
9. Center for Drug Evaluation and Research Clinical Pharmacology and Biopharmaceutics Review(s), Application Number 22-371s000. 2008. Available online: https://www.accessdata.fda.gov/drugsatfda_docs/nda/2009/022371s000ClinPharm.pdf (accessed on 23 September 2022).
10. Park, Y.S.; Kim, S.H.; Kim, Y.J.; Yang, S.C.; Lee, M.H.; Shaw, L.M.; Kang, J.S. Determination of Azelastine in Human Plasma by Validated Liquid Chromatography Coupled to Tandom Mass Spectrometry (LC-ESI/MS/MS) for the Clinical Studies. *Int. J. Biomed. Sci.* **2010**, *6*, 120–127.
11. Wojtyniak, J.G.; Britz, H.; Selzer, D.; Schwab, M.; Lehr, T. Data Digitizing: Accurate and Precise Data Extraction for Quantitative Systems Pharmacology and Physiologically-Based Pharmacokinetic Modeling. *CPT Pharmacomet. Syst. Pharmacol.* **2020**, *9*, 322–331. [CrossRef]
12. Mould, D.R.; Upton, R.N. Basic Concepts in Population Modeling, Simulation, and Model-Based Drug Development-Part 2: Introduction to Pharmacokinetic Modeling Methods. *CPT Pharmacomet. Syst. Pharmacol.* **2013**, *2*, e38. [CrossRef]
13. Goyal, A.; Duke, E.R.; Cardozo-Ojeda, E.F.; Schiffer, J.T. Modeling explains prolonged SARS-CoV-2 nasal shedding relative to lung shedding in remdesivir-treated rhesus macaques. *iScience* **2022**, *25*, 104448. [CrossRef] [PubMed]
14. Goyal, A.; Cardozo-Ojeda, E.F.; Schiffer, J.T. Potency and Timing of Antiviral Therapy as Determinants of Duration of SARS-CoV-2 Shedding and Intensity of Inflammatory Response. *Sci. Adv.* **2020**, *6*, eabc7112. [CrossRef] [PubMed]
15. Néant, N.; Lingas, G.; Le Hingrat, Q.; Ghosn, J.; Engelmann, I.; Lepiller, Q.; Gaymard, A.; Ferré, V.; Hartard, C.; Plantier, J.C.; et al. Modeling SARS-CoV-2 Viral Kinetics and Association with Mortality in Hospitalized Patients from the French COVID Cohort. *Proc. Natl. Acad. Sci. USA* **2021**, *118*, e2017962118. [CrossRef] [PubMed]

16. Perelson, A.S.; Ke, R. Mechanistic Modeling of SARS-CoV-2 and Other Infectious Diseases and the Effects of Therapeutics. *Clin. Pharmacol. Ther.* **2021**, *109*, 829–840. [CrossRef]
17. Wählby, U.; Jonsson, E.N.; Karlsson, M.O. Comparison of Stepwise Covariate Model Building Strategies in Population Pharmacokinetic-Pharmacodynamic Analysis. *AAPS PharmSci* **2002**, *4*, E27. [CrossRef]
18. Goyal, A.; Reeves, D.B.; Fabian Cardozo-Ojeda, E.; Schiffer, J.T.; Mayer, B.T. Viral Load and Contact Heterogeneity Predict SARS-CoV-2 Transmission and Super-Spreading Events. *eLife* **2021**, *10*, e63537. [CrossRef]
19. an der Heiden, M. *SARS-CoV-2-Nowcasting Und -R-Schaetzung*; Zenodo: Berlin, Germany, 2022.
20. Schipper, N.G.M.; Verhoef, J.C.; Merkus, F.W.H.M. The Nasal Mucociliary Clearance: Relevance to Nasal Drug Delivery. *Pharm. Res.* **1991**, *8*, 807–814. [CrossRef]
21. Furubayashi, T.; Kamaguchi, A.; Kawaharada, K.; Masaoka, Y.; Kataoka, M.; Yamashita, S.; Higashi, Y.; Sakane, T. Evaluation of the Contribution of the Nasal Cavity and Gastrointestinal Tract to Drug Absorption Following Nasal Application to Rats. *Biol. Pharm. Bull.* **2007**, *30*, 608–611. [CrossRef]
22. Furubayashi, T.; Kamaguchi, A.; Kawaharada, K.; Masaoka, Y.; Kataoka, M.; Yamashita, S.; Higashi, Y.; Sakane, T. Kinetic Model to Predict the Absorption of Nasally Applied Drugs from in Vitro Transcellular Permeability of Drugs. *Biol. Pharm. Bull.* **2007**, *30*, 1007–1010. [CrossRef]
23. Marc, A.; Kerioui, M.; Blanquart, F.; Bertrand, J.; Mitjà, O.; Corbacho-Monné, M.; Marks, M.; Guedj, J. Quantifying the Relationship between Sars-Cov-2 Viral Load and Infectiousness. *eLife* **2021**, *10*, e69302. [CrossRef]
24. Robert Koch Institute. *Wöchentlicher Lagebericht Des RKI Zur Coronavirus-Krankheit-2019 (COVID-19)*; Robert Koch Institute: Berlin, Germany, 2022.
25. Takahashi, T.; Ellingson, M.K.; Wong, P.; Israelow, B.; Lucas, C.; Klein, J.; Silva, J.; Mao, T.; Oh, J.E.; Tokuyama, M.; et al. Sex Differences in Immune Responses That Underlie COVID-19 Disease Outcomes. *Nature* **2020**, *588*, 315–320. [CrossRef] [PubMed]
26. Starke, K.R.; Petereit-Haack, G.; Schubert, M.; Kämpf, D.; Schliebner, A.; Hegewald, J.; Seidler, A. The Age-Related Risk of Severe Outcomes Due to COVID-19 Infection: A Rapid Review, Meta-Analysis, and Meta-Regression. *Int. J. Environ. Res. Public Health* **2020**, *17*, 5974. [CrossRef] [PubMed]
27. Jun, T.; Nirenberg, S.; Weinberger, T.; Sharma, N.; Pujadas, E.; Cordon-Cardo, C.; Kovatch, P.; Huang, K. Analysis of Sex-Specific Risk Factors and Clinical Outcomes in COVID-19. *Commun. Med.* **2021**, *1*, 3. [CrossRef] [PubMed]

# 5 DISCUSSION

## 5.1 General Remarks

This work presents a comprehensive overview of the possibilities NLME modelling provides in infectious disease and pharmacometric modelling: The epidemiologic models developed in Projects I and II focused on the identification of risk factors for the spreading of the virus and the occurrence of severe disease centred around the incidence of infections in Germany. The viral load model developed in Project III investigates individual disease courses and the influence of treatment and demographic variables. Still, both approaches were applied successfully with the same aim: to gain insights into preventive measures.

Compartmental models have been used for the description of epidemics for more than a century[91]. In these models, populations transfer through different disease-relevant stages. The definition of these stages depends on the disease as well as on the research question. Projects I and II show different examples for extensions of the basic SIR model to facilitate the investigation of various pandemic parameters.

Project I aimed at describing and predicting the number of cases, hospitalizations, patients requiring ICU treatment and the consequential fatalities due to COVID-19. The disease stages were extended accordingly and the influence of age, sex and VOCs of the patients was implemented as covariate effects. The model was used to estimate the impact of the testing strategy, which impacted the hospitalisation and case-fatality rate (CFR). This was expected and is in line with previous findings, as a more thorough screening for COVID-19 results in the increased detection of asymptomatic cases, which do not require hospitalization[92]. Furthermore, the modelling analysis facilitated a thorough analysis of the CFR. Previous studies identified shifts of the CFR over time in Germany, some of which explained these with shifts within the demographics of cases or different treatment strategies between federal states[93,94]. Our approach combined all knowledge, distinctly describing the number of fatalities in relation to the age and sex distribution of cases, the testing strategy and VOC in each federal state. Thereby, our analysis confirmed the findings of Morwinsky et al.[94], who identified a decrease in the CFR between spring and autumn 2020 related to the younger age of confirmed infections. Wjst et al.[93] identified differences in the CFR between ICU patients in Munich and Hamburg and could show that these differences arose from different management of hypoxaemia. Similarly, a difference between federal states was identified in our analysis, where the fraction of patients requiring ICU treatment differed between several federal states. However, of all identified influences, our analysis revealed age as the strongest

predictor for severe disease and fatality. This underlines that the older population should be subject to protective measures, which was the research focus of Project II.

Finally, while the impact of NPIs was not implemented as a covariate effect, the model still provided valuable insight into the effect of changing governmental regulations within its framework of stepwise Rt-changes. While the estimation of Rt within fixed time frames (i.e. daily or weekly) is most commonly used for these purposes[83,95], the estimation of stepwise Rt-changes has been successfully applied in our Projects I and II as well as by other researchers[96]. It provides the opportunity to compare the timing and extent of Rt-changes with NPI-changes.

In contrast to Project I, which focused on quantifying the impact variables on hospitalization and fatality rates, Project II focused on the spreading of SARS-CoV-2 with the aim to differentiate the impact of NPIs between age groups, concentrating on NPIs that concern mostly children and adolescents, such as school closures. Here, the staggered timing of school holidays and the varying vaccination levels between federal states and age groups provided the possibility to precisely determine the impact of both on the spreading of infections. Via the combined approach of describing the overall Rt changes within each federal state while estimating the relative impact of the NPIs on each age group, shifts in infection rates due to school closures and holidays could be determined independently of the overall trend in infections caused by other measures or, for example, increases due to increased travel during school holiday periods, which other researches could not distinguish between[97,98].

Thereby, Projects I and II emphasise the broad applicability of compartmental models and their flexibility to be adjusted according to the questions they should answer. Both projects highlight the benefits of approaching epidemiologic modelling using NLME techniques, which has only recently gained popularity[64].

Project III integrated different models that were developed independently of each other to obtain the desired information: A PK model for azelastine was developed using concentration-time profiles and physiological information gathered from literature after nasal and intravenous application. The resulting PK model was linked to PD and outcome models developed using data from the CARVIN study[45]. To evaluate the potential effect of azelastine on the prevention of the spreading of infections, a transmission model developed by Goyal et al.[59] was used, where the transmission risk is calculated based on the viral load. Finally, the model was used to perform simulations of various infectiousness scenarios to answer the question if prophylactic treatment with azelastine cannot only lessen COVID-19 symptoms but can also prevent secondary infections, which is a concept currently evaluated in a dedicated study.

Therefore, Project III illustrates how the integration of several models that are developed using different approaches can answer specific research questions, which is a concept that has been used in drug development for many years[95].

## 5.2 Data Availability

Models are by definition only a simplified representation of the underlying system[99], which is of biological nature in the case of Project III or of epidemiological nature in case of Projects I and II. Simplifications are needed for the sake of computational time and are necessitated by limited input knowledge. Time and background knowledge were particularly restricted in the early stages of the pandemic[100], during which the model presented in Project I was developed. This model was continuously updated as the pandemic progressed and hence, at each point in time only represented the state of the current knowledge.

During the COVID-19 pandemic, the availability as well as the format and informational content of data posed limitations[100]. In Germany, the number of cases, hospitalized patients and ICU patients was not reported from the same source, leading to effortful collection of the data from multiple sources. Additionally, data was not recorded on an individual level, i.e. it was not registered whether a confirmed case required inpatient treatment, neither was all data reported stratified by age. However, for such inconsistent reporting, mathematical modelling provides a powerful tool as it facilitates the combination of knowledge gained from various sources. In Project I, both individual-level data and data available on population level were utilized. In addition to the number of age- and sex-stratified confirmed cases on a population level, a database was available from the hospital financial information system MetaKIS including individual information for 30,723 hospitalized COVID-19 patients, which covered approximately 10% of hospitalized COVID-19 patients in Germany at that time. This database provided the possibility to determine the fraction of patients requiring treatment at general ward, ICU or mechanical ventilation, and to stratify this information by age group and sex. Furthermore, for each stratification group, fatality rates could be derived for each hospital ward. This knowledge was used as prior information during model development, which lowered the number of parameters that needed to be estimated and accelerated model development in the early phases of the pandemic.

As previously discussed, simplifications lie in the nature of model development. However, simplifications need to be weighed against the intended use and/or interpretation of the model. Here, the model needs to be fit for the intended purpose of the model rather than always displaying the closest possible representation of the underlying "true" system[53]. In Project I, for example, when simulating the number of ICU patients in German districts, a discrepancy between model predictions and observations was observed. Nonetheless, the model can still be considered valid, as the differences between model predictions and observations likely arise from discrepancies in the data records: The number of cases in each district was recorded based on the place of residency of the patient[101], while the number of ICU patients was recorded based on the location of the

hospital[102]. Here, the model did not adjust its predictions for patients crossing district borders to reach a hospital with ICU capacities. This theory was confirmed by comparing model predictions of districts comprising big cities (and therefore hospitals with ICU capacities) to smaller districts without appropriate ICU units.

The simplifications made in Project I were appropriate for the description of the first two years of the pandemic in Germany, when the model was updated on a biweekly basis. However, at the end of the year 2022, the updating of the model was terminated due to rising issues of data availability and accuracy of the simplifications. Caused by the increased usage of quick tests, PCR testing for SARS-CoV-2 decreased[103]. However, in Germany, only cases confirmed by PCR test enter official statistics[104]. Thereby, the dark figure rose, which could be observed exemplarily by the discrepancy between recorded cases and the measured viral load in wastewater in Berlin, which had previously been shown to be a good surrogate for the incidence of the virus[105]. Additionally, a decrease in vaccination effectiveness over time has been observed in dedicated studies[37]. However, the increasing spread of sublineages of the VOC Omicron and the stratification criteria of vaccination records being inconclusive impeded the precise implementation of the vaccination effect with the progression of the pandemic.

In Project II, limitations arose from the number of undetected infections. Various studies evaluated the fraction of infections that are not part of the registered confirmed cases by leveraging seropositivity tests[106,107,108,109]. Here, time-dependent changes, as well as an age-dependency of the undetected infections could be observed[106]. However, these studies are limited to the time before the emergence of vaccinations, as seropositivity can also be ascribed to vaccinations[110]. For the interpretation of the results of Project II, this limitation entails that the observed differences between settings and age groups need to be interpreted with caution. For example, the reduction of confirmed cases among school children during remote teaching could be attributed to both the reduced infection risk due to a limited number of daily contacts as well as to the ceasing in-school routine testing of the children.

Overall, Projects I and II show how the uncoordinated collection and reporting of data vital to determining pandemic characteristics can hinder the fast and sufficient implementation of precise models for the prediction of trajectories. Here, the concertation of data reporting could even be improved further if performed on a multinational level, e.g. as dictated by European health agencies[100]. A European database might streamline the generation of knowledge especially regarding the impact of NPIs, as national regulations differed vastly. Additionally, some of the data regarding hospitalized patients was only shown in pdf-reports or in varying formats on online websites and therefore needed to be entered manually into the data set. Especially in the setting at hand, where data was updated on a daily basis, the provision of data in a format that can be processed in automated procedures could substantially reduce processing times and the errors caused

by typos.

In Project III, a previously published SARS-CoV-2 viral replication model by Goyal et al.[87] was adapted to describe the viral load measured in the CARVIN study, which investigated the impact of azelastine and placebo nasal spray on the viral load and symptoms of COVID-19 patients[45]. Virus replication follows highly complex non-linear time-dependent processes and NLME modelling techniques provide the opportunity to analyse such systems. Correspondingly, virus replication models of varying complexity have been developed used to estimate the impact of various potential antiviral drugs and the timing of their administration[111,112,113,114]. These models all include the effect of the immune responses to various degrees, depending on the time of their development and the available data.

In Project III, the availability of more precise information could have lessened the necessity of simplifications and could have increased the identifiability of model parameters. Instead, most parameters were fixed to values identified by Goyal et al. and only slight adjustments were made to account for the lower disease severity of the mild COVID-19 patients in the CARVIN study compared to the hospitalized patients investigated by Goyal et al.[87]. Information regarding, for example, the time of infection or symptom onset was not available but would have provided valuable insights regarding the time scale of the infection.

Additionally, the precise time points of nasal spray application were not recorded. Here, the rinse effect of the placebo or azelastine nasal spray might have an influence on the measured viral load[115] and thereby be responsible for the high intra-individual fluctuations in viral load. As an online system for the recording of symptoms was already available during the study, the addition of a system that reminds the study participant to apply the study medication and that records the actual time of administration could have been an easy extension, especially as such reminder applications are already widely available[116].

## 5.3 Simulation and Forecasting

Especially in the beginning of the pandemic, before vaccinations and adequate treatment options were available, it was of vital importance to control the spreading of SARS-CoV-2 in order to limit the number of ICU patients. Therefore, it was of high interest to predict the trajectories of cases and ICU patients in order to manage health care resources and justify appropriate NPIs. The model presented in Project I describes the number of cases, patients, and fatalities and was developed in parallel with the progressing pandemic. Interestingly, for the description of short-term trajectories, a model exploiting stepwise changes of Rt instead of estimating a daily Rt based on the day-to-day fluctuations of the number of cases proved to be sufficient for the prediction of short-term trajectories. With

a mean period of 15.5 days between changes in the Rt, it was shown that the observed number of cases and patients could be accurately described without the need for a daily adaptation of the infection dynamics. The timing of Rt change points often correlated with rule changes regarding contact restrictions by the federal or state government. Consequently, it could be observed that the average variability of Rt between federal states decreased from 23.2 %CV to 11.2 %CV when the "Bundesnotbremse" came into force, meaning that the German government enacted contact restriction measures instead of federal state government implementing their own rules. This finding underlines that varying NPIs between federal states show varying effectiveness.

Interestingly, changes in the Rt often already occurred on the day that governmental rule changes were decided upon but not yet in effect. This suggests that the awareness for the pandemic in the population was influenced by governmental decisions and has an impact on the risk perception of the population regarding infections. Unfortunately, at the same time, this renders the forecast of the pandemic trajectory much harder, as human behaviour is hard to predict, especially during times of quickly spreading fake news over social media.

Conclusively, while it is possible to adjust predictions for increasing vaccination rates and the spreading of VOCs, predicting changes in risk perception proves difficult. Therefore, predictions should only be performed keeping in mind various possible scenarios and the unpredictability of human behaviour. Nonetheless, despite the aforementioned uncertainties around some model inputs and assumptions, modelling and simulation tools can be used to explore these uncertainties and predict plausible ranges for the pandemic's short-term trajectories[20,19].

Despite these challenges, publicly available simulation tools provide the possibility to visualize the pandemic's trajectories and can thereby help both authorities and the general public to understand the impact of NPIs[19]. The model developed in Project I was translated to an interactive online simulation tool accessible to the public via web browser (`www.covid-simulator.com`). Here, the impact of different Rt trajectories could be simulated with respect to their impact on the number of hospitalized patients, ICU patients and fatalities. Additional configuration options depended on the current major impact factors or uncertainties, such as the change of Rt due to currently emerging VOCs or vaccination willingness of the population. Next to the parameters included in the model for data description, the simulation tool included the impact of a seasonal amplitude based on observations from Gavenciak et al[117] who analysed data from 143 European regions. The Bayesian model identified a seasonal variation of viral transmission with a median reduction of 42.1% from the peak in winter (January 1$^{st}$) to the nadir in summer (July 1$^{st}$). This feature was included in order to provide more accurate long-term trajectories.

In contrast to webpages that visualize the trajectories of the pandemic based on a sin-

gle estimate and its confidence interval, public simulation tools are of the advantage that users can explore the impact of various measures on their own. For example, the simulation tools could provide trajectories for requested decreases or increases in the effective reproductive number. During the COVID-19 pandemic, they were frequently used by the press, politicians and private users in order to simulate the pandemic trajectories[118,119].

Finally, the availability of simulation tools to the public might improve adherence to the measures resolved by the government: Many studies identified autonomous motivation to be the strongest predictor for adhering to COVID-19 measures[120,121], while other studies showed that simulation tools can be of great use to increase this motivation[122]. Furthermore, compliance with preventive measures was linked to an individual's trust in science as well as to the individual´s risk perception[123]. Here, forecasting various scenarios might provide valuable insights and improve the user's understanding of their personal and the population's risk.

# 6 CONCLUSION

The presented work shows that mathematical modelling can widely support the understanding of the spread of viral infections, both within as well as between individuals.

Pharmacometric modelling of viral load-time profiles and disease severity can be used to describe impact of treatment and for the identification of individual risk factors. In this work, the combination of the azelastine-viral load PK/PD model and a viral load-infectivity model enabled to simulate the impact of azelastine on the infectivity of individuals infected with SARS-CoV-2.

Epidemiological models proved to be helpful for the understanding and prediction of pandemic trajectories. In this work, it was highlighted how the application of NLME modelling techniques for the analysis of the COVID-19 pandemic in the 16 German federal states supported the quantification of the impact of NPIs, vaccinations and testing strategies on the COVID-19 pandemic in Germany. Thereby, the effects of improved treatment options and vaccinations could be identified on the trajectory of ICU patients. Furthermore, the impact of school holidays and remote schooling could be quantified stratified by age group. Finally, simulation tools such as www.covid-simulator.com provided visualisations of future trends and made the pandemic situation more accessible for the general public.

However, in all three modelling analyses, access to data of high quality was the limiting factor: In the viral load modelling analysis, missing information necessitated that some model parameters had to be informed from literature. In the epidemiological modelling analyses, the access to data varied between federal states and the age-stratification of case notifications and vaccinations did not coincide. These limitations resulted in simplifications of the models which in return can lead to reduced model robustness with respect to predictions.

# BIBLIOGRAPHY


[1] Christiane Dings et al. “Model-Based Analysis of SARS-CoV-2 Infections, Hospitalization and Outcome in Germany, the Federal States and Districts”. In: *Viruses* 14.10 (2022). ISSN: 1999-4915. DOI: 10.3390/v14102114.

[2] Christiane Dings et al. “Effect of vaccinations and school restrictions on the spread of COVID-19 in different age groups in Germany”. In: *Infectious Disease Modelling* 9.4 (2024), pp. 1250–1264. ISSN: 2468-0427. DOI: 10.1016/j.idm.2024.07.004.

[3] Christiane Dings et al. “Pharmacometric Modeling of the Impact of Azelastine Nasal Spray on SARS-CoV-2 Viral Load and Related Symptoms in COVID-19 Patients”. In: *Pharmaceutics* 14.10 (2022). ISSN: 1999-4923. DOI: 10.3390/pharmaceutics14102059.

[4] Alex O. Holcombe. “Contributorship, Not Authorship: Use CRediT to Indicate Who Did What”. In: *Publications* 7.3 (2019). ISSN: 2304-6775. DOI: 10.3390/publications7030048.

[5] Amy Brand et al. “Beyond authorship: attribution, contribution, collaboration, and credit”. In: *Learned Publishing* 28.2 (2015), pp. 151–155. DOI: 10.1087/20150211.

[6] World Health Organization. *WHO Coronavirus Disease (COVID-19) Dashboard*. 2024. URL: covid19.who.int/ (Accessed: 10/13/2024).

[7] Ben Hu et al. “Characteristics of SARS-CoV-2 and COVID-19”. In: *Nature Reviews Microbiology* 19.3 (2021), pp. 141–154. ISSN: 1740-1534. DOI: 10.1038/s41579-020-00459-7.

[8] Yousef Alimohamadi et al. “Determine the most common clinical symptoms in COVID-19 patients: a systematic review and meta-analysis.” eng. In: *Journal of preventive medicine and hygiene* 61.3 (Sept. 2020), E304–E312. ISSN: 2421-4248 (Electronic). DOI: 10.15167/2421-4248/jpmh2020.61.3.1530.

[9] COVID-19 Treatment Guidelines Panel. *Coronavirus Disease 2019 (COVID-19) Treatment Guidelines. National Institutes of Health.* 2023. URL: www.covid19treatmentguidelines.nih.gov (Accessed: 09/06/2023).

[10] Xi He et al. “Temporal dynamics in viral shedding and transmissibility of COVID-19”. In: *Nature Medicine* 26.5 (2020), pp. 672–675. ISSN: 1546-170X. DOI: 10.1038/s41591-020-0869-5.

[11] Arif Billah, Mamun Miah, and Nuruzzaman Khan. “Reproductive number of coronavirus: A systematic review and meta-analysis based on global level evidence.” eng. In: *PloS one* 15.11 (2020), e0242128. ISSN: 1932-6203 (Electronic). DOI: 10.1371/journal.pone.0242128.

[12] Luke Taylor. “Covid-19: Brazil’s hospitals close to collapse as cases reach record high”. In: *BMJ* (Mar. 2021), 372:n800. ISSN: 1756-1833. DOI: 10.1136/bmj.n800.

[13] Michael Klompas, Meghan A. Baker, and Chanu Rhee. “Airborne Transmission of SARS-CoV-2: Theoretical Considerations and Available Evidence”. In: *JAMA* 324.5 (Aug. 2020), pp. 441–442. ISSN: 0098-7484. DOI: 10.1001/jama.2020.12458.

[14] Rami Sommerstein et al. “Risk of SARS-CoV-2 transmission by aerosols, the rational use of masks, and protection of healthcare workers from COVID-19”. In: *Antimicrobial Resistance & Infection Control* 9.1 (2020), p. 100. ISSN: 2047-2994. DOI: 10.1186/s13756-020-00763-0.

[15] Christoph Josef Hemmer et al. “Protection From COVID-19–The Efficacy of Face Masks.” eng. In: *Deutsches Arzteblatt international* 118.5 (Feb. 2021), pp. 59–65. ISSN: 1866-0452 (Electronic). DOI: 10.3238/arztebl.m2021.0119.

[16] Thomas J Layden et al. “Mathematical modeling of viral kinetics:: a tool to understand and optimize therapy”. In: *Clinics in Liver Disease* 7.1 (2003), pp. 163–178. ISSN: 1089-3261. DOI: 10.1016/S1089-3261(02)00063-6.

[17] Scott Marshall et al. “Model-Informed Drug Discovery and Development: Current Industry Good Practice and Regulatory Expectations and Future Perspectives”. In: *CPT: Pharmacometrics & Systems Pharmacology* 8.2 (2019), pp. 87–96. DOI: 10.1002/psp4.12372.

[18] Efthymios Manolis and Ralf Herold. “Pharmacometrics for Regulatory Decision Making”. In: *Clinical Pharmacokinetics* 50.10 (2011), pp. 625–626. ISSN: 1179-1926. DOI: 10.2165/11594340-000000000-00000.

[19] Asif Afzal et al. “Merits and Limitations of Mathematical Modeling and Computational Simulations in Mitigation of COVID-19 Pandemic: A Comprehensive Review”. In: *Archives of Computational Methods in Engineering* 29.2 (2022), pp. 1311–1337. ISSN: 1886-1784. DOI: 10.1007/s11831-021-09634-2.

[20] Lyndon P. James et al. “The Use and Misuse of Mathematical Modeling for Infectious Disease Policymaking: Lessons for the COVID-19 Pandemic”. In: *Medical Decision Making* 41.4 (2021), pp. 379–385. DOI: 10.1177/0272989X21990391.

[21] Martin Schonger and Daniela Sele. “Intuition and exponential growth: bias and the roles of parameterization and complexity”. In: *Mathematische Semesterberichte* 68.2 (2021), pp. 221–235. ISSN: 1432-1815. DOI: 10.1007/s00591-021-00306-7.

[22] Geoffrey Rose. “Sick individuals and sick populations”. In: *International Journal of Epidemiology* 30.3 (June 2001), pp. 427–432. ISSN: 0300-5771. DOI: 10.1093/ije/30.3.427.

[23] Yong Ge et al. “Impacts of worldwide individual non-pharmaceutical interventions on COVID-19 transmission across waves and space”. In: *International Journal of Applied Earth Observation and Geoinformation* 106 (2022), p. 102649. ISSN: 1569-8432. DOI: 10.1016/j.jag.2021.102649.

[24] Derek K Chu et al. “Physical distancing, face masks, and eye protection to prevent person-to-person transmission of SARS-CoV-2 and COVID-19: a systematic review and meta-analysis”. In: *The Lancet* 395.10242 (2020), pp. 1973–1987. ISSN: 0140-6736. DOI: 10.1016/S0140-6736(20)31142-9.

[25] Jorge Hernández-Bello et al. “Neutralizing Antibodies against SARS-CoV-2, Anti-Ad5 Antibodies, and Reactogenicity in Response to Ad5-nCoV (CanSino Biologics) Vaccine in Individuals with and without Prior SARS-CoV-2”. In: *Vaccines* 9.9 (2021). ISSN: 2076-393X. DOI: 10.3390/vaccines9091047.

[26] Mario Cazzola et al. “Controversy surrounding the Sputnik V vaccine”. In: *Respiratory Medicine* 187 (2021), p. 106569. ISSN: 0954-6111. DOI: 10.1016/j.rmed.2021.106569.

[27] European Medicines Agency (EMA). *EMA recommends first COVID-19 vaccine for authorisation in the EU*. 2020. URL: www.ema.europa.eu/en/news/ema-recommends-first-covid-19-vaccine-authorisation-eu (Accessed: 09/14/2023).

[28] European Medicines Agency (EMA). *EMA recommends COVID-19 Vaccine AstraZeneca for authorisation in the EU*. 2021. URL: www.ema.europa.eu/en/news/ema-recommends-covid-19-vaccine-astrazeneca-authorisation-eu (Accessed: 09/15/2023).

[29] Bundesministerium für Gesundheit (BMG). *Impfdashboard*. 2023. URL: www.impfdashboard.de (Accessed: 09/15/2023).

[30] Centers for Disease Control and Prevention (CDC). *SARS-CoV-2 Variant Classifications and Definitions*. 2023. URL: www.cdc.gov/coronavirus/2019-ncov/variants/variant-classifications.html (Accessed: 09/17/2023).

[31] Yuan Huang et al. “Structural and functional properties of SARS-CoV-2 spike protein: potential antivirus drug development for COVID-19”. In: *Acta Pharmacologica Sinica* 41.9 (2020), pp. 1141–1149. ISSN: 1745-7254. DOI: 10.1038/s41401-020-0485-4.

[32] Kai-Wei K Chen, Daniel Tsung-Ning Huang, and Li-Min Huang. “SARS-CoV-2 variants - Evolution, spike protein, and vaccines.” eng. In: *Biomedical journal* 45.4 (2022), pp. 573–579. ISSN: 2320-2890 (Electronic). DOI: 10.1016/j.bj.2022.04.006.

[33] Mona Sadat Mirtaleb et al. “An insight overview on COVID-19 mRNA vaccines: Advantageous, pharmacology, mechanism of action, and prospective considerations”. In: *International Immunopharmacology* 117 (2023), p. 109934. ISSN: 18781705. DOI: 10.1016/J.INTIMP.2023.109934.

[34] Weihao Shao et al. “Effectiveness of COVID-19 vaccines against SARS-CoV-2 variants of concern in real-world: a literature review and meta-analysis”. In: *Emerging Microbes & Infections* 11.1 (2022). PMID: 36069511, pp. 2383–2392. DOI: 10.1080/22221751.2022.2122582.

[35] Raj S Patel and Babita Agrawal. “Heterologous immunity induced by 1(st) generation COVID-19 vaccines and its role in developing a pan-coronavirus vaccine.” eng. In: *Frontiers in immunology* 13 (2022), p. 952229. ISSN: 1664-3224 (Electronic). DOI: 10.3389/fimmu.2022.952229.

[36] Shanti Pather et al. “Clinical development of variant-adapted BNT162b2 COVID-19 vaccines: the early Omicron era”. In: *Expert Review of Vaccines* 22.1 (2023). PMID: 37417000, pp. 650–661. DOI: 10.1080/14760584.2023.2232851.

[37] Massimo Fabiani et al. “Effectiveness of mRNA vaccines and waning of protection against SARS-CoV-2 infection and severe covid-19 during predominant circulation of the delta variant in Italy: retrospective cohort study”. In: *BMJ* 376 (2022). DOI: 10.1136/bmj-2021-069052.

[38] Deborah Cromer et al. “Predicting vaccine effectiveness against severe COVID-19 over time and against variants: a meta-analysis”. In: *Nature Communications* 14.1 (2023), p. 1633. ISSN: 2041-1723. DOI: 10.1038/s41467-023-37176-7.

[39] Yannan Shen et al. “Monitoring non-pharmaceutical public health interventions during the COVID-19 pandemic”. In: *Scientific Data* 8.1 (2021), p. 225. ISSN: 2052-4463. DOI: 10.1038/s41597-021-01001-x.

[40] Moran Bodas et al. “Lockdown Efficacy in Controlling the Spread of COVID-19 May Be Waning Due to Decline in Public Compliance, Especially among Unvaccinated Individuals: A Cross-Sectional Study in Israel”. In: *International Journal*

*of Environmental Research and Public Health* 19.9 (2022). ISSN: 1660-4601. DOI: 10.3390/ijerph19094943.

[41] Naoka Murakami et al. "Therapeutic advances in COVID-19". In: *Nature Reviews Nephrology* 19.1 (2023), pp. 38–52. ISSN: 1759-507X. DOI: 10.1038/s41581-022-00642-4.

[42] Deutsche Gesellschaft für Internistische Intensivmedizin und Notfallmedizin e.V. (DGIIN) et al. *S3-Leitlinie - Empfehlungen zur Therapie von Patienten mit COVID-19, Version März 2023*. 2023. URL: www.register.awmf.org/assets/guidelines/113-001LGl_S3_Empfehlungen-zur-stationaeren-Therapie-von-Patienten-mit-COVID-19_2023-03.pdf (Accessed: 09/18/2023).

[43] Leah R. Reznikov et al. "Identification of antiviral antihistamines for COVID-19 repurposing". In: *Biochemical and Biophysical Research Communications* 538 (2021), pp. 173–179. ISSN: 10902104. DOI: 10.1016/j.bbrc.2020.11.095.

[44] Jonathan A. Bernstein. "Azelastine hydrochloride: a review of pharmacology, pharmacokinetics, clinical efficacy and tolerability". In: *Currend Medical research and Opinions* 23.10 (2007), pp. 2442 –2452. DOI: 10.1185/030079907X226302.

[45] Jens Peter Klussmann et al. "Early intervention with azelastine nasal spray may reduce viral load in SARS-CoV-2 infected patients". In: *Scientific Reports* 13.1 (2023), p. 6839. ISSN: 2045-2322. DOI: 10.1038/s41598-023-32546-z.

[46] Christina Lee and Jonathan Corren. "Review of azelastine nasal spray in the treatment of allergic and non-allergic rhinitis". In: *Expert Opinion on Pharmacotherapy* 8.5 (2007). PMID: 17376024, pp. 701–709. DOI: 10.1517/14656566.8.5.701.

[47] Shuai Ge et al. "Azelastine inhibits viropexis of SARS-CoV-2 spike pseudovirus by binding to SARS-CoV-2 entry receptor ACE2". In: *Virology* 560 (2021), pp. 110–115. ISSN: 0042-6822. DOI: 10.1016/j.virol.2021.05.009.

[48] Mohammad M Ghahremanpour et al. *Identification of 14 Known Drugs as Inhibitors of the Main Protease of SARS-CoV-2.* eng. 2020. DOI: 10.1101/2020.08.28.271957.

[49] Hasanain Abdulhameed Odhar et al. "Molecular docking and dynamics simulation of FDA approved drugs with the main protease from 2019 novel coronavirus". eng. In: *Bioinformation* 16.3 (2020), pp. 236–244. ISSN: 0973-2063. DOI: 10.6026/97320630016236.

[50] Li Yang et al. "Identification of SARS-CoV-2 entry inhibitors among already approved drugs". In: *Acta Pharmacologica Sinica* 42.8 (2021), pp. 1347–1353. ISSN: 1745-7254. DOI: 10.1038/s41401-020-00556-6.

[51] Robert Konrat et al. “The Anti-Histamine Azelastine, Identified by Computational Drug Repurposing, Inhibits Infection by Major Variants of SARS-CoV-2 in Cell Cultures and Reconstituted Human Nasal Tissue”. In: *Frontiers in Pharmacology* 13 (2022). ISSN: 1663-9812. DOI: 10.3389/fphar.2022.861295.

[52] EFPIA MID3 Workgroup et al. “Good Practices in Model-Informed Drug Discovery and Development: Practice, Application, and Documentation”. In: *CPT: Pharmacometrics & Systems Pharmacology* 5.3 (2016), pp. 93–122. DOI: 10.1002/psp4.12049.

[53] D. R. Mould and R. N. Upton. “Basic concepts in population modeling, simulation, and model-based drug development”. In: *CPT: Pharmacometrics and Systems Pharmacology* 1.1 (2012), pp. 1–14. ISSN: 21638306. DOI: 10.1038/psp.2012.4.

[54] EMA. “Guideline on reporting the results of population pharmacokinetic analyses”. 2008.

[55] FDA. “Guidance for Industry Population Pharmacokinetics Guidance for Industry Population Pharmacokinetics”. Feb. 2022.

[56] Hannah M Jones, Iain B Gardner, and Kenny J Watson. “Modelling and PBPK Simulation in Drug Discovery”. In: *The AAPS Journal* 11.1 (2009), pp. 155–166. ISSN: 1550-7416. DOI: 10.1208/s12248-009-9088-1.

[57] Piet H van der Graaf and Neil Benson. “Systems Pharmacology: Bridging Systems Biology and Pharmacokinetics-Pharmacodynamics (PKPD) in Drug Discovery and Development”. In: *Pharmaceutical Research* 28.7 (2011), pp. 1460–1464. ISSN: 1573-904X. DOI: 10.1007/s11095-011-0467-9.

[58] Angela R McLean. *Infectious Disease Modeling.* eng. 2012. DOI: 10.1007/978-1-4614-5719-0_5.

[59] Ashish Goyal et al. “Viral load and contact heterogeneity predict SARS-CoV-2 transmission and super-spreading events”. In: *eLife* 10 (2021), pp. 1–63. ISSN: 2050084X. DOI: 10.7554/ELIFE.63537.

[60] Peter J White. *Mathematical Models in Infectious Disease Epidemiology.* eng. 2017. DOI: 10.1016/B978-0-7020-6285-8.00005-8.

[61] Oluwakemi Abiodun, Adebimpe Olukayode, and James Ndako. “Mathematical Modeling and Its Methodological Approach: Application to Infectious Disease”. In: *2023 International Conference on Science, Engineering and Business for Sustainable Development Goals (SEB-SDG).* Vol. 1. 2023, pp. 1–14. DOI: 10.1109/SEB-SDG57117.2023.10124470.

[62] William Ogilvy Kermack, Anderson G. McKendrick, and Gilbert Thomas Walker. "A contribution to the mathematical theory of epidemics". In: *Proceedings of the Royal Society of London. Series A, Containing Papers of a Mathematical and Physical Character* 115.772 (1927), pp. 700–721. DOI: 10.1098/rspa.1927.0118.

[63] Teddy Lazebnik. "Computational applications of extended SIR models: A review focused on airborne pandemics". In: *Ecological Modelling* 483 (2023), p. 110422. ISSN: 0304-3800. DOI: 10.1016/j.ecolmodel.2023.110422.

[64] Romain Narci et al. "Inference in Gaussian state-space models with mixed effects for multiple epidemic dynamics". In: *Journal of Mathematical Biology* 85.4 (2022), p. 40. ISSN: 1432-1416. DOI: 10.1007/s00285-022-01806-3.

[65] Carolin Zitzmann and Lars Kaderali. "Mathematical Analysis of Viral Replication Dynamics and Antiviral Treatment Strategies: From Basic Models to Age-Based Multi-Scale Modeling". In: *Frontiers in Microbiology* 9 (2018). ISSN: 1664-302X. DOI: 10.3389/fmicb.2018.01546.

[66] Ali A. Rabaan et al. "Viral Dynamics and Real-Time RT-PCR Ct Values Correlation with Disease Severity in COVID-19". In: *Diagnostics* 11.6 (2021). ISSN: 2075-4418. DOI: 10.3390/diagnostics11061091.

[67] José C. Pinheiro and Douglas M. Bates. *Mixed-Effects Models in S and S-PLUS*. Springer-Verlag, 2000. DOI: 10.1007/B98882.

[68] Lewis B Sheiner and Stuart L Beal. "Evaluation of methods for estimating population pharmacokinetic parameters. I. Michaelis-menten model: Routine clinical pharmacokinetic data". In: *Journal of Pharmacokinetics and Biopharmaceutics* 8.6 (1980), pp. 553–571. ISSN: 0090-466X. DOI: 10.1007/BF01060053.

[69] Lewis B Sheiner and Stuart L Beal. "Evaluation of methods for estimating population pharmacokinetic parameters II. Biexponential model and experimental pharmacokinetic data". In: *Journal of Pharmacokinetics and Biopharmaceutics* 9.5 (1981), pp. 635–651. ISSN: 0090-466X. DOI: 10.1007/BF01061030.

[70] Robert J. Bauer. "NONMEM Tutorial Part I: Description of Commands and Options, With Simple Examples of Population Analysis". In: *CPT: Pharmacometrics & Systems Pharmacology* 8.8 (2019), pp. 525–537. DOI: 10.1002/psp4.12404.

[71] Mats Karlsson et al. "Assumption Testing in Population Pharmacokinetic Models: Illustrated with an Analysis of Moxonidine Data from Congestive Heart Failure Patients". In: *Journal of pharmacokinetics and biopharmaceutics* 26 (May 1998), pp. 207–46. DOI: 10.1023/A:1020561807903.

[72] Larry F. Lacey et al. “Common noncompartmental pharmacokinetic variables: are they normally or log-normally distributed?” In: *Journal of biopharmaceutical statistics* 7.1 (1997), pp. 171–178. ISSN: 1054-3406. DOI: 10.1080/10543409708835177.

[73] Steven A. Julious and Camille A.M. Debarnot. “Why are pharmacokinetic data summarized by arithmetic means?” In: *Journal of biopharmaceutical statistics* 10.1 (2000), pp. 55–71. ISSN: 1054-3406. DOI: 10.1081/BIP-100101013.

[74] Ulrika Wählby et al. “Models for time-varying covariates in population pharmacokinetic- pharmacodynamic analysis”. In: *British Journal of Clinical Pharmacology* 58.4 (2004), pp. 367–377. ISSN: 03065251. DOI: 10.1111/j.1365-2125.2004.02170.x.

[75] Matthew M Hutmacher and Kenneth G Kowalski. “Covariate selection in pharmacometric analyses: a review of methods”. In: *Br J Clin Pharmacol* 79.1 (2015), pp. 132–47. DOI: 10.1111/bcp.12451.

[76] Ulrika Waehlby, E. Niclas Jonsson, and Mats O. Karlsson. “Comparison of stepwise covariate model building strategies in population pharmacokinetic-pharmacodynamic analysis”. In: *AAPS PharmSci* 4.4 (2002), pp. 68–79. DOI: 10.1208/ps040427.

[77] Pauline van den Driessche. “Reproduction numbers of infectious disease models.” eng. In: *Infectious Disease Modelling* 2.3 (2017), pp. 288–303. ISSN: 2468-0427 (Electronic). DOI: 10.1016/j.idm.2017.06.002.

[78] Michael G Roberts and Johan A P Heesterbeek. “Model-consistent estimation of the basic reproduction number from the incidence of an emerging infection”. In: *Journal of Mathematical Biology* 55.5 (2007), pp. 803–816. ISSN: 1432-1416. DOI: 10.1007/s00285-007-0112-8.

[79] Thomas V. Inglesby. “Public Health Measures and the Reproduction Number of SARS-CoV-2”. In: *JAMA* 323.21 (June 2020), pp. 2186–2187. ISSN: 0098-7484. DOI: 10.1001/jama.2020.7878.

[80] Laura F White et al. “Statistical Estimation of the Reproductive Number From Case Notification Data”. In: *American Journal of Epidemiology* 190.4 (Oct. 2020), pp. 611–620. ISSN: 0002-9262. DOI: 10.1093/aje/kwaa211.

[81] Anne Cori et al. “A New Framework and Software to Estimate Time-Varying Reproduction Numbers During Epidemics”. In: *American Journal of Epidemiology* 178.9 (Sept. 2013), pp. 1505–1512. ISSN: 0002-9262. DOI: 10.1093/aje/kwt133.

[82] Jacco Wallinga and Peter Teunis. “Different Epidemic Curves for Severe Acute Respiratory Syndrome Reveal Similar Impacts of Control Measures”. In: *American Journal of Epidemiology* 160.6 (Sept. 2004), pp. 509–516. DOI: 10.1093/aje/kwh255.

[83] Matthias an der Heiden and Osamah Hamouda. “Schätzung der aktuellen Entwicklung der SARS-CoV-2-Epidemie in Deutschland – Nowcasting”. In: *Epid Bull* 17 (2020), pp. 10–16. DOI: 10.25646/6692.4.

[84] Rahil Sachak-Patwa et al. “A target-cell limited model can reproduce influenza infection dynamics in hosts with differing immune responses”. In: *Journal of Theoretical Biology* 567 (2023), p. 111491. ISSN: 0022-5193. DOI: 10.1016/j.jtbi.2023.111491.

[85] Esteban A. Hernandez-Vargas and Jorge X. Velasco-Hernandez. “In-host Mathematical Modelling of COVID-19 in Humans”. In: *Annual Reviews in Control* 50 (2020), pp. 448–456. ISSN: 1367-5788. DOI: 10.1016/j.arcontrol.2020.09.006.

[86] Rob J. De Boer and Alan S. Perelson. “Target Cell Limited and Immune Control Models of HIV Infection: A Comparison”. In: *Journal of Theoretical Biology* 190.3 (1998), pp. 201–214. ISSN: 0022-5193. DOI: 10.1006/jtbi.1997.0548.

[87] Ashish Goyal, E Fabian Cardozo-Ojeda, and Joshua T Schiffer. “Potency and timing of antiviral therapy as determinants of duration of SARS-CoV-2 shedding and intensity of inflammatory response.” eng. In: *Science advances* 6.47 (2020). ISSN: 2375-2548 (Electronic). DOI: 10.1126/sciadv.abc7112.

[88] Cristina Leon et al. “Modelling of the Innate and Adaptive Immune Response to SARS Viral Infection, Cytokine Storm and Vaccination”. In: *Vaccines* 11.1 (2023). ISSN: 2076-393X. DOI: 10.3390/vaccines11010127.

[89] Sean Quan Du and Weiming Yuan. “Mathematical modeling of interaction between innate and adaptive immune responses in COVID-19 and implications for viral pathogenesis”. In: *Journal of Medical Virology* 92.9 (2020), pp. 1615–1628. DOI: 10.1002/jmv.25866.

[90] Nicholas H.G. Holford and Lewis B. Sheiner. “Kinetics of pharmacologic response”. In: *Pharmacology & Therapeutics* 16.2 (1982), pp. 143–166. ISSN: 0163-7258. DOI: 10.1016/0163-7258(82)90051-1.

[91] William O Kermack and Anderson G McKendrick. “Contributions to the mathematical theory of epidemics—I”. In: *Bulletin of Mathematical Biology* 53.1 (1991), pp. 33–55. ISSN: 1522-9602. DOI: 10.1007/BF02464423.

[92] Jayakrishnan Unnikrishnan, Sujith Mangalathu, and Raman V Kutty. "Estimating under-reporting of COVID-19 cases in Indian states: an approach using a delay-adjusted case fatality ratio". In: *BMJ Open* 11.1 (2021). ISSN: 2044-6055. DOI: 10.1136/bmjopen-2020-042584.

[93] Matthias Wjst and Clemens Wendtner. "High variability of COVID-19 case fatality rate in Germany". In: *BMC Public Health* 23.1 (2023), p. 416. ISSN: 1471-2458. DOI: 10.1186/s12889-023-15112-0.

[94] Saskia Morwinsky, Natalie Nitsche, and Enrique Acosta. "COVID-19 fatality in Germany: Demographic determinants of variation in case-fatality rates across and within German federal states during the first and second waves". In: *Demographic Research* 45 (2021), pp. 1355–1372. ISSN: 14359871, 23637064. DOI: 10.4054/DemRes.2021.45.45.

[95] Mark B Shapiro et al. "Adaptive Susceptible-Infectious-Removed Model for Continuous Estimation of the COVID-19 Infection Rate and Reproduction Number in the United States: Modeling Study." eng. In: *Journal of medical Internet research* 23.4 (2021), e24389. ISSN: 1438-8871 (Electronic). DOI: 10.2196/24389.

[96] Manuel Pájaro et al. "Stochastic SIR model predicts the evolution of COVID-19 epidemics from public health and wastewater data in small and medium-sized municipalities: A one year study". In: *Chaos, Solitons & Fractals* 164 (2022), p. 112671. ISSN: 0960-0779. DOI: 10.1016/j.chaos.2022.112671.

[97] Thomas Plümper and Eric Neumayer. "Fueling the Covid-19 pandemic: summer school holidays and incidence rates in German districts". In: *Journal of Public Health* 43.3 (Mar. 2021), e415–e422. ISSN: 1741-3842. DOI: 10.1093/pubmed/fdab080.

[98] Clara von Bismarck-Osten, Kirill Borusyak, and Uta Schönberg. "The role of schools in transmission of the SARS-CoV-2 virus: quasi-experimental evidence from Germany". In: *Economic Policy* 37.109 (Jan. 2022), pp. 87–130. ISSN: 0266-4658. DOI: 10.1093/epolic/eiac001.

[99] Amit Huppert and Guy Katriel. "Mathematical modelling and prediction in infectious disease epidemiology". In: *Clinical Microbiology and Infection* 19.11 (2013), pp. 999–1005. ISSN: 1198-743X. DOI: 10.1111/1469-0691.12308.

[100] Marta C. Nunes et al. "Redefining pandemic preparedness: Multidisciplinary insights from the CERP modelling workshop in infectious diseases, workshop report". In: *Infectious Disease Modelling* 9.2 (2024), pp. 501–518. ISSN: 2468-0427. DOI: 10.1016/j.idm.2024.02.008.

[101] *Infektionsschutzgesetz vom 20. Juli 2000 (BGBl. I S. 1045), das zuletzt durch Artikel 8v des Gesetzes vom 12. Dezember 2023 (BGBl. 2023 I Nr. 359) geändert worden ist*. URL: www.gesetze-im-internet.de/ifsg/IfSG.pdf (Accessed: 08/18/2024).

[102] Robert Koch-Institut. *Intensivkapazitäten und COVID-19-Intensivbettenbelegung in Deutschland*. 2024. DOI: 10.5281/zenodo.13168944.

[103] Niklas Willrich et al. "Update: Erfassung der SARS-CoV-2-PCR-Testzahlen in Deutschland und die Entwicklung der Testzahlen in ärztlichen Praxen". In: 47 (2021), pp. 18–25. DOI: 10.25646/9306.

[104] Robert Koch-Institut. *SARS-CoV-2-PCR-Testungen in Deutschland*. 2023. DOI: 10.5281/zenodo.8069452.

[105] Oliver McManus et al. "Predicting COVID-19 Incidence Using Wastewater Surveillance Data, Denmark, October 2021–June 2022". In: *Emerging Infectious Disease journal* 29.8 (2023), p. 1589. ISSN: 1080-6059. DOI: 10.3201/eid2908.221634.

[106] Marc Schneble et al. "A statistical model for the dynamics of COVID-19 infections and their case detection ratio in 2020". In: *Biometrical Journal* 63.8 (2021), pp. 1623–1632. DOI: 10.1002/bimj.202100125.

[107] Maria Vittoria Barbarossa et al. "Modeling the spread of COVID-19 in Germany: Early assessment and possible scenarios." eng. In: *PloS one* 15.9 (2020), e0238559. ISSN: 1932-6203 (Electronic). DOI: 10.1371/journal.pone.0238559.

[108] Irene Rocchetti et al. "Estimating the size of undetected cases of the COVID-19 outbreak in Europe: an upper bound estimator". In: *Epidemiologic Methods* 9.s1 (2020), p. 20200024. DOI: doi:10.1515/em-2020-0024.

[109] Christian Staerk, Tobias Wistuba, and Andreas Mayr. "Estimating effective infection fatality rates during the course of the COVID-19 pandemic in Germany". In: *BMC Public Health* 21.1 (2021), p. 1073. ISSN: 1471-2458. DOI: 10.1186/s12889-021-11127-7.

[110] Emanuele Amodio et al. "Antibodies Responses to SARS-CoV-2 in a Large Cohort of Vaccinated Subjects and Seropositive Patients". In: *Vaccines* 9.7 (2021). DOI: 10.3390/vaccines9070714.

[111] Isam Al-Darabsah, Kang-Ling Liao, and Stéphanie Portet. "A simple in-host model for COVID-19 with treatments: model prediction and calibration". In: *Journal of Mathematical Biology* 86.2 (2023), p. 20. ISSN: 1432-1416. DOI: 10.1007/s00285-022-01849-6.

[112] Shengyuan Zhang et al. “SARS-CoV-2 viral dynamic modeling to inform model selection and timing and efficacy of antiviral therapy”. In: *CPT: Pharmacometrics & Systems Pharmacology* 12.10 (2023), pp. 1450–1460. DOI: 10.1002/psp4.13022.

[113] Antonio Gonçalves et al. “Timing of Antiviral Treatment Initiation is Critical to Reduce SARS-CoV-2 Viral Load”. In: *CPT: Pharmacometrics & Systems Pharmacology* 9.9 (2020), pp. 509–514. DOI: 10.1002/psp4.12543.

[114] Steven Sanche et al. “A simple model of COVID-19 explains disease severity and the effect of treatments”. In: *Scientific Reports* 12.1 (2022), p. 14210. ISSN: 2045-2322. DOI: 10.1038/s41598-022-18244-2.

[115] Suzy Huijghebaert et al. “Saline nasal irrigation and gargling in COVID-19: a multidisciplinary review of effects on viral load, mucosal dynamics, and patient outcomes”. In: *Frontiers in Public Health* 11 (2023). ISSN: 2296-2565. DOI: 10.3389/fpubh.2023.1161881.

[116] Katarzyna Stawarz, Anna L. Cox, and Ann Blandford. “Don’t forget your pill! designing effective medication reminder apps that support users’ daily routines”. In: *Proceedings of the SIGCHI Conference on Human Factors in Computing Systems*. CHI ’14. Toronto, Ontario, Canada: Association for Computing Machinery, 2014, 2269–2278. ISBN: 9781450324731. DOI: 10.1145/2556288.2557079.

[117] Tomáš Gavenčiak et al. “Seasonal variation in SARS-CoV-2 transmission in temperate climates: A Bayesian modelling study in 143 European regions”. In: *PLOS Computational Biology* 18.8 (Aug. 2022), pp. 1–14. DOI: 10.1371/journal.pcbi.1010435.

[118] Bohdan Nosyk et al. “Dissemination Science to Advance the Use of Simulation Modeling: Our Obligation Moving Forward”. In: *Medical Decision Making* 40.6 (2020). PMID: 32755285, pp. 718–721. DOI: 10.1177/0272989X20945308.

[119] ZDF heute show. *Die Bundesnotbremse kommt. Bald. Demnächst. Hoffentlich. | heute-show vom 16.04.2021*. Youtube. URL: www.youtube.com/watch?v=pQignyIcyB8.

[120] Psychological Science Accelerator Self-Determination Theory Collaboration. “A global experiment on motivating social distancing during the COVID-19 pandemic”. In: *Proceedings of the National Academy of Sciences* 119.22 (2022), e2111091119. DOI: 10.1073/pnas.2111091119.

[121] Sofie Morbée et al. “Adherence to COVID-19 measures: The critical role of autonomous motivation on a short- and long-term basis.” In: *Motivation Science* 7.4 (2021), pp. 487–496. DOI: 10.1037/mot0000250.

[122] Isabel Buil, Sara Catalán, and Eva Martínez. “Encouraging intrinsic motivation in management training: The use of business simulation games”. In: *The International Journal of Management Education* 17.2 (2019), pp. 162–171. ISSN: 1472-8117. DOI: 10.1016/j.ijme.2019.02.002.

[123] Nejc Plohl and Bojan Musil. “Modeling compliance with COVID-19 prevention guidelines: the critical role of trust in science”. In: *Psychology, Health & Medicine* 26.1 (2021). PMID: 32479113, pp. 1–12. DOI: 10.1080/13548506.2020.1772988.

# APPENDIX

## A Supplementary Material to the Publications

### *A1 Project I: COVID-19 Hospitalizations and Deaths*

### *A1.1 Supplementary Document and Tables*

Attached as PDF: Figure S1.pdf

**Figure S1.** Descriptive performance plots for Germany and all federal states. Points: observations, lines: model simulations. Information about the number of inpatients was not available for Germany and several federal states.

Attached as PDF: Figure S2.pdf

**Figure S2.** Descriptive performance plots for German districts (NUTS-3). Points: observations, lines: model simulations. Information about the number of ICU and ventilated patients was not available for 4 districts.

Attached as .mod-file: ModelFile S1.mod

**Model File S1.** NONMEM model file of the infectiousness model

Attached as .mod-file: ModelFile S2. mod

**Model File S2.** NONMEM model file of the full model

**Supplementary Table S1.** Data Sources

| Area | Data | Source |
|---|---|---|
| Germany and federal states | Cases, recoveries, fatalities | Berliner Morgenpost [18] |
| Germany and federal states | ICU with and without ventilation | DIVI Intensivregister [33] |
| Germany and federal states | Number of tests and positive rates | RKI [19] |
| German districts | Cases with age groups and sex distribution | RKI [19] |
| German districts | ICU with and without ventilation | RKI documentation of DIVI data [34] |
| Bavaria | Occupied hospital beds | Bavarian government [20] |
| Berlin | Occupied hospital beds and daily hospitalizations | Berlin government [21] |
| Brandenburg | Occupied hospital beds | Brandenburg government [25] |
| Bremen | Occupied hospital beds | Bremen government [26] |
| Hamburg | Occupied hospital beds | Hamburg government [27] |
| Hesse | Occupied hospital beds and daily hospitalizations | Hesse government, via email |
| Lower Saxony | Occupied hospital beds | Lower Saxony government [28] |
| Mecklenburg-Vorpommern | Occupied hospital beds and daily hospitalizations | Mecklenburg-Vorpommern government [29] |
| North Rhine-Westphalia | Occupied hospital beds and daily hospitalizations | North Rhine-Westphalia government [30] |

| | | |
|---|---|---|
| Rhineland-Palatinate | Occupied hospital beds and daily hospitalizations | Rhineland-Palatinate government, via email |
| Rhineland-Palatinate | Daily hospitalizations | Rhineland-Palatinate government [31] |
| Saarland | Occupied hospital beds | Saarland government, via email |
| Saxony | Occupied hospital beds | Saxony government [32] |
| Saxony-Anhalt | Daily hospitalizations | Saxony-Anhalt government [22] |
| Schleswig-Holstein | Occupied hospital beds and daily hospitalizations | Christian-Albrechts-Universität zu Kiel [23] |
| Thuringia | Daily hospitalizations | Thuringia government [24] |

**Table S2.** Summary of the clinical database. Age is summarized as median and interquartile range.

| | | **Total inpatients** | **General ward patients** | **ICU patients** | **ICU patients not ventilated** | **ICU patients ventilated** |
|---|---|---|---|---|---|---|
| N | | 28847 | 23612 | 5235 | 1727 | 3508 |
| Age [years] | | 73 (57-83) | 73 (56-83) | 72 (61-80) | 71 (57-81) | 73 (63-80) |
| Sex | Male | 15300 (53%) | 11869 (50%) | 3431 (66%) | 1078 (62%) | 2353 (67%) |
| | Female | 13547 (47%) | 11743 (50%) | 1804 (34%) | 649 (38%) | 1155 (33%) |
| Fatalities | | 6913 (24%) | 4204 (18%) | 2709 (52%) | 412 (24%) | 2297 (65%) |

**Table S3.** Changes in infectiousness (Rt) according to NPIs and model estimated changepoints (CP).

| **Date of CP** | **NPI/Explanation for change in infectiousness** | **Model estimated CP** | **Rt Germany (lowest – highest in federal states)** | **Relative Change** | **Inter-state variability [%CV]** |
|---|---|---|---|---|---|
| Initial R | No NPIs in action | - | 2.78 | - | - |
| 16-19 Mar 2020 | School closure (differs between federal states) | No | 1.92 (1.37-2.79) | -31% | 18.7% |
| 21-23 Mar 2020 | Curfew or restraining order (differs between federal states) | No | 1.1 (0.70-1.83) | -43% | 24.1% |
| 1 Apr 2020 | No distinguishable NPIs, might be accountable to a raised awareness in population | Yes | 0.64 (0.41-1.13) | -42% | 25.5% |
| 26 Apr 2020 | Mandatory face masks in public buildings and public transport becoming effective between 22 and 29 April (differs between federal states); the average Rt in Germany is stable, however, there are significant changes between the federal state Rts | Yes | 0.64 (0.29-1.05) | 0% | 36.7% |
| 7 May 2020 | Lifting of some restrictions on 6 May | Yes | 0.72 (0.50-1.07) | +13% | 21.7% |

| | | | | | |
|---|---|---|---|---|---|
| 6 Jun 2020 | Local hotspots with many infected individuals while the total number of weekly cases is low leading to local short term changes of Rt | Yes | 1.08 (0.55-2.01) | +51% | 40.6% |
| 18 Jun 2020 | Local hotspots with many infected individuals while the total number of weekly cases is low leading to local short term changes of Rt | Yes | 0.86 (0.58-1.35) | -21% | 27.2% |
| 12 Jul 2020 | Many infections among travelers returning to Germany | Yes | 1.33 (1.19-1.58) | +55% | 6.9% |
| 10 Aug 2020 | Obligatory PCR test for travelers since 8 August | Yes | 1.05 (0.57-1.70) | -21% | 34.1% |
| 20 Aug 2020 | Various local increases or liftings of restrictions over the course of August -September | Yes | 0.95 (0.68-1.33) | -10% | 31.6% |
| 7 Sep 2020 | Various local increases or liftings of restrictions over the course of August -September | Yes | 1.25 (0.99-1.50) | +32% | 10.2% |
| 4 Oct 2020 | - | Yes | 1.51 (1.07-2.18) | +21% | 18.3% |
| 12 Oct 2020 | 14 October new local resolution for counties with high incidence | Yes | 1.55 (1.34-1.81) | +3% | 6.3% |
| 28 Oct 2020 | Resolution of “Lockdown light” | Yes | 1.12 (0.92-1.44) | -28% | 11.3% |
| 6 Nov 2020 | Resolutions of “Lockdown light” effective on 2 November | Yes | 1.00 (0.75-1.31) | -11% | 12.6% |
| 19 Nov 2020 | New infection protection law resoluted on 18 November | Yes | 0.98 (0.75-1.36) | -2% | 15.1% |
| 30 Nov 2020 | - | Yes | 1.2 (1.1-1.36) | +25% | 6.2% |
| 18 Dec 2020 | Further lockdown restrictions in force at 16 December | Yes | 0.67 (0.53-0.89) | -45% | 14.6% |
| 28 Dec 2020 | Increase of personal contacts and delay in reporting during the Christmas holidays | Yes | 1.22 (1.08-1.45) | 83% | 6.3% |
| 8 Jan 2021 | Further lockdown restrictions in force an 11 January | Yes | 0.80 (0.64-0.95) | -35% | 9.3% |
| 22 Jan 2021 | Differing reopening of schools between federal states, 19 January: expansion of federal lockdown until 14 February | Yes | 0.82 (0.48-1.42) | +4% | 29% |
| 29 Jan 2021 | Travel restrictions from countries with high incidence of VOC B.1.1.7 at 30 January | Yes | 0.76 (0.67-0.87) | -8% | 8.6% |
| 11 Feb 2021 | Federal government expands lockdown until 7 March; only some restrictions are lifted | Yes | 0.93 (0.82-0.99) | +23% | 6.1% |
| 8 Mar 2021 | Lifting of several restrictions by the German federal government | No | 0.99 (0.94-1.04) | +6% | 3.9% |

**Table S4.** Fractions of confirmed cases hospitalized, treated at ICU, ventilated and death rates as functions of age (a) and sex (s) as extracted from the clinical database.

| | Model function | Age group [years] | Female (F) [%] | Male (M) [%] |
|---|---|---|---|---|
| Fraction hospitalized | fh(a, s) | 0 to 4 | 3.02 | 3.70 |
| | | 5 to 14 | 0.90 | 0.90 |
| | | 15 to 35 | 2.38 | 1.54 |
| | | 35 to 59 | 4.45 | 7.45 |
| | | 60 to 79 | 20.6 | 29.1 |
| | | 80+ | 29.6 | 50.3 |
| Fraction treated at ICU of inpatients | fi(a, s) | 0 to 4 | 6.05 | 23.7 |
| | | 5 to 14 | 5.87 | 19.6 |
| | | 15 to 35 | 9.64 | 22.2 |
| | | 35 to 59 | 21.4 | 35.7 |
| | | 60 to 79 | 35.3 | 54.1 |
| | | 80+ | 21.4 | 35.1 |
| Fraction ventilated of ICU patients | fv(a, s) | 0 to 4 | 30.8 | 30.8 |
| | | 5 to 14 | 44.4 | 44.4 |
| | | 15 to 35 | 46.3 | 46.3 |
| | | 35 to 59 | 60.0 | 60.0 |
| | | 60 to 79 | 71.9 | 71.9 |
| | | 80+ | 66.6 | 66.6 |
| Fraction death (general ward) | fdh(a, s) | 0 to 34 | 0 | 0 |
| | | 35 to 59 | 1.25 | 1.25 |
| | | 60 to 79 | 10.1 | 14.7 |
| | | 80+ | 33.4 | 41.4 |
| Fraction death (ICU not ventilated) | fdi(a, s) | 0 to 34 | 0 | 0 |
| | | 35 to 59 | 4.53 | 4.53 |
| | | 60 to 79 | 19.4 | 19.4 |
| | | 80+ | 33.4 | 33.4 |
| Fraction death (ICU ventilated) | fdv(a, s) | 0 to 4 | 0 | 0 |
| | | 5 to 14 | 25.0 | 25.0 |
| | | 15 to 35 | 18.0 | 18.0 |
| | | 35 to 59 | 37.2 | 37.2 |
| | | 60 to 79 | 65.3 | 65.3 |
| | | 80+ | 84.1 | 84.1 |
| Fraction death (outpatients) | fda(a, s) | 0 to 59 | 0 | 0 |
| | | 60 to 79 | 1.72 | 2.73 |
| | | 80+ | 18.3 | 22.6 |

**References**

18. Corona Zahlen Aktuell: Karte Für Deutschland + Weltweit. Available online: https://interaktiv.morgenpost.de/corona-virus-karte-infektionen-deutschland-weltweit/ (accessed on 4 August 2022).
19. SurvStat@RKI 2.0. Available online: https://survstat.rki.de/Content/Query/Create.aspx (accessed on 4 August 2022).

20. Informationen Zu Corona: Häufige Fragen-Bayerisches Staatsministerium Des Innern, Für Sport Und Integration. Available online: https://www.stmi.bayern.de/miniwebs/coronavirus/lage/index.php (accessed on 4 August 2022).
21. COVID-19 Berlin. Available online: https://www.berlin.de/corona/lagebericht/desktop/corona.html#stationäre-behandlung (accessed on 4 August 2022).
22. Pressemitteilungen|Ministerium Für Soziales, Gesundheit, Integration Und Verbraucherschutz. Available online: https://msgiv.brandenburg.de/msgiv/de/presse/pressemitteilungen/ (accessed on 4 August 2022).
23. Corona-Fallzahlen-Die Senatorin Für Gesundheit, Frauen Und Verbraucherschutz. Available online: https://www.gesundheit.bremen.de/corona/zahlen/corona-fallzahlen-37649 (accessed on 4 August 2022).
24. Corona: Zahlen, Fälle, Statistik von COVID-19-Hamburg.De. Available online: https://www.hamburg.de/corona-zahlen/ (accessed on 4 August 2022).
25. Presseinformationen|Nds. Ministerium Für Soziales, Gesundheit Und Gleichstellung. Available online: https://www.ms.niedersachsen.de/startseite/service_kontakt/presseinformationen/ (accessed on 4 August 2022).
26. Daten Zur Corona-Pandemie-LAGuS. Available online: https://www.lagus.mv-regierung.de/Gesundheit/InfektionsschutzPraevention/Daten-Corona-Pandemie (accessed on 4 August 2022).
27. NRW-Dashboard Zur Corona-Pandemie. Available online: https://www.giscloud.nrw.de/corona-dashboard.html (accessed on 4 August 2022).
28. Coronavirus SARS-CoV-2: Aktuelle Fallzahlen Für Rheinland-Pfalz. Available online: https://lua.rlp.de/de/presse/detail/news/News/detail/coronavirus-sars-cov-2-aktuelle-fallzahlen-fuer-rheinland-pfalz/ (accessed on 4 August 2022).
29. Infektionsfälle in Sachsen-Coronavirus in Sachsen-Sachsen.De. Available online: https://www.coronavirus.sachsen.de/infektionsfaelle-in-sachsen-4151.html (accessed on 4 August 2022).
30. Pressemitteilungen. Available online: https://ms.sachsen-anhalt.de/presse/pressemitteilungen/ (accessed on 4 August 2022).
31. COVID-19—Institut Für Infektionsmedizin. Available online: https://www.infmed.uni-kiel.de/de/epidemiologie/covid-19 (accessed on 4 August 2022).
32. TMASGFF: Infektionslage. Available online: https://www.tmasgff.de/covid-19/fallzahlen (accessed on 4 August 2022).
33. DIVI Intensivregister. Available online: https://www.intensivregister.de/#/aktuelle-lage/laendertabelle (accessed on 4 August 2022).
34. Tagesdaten-CSV Aus Dem DIVI-Intensivregister. Available online: https://edoc.rki.de/ (accessed on 4 August 2022).

## *A1.2 Supplementary Figure S1*

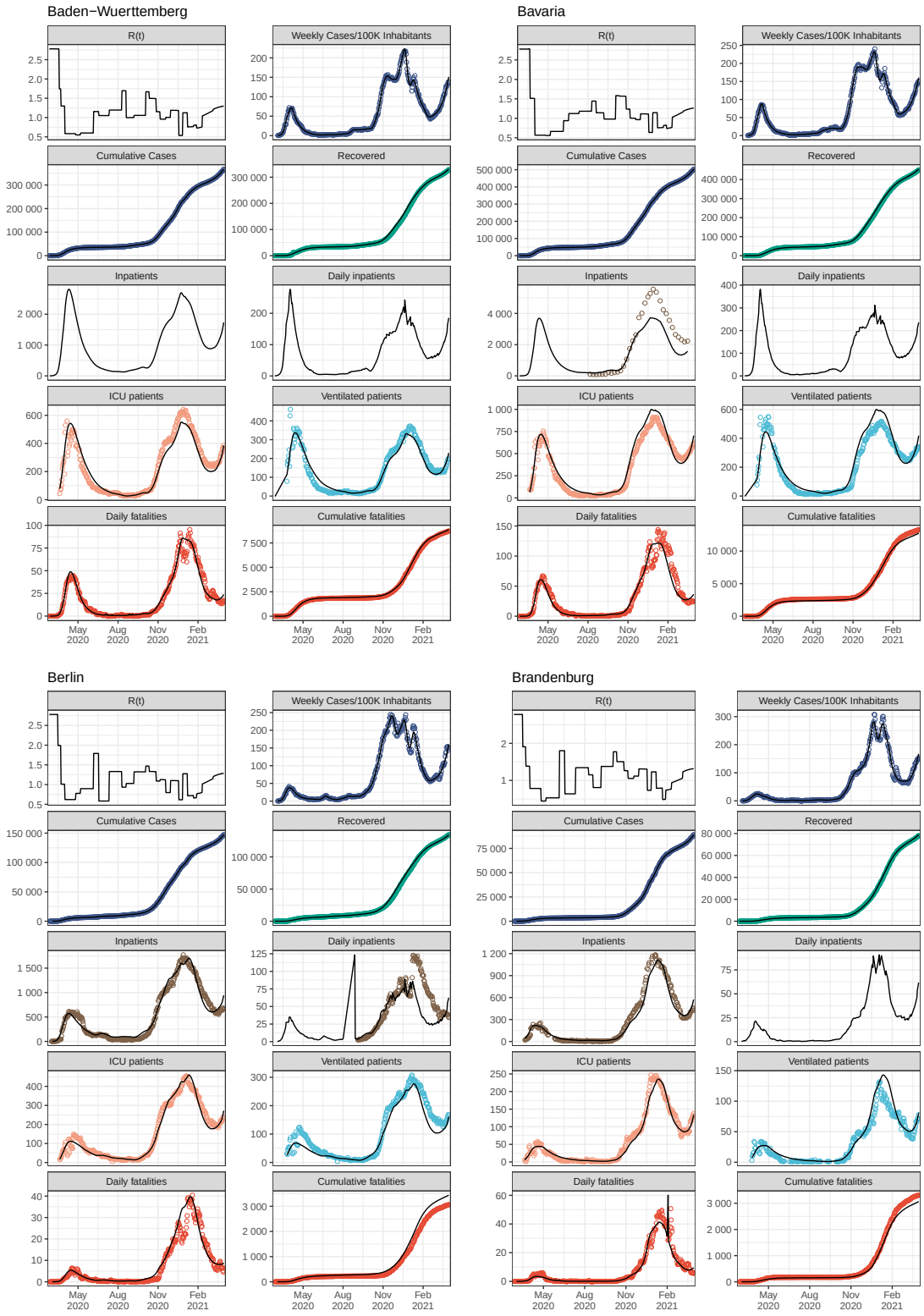

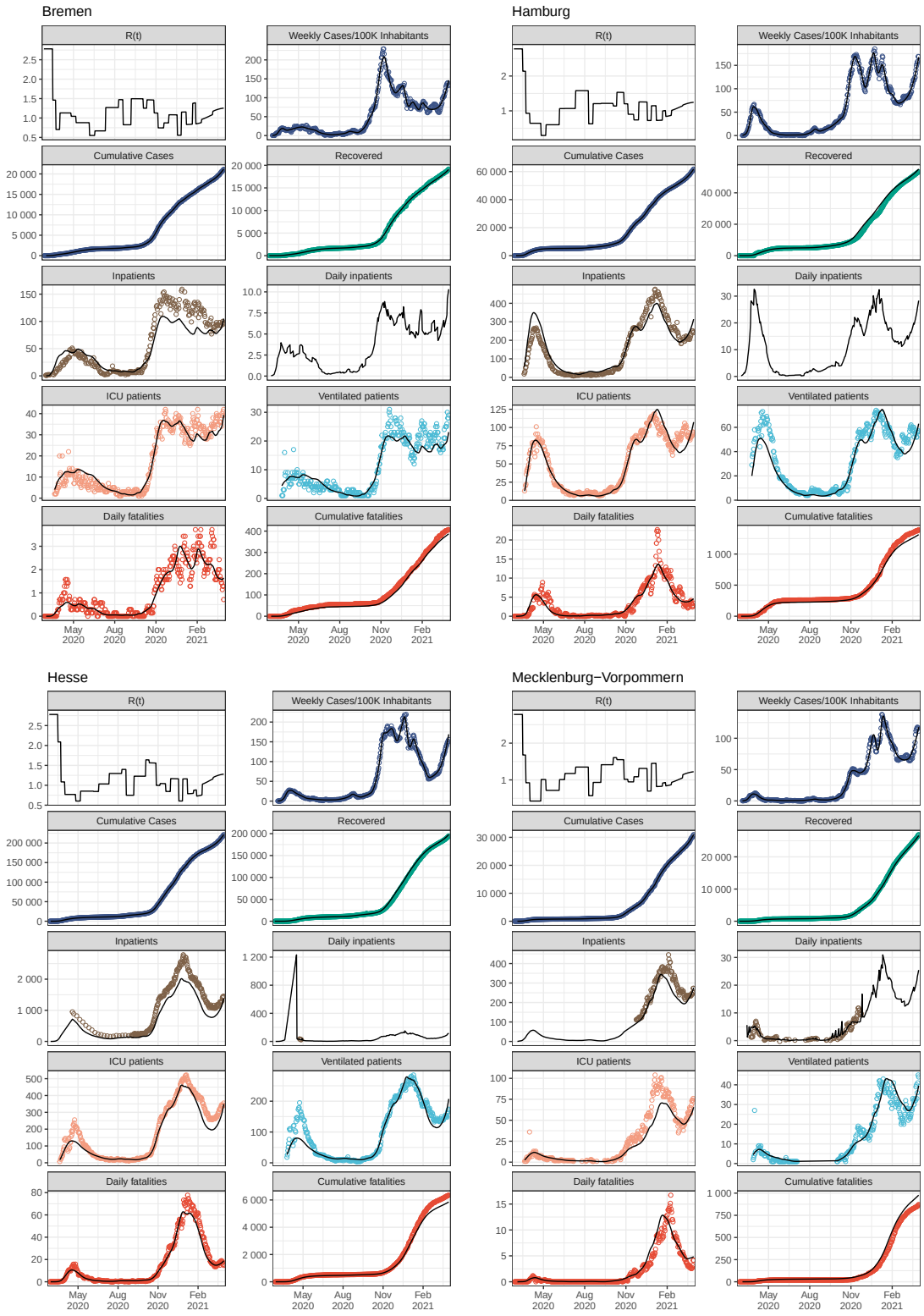
Bremen
Hamburg
Hesse
Mecklenburg−Vorpommern
R(t)
Weekly Cases/100K Inhabitants
Cumulative Cases
Recovered
Inpatients
Daily inpatients
ICU patients
Ventilated patients
Daily fatalities
Cumulative fatalities
May 2020
Aug 2020
Nov 2020
Feb 2021

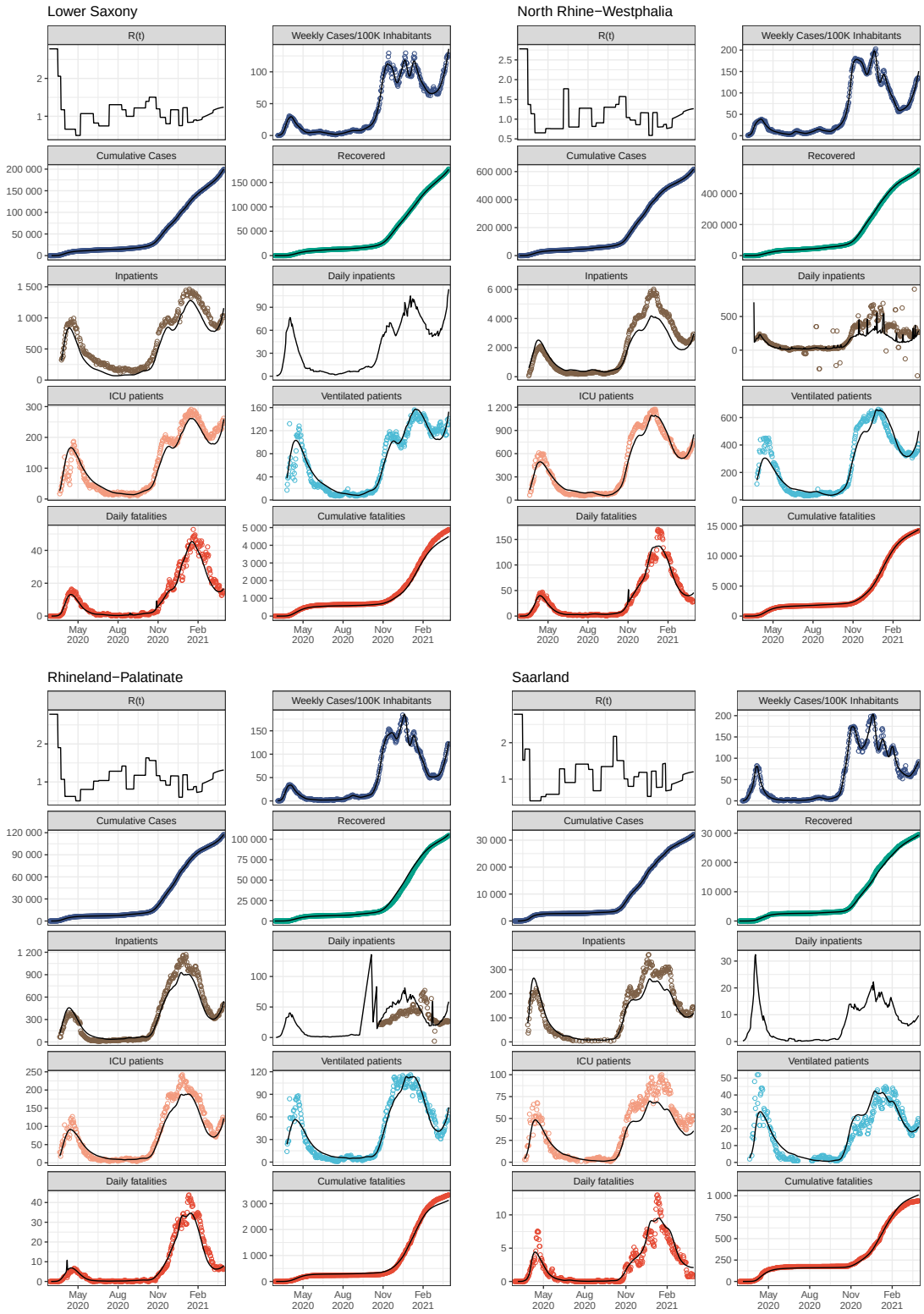
Lower Saxony
North Rhine−Westphalia
Rhineland−Palatinate
Saarland
R(t)
Weekly Cases/100K Inhabitants
Cumulative Cases
Recovered
Inpatients
Daily inpatients
ICU patients
Ventilated patients
Daily fatalities
Cumulative fatalities
May 2020
Aug 2020
Nov 2020
Feb 2021

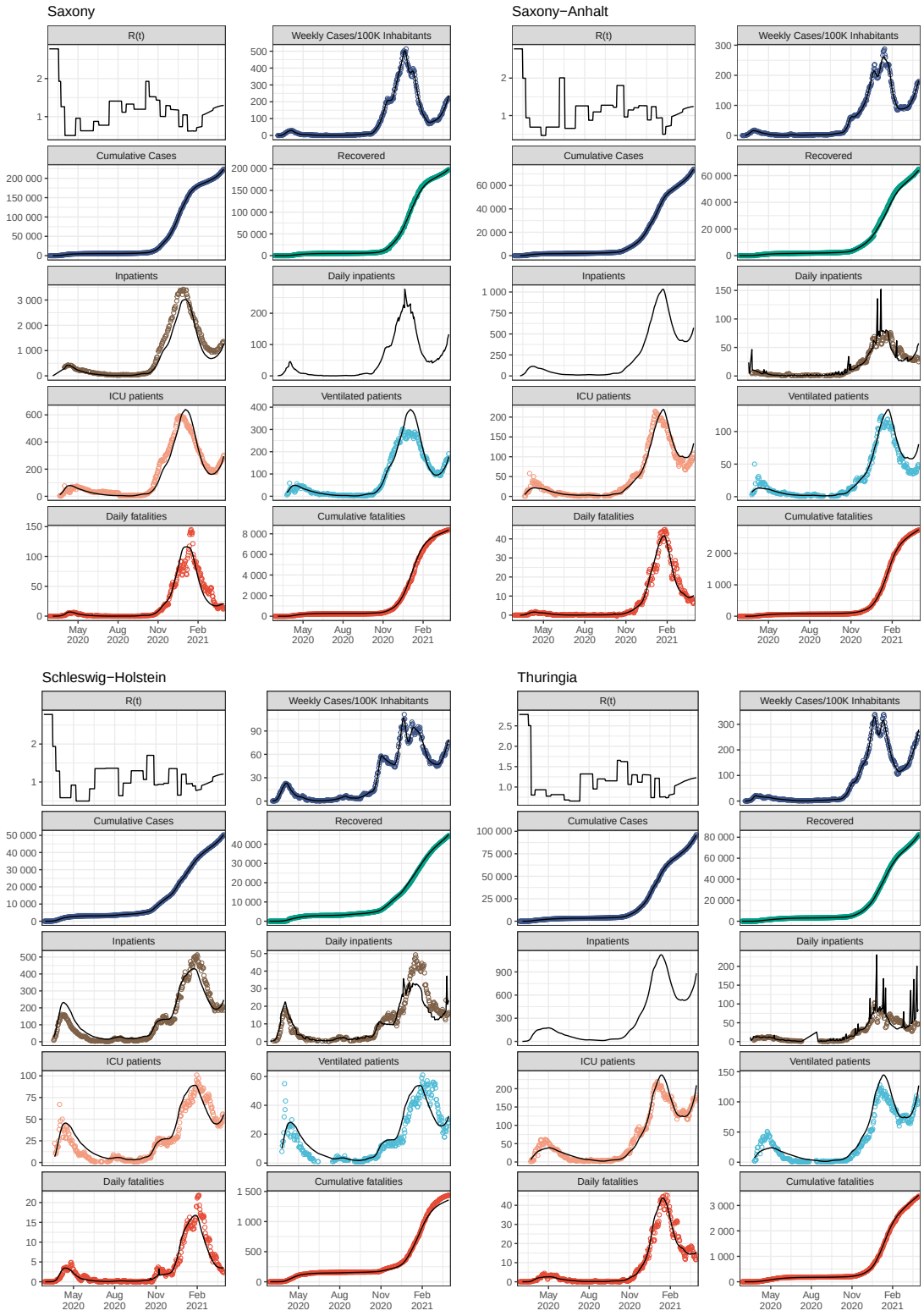
Saxony
R(t)
Weekly Cases/100K Inhabitants
Cumulative Cases
Recovered
Inpatients
Daily inpatients
ICU patients
Ventilated patients
Daily fatalities
Cumulative fatalities
Saxony−Anhalt
Schleswig−Holstein
Thuringia
May 2020
Aug 2020
Nov 2020
Feb 2021

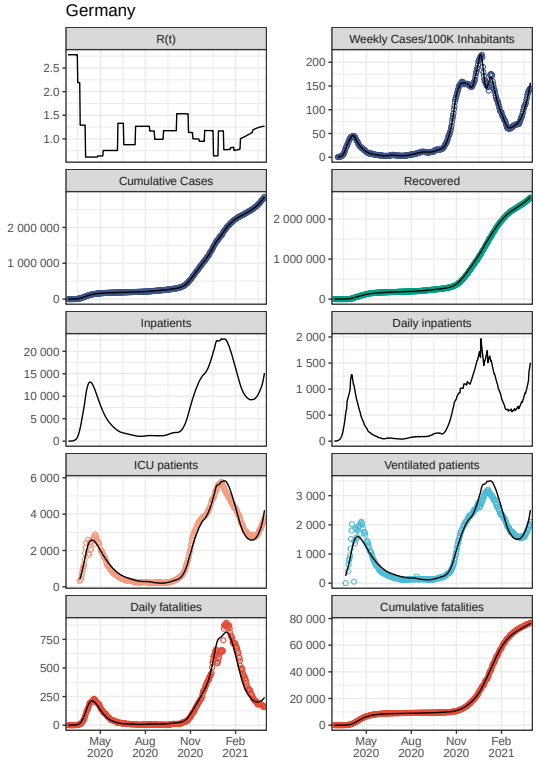
Germany
R(t)
2.5
2.0
1.5
1.0
Weekly Cases/100K Inhabitants
200
150
100
50
0
Cumulative Cases
2 000 000
1 000 000
0
Recovered
2 000 000
1 000 000
0
Inpatients
20 000
15 000
10 000
5 000
0
Daily inpatients
2 000
1 500
1 000
500
0
ICU patients
6 000
4 000
2 000
0
Ventilated patients
3 000
2 000
1 000
0
Daily fatalities
750
500
250
0
Cumulative fatalities
80 000
60 000
40 000
20 000
0
May 2020
Aug 2020
Nov 2020
Feb 2021
May 2020
Aug 2020
Nov 2020
Feb 2021

## *A1.3 Supplementary Figure S2*

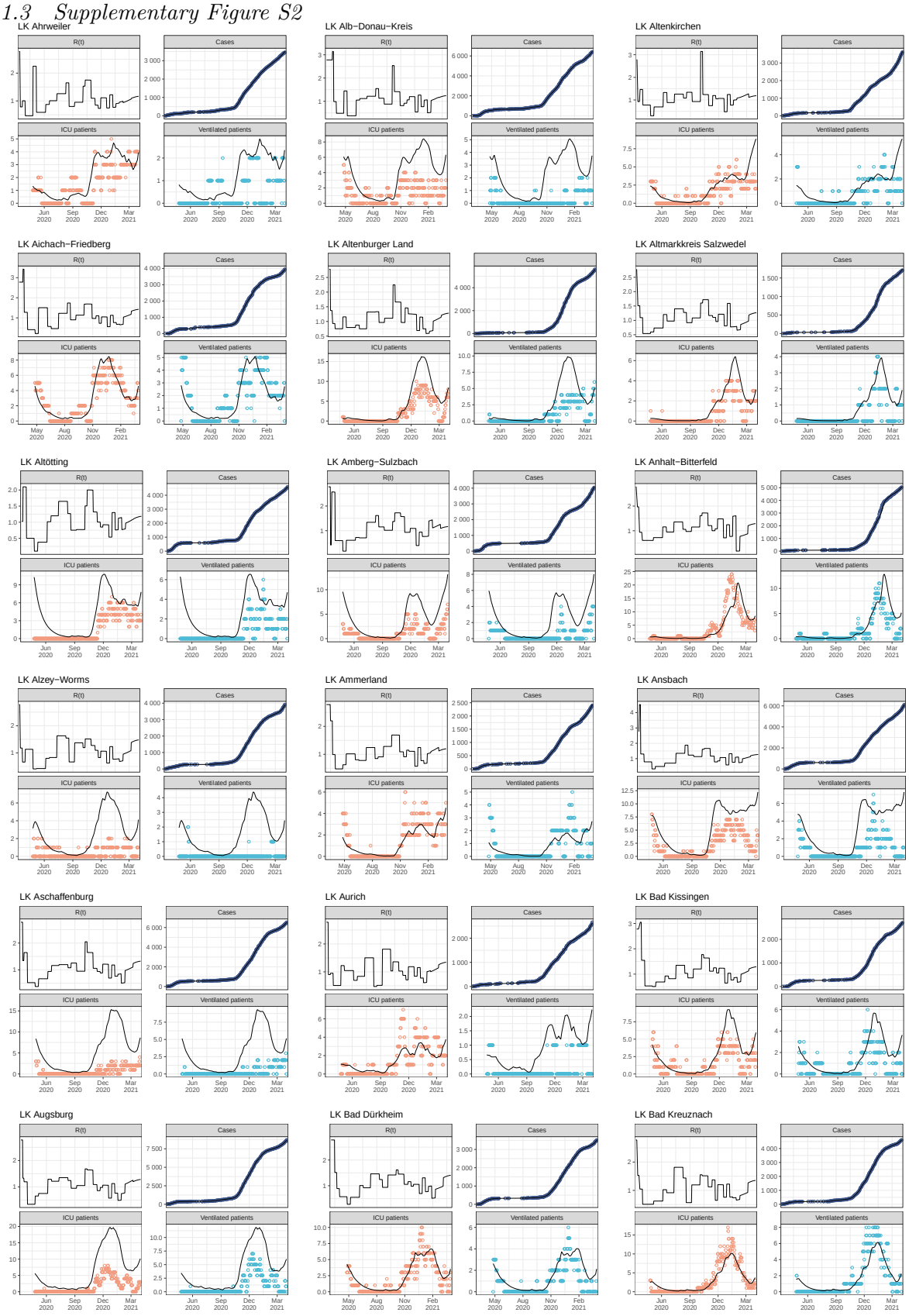

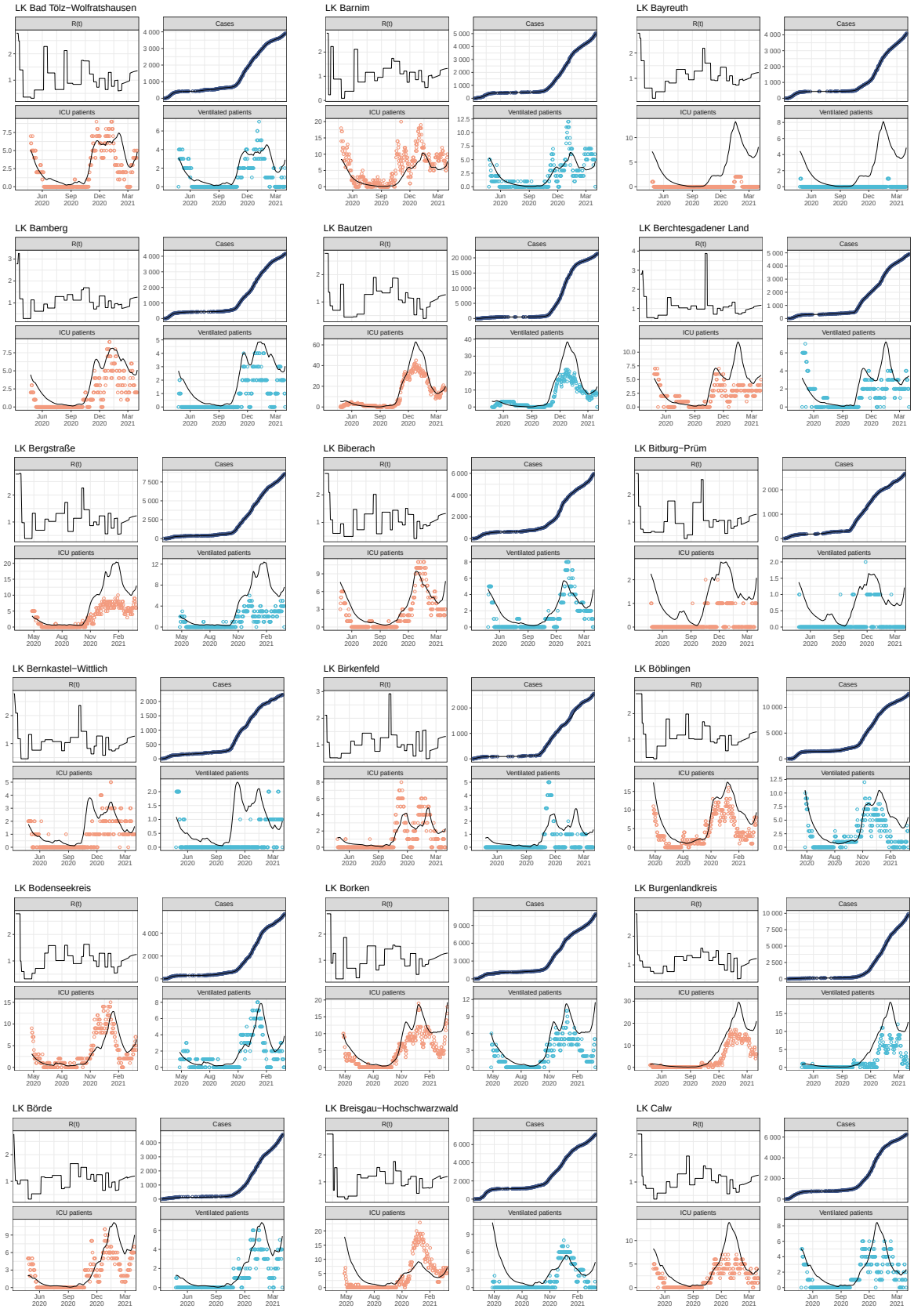
LK Bad Tölz−Wolfratshausen
LK Barnim
LK Bayreuth
LK Bamberg
LK Bautzen
LK Berchtesgadener Land
LK Bergstraße
LK Biberach
LK Bitburg−Prüm
LK Bernkastel−Wittlich
LK Birkenfeld
LK Böblingen
LK Bodenseekreis
LK Borken
LK Burgenlandkreis
LK Börde
LK Breisgau−Hochschwarzwald
LK Calw
R(t)
Cases
ICU patients
Ventilated patients

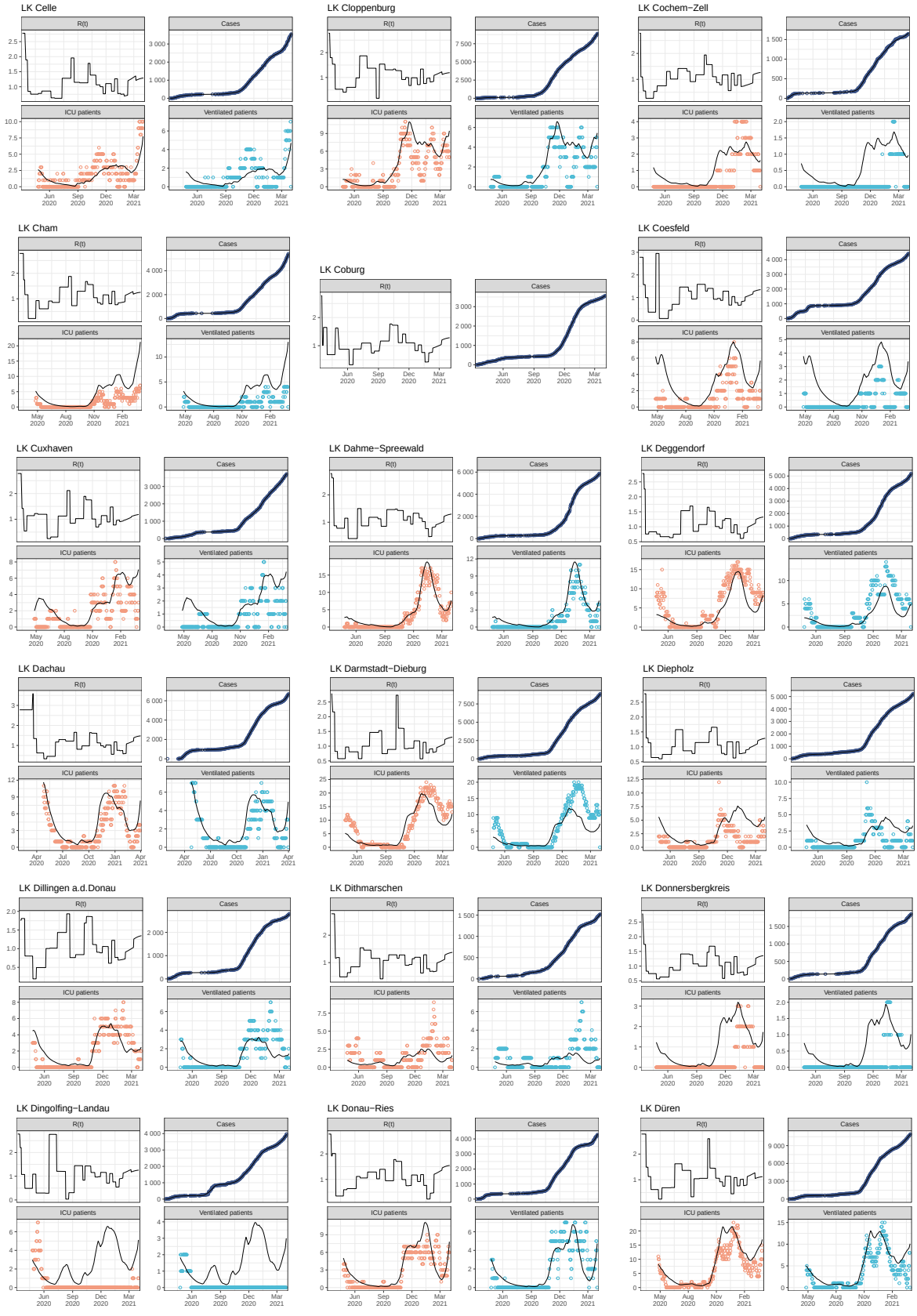
LK Celle
LK Cloppenburg
LK Cochem−Zell
LK Cham
LK Coburg
LK Coesfeld
LK Cuxhaven
LK Dahme−Spreewald
LK Deggendorf
LK Dachau
LK Darmstadt−Dieburg
LK Diepholz
LK Dillingen a.d.Donau
LK Dithmarschen
LK Donnersbergkreis
LK Dingolfing−Landau
LK Donau−Ries
LK Düren
R(t)
Cases
ICU patients
Ventilated patients

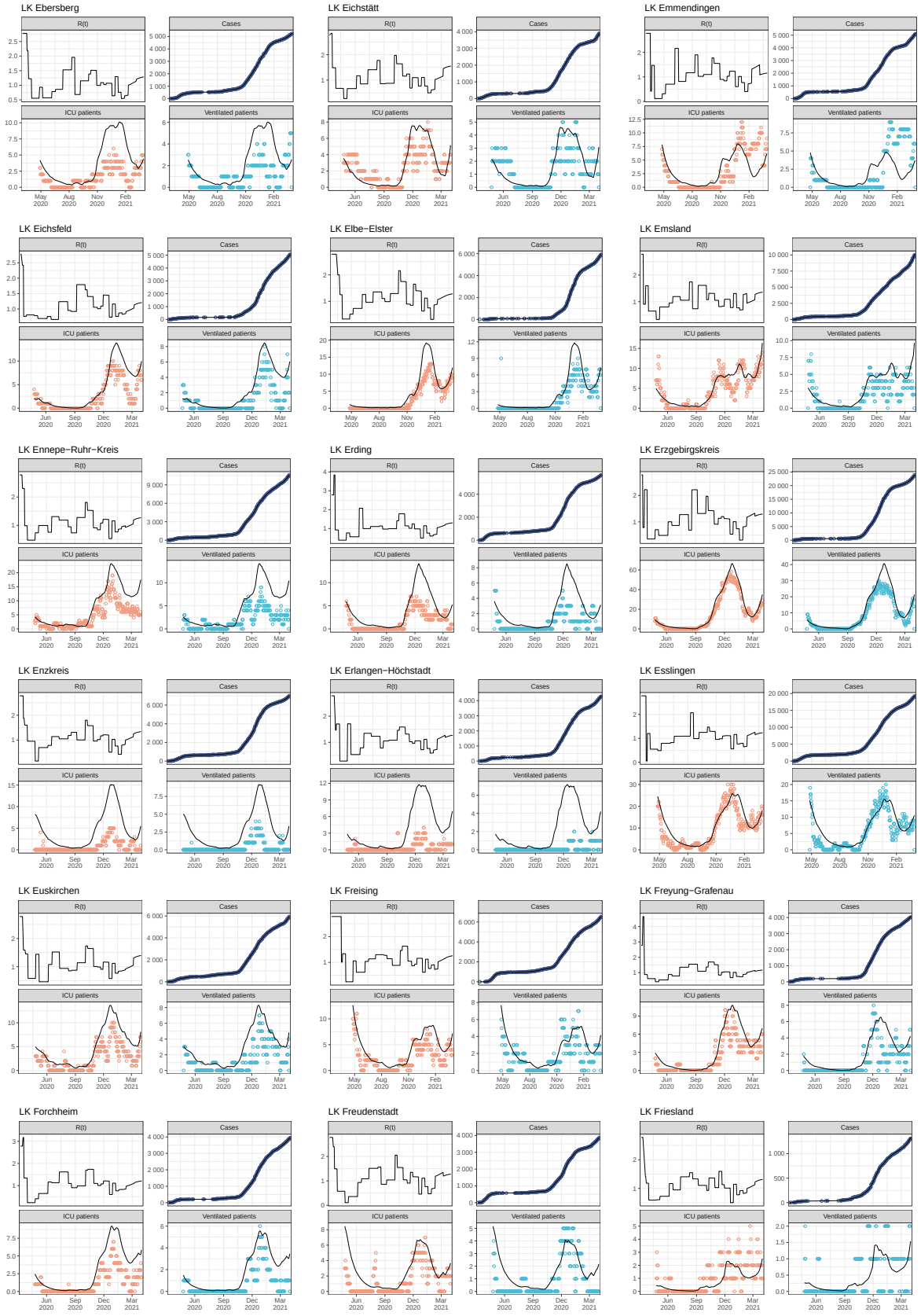
LK Ebersberg
LK Eichstätt
LK Emmendingen
LK Eichsfeld
LK Elbe−Elster
LK Emsland
LK Ennepe−Ruhr−Kreis
LK Erding
LK Erzgebirgskreis
LK Enzkreis
LK Erlangen−Höchstadt
LK Esslingen
LK Euskirchen
LK Freising
LK Freyung−Grafenau
LK Forchheim
LK Freudenstadt
LK Friesland
R(t)
Cases
ICU patients
Ventilated patients

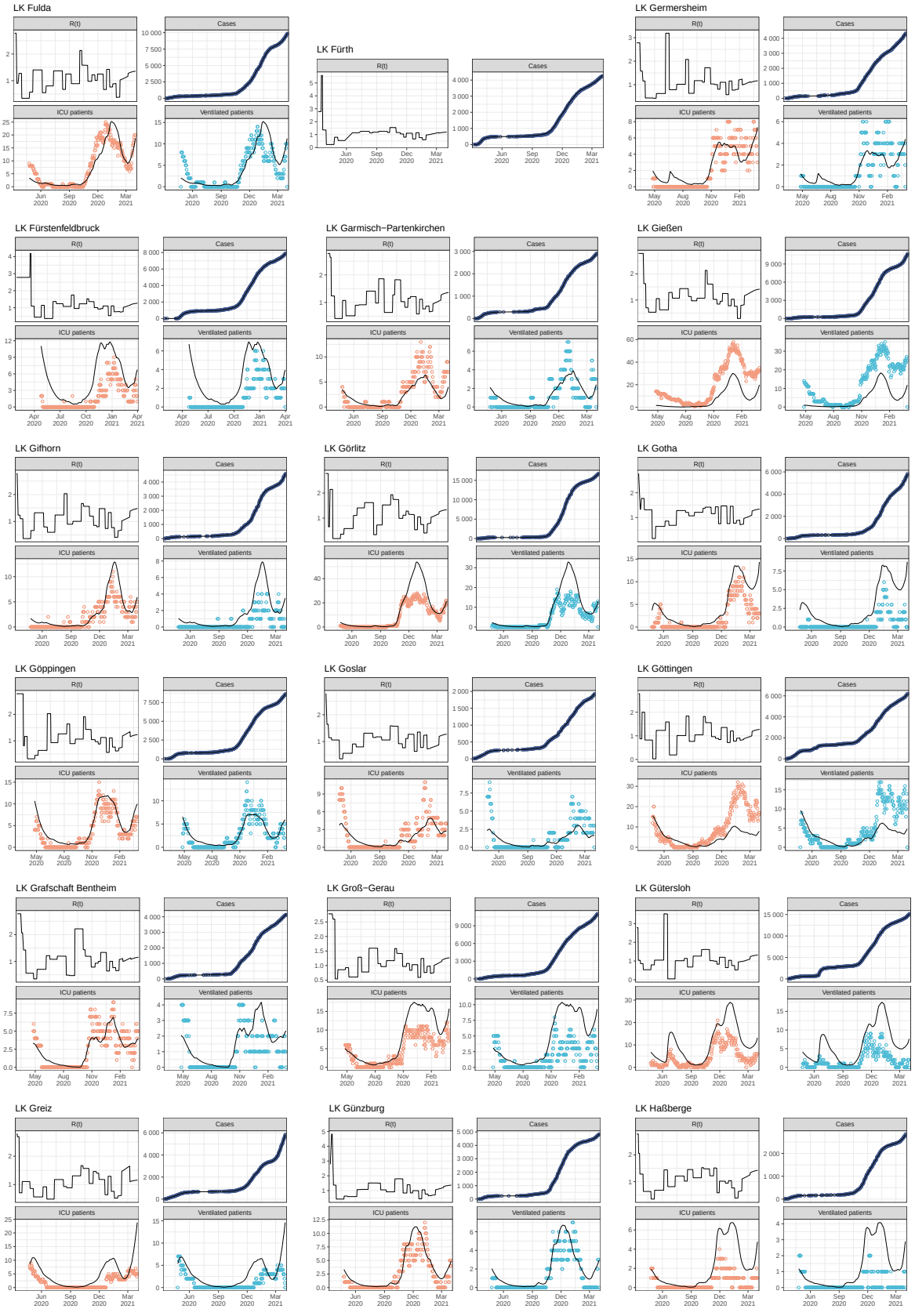
LK Fulda
LK Fürth
LK Germersheim
LK Fürstenfeldbruck
LK Garmisch−Partenkirchen
LK Gießen
LK Gifhorn
LK Görlitz
LK Gotha
LK Göppingen
LK Goslar
LK Göttingen
LK Grafschaft Bentheim
LK Groß−Gerau
LK Gütersloh
LK Greiz
LK Günzburg
LK Haßberge
R(t)
Cases
ICU patients
Ventilated patients

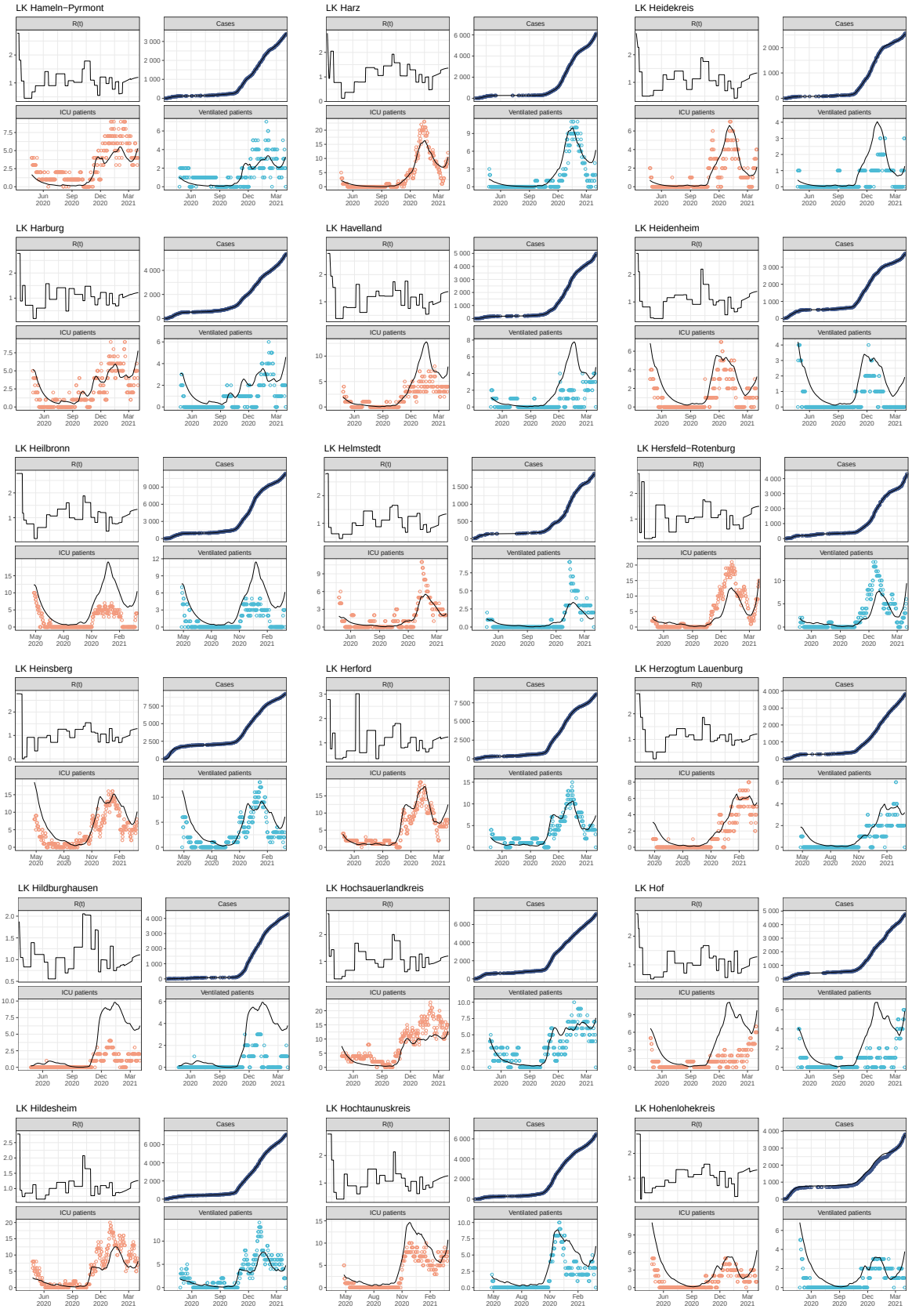
LK Hameln−Pyrmont
LK Harz
LK Heidekreis
LK Harburg
LK Havelland
LK Heidenheim
LK Heilbronn
LK Helmstedt
LK Hersfeld−Rotenburg
LK Heinsberg
LK Herford
LK Herzogtum Lauenburg
LK Hildburghausen
LK Hochsauerlandkreis
LK Hof
LK Hildesheim
LK Hochtaunuskreis
LK Hohenlohekreis
R(t)
Cases
ICU patients
Ventilated patients

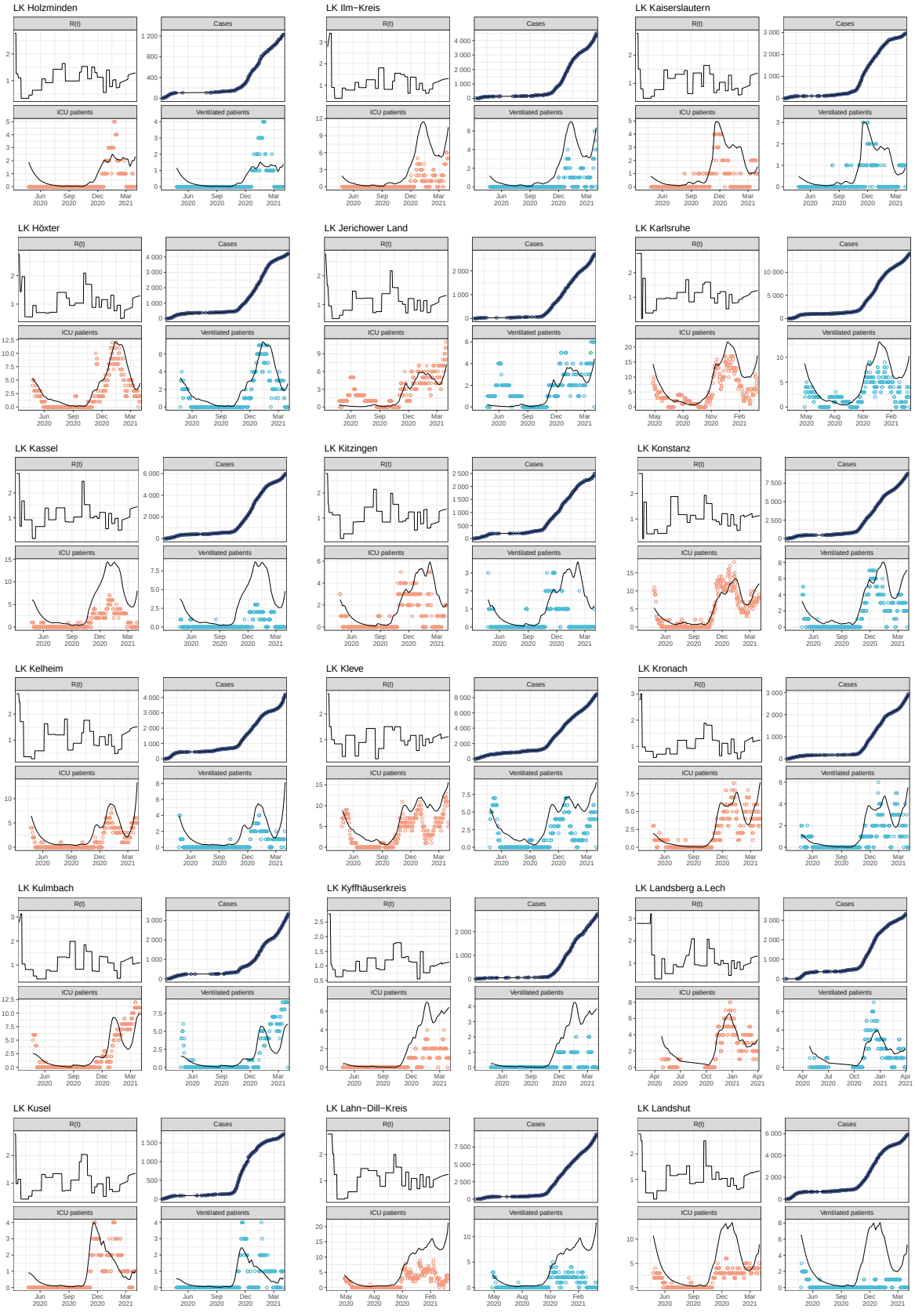
LK Holzminden
LK Ilm−Kreis
LK Kaiserslautern
LK Höxter
LK Jerichower Land
LK Karlsruhe
LK Kassel
LK Kitzingen
LK Konstanz
LK Kelheim
LK Kleve
LK Kronach
LK Kulmbach
LK Kyffhäuserkreis
LK Landsberg a.Lech
LK Kusel
LK Lahn−Dill−Kreis
LK Landshut
R(t)
Cases
ICU patients
Ventilated patients

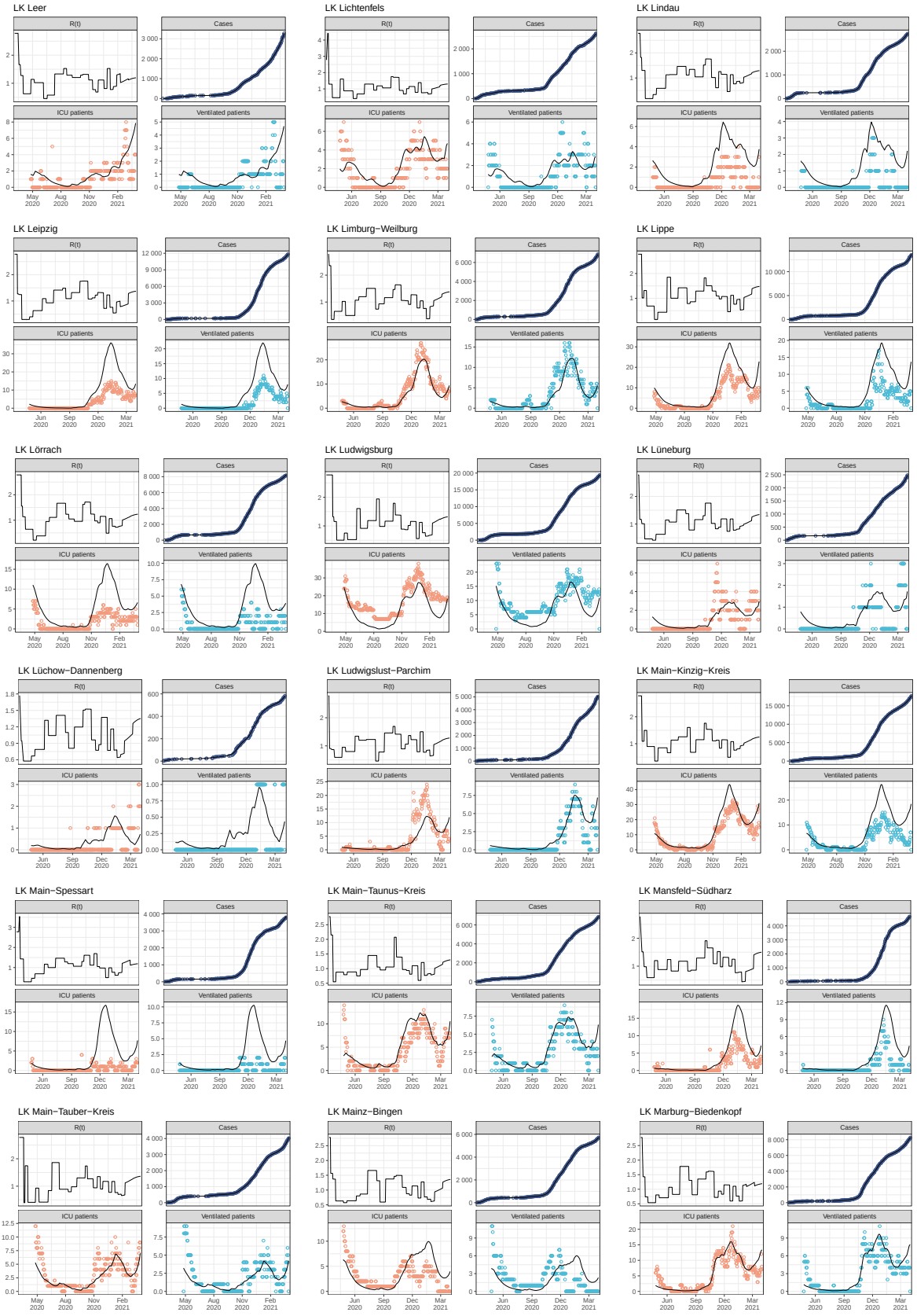
LK Leer
LK Lichtenfels
LK Lindau
LK Leipzig
LK Limburg−Weilburg
LK Lippe
LK Lörrach
LK Ludwigsburg
LK Lüneburg
LK Lüchow−Dannenberg
LK Ludwigslust−Parchim
LK Main−Kinzig−Kreis
LK Main−Spessart
LK Main−Taunus−Kreis
LK Mansfeld−Südharz
LK Main−Tauber−Kreis
LK Mainz−Bingen
LK Marburg−Biedenkopf
R(t)
Cases
ICU patients
Ventilated patients

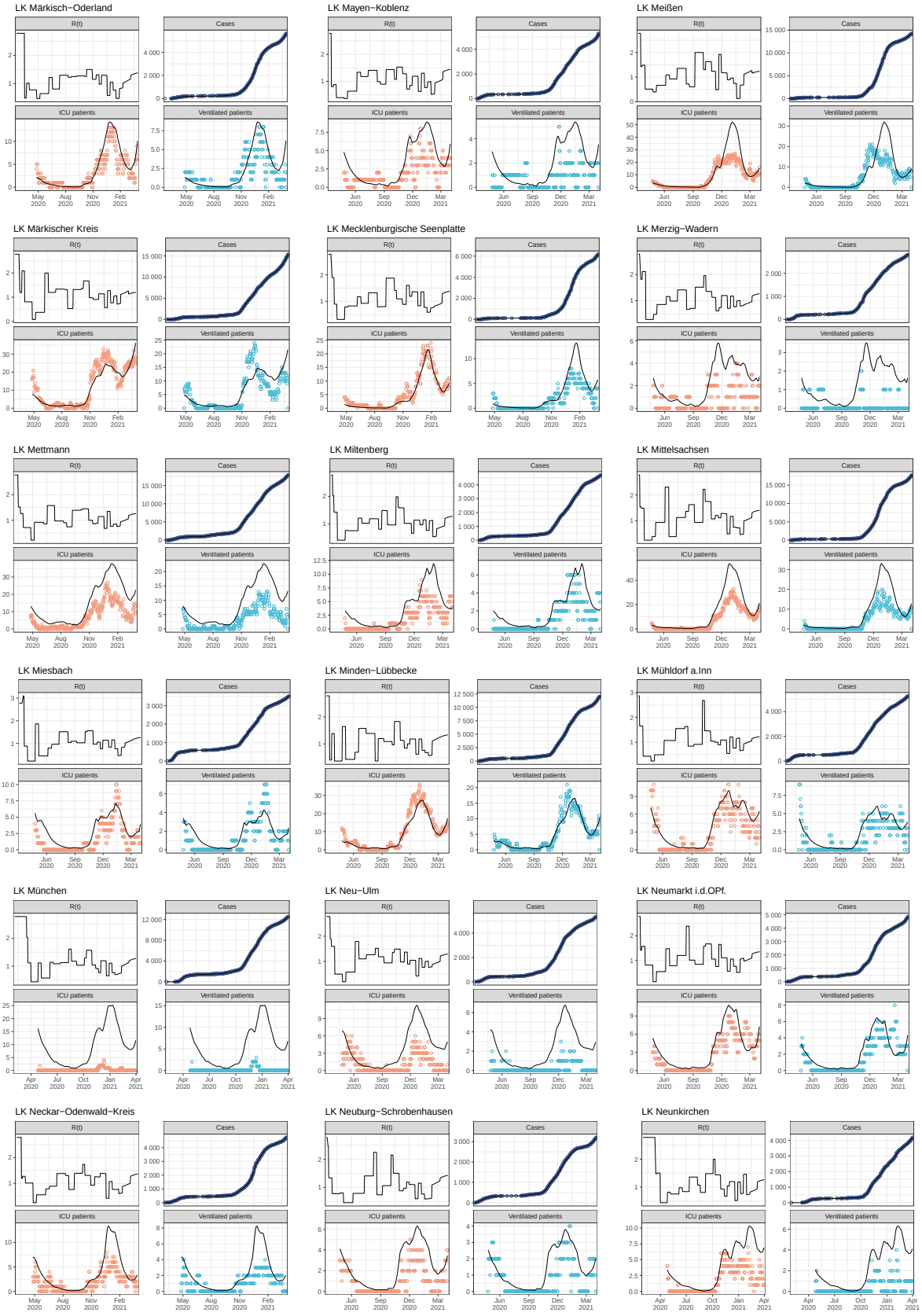
LK Märkisch−Oderland
LK Mayen−Koblenz
LK Meißen
LK Märkischer Kreis
LK Mecklenburgische Seenplatte
LK Merzig−Wadern
LK Mettmann
LK Miltenberg
LK Mittelsachsen
LK Miesbach
LK Minden−Lübbecke
LK Mühldorf a.Inn
LK München
LK Neu−Ulm
LK Neumarkt i.d.OPf.
LK Neckar−Odenwald−Kreis
LK Neuburg−Schrobenhausen
LK Neunkirchen
R(t)
Cases
ICU patients
Ventilated patients

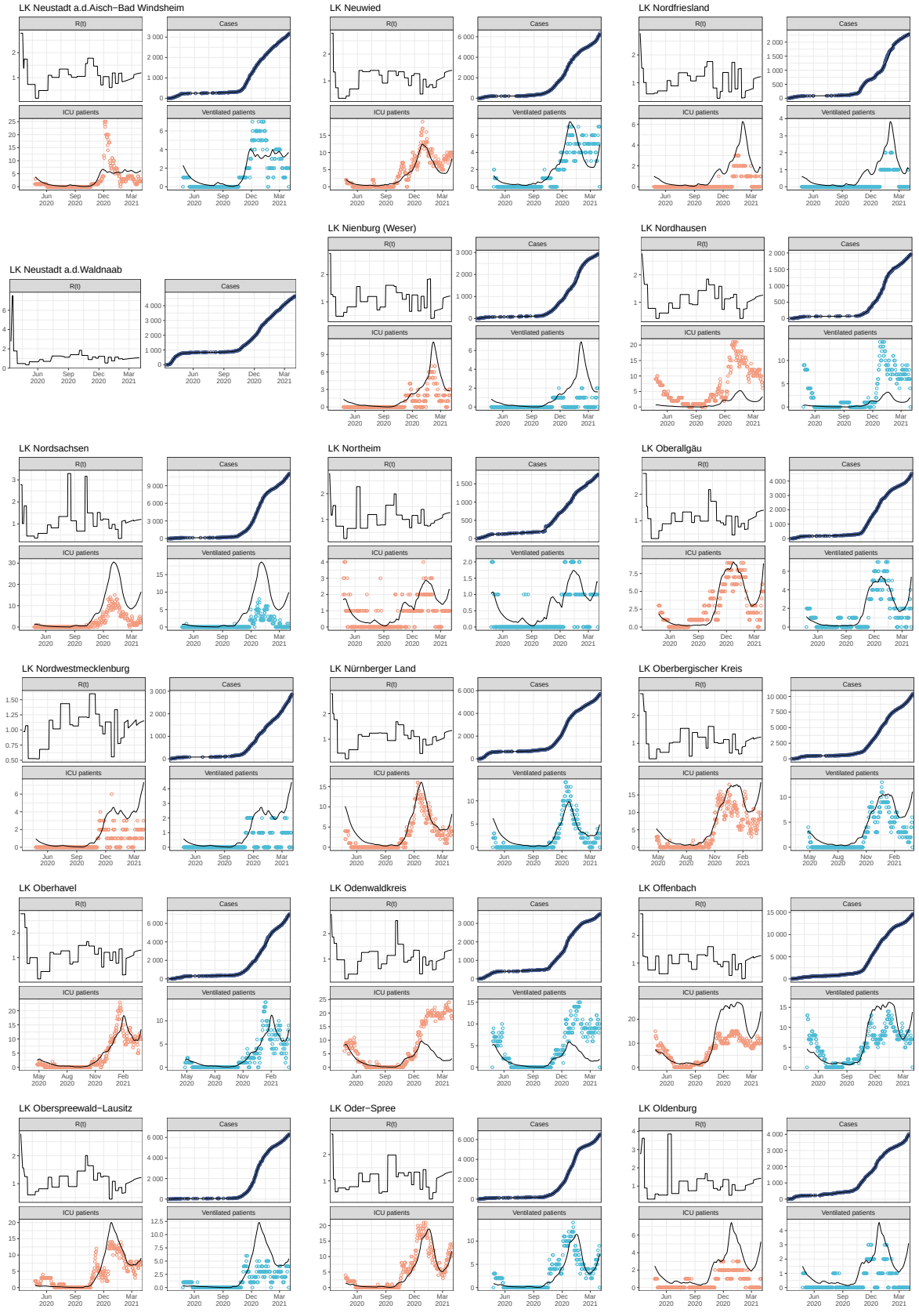
LK Neustadt a.d.Aisch−Bad Windsheim
LK Neuwied
LK Nordfriesland
LK Neustadt a.d.Waldnaab
LK Nienburg (Weser)
LK Nordhausen
LK Nordsachsen
LK Northeim
LK Oberallgäu
LK Nordwestmecklenburg
LK Nürnberger Land
LK Oberbergischer Kreis
LK Oberhavel
LK Odenwaldkreis
LK Offenbach
LK Oberspreewald−Lausitz
LK Oder−Spree
LK Oldenburg
R(t)
Cases
ICU patients
Ventilated patients

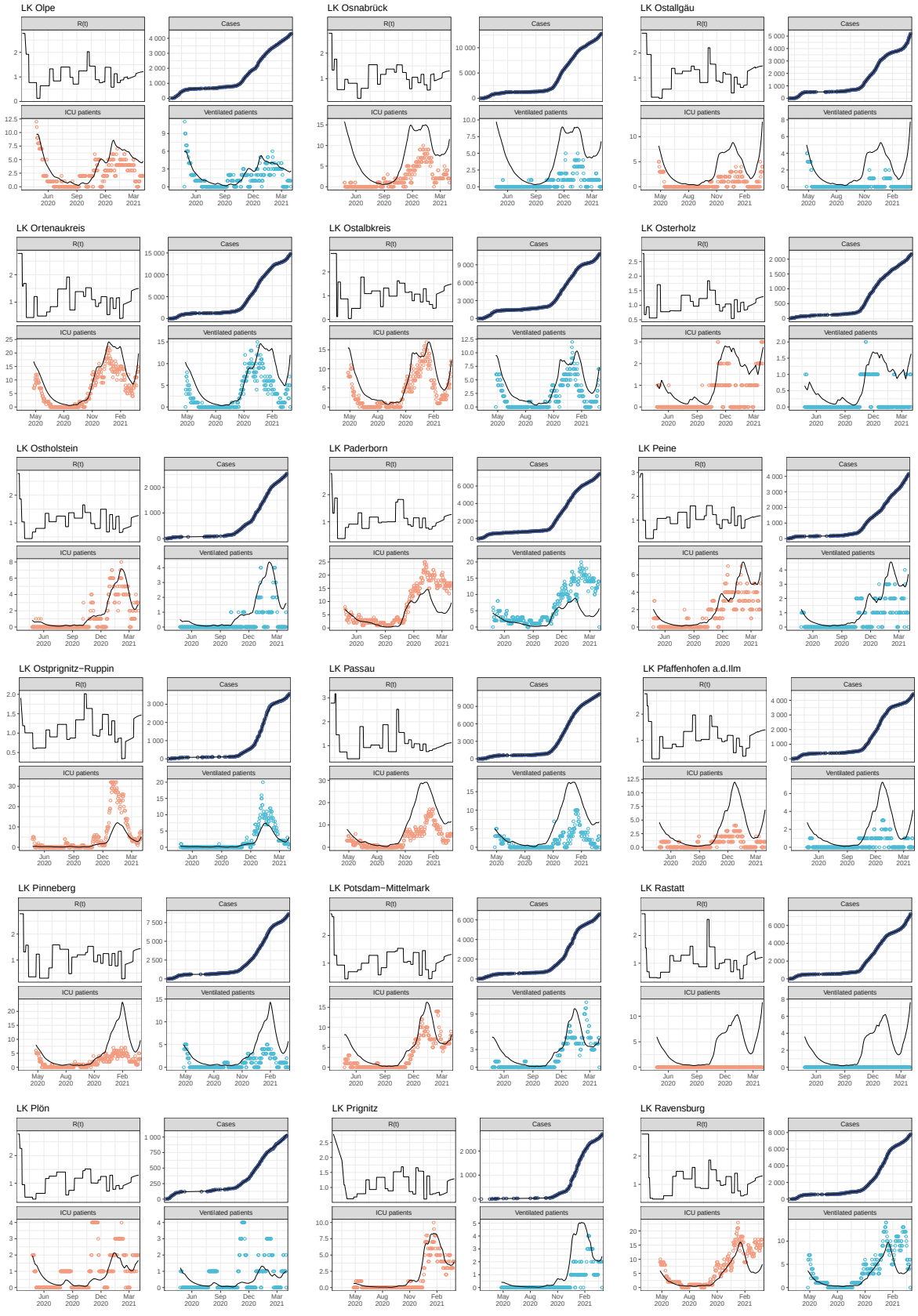
LK Olpe
LK Osnabrück
LK Ostallgäu
LK Ortenaukreis
LK Ostalbkreis
LK Osterholz
LK Ostholstein
LK Paderborn
LK Peine
LK Ostprignitz−Ruppin
LK Passau
LK Pfaffenhofen a.d.Ilm
LK Pinneberg
LK Potsdam−Mittelmark
LK Rastatt
LK Plön
LK Prignitz
LK Ravensburg
R(t)
Cases
ICU patients
Ventilated patients

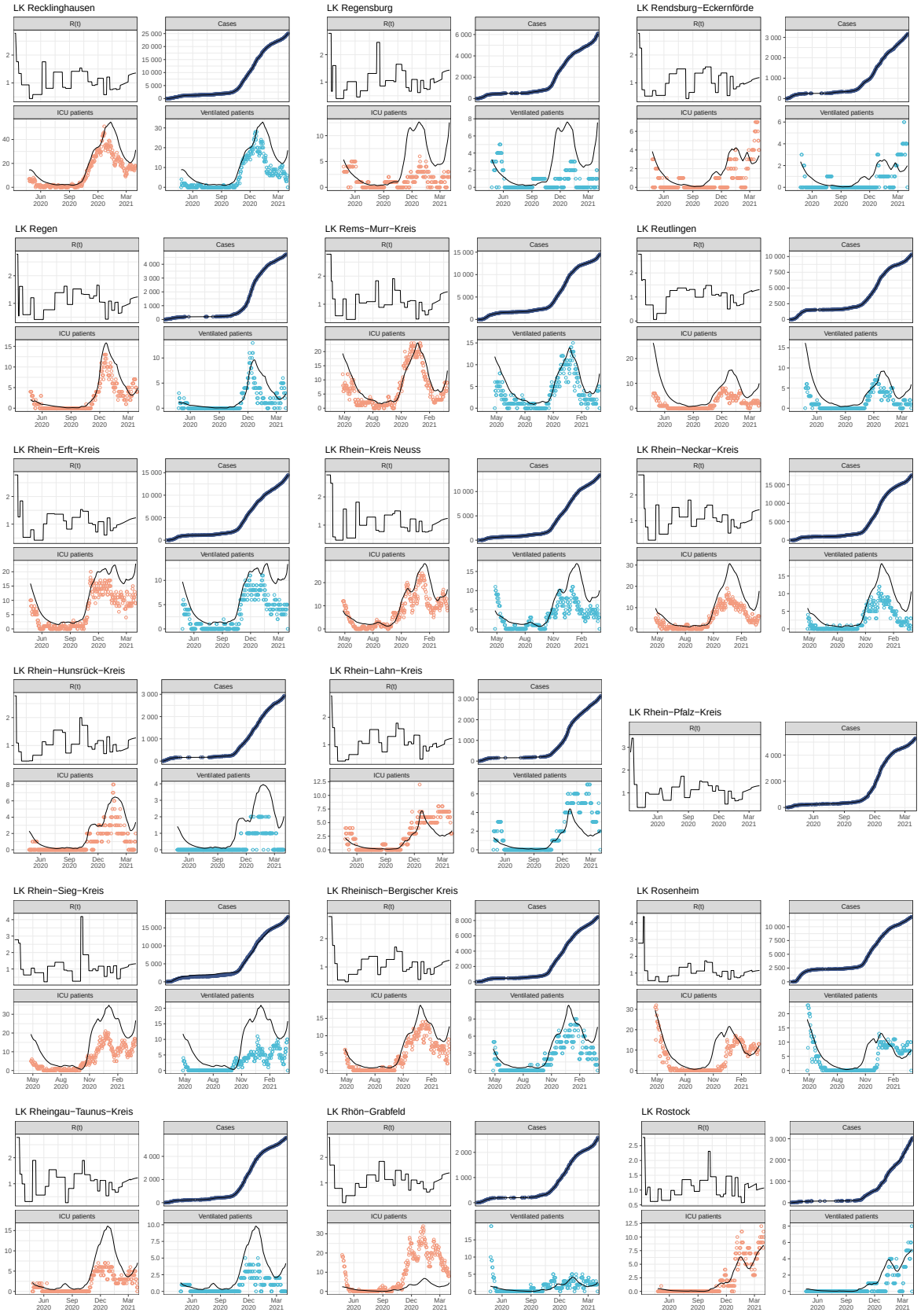
LK Recklinghausen
LK Regensburg
LK Rendsburg−Eckernförde
LK Regen
LK Rems−Murr−Kreis
LK Reutlingen
LK Rhein−Erft−Kreis
LK Rhein−Kreis Neuss
LK Rhein−Neckar−Kreis
LK Rhein−Hunsrück−Kreis
LK Rhein−Lahn−Kreis
LK Rhein−Pfalz−Kreis
LK Rhein−Sieg−Kreis
LK Rheinisch−Bergischer Kreis
LK Rosenheim
LK Rheingau−Taunus−Kreis
LK Rhön−Grabfeld
LK Rostock
R(t)
Cases
ICU patients
Ventilated patients

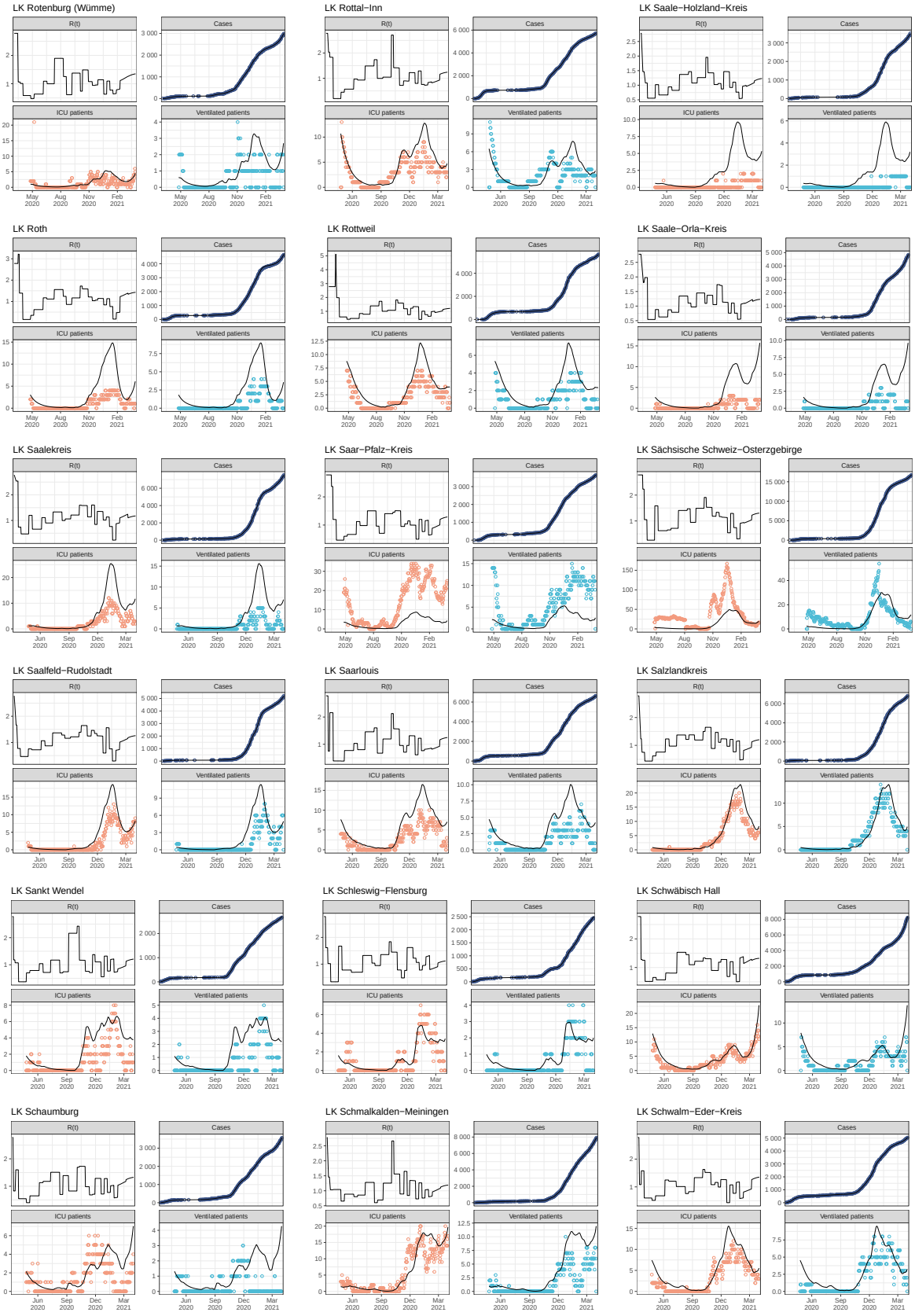
LK Rotenburg (Wümme)
LK Rottal−Inn
LK Saale−Holzland−Kreis
LK Roth
LK Rottweil
LK Saale−Orla−Kreis
LK Saalekreis
LK Saar−Pfalz−Kreis
LK Sächsische Schweiz−Osterzgebirge
LK Saalfeld−Rudolstadt
LK Saarlouis
LK Salzlandkreis
LK Sankt Wendel
LK Schleswig−Flensburg
LK Schwäbisch Hall
LK Schaumburg
LK Schmalkalden−Meiningen
LK Schwalm−Eder−Kreis
R(t)
Cases
ICU patients
Ventilated patients

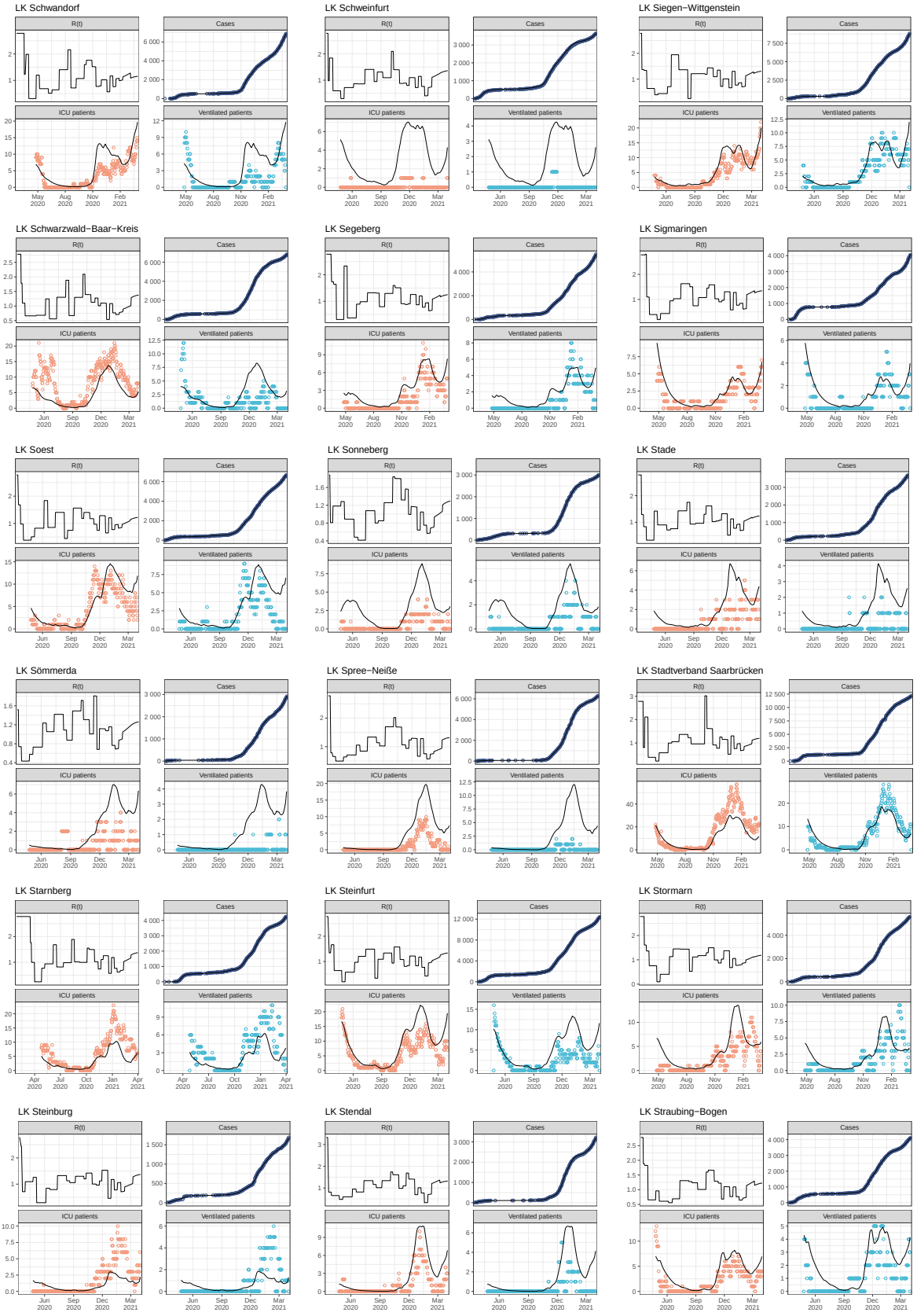
LK Schwandorf
LK Schweinfurt
LK Siegen−Wittgenstein
LK Schwarzwald−Baar−Kreis
LK Segeberg
LK Sigmaringen
LK Soest
LK Sonneberg
LK Stade
LK Sömmerda
LK Spree−Neiße
LK Stadtverband Saarbrücken
LK Starnberg
LK Steinfurt
LK Stormarn
LK Steinburg
LK Stendal
LK Straubing−Bogen
R(t)
Cases
ICU patients
Ventilated patients

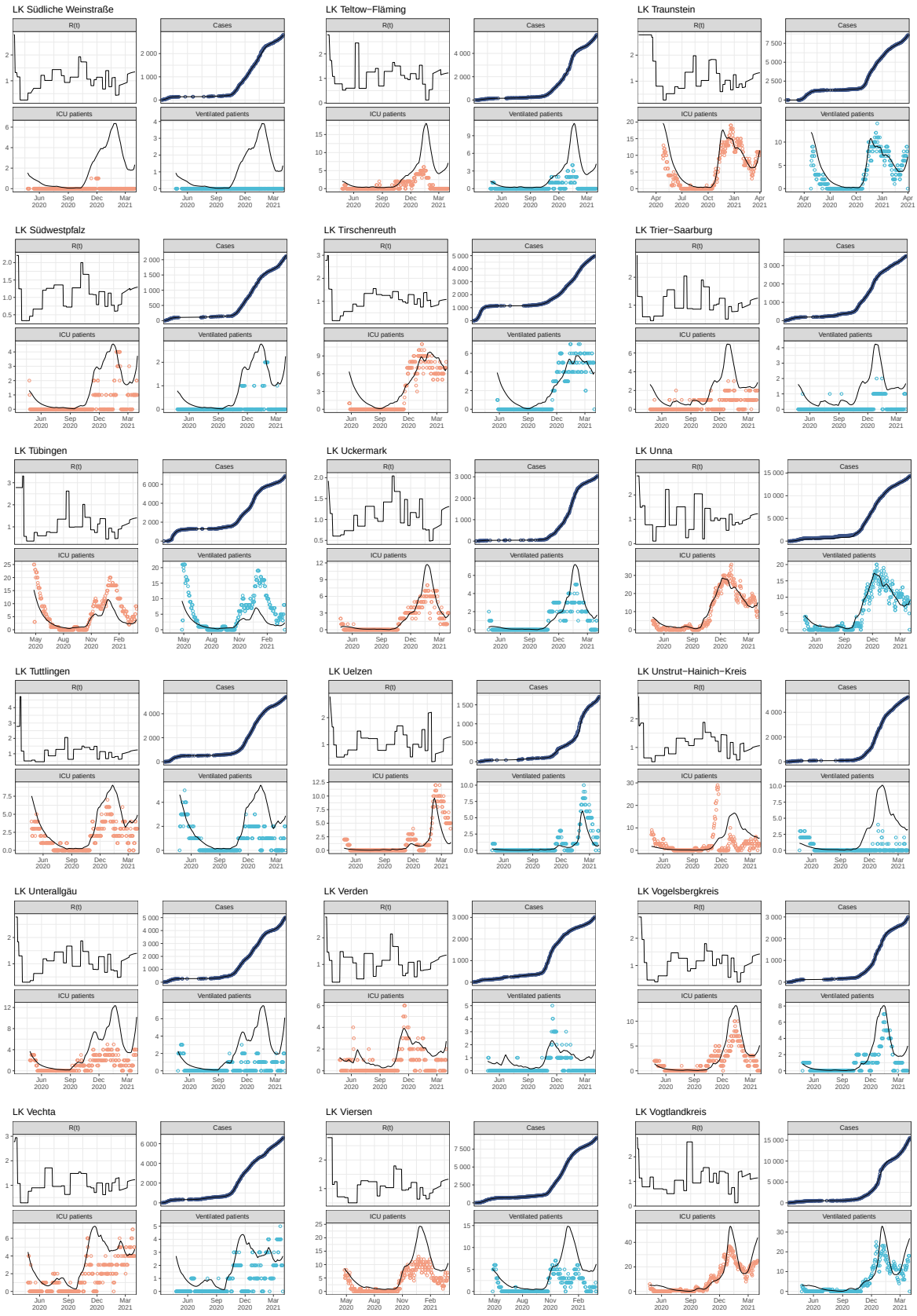
LK Südliche Weinstraße
LK Teltow−Fläming
LK Traunstein
LK Südwestpfalz
LK Tirschenreuth
LK Trier−Saarburg
LK Tübingen
LK Uckermark
LK Unna
LK Tuttlingen
LK Uelzen
LK Unstrut−Hainich−Kreis
LK Unterallgäu
LK Verden
LK Vogelsbergkreis
LK Vechta
LK Viersen
LK Vogtlandkreis
R(t)
Cases
ICU patients
Ventilated patients

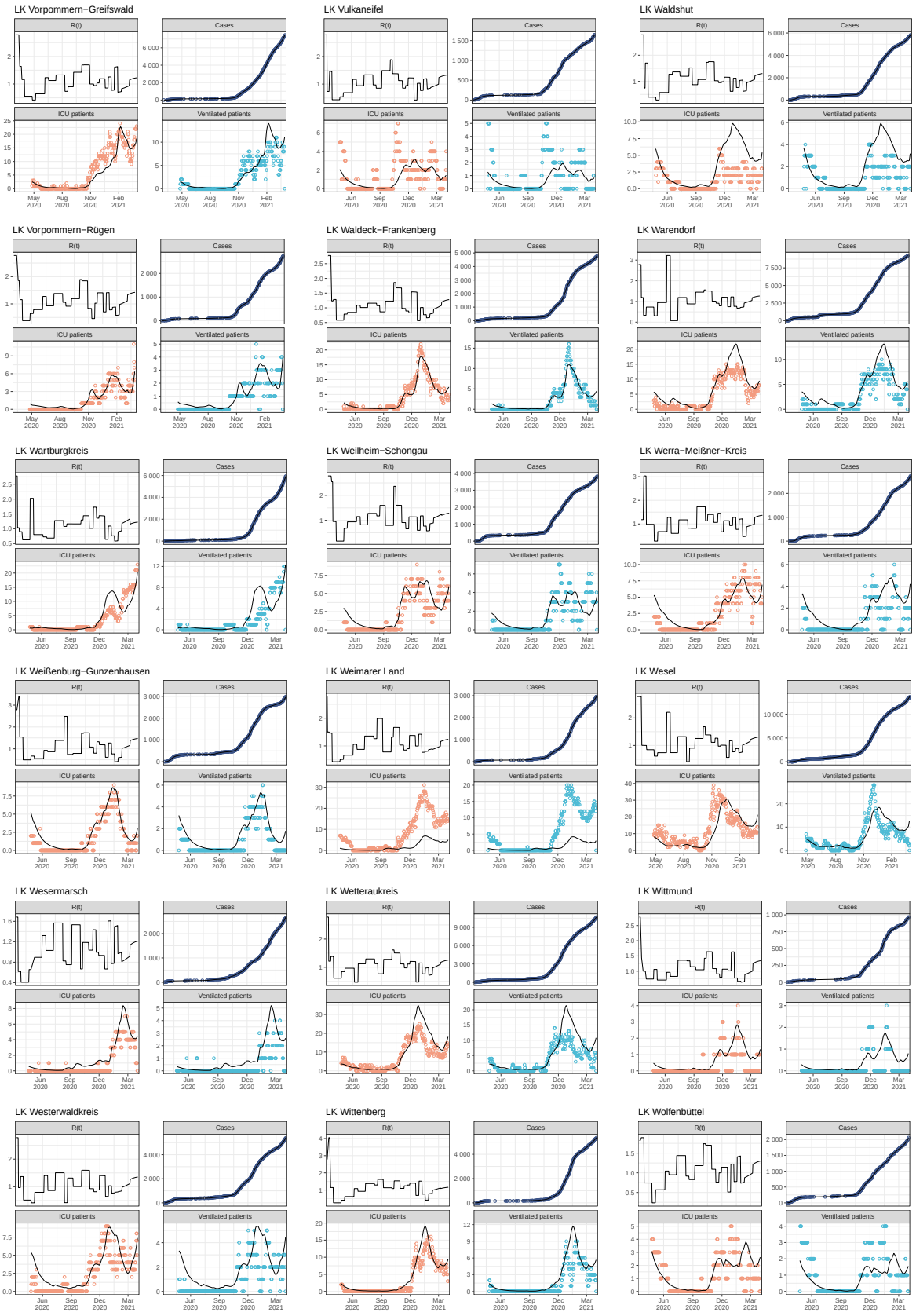
LK Vorpommern−Greifswald
LK Vulkaneifel
LK Waldshut
LK Vorpommern−Rügen
LK Waldeck−Frankenberg
LK Warendorf
LK Wartburgkreis
LK Weilheim−Schongau
LK Werra−Meißner−Kreis
LK Weißenburg−Gunzenhausen
LK Weimarer Land
LK Wesel
LK Wesermarsch
LK Wetteraukreis
LK Wittmund
LK Westerwaldkreis
LK Wittenberg
LK Wolfenbüttel
R(t)
Cases
ICU patients
Ventilated patients

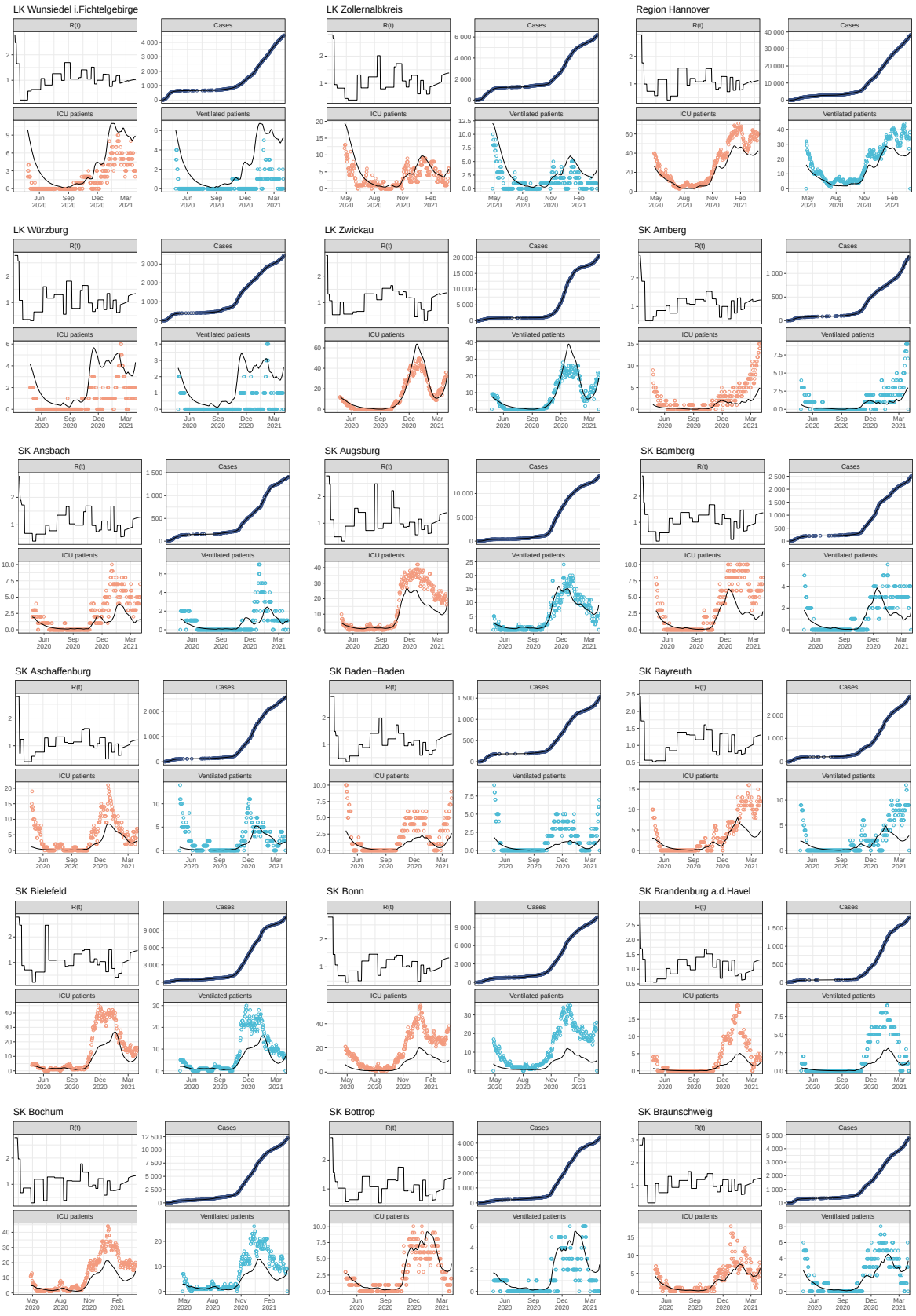
LK Wunsiedel i.Fichtelgebirge
LK Zollernalbkreis
Region Hannover
LK Würzburg
LK Zwickau
SK Amberg
SK Ansbach
SK Augsburg
SK Bamberg
SK Aschaffenburg
SK Baden−Baden
SK Bayreuth
SK Bielefeld
SK Bonn
SK Brandenburg a.d.Havel
SK Bochum
SK Bottrop
SK Braunschweig
R(t)
Cases
ICU patients
Ventilated patients

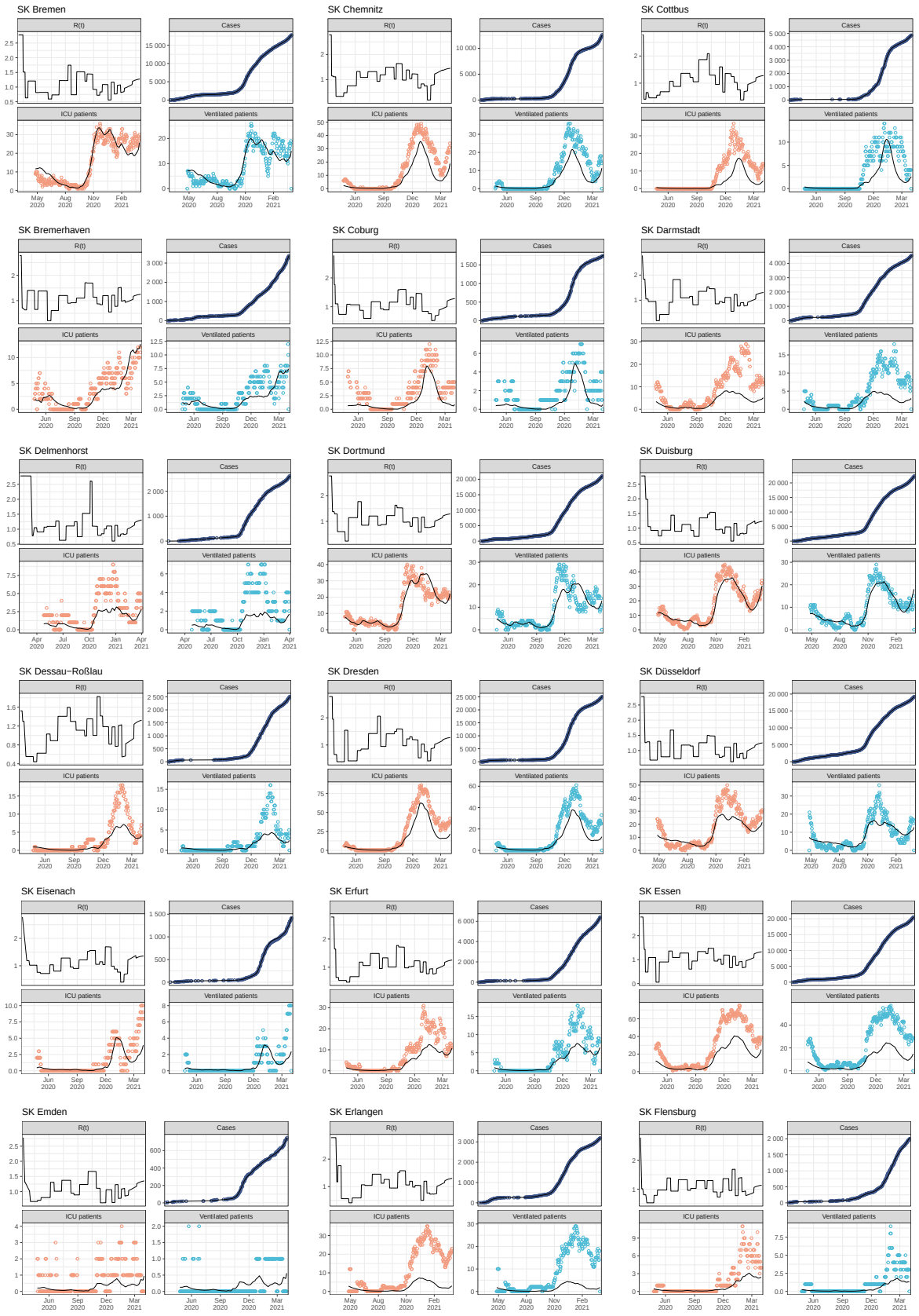
SK Bremen
SK Chemnitz
SK Cottbus
SK Bremerhaven
SK Coburg
SK Darmstadt
SK Delmenhorst
SK Dortmund
SK Duisburg
SK Dessau−Roßlau
SK Dresden
SK Düsseldorf
SK Eisenach
SK Erfurt
SK Essen
SK Emden
SK Erlangen
SK Flensburg
R(t)
Cases
ICU patients
Ventilated patients

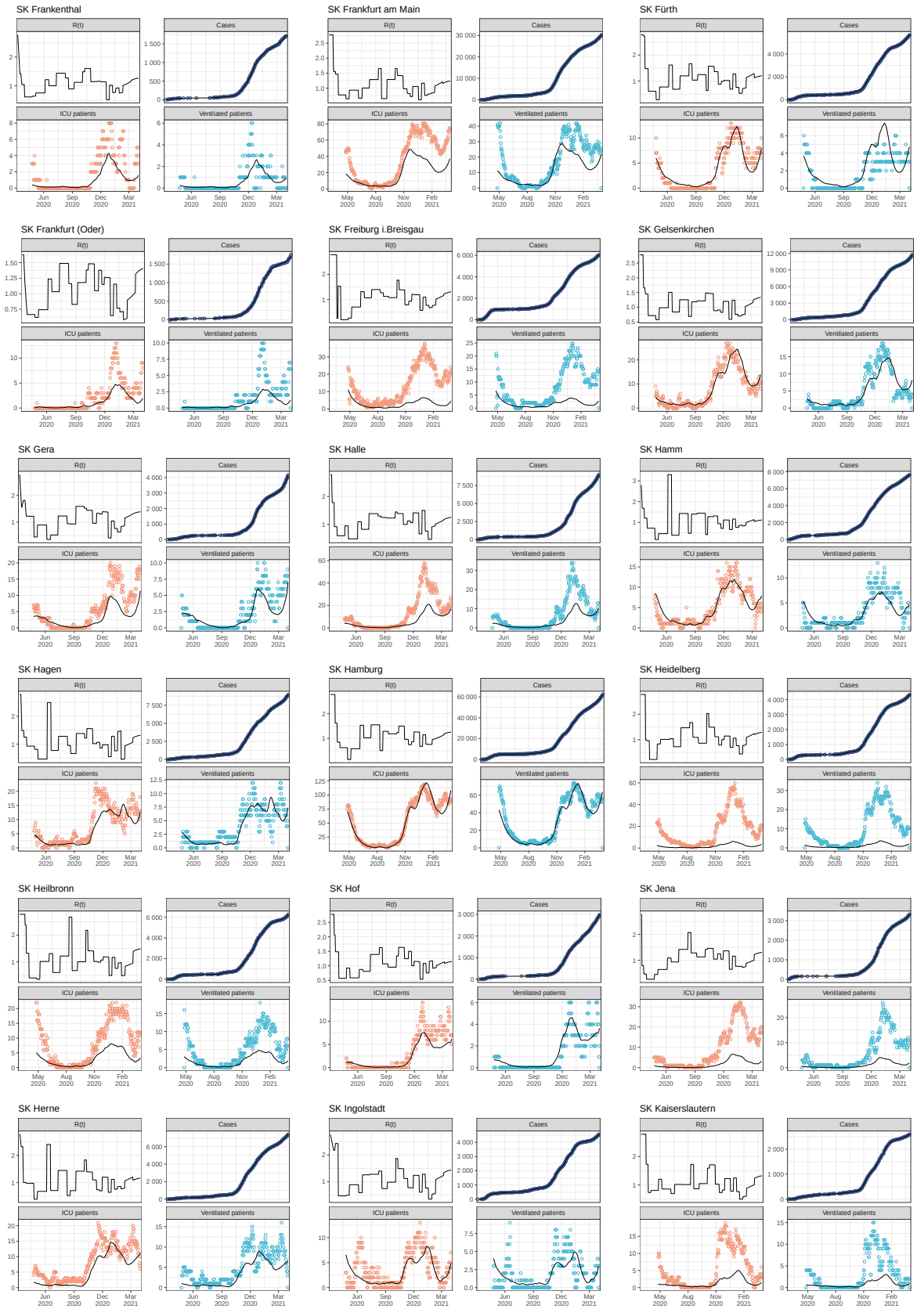
SK Frankenthal
SK Frankfurt am Main
SK Fürth
SK Frankfurt (Oder)
SK Freiburg i.Breisgau
SK Gelsenkirchen
SK Gera
SK Halle
SK Hamm
SK Hagen
SK Hamburg
SK Heidelberg
SK Heilbronn
SK Hof
SK Jena
SK Herne
SK Ingolstadt
SK Kaiserslautern
R(t)
Cases
ICU patients
Ventilated patients

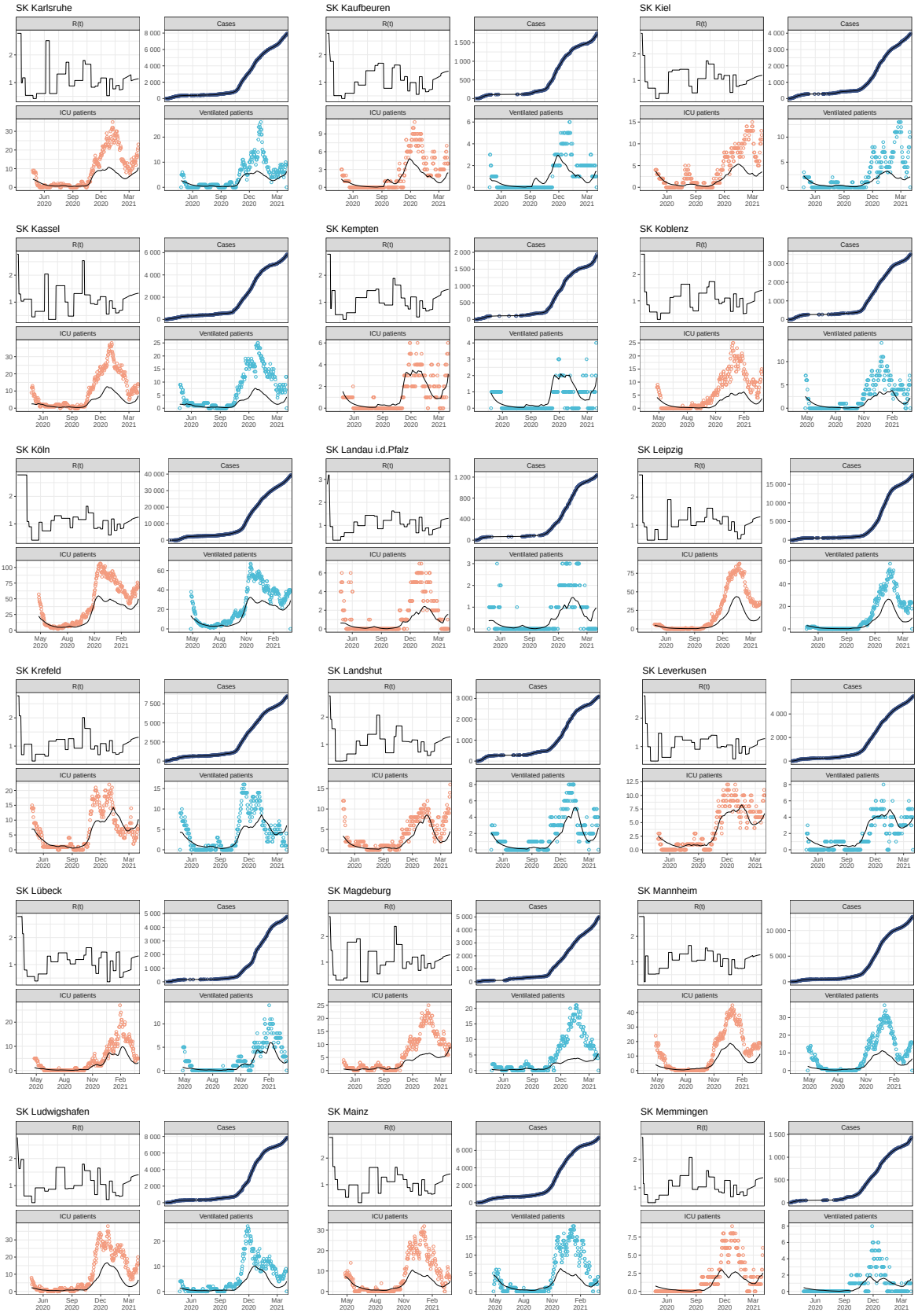
SK Karlsruhe
SK Kaufbeuren
SK Kiel
SK Kassel
SK Kempten
SK Koblenz
SK Köln
SK Landau i.d.Pfalz
SK Leipzig
SK Krefeld
SK Landshut
SK Leverkusen
SK Lübeck
SK Magdeburg
SK Mannheim
SK Ludwigshafen
SK Mainz
SK Memmingen
R(t)
Cases
ICU patients
Ventilated patients

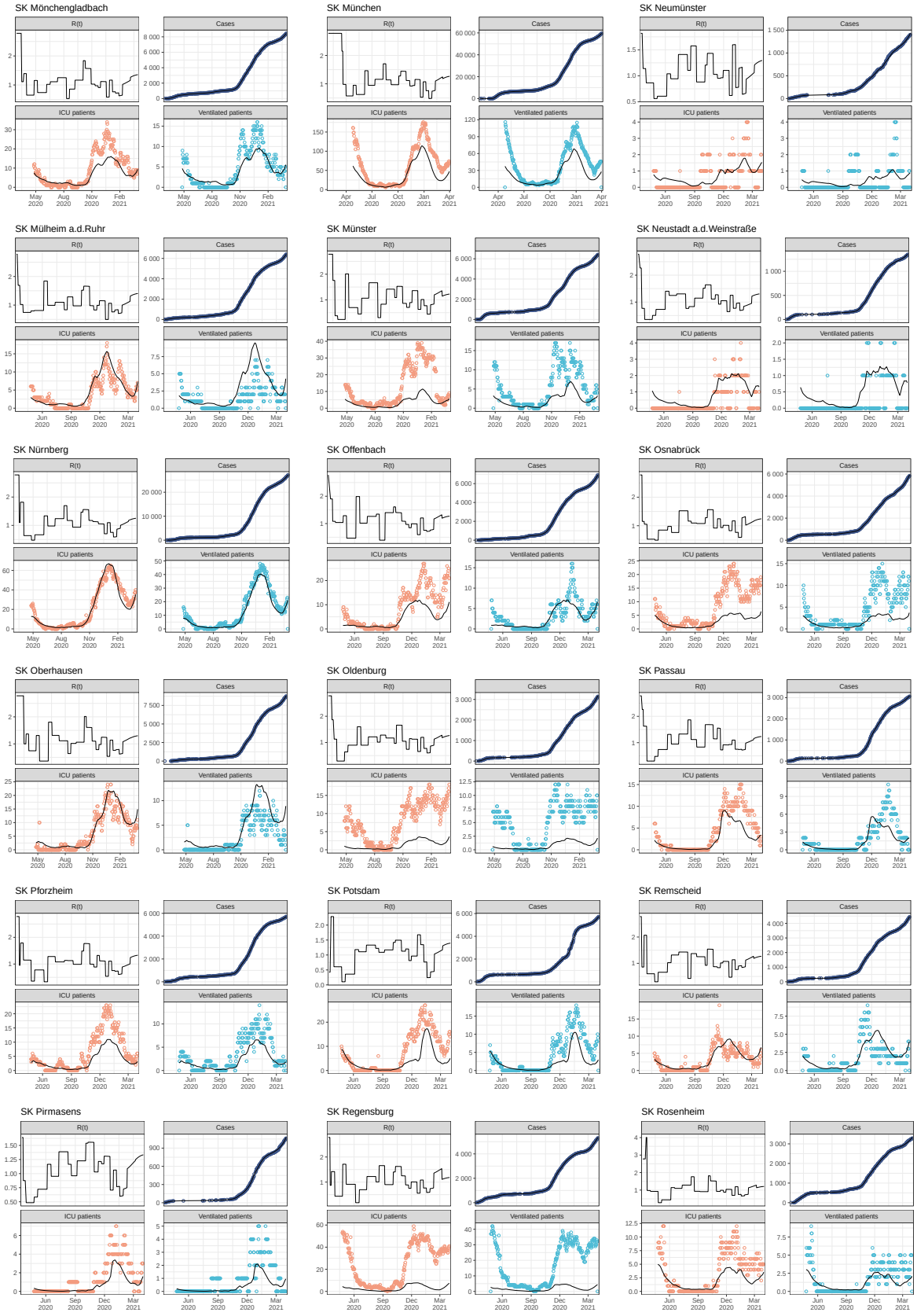
SK Mönchengladbach
SK München
SK Neumünster
SK Mülheim a.d.Ruhr
SK Münster
SK Neustadt a.d.Weinstraße
SK Nürnberg
SK Offenbach
SK Osnabrück
SK Oberhausen
SK Oldenburg
SK Passau
SK Pforzheim
SK Potsdam
SK Remscheid
SK Pirmasens
SK Regensburg
SK Rosenheim
R(t)
Cases
ICU patients
Ventilated patients

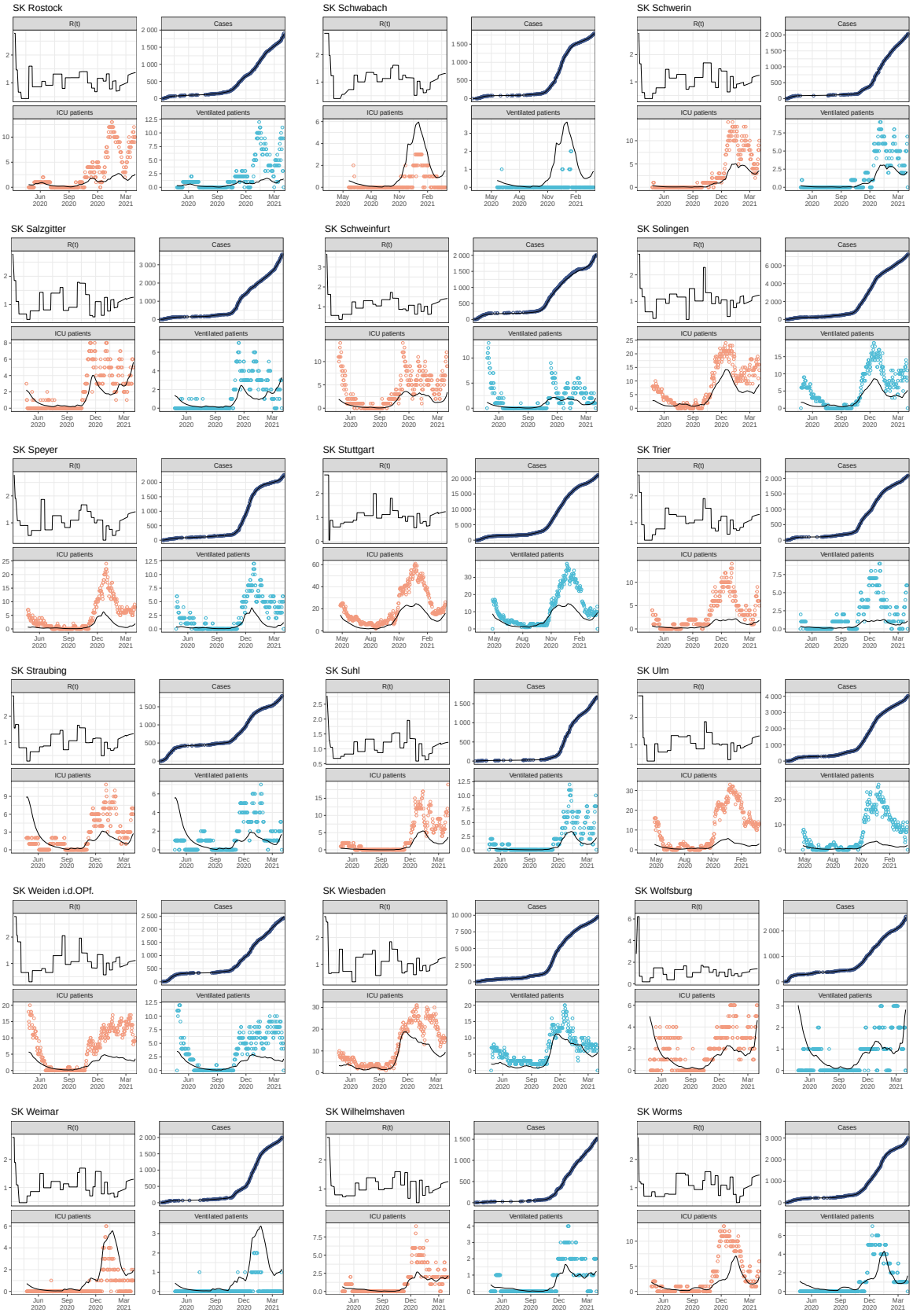
SK Rostock
SK Schwabach
SK Schwerin
SK Salzgitter
SK Schweinfurt
SK Solingen
SK Speyer
SK Stuttgart
SK Trier
SK Straubing
SK Suhl
SK Ulm
SK Weiden i.d.OPf.
SK Wiesbaden
SK Wolfsburg
SK Weimar
SK Wilhelmshaven
SK Worms
R(t)
Cases
ICU patients
Ventilated patients

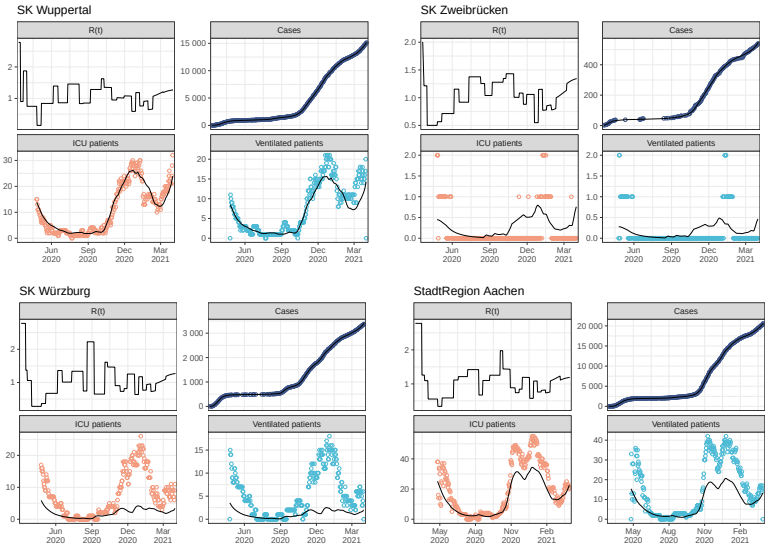
SK Wuppertal
R(t)
Cases
ICU patients
Ventilated patients
SK Zweibrücken
SK Würzburg
StadtRegion Aachen
Jun 2020
Sep 2020
Dec 2020
Mar 2021
May 2020
Aug 2020
Nov 2020
Feb 2021

## *A1.4 Supplementary Model File S1*

```
;Model file S1: NONMEM model file of the infectiousness model

$SIZES NO=5000 PD=-100 LVR=50

$PROBLEM COVID-19 cases

$INPUT ID TIME STATE=DROP TIME2 DROP DV LNDV LNDVCR OBS CMT AMT EVID MDV NUMBER CASE0 ICUDATASET DIVIFLAG SCHOOLS STORECLOSURE
      CURFEW RESTRAININGORDER CARNIVAL FLAGZEROOBS FLAGRKI FLAGMP DOSING2 MAXIMUMICU FLAG20200714 MDV20200714 FLAG20200804
      RKIDEATHS MPCASES MPCASESRECOVRKIDEATH Zweitimpfungen secondDosesCumulative tglImpfungen Datenende LastTimeImpfungen
      CumTglImpfungen fixRt_0 fixRt_1 fixRt_2 fixRt_3 fixRt_4 fixRt_5 fixRt_6 fixRt_7 fixRt_8 fixRt_9 fixRt_10 fixRt_11 fixRt_12
      fixRt_13 fixRt_14 fixRt_15 fixRt_16 fixRt_17 fixRt_18 fixRt_19 fixRt_20 fixRt_21 fixRt_22 fixRt_23 fixRt_24 fixRt_25
      fixRt_26 fixRt_27 fixCP_4 fixCP_5 fixCP_6 fixCP_7 fixCP_8 fixCP_9 fixCP_10 fixCP_11 fixCP_12 fixCP_13 fixCP_14 fixCP_15
      fixCP_16 fixCP_17 fixCP_18 fixCP_19 fixCP_20 fixCP_21 fixCP_22 fixCP_23 fixCP_24 fixCP_25 fixCP_26 fixCP_27 fixF2 PREDIC
      MDVLAST
$DATA DATASET.csv IGNORE=@ IGNORE(DOSING2.EQ.1) IGNORE(CMT.GT.3) IGNORE(FLAGZEROOBS.EQ.1) IGNORE(ID.EQ.17) IGNORE(FLAGRKI.EQ.1)
      IGNORE(TIME.GE.466)

$SUBROUTINES ADVAN13 TOL=5
$MODEL NCOMPS=3

$PK
;Changepoints (COVi) and Rt-values (Ei) fixed to previously estimated values until the most recent ones (COV22, E22 and following)
      to save computational time
Q_0 = 0
RtSTART = fixRt_0
COV1 = SCHOOLS                  ;Time of school closing, covariate in dataset
E1 = fixRt_1
COV2 = CARNIVAL                 ;Time of German carnival, covariate in dataset
E2 = fixRt_2
COV3 = MAX(CURFEW,RESTRAININGORDER) ;Time of restraining order, covariate in dataset
E3 = fixRt_3
MTDIFF = 1
MTIME(1) = fixCP_4
COV4 = MPAST(1)
E4 = fixRt_4
MTIME(2) = fixCP_5
COV5 = MPAST(2)
E5 = fixRt_5
MTIME(3) = fixCP_6
COV6 = MPAST(3)
E6 = fixRt_6
MTIME(4) = fixCP_7
COV7 = MPAST(4)
E7 = fixRt_7
MTIME(5) = fixCP_8
COV8 = MPAST(5)
E8 = fixRt_8
MTIME(7) = fixCP_9
COV9 = MPAST(7)
E9 = fixRt_9
MTIME(8) = fixCP_10
COV10 = MPAST(8)
E10 = fixRt_10
MTIME(9) = fixCP_11
COV11 = MPAST(9)
E11 = fixRt_11
MTIME(10) =fixCP_12
COV12 = MPAST(10)
E12 = fixRt_12
MTIME(11) = fixCP_13
COV13 = MPAST(11)
E13 = fixRt_13
MTIME(12) = fixCP_14
COV14 = MPAST(12)
E14 = fixRt_14
MTIME(13) = fixCP_15
COV15 = MPAST(13)
E15 = fixRt_15
MTIME(14) =fixCP_16
COV16 = MPAST(14)
E16 = fixRt_16
MTIME(15) = fixCP_17
COV17 = MPAST(15)
```

```
E17 = fixRt_17
MTIME(16) = fixCP_18
COV18 = MPAST(16)
E18 = fixRt_18
MTIME(17) = fixCP_19
COV19 = MPAST(17)
E19 = fixRt_19
MTIME(18) = fixCP_20
COV20 = MPAST(18)
E20 = fixRt_20
MTIME(19) = fixCP_21
COV21 = MPAST(19)
E21 = fixRt_21
;Estimated most recent changepoints and Rt-values
MTIME(20) = MTIME(19)+THETA(41)
COV22 = MPAST(20)
E22 = THETA(42)*EXP(ETA(24))
MTIME(21) = MTIME(20)+THETA(43)
COV23 = MPAST(21)
E23 = THETA(44)*EXP(ETA(25))
MTIME(22) = MTIME(21)+THETA(45)
COV24 = MPAST(22)
E24 = THETA(46)*EXP(ETA(26))
MTIME(23) = THETA(47)
COV25 = MPAST(23)
E25 = THETA(48)*EXP(ETA(27))

k=0.072
initVOC=0.002

RtFREE_OLD = RtSTART*(1-COV1)+E2*COV2+E1*(COV1-COV3)+E3*(COV3-COV4)+E4*(COV4-COV5)+E5*(COV5-COV6)+E6*(COV6-COV7)+E7*(COV7-COV8)+E8
       *(COV8-COV9)+E9*(COV9-COV10)+E10*(COV10-COV11)+E11*(COV11-COV12)+E12*(COV12-COV13)+E13*(COV13-COV14)+E14*(COV14-COV15)+E15*(
       COV15-COV16)+E16*(COV16-COV17)+E17*(COV17-COV18)+E18*(COV18-COV19)+E19*(COV19-COV20)+E20*(COV20-COV21)+E21*(COV21-COV22)+E22
       *(COV22-COV23)+E23*(COV23-COV24)+E24*(COV24-COV25)+E25*COV25

RtBASE = RtSTART
Rt_0 = RtSTART
Rt_1 = E1
Rt_2 = E2
Rt_3 = E3
Rt_4 = E4
CP_4 = MTIME(1)
Rt_5 = E5
CP_5 = MTIME(2)
Rt_6 = E6
CP_6 = MTIME(3)
Rt_7 = E7
CP_7 = MTIME(4)
Rt_8 = E8
CP_8 = MTIME(5)
Rt_9 = E9
CP_9 = MTIME(7)
Rt_10 = E10
CP_10 = MTIME(8)
Rt_11 = E11
CP_11 = MTIME(9)
Rt_12 = E12
CP_12 = MTIME(10)
Rt_13 = E13
CP_13 = MTIME(11)
Rt_14 = E14
CP_14 = MTIME(12)
Rt_15 = E15
CP_15 = MTIME(13)
Rt_16 = E16
CP_16 = MTIME(14)
Rt_17 = E17
CP_17 = MTIME(15)
Rt_18 = E18
CP_18 = MTIME(16)
Rt_19 = E19
CP_19 = MTIME(17)
Rt_20 = E20
CP_20 = MTIME(18)
Rt_21 = E21
```

```
CP_21 = MTIME(19)
Rt_22 = E22
CP_22 = MTIME(20)
Rt_23 = E23
CP_23 = MTIME(21)
Rt_24 = E24
CP_24 = MTIME(22)
Rt_25 = E25
CP_25 = MTIME(23)

F2 = fixF2
ALAG2 = 9

isolation = 100
infectious = 7

gamma = 1/(infectious)

A_0(1) = NUMBER

InitDay = 347
FractionInfectious = 0.08
FractionUninfetious = 1-FractionInfectious

$DES
DaysSinceVOC = T-InitDay
IF(T.LT.InitDay) DaysSinceVOC = 0
VOC = 1/(1+((1-initVOC)/initVOC)*EXP(-k*DaysSinceVOC))
IF(T.LT.InitDay) VOC = 0
RtFREE = RtFREE_OLD*(1-VOC)+RtFREE_OLD*1.35*VOC
beta = RtFREE*gamma

DADT(1) = -beta*A(1)/NUMBER*A(2)               ;S
DADT(2) = beta*A(1)/NUMBER*A(2) - gamma*A(2)   ;I
DADT(3) = gamma*A(2)                           ;C

$ERROR
DaysSinceVOC_Err = TIME-InitDay
IF(TIME.LT.InitDay) DaysSinceVOC_Err = 0
VOC_Err = 1/(1+((1-initVOC)/initVOC)*EXP(-k*DaysSinceVOC_Err))
IF(TIME.LT.InitDay) VOC_Err = 0
Rt = RtFREE_OLD*(1-VOC_Err)+RtFREE_OLD*1.35*VOC_Err
SUSCEPTIBLES = A(1)
Rt = Rt*SUSCEPTIBLES/NUMBER
CASES = A(3)+Q_0

IPRED = CASES
W = IPRED
DEL = 0
IF(IPRED.EQ.0) DEL = 0.001
IRES   = DV - IPRED
IWRES  = IRES/(W+DEL)
Y  = IPRED *EXP(EPS(1)) + EPS(2)

$THETA
(0, 2.78,15) FIX ;1 RtFREE
(0.1, 1.92,5) FIX ;2 SCHOOLS
(0) FIX ;3 CARNIVAL
(0.1, 1.1,5) FIX ;4 RESTRAIN
(0.1, 0.636,5) FIX ;5 EFFECT4
(0, 0.636,5) FIX ;6 EFFECT5
(0, 0.716) FIX ;7 EFFECT6
(90, 101) FIX ;8 MTIME4
(0, 24.9) FIX ;9 +MTIME5
(1, 10.6) FIX ;10 +MTIME6
(0, 30) FIX ;11 +MTIME7
(0, 1.08,5) FIX ;12 EFFECT7
(0, 11.6) FIX ;13 +MTIME8
(0, 0.857,5) FIX ;14 EFFECT8
(0, 24.9) FIX ;15 +MTIME9
(0, 1.33,5) FIX ;16 EFFECT9
(0, 28.6,40) FIX ;17 +MTIME10
(0, 1.05,5) FIX ;18 EFFECT10
(0, 9.92,30) FIX ;19 +MTIME11
(0, 0.946,5) FIX ;20 EFFECT11
```

```
(0, 18.4,40) FIX ;21 +MTIME12
(0, 1.25,5) FIX ;22 EFFECT12
(0, 26.1,40) FIX ;23 +MTIME13
(0, 1.51,5) FIX ;24 EFFECT13
(0, 8.7,40) FIX ;25 +MTIME14
(0, 1.55,5) FIX ;26 EFFECT14
(5, 15.8,40) FIX ;27 +MTIME15
(0, 1.12,5) FIX ;28 EFFECT15
(5, 9.08,40) FIX ;29 +MTIME16
(0, 0.998,5) FIX ;30 EFFECT16
(5, 13.3,40) FIX ;31 +MTIME17
(0, 0.978,5) FIX ;32 EFFECT17
(5, 10.9,40) FIX ;33 +MTIME18
(0, 1.22,5) FIX ;34 EFFECT18
(7, 18.4,40) FIX ;35 MTIME19
(0, 0.667,5) FIX ;36 EFFECT19
(7, 9.89,40) FIX ;37 +MTIME20
(0, 1.22,5) FIX ;38 EFFECT20
(7, 10.4,20) FIX;39 +MTIME21
(0, 0.796,5) FIX;40 EFFECT21
(7, 14,20) ;41 +MTIME22
(0, 0.8,5) ;42 EFFECT22
(5, 6,20) ;43 +MTIME23
(0, 0.7,5) ;44 EFFECT23
(7, 11,20) ;45 +MTIME24
(0, 0.9,1.5) ;46 EFFECT24
(442) FIX ;47 MTIME25
(0, 1,1.5) ;48 EFFECT25

$OMEGA
 0 FIX ;1 RtFREE
 0 FIX ;2 SCHOOLS
 0 FIX ;3 CARNIVAL
 0 FIX ;4 RESTRAIN
 0 FIX ;5 EFFECT4
 0 FIX ;6 EFFECT5
 0 FIX ;7 EFFECT6
 0 FIX ;8 F2
 0 FIX ;9 EFFECT7
 0 FIX ;10 EFFECT8
 0 FIX ;11 EFFECT9
 0 FIX ;12 EFFECT10
 0 FIX ;13 EFFECT11
 0 FIX ;14 EFFECT12
 0 FIX ;15 EFFECT13
 0 FIX ;16 EFFECT14
 0 FIX ;17 EFFECT15
 0 FIX ;18 EFFECT16
 0 FIX ;19 EFFECT17
 0 FIX ;20 EFFECT18
 0 FIX ;21 EFFECT19
 0 FIX ;22 EFFECT20
 0 FIX ;23 EFFECT21
 0.01 ;24 EFFECT22
 0.01 ;25 EFFECT23
 0.01 ;26 EFFECT24
 0.01 ;27 EFFECT25

$SIGMA
 0.00003 ;prop c
 1100 ;add c

$EST METHOD=1 INTER MAXEVAL=9999 NOABORT NSIG=3 SIGL=6 PRINT=1 POSTHOC

$COV UNCONDITIONAL

$TABLE ID TIME TIME2 DV OBS CMT EVID MDV IPRED Rt Rt_0 Rt_1 Rt_2 Rt_3 Rt_4 Rt_5 Rt_6 Rt_7 Rt_8 Rt_9 Rt_10 Rt_11 Rt_12 Rt_13 Rt_14
      Rt_15 Rt_16 Rt_17 Rt_18 Rt_19 Rt_20 Rt_21 Rt_22 Rt_23 Rt_24 Rt_25 CP_4 CP_5 CP_6 CP_7 CP_8 CP_9 CP_10 CP_11 CP_12 CP_13
      CP_14 CP_15 CP_16 CP_17 CP_18 CP_19 CP_20 CP_21 CP_22 CP_23 CP_24 CP_25 F2 RtFREE RtFREE_OLD ONEHEADER NOPRINT FILE=
      sdtab2001
```

## *A1.5 Supplementary Model File S2*

```
;Model file S2: NONMEM model file of the full model

$SIZES NO=-10000 PD=-5000 LVR=50 PC=35

$PROBLEM COVID-19 full model

$INPUT ID Week Year STATE=DROP TIME TIME2 DROP DV LNDV LNDVCR OBS CMT AMT EVID MDV NUMBER CASE0 ICUDATASET DIVIFLAG SCHOOLS
      STORECLOSURE CURFEW RESTRAININGORDER CARNIVAL FLAGZEROOBS FLAGRKI FLAGMP DOSING2 MAXIMUMICU FLAG20200714 MDV20200714
      FLAG20200804 RKIDEATHS MPCASES MPCASESRECOVRKIDEATH Zweitimpfungen secondDosesCumulative tglImpfungen Datenende
      LastTimeImpfungen CumTglImpfungen A00toA04_M A00toA04_W A05toA14_M A05toA14_W A15toA34_M A15toA34_W A35toA59_M A35toA59_W
      A60toA79_M A60toA79_W A80_M A80_W PositiveRate numberTests PREDIC fixRt_0 fixRt_1 fixRt_2 fixRt_3 fixRt_4 fixRt_5 fixRt_6
      fixRt_7 fixRt_8 fixRt_9 fixRt_10 fixRt_11 fixRt_12 fixRt_13 fixRt_14 fixRt_15 fixRt_16 fixRt_17 fixRt_18 fixRt_19 fixRt_20
      fixRt_21 fixRt_22 fixRt_23 fixRt_24 fixRt_25 fixCP_4 fixCP_5 fixCP_6 fixCP_7 fixCP_8 fixCP_9 fixCP_10 fixCP_11 fixCP_12
      fixCP_13 fixCP_14 fixCP_15 fixCP_16 fixCP_17 fixCP_18 fixCP_19 fixCP_20 fixCP_21 fixCP_22 fixCP_23 fixCP_24 fixCP_25 fixF2
      MDVLAST
$DATA DATASET.csv IGNORE=@ IGNORE(CMT.EQ.4) IGNORE(DOSING2.EQ.1) IGNORE(DIVIFLAG.EQ.2) IGNORE(CMT.EQ.8) IGNORE(CMT.EQ.11) IGNORE(
      CMT.EQ.12) IGNORE(CMT.EQ.9) IGNORE(FLAGZEROOBS.EQ.1) IGNORE(ID.EQ.17) IGNORE(FLAGRKI.EQ.1) IGNORE(PREDIC.EQ.1) IGNORE(TIME.
      GT.466)

$SUBROUTINES ADVAN6 TOL=6
$MODEL NCOMPS=30

$PK
;Parameters for infectious model
Q_0 = 0
A_0(1) = NUMBER
RtSTART = fixRt_0
COV1 = SCHOOLS
E1 = fixRt_1
COV2 = CARNIVAL
E2 = fixRt_2
COV3 = MAX(CURFEW,RESTRAININGORDER)
E3 = fixRt_3
MTDIFF = 1
MTIME(1) = fixCP_4
COV4 = MPAST(1)
E4 = fixRt_4
MTIME(2) = fixCP_5
COV5 = MPAST(2)
E5 = fixRt_5
MTIME(3) = fixCP_6
COV6 = MPAST(3)
E6 = fixRt_6
MTIME(4) = fixCP_7
COV7 = MPAST(4)
E7 = fixRt_7
MTIME(7) = fixCP_8
COV8 = MPAST(7)
E8 = fixRt_8
MTIME(8) = fixCP_9
COV9 = MPAST(8)
E9 = fixRt_9
MTIME(9) = fixCP_10
COV10 = MPAST(9)
E10 = fixRt_10
MTIME(11) = fixCP_11
COV11 = MPAST(11)
E11 =fixRt_11
MTIME(12) = fixCP_12
COV12 = MPAST(12)
E12 = fixRt_12
MTIME(13) = fixCP_13
COV13 = MPAST(13)
E13 = fixRt_13
MTIME(14) = fixCP_14
COV14 = MPAST(14)
E14 = fixRt_14
MTIME(16) = fixCP_15
COV15 = MPAST(16)
E15= fixRt_15
MTIME(17) = fixCP_16
COV16= MPAST(17)
E16= fixRt_16
```

```
MTIME(18) = fixCP_17
COV17= MPAST(18)
E17= fixRt_17
MTIME(19) = fixCP_18
COV18= MPAST(19)
E18= fixRt_18
MTIME(20) = fixCP_19
COV19= MPAST(20)
E19= fixRt_19
MTIME(21) = fixCP_20
COV20 = MPAST(21)
E20= fixRt_20
MTIME(22) = fixCP_21
COV21 = MPAST(22)
E21 = fixRt_21
MTIME(23) = fixCP_22
COV22 = MPAST(23)
E22 = fixRt_22
MTIME(24) = fixCP_23
COV23 = MPAST(24)
E23 = fixRt_23
MTIME(25) = fixCP_24
COV24 = MPAST(25)
E24 = fixRt_24
MTIME(26) = fixCP_25
COV25 = MPAST(26)
E25= fixRt_25
MTIME(26) = fixCP_25
COV25 = MPAST(26)
E25= fixRt_25

RtFREE_OLD = RtSTART*(1-COV1)+E2*COV2+E1*(COV1-COV3)+E3*(COV3-COV4)+E4*(COV4-COV5)+E5*(COV5-COV6)+E6*(COV6-COV7)+E7*(COV7-COV8)+E8
       *(COV8-COV9)+E9*(COV9-COV10)+E10*(COV10-COV11)+E11*(COV11-COV12)+E12*(COV12-COV13)+E13*(COV13-COV14)+E14*(COV14-COV15)+E15*(
       COV15-COV16)+E16*(COV16-COV17)+E17*(COV17-COV18)+E18*(COV18-COV19)+E19*(COV19-COV20)+E20*(COV20-COV21)+E21*(COV21-COV22)+E22
       *(COV22-COV23)+E23*(COV23-COV24)+E24*(COV24-COV25)+E25*COV25

F2 = fixF2
ALAG2 = 9

isolation = 100
infectious = 7

gamma = 1/(infectious)

PR= PositiveRate
IF(PositiveRate.LT.0.1) PR=0.1

;VOC Alpha model parameters
InitDay = 347
k=0.072
initVOC=0.002
DSM = TIME-InitDay
IF(TIME.LT.InitDay) DSM = 0
FractionVOC = 1/(1+((1-initVOC)/initVOC)*EXP(-k*DSM))

;time until discharge, proportion of time on ICU and on a mechanical ventilator as extracted of clinical database
IIV1 = EXP(ETA(1))
hill1 = THETA(14)
F_LD_VENT_L = THETA(2)-(THETA(2)*THETA(3))*TIME**hill1/(TIME**hill1+THETA(15)**hill1)
LD_VENT_D = 15.5                ;Duration until discharge ICU with ventilation death
LD_VENT_L = 28.6*F_LD_VENT_L    ;Duration until discharge ICU with ventilation recovery
LD_ICU_D = 20                   ;Duration until discharge ICU without ventilation death
LD_ICU_L = 20.4                 ;Duration until discharge ICU without ventilation recovery
LD_HOSP_D = 10.6                ;Duration until discharge general ward only death
LD_HOSP_L = 11.5                ;Duration until discharge general ward only recovery
P_VENT_STAY_D = 0.63            ;Proportion of time ventilated of ICU with ventilation death
P_VENT_STAY_L = 0.28            ;Proportion of time ventilated of ICU with ventilation recovery
P_VENT_on_ICU_STAY_D = 0.68     ;Proportion of time on ICU of ICU with ventilation death
P_VENT_on_ICU_STAY_L = 0.43     ;Proportion of time on ICU of ICU with ventilation recovery
P_ICU_STAY_D = 0.44             ;Proportion of time on ICU of ICU without ventilation death
P_ICU_STAY_L = 0.29             ;Proportion of time on ICU of ICU without ventilation recovery

;Correction factors for federal states with different reporting
fBER = 1
IF(ID.EQ.3) fBER = THETA(8)
```

```
fHE = 1
IF(ID.EQ.7) fHE = 1.15
fBR = 1
IF(ID.EQ.5) fBR = 1.3
fHH = 1
IF(ID.EQ.6) fHH = 1.2

;Hospitalized fractions by age group, corrected by factor
Hosp80= THETA(1)
Hosp60= 0.578*THETA(1)
Hosp0 = 0.0735*THETA(1)
Hosp5 = 0.0178*THETA(1)
Hosp15= 0.0305*THETA(1)
Hosp35= 0.148*THETA(1)

;Hospitalized fractions by age, sex and time
H0 = Hosp0*(A00toA04_M+A00toA04_W*0.817)
H5 = Hosp5*(A05toA14_M+A05toA14_W)
H15 = Hosp15*(A15toA34_M+A15toA34_W*1.55)
H35 = Hosp35*(A35toA59_M+A35toA59_W*0.597)
H60 = Hosp60*(A60toA79_M+A60toA79_W*0.708)
H80 = Hosp80*(A80_M+A80_W*0.588)

;Covariate impact and changes of hospitalization rate
MTIME(15) = THETA(10)
FHOSP = THETA(5)
hill2 = THETA(22)
FHOSPnTEST = THETA(11)

hosptrans = THETA(10)
hosp_TV = H0+H5+H15+H35+H60+H80
hospfactor = (1-FHOSP*TIME**hill2/(THETA(4)**hill2+TIME**hill2))*EXP(-FHOSPnTEST*numberTests/1000000)*(1+FractionVOC*THETA(20))
hosp = hosp_TV*hospfactor
isolated = (1-hosp)*isolation
hospitalized = hosp*isolation

;Fraction treated at ICU
POP1 = 0
POP2 = 0
IF(ID.EQ.2) POP1 = 1
IF(ID.EQ.3) POP1 = 1
IF(ID.EQ.5) POP1 = 1
IF(ID.EQ.6) POP1 = 1
IF(ID.EQ.7) POP1 = 1
IF(ID.EQ.10) POP1 = 1
IF(ID.EQ.12) POP1 = 1
IF(ID.EQ.17) POP2 = 1
FICU= (THETA(6)+(POP1*THETA(13)+(1-POP1)*THETA(24)+POP2*THETA(25))*TIME**hill2/(THETA(4)**hill2+TIME**hill2))*(1+FractionVOC*THETA
      (21))

ICU0 = Hosp0*(A00toA04_M+A00toA04_W*0.817*0.255)*0.439*FICU/hosp_TV
ICU5 = Hosp5*(A05toA14_M+A05toA14_W*0.299)*0.363*FICU/hosp_TV
ICU15 = Hosp15*(A15toA34_M+A15toA34_W*1.55*0.435)*0.41*FICU/hosp_TV
ICU35 = Hosp35*(A35toA59_M+A35toA59_W*0.597*0.600)*0.66*FICU/hosp_TV
ICU60 = Hosp60*(A60toA79_M+A60toA79_W*0.708*0.652)*FICU/hosp_TV
ICU80 = Hosp80*(A80_M+A80_W*0.588*0.608)*0.65*FICU/hosp_TV

revFRACTHOSP =(ICU0+ICU5+ICU15+ICU35+ICU60+ICU80)
FRACTHOSP = 1-revFRACTHOSP
toHOSP = hosptrans*FRACTHOSP

;Fraction ICU (ventilated)
B0 = ICU0/revFRACTHOSP*0.308
B5 = ICU5/revFRACTHOSP*0.444
B15 = ICU15/revFRACTHOSP*0.463
B35 = ICU35/revFRACTHOSP*0.600
B60 = ICU60/revFRACTHOSP*0.719
B80 = ICU80/revFRACTHOSP*0.666
FRACTVENT = (B0+B5+B15+B35+B60+B80)
FRACTICU = 1-FRACTVENT
toICU = hosptrans*(1-FRACTHOSP)*FRACTICU
toVENT = hosptrans*(1-FRACTHOSP)*(1-FRACTICU)

;Proportion of patients at respective wards and of respective age and sex calculated for death
HOSPu60_M = (1-0.66*FICU)*(Hosp35*A35toA59_M)/hosp_TV/FRACTHOSP
```

```
HOSPo60_M = (1-FICU)*(Hosp60*A60toA79_M)/hosp_TV/FRACTHOSP
HOSPo80_M = (1-0.65*FICU)*(Hosp80*A80_M)/hosp_TV/FRACTHOSP
HOSPu60_W = (1-0.600*0.66*FICU)*(Hosp35*A35toA59_W*0.597)/hosp_TV/FRACTHOSP
HOSPo60_W = (1-0.652*FICU)*(Hosp60*A60toA79_W*0.708)/hosp_TV/FRACTHOSP
HOSPo80_W = (1-0.608*0.65*FICU)*(Hosp80*A80_W*0.588)/hosp_TV/FRACTHOSP
ICUo35 = ICU35*(1-0.6)/revFRACTHOSP/FRACTICU
ICUo60 = ICU60*(1-0.719)/revFRACTHOSP/FRACTICU
ICUo80 = ICU80*(1-0.666)/revFRACTHOSP/FRACTICU
Bo05 = (B5)/(FRACTVENT+0.001)
Bo15 = (B15)/(FRACTVENT+0.001)
Bo35 = (B35)/(FRACTVENT+0.001)
Bo60 = (B60)/(FRACTVENT+0.001)
Bo80 = (B80)/(FRACTVENT+0.001)

;Death rates inpatients
PRdeath = (THETA(7)-THETA(7)*THETA(12)*EXP(-PR*THETA(9)))
PRdeathICU = (THETA(7)-THETA(7)*THETA(12)*EXP(-3.12*THETA(9)))
HOSPd = (0.0125*HOSPu60_M+0.0125*HOSPu60_W+0.147*HOSPo60_M+0.101*HOSPo60_W+0.414*HOSPo80_M+0.334*HOSPo80_W)*(1+FractionVOC*THETA
      (19))*PRdeath
ICUd = (0.0453*ICUo35+0.193*ICUo60+0.477*ICUo80) *(1+FractionVOC*THETA(19))*PRdeathICU
VENTd = (0.25*Bo05+0.18*Bo15+0.372*Bo35+0.653*Bo60+0.841*Bo80) *(1+FractionVOC*THETA(19))*PRdeathICU

;Death rates outpatient
MTIME(10) = THETA(18)
hill3 = THETA(23)
FDOUT = THETA(17)*TIME**hill3/(TIME**hill3+THETA(18)**hill3)
FDOUT2 = THETA(26)*THETA(17)*TIME**hill3/(TIME**hill3+THETA(27)**hill3)
RR_Death = 0.16
out80M = A80_M*(1-Hosp80*hospfactor)
out80W = A80_W*(1-Hosp80*0.588*hospfactor)
out60M = A60toA79_M*(1-Hosp60*hospfactor)
out60W = A60toA79_W*(1-Hosp60*0.708*hospfactor)
OUTd = (THETA(16)+FDOUT-FDOUT2)*PRdeath*(1+FractionVOC*THETA(19))
death = (out80M+out80W*0.334/0.414+(out60M+out60W*0.101/0.147)*1.22/10.1)/(1-hosp)*OUTd

;transit rates for different wards and outcomes
deathHOSP = 2/(LD_HOSP_D)
deathICU = 2/(LD_ICU_D)
deathVENT = 2/(LD_VENT_D)
recovery_rateHOSP = 2/(LD_HOSP_L)
recovery_rateICU = 2/(LD_ICU_L)
recovery_rateVENT = 2/(LD_VENT_L)

MTIME(5) = 70
REC_TIME = MPAST(5)
recovery = 14
recovery_rate = 2/recovery
recovery_hosp = 14
recovery_ratehosp = 2/recovery_hosp
death_rate = 2/LD_HOSP_D

HOSPl = 1-HOSPd
ICUl = 1-ICUd
VENTl = 1-VENTd

$DES
DaysSinceVOC = T-InitDay
IF(T.LT.InitDay) DaysSinceVOC = 0
VOC = 1/(1+((1-initVOC)/initVOC)*EXP(-k*DaysSinceVOC))
IF(T.LT.InitDay) VOC = 0
RtFREE = RtFREE_OLD*(1-VOC)+RtFREE_OLD*1.35*VOC
beta = RtFREE*gamma
DADT(1) = -beta*A(1)/NUMBER*A(2)                                ;S
DADT(2) = beta*A(1)/NUMBER*A(2) - gamma*A(2)                    ;I
DADT(3) = gamma*A(2) - isolated*A(3) - hospitalized*A(3)        ;A
DADT(4) = isolated*A(3)*(1-death) - recovery_rate*A(4)          ;QR1
DADT(5) = HOSPl*toHOSP*A(26) - recovery_rateHOSP*A(5)                   ;Halive1
DADT(6) = recovery_rateHOSP*A(5) - recovery_rateHOSP*A(6)               ;Halive2
DADT(7) = HOSPd*toHOSP*A(26)- deathHOSP*A(7)                                    ;Hdeath1
DADT(8) = deathHOSP*A(7) - deathHOSP*A(8)                                               ;Hdeath2
DADT(9) = ICUl*toICU*A(26) - recovery_rateICU*A(9)                              ;ICUalive1
DADT(10) = recovery_rateICU*A(9) - recovery_rateICU*A(10)               ;ICUalive2
DADT(11) = ICUd*toICU*A(26)- deathICU*A(11)                                     ;ICUdeath1
DADT(12) = deathICU*A(11)- deathICU*A(12)                                               ;ICUdeath2
DADT(13) = VENTl*toVENT*A(26) - recovery_rateVENT*A(13)                 ;Valive1
```

```
DADT(14) = recovery_rateVENT*A(13) - recovery_rateVENT*A(14)     ;Valive2
DADT(15) = VENTd*toVENT*A(26) - deathVENT*A(15)                                  ;Vdeath1
DADT(16) = deathVENT*A(15)- deathVENT*A(16)                                      ;Vdeath2
DADT(17) = recovery_rate*A(20) + recovery_ratehosp*A(24)      ;R
DADT(18) = death_rate*A(29) +deathHOSP*A(8) + deathICU*A(12) + deathVENT*A(16);D daily
DADT(19) = gamma*A(2)                                         ;total cases
DADT(20) = recovery_rate*A(4) - recovery_rate*A(20)           ;QR2
DADT(21) = (toICU + toVENT + toHOSP)*A(26)                    ;daily hospitalizations
DADT(22) = (toICU + toVENT)*A(26)                             ;daily ICU patients
DADT(23) = recovery_rateHOSP*A(6) + recovery_rateICU*A(10) + recovery_rateVENT*A(14) - recovery_ratehosp*A(23) ;R1hospital
DADT(24) = recovery_ratehosp*A(23) - recovery_ratehosp*A(24) ;R2hospital
DADT(25) = hospitalized*A(3) - hosptrans*A(25)                ;T1hosp
DADT(26) = hosptrans*A(25) - hosptrans*A(26)                  ;T2hosp
DADT(27) = death_rate*A(29) +deathHOSP*A(8) + deathICU*A(12) + deathVENT*A(16);D
DADT(28) = isolated*A(3)*death - death_rate*A(28)             ;QD1
DADT(29) = death_rate*A(28) - death_rate*A(29)                ;QD2

$ERROR
DaysSinceVOC_Err = TIME-InitDay
IF(TIME.LT.InitDay) DaysSinceVOC_Err = 0
VOC_Err = 1/(1+((1-initVOC)/initVOC)*EXP(-k*DaysSinceVOC_Err))
IF(TIME.LT.InitDay) VOC_Err = 0
RtFREE_Err = RtFREE_OLD*(1-VOC_Err)+RtFREE_OLD*1.35*VOC_Err
Rt = RtFREE_Err*A(1)/NUMBER
CASES = A(19)+Q_0
VENTILATED = P_VENT_STAY_L*(A(13)+A(14))+P_VENT_STAY_D*(A(15)+A(16))
VENTILATED_ABS = VENTILATED
VENTILATED_ICU = P_VENT_on_ICU_STAY_L*(A(13)+A(14))+P_VENT_on_ICU_STAY_D*(A(15)+A(16))
ICUtotal = P_ICU_STAY_L*(A(9)+A(10))+ P_ICU_STAY_D*(A(11)+A(12))+VENTILATED_ICU
ICU_ABS = ICUtotal
HOSPtotal = A(5)+A(6)+A(7)+A(8)+A(9)+A(10)+A(11)+A(12)+A(13)+A(14)+A(15)+A(16)
DAILY_DEAD = A(18)
DAILY_HOSP = A(21)
DEAD = A(27)
RECOVERED = CASE0+Q_0+A(17)*REC_TIME

IPRED = CASES
IF(CMT.EQ.4) IPRED = RECOVERED
IF(CMT.EQ.5) IPRED = ICU_ABS*fBER*fBR*fHH
IF(CMT.EQ.6) IPRED = DEAD
IF(CMT.EQ.7) IPRED = HOSPtotal*fBER*fHE
IF(CMT.EQ.10) IPRED = VENTILATED_ABS*fBER*fBR*fHH
IF(CMT.EQ.18) IPRED = DAILY_DEAD
IF(CMT.EQ.21) IPRED = DAILY_HOSP
W = IPRED
DEL = 0
IF(IPRED.EQ.0) DEL = 0.001
IRES   = DV - IPRED
IWRES  = IRES/(W+DEL)
Y  = IPRED *EXP(EPS(1)) + EPS(2)           ;cases
IF(CMT.EQ.5) Y = IPRED + W*EPS(3) + EPS(4) ;ICU
IF(CMT.EQ.6) Y = IPRED + W*EPS(5) + EPS(6) ;death
IF(CMT.EQ.7) Y = IPRED + W*EPS(7) + EPS(8) ;hospital
IF(CMT.EQ.10) Y = IPRED + W*EPS(9) + EPS(10) ;ventilated
IF(CMT.EQ.18) Y = IPRED + W*EPS(11) + EPS(12) ;daily deaths
IF(CMT.EQ.21) Y = IPRED + W*EPS(13) + EPS(14) ;daily hospitalizations

$THETA
(0.8, 0.999,1) FIX ;1 hosp80
(1, 1.69,2) ;2 ftoVENT1
(0, 0.648,1) ;3 factor ftoVENT2
(50, 281,400) ;4 MTHOSP
(0.1, 0.496,1) ;5 fHOSP
(0, 0.476,1) ;6 toICU
(0.5, 1.05,1.7) ;7 fdeath
(0.3, 1.52,2) FIX ;8 fBER
(0, 0.129) ;9 PR death
(100) FIX ; 10 hosptrans
(0, 0.334) ;11 FHOSPnTEST
(0, 0.48,1) ;12 fmin PR Death
(0, 0.29,1) ;13 +toICU POP1
(100) FIX ;14 hill1 vent
(50, 228,350) ;15 MTICU
0 FIX ;16 dout
(0, 0.226,1) ;17 dout2
```

```
(0, 348,450) ;18 MTIME FDOUT
0 FIX ;19 factor D VOC
(0, 0.395,1) ;20 factor H VOC
(0, 0.162,1) ;21 factor ICU VOC
(100) FIX ;22 hill2 hosp+ICU
(0, 29.57,100) ;23 hill3 dout
(-0.2, 0.0904,1) ;24 +toICU 1-POP1
(-0.2, 0.136,1) FIX;25 +toICU Germany
1 FIX; 26 Fraction -FDOUT
(360,446, 500);27 MTIME FDOUT2

$OMEGA
 0 FIX ;1 dummy IIV

$SIGMA
 0.000032 ;prop ccases
 1060 ;add cases
 0.0544 ;prop icu
 20.8 ;add icu
 0.00957 ;prop death
 140 ;add death
 0.124 ;prop hospital
 175 ;add hospital
 0.0884 ;prop ventilated
 2.19 ;add ventilated
 0.647 ;prop daily death
 0.13 ;add daily death
 6.82 ;prop daily hospitalizations
 2.12 ;add dkdaily hospitalizations

$EST METHOD=1 INTER MAXEVAL=9999 NOABORT NSIG=3 SIGL=6 PRINT=1 POSTHOC
$COV UNCOND MATRIX=R

$TABLE ID TIME DV OBS CMT EVID MDV IPRED DIVIFLAG Rt RtFREE RtFREE_OLD hosp FRACTHOSP FRACTICU HOSPd ICUd VENTd OUTd death
       ONEHEADER NOPRINT FILE=sdtab2101i
```

## *A2 Project II: COVID-19 Spreading in Different Age Groups*

**Supplement**

### Effect of vaccinations and school restrictions on the spread of COVID-19 in different age groups in Germany

Christiane Dings[1], Dominik Selzer[1], Nicola Luigi Bragazzi[1], Eva Möhler[2], Markus Wenning[3], Thomas Gehrke[3], Ulf Richter[4], Alexandra Nonnenmacher[4], Folke Brinkmann[5,6], Tobias Rothoeft[5], Michael Zemlin[7], Thomas Lücke[3,5] and Thorsten Lehr[1]*

1 Department of Clinical Pharmacy, Saarland University, 66123 Saarbrücken, Germany

2 Department of Child and Adolescent Psychiatry, Saarland University Hospital, 66421 Homburg, Germany

3 Medical Association, Westfalen-Lippe, 48151 Münster, Germany

4 School of Education and Psychology, Siegen University, 57072 Siegen, Germany

5 University Children's Hospital, Ruhr University, 44791 Bochum, Germany

6 University Children's Hospital, Airway Research Center North (ARCN), German Center for Lung Research (DZL), Lübeck, Germany

7 Department of General Pediatrics and Neonatology, Saarland University Hospital, 66421 Homburg, Germany

* Corresponding author: thorsten.lehr@mx.uni-saarland.de; Tel.: +49 681 302 70255

**Supplementary Table 1:** Growth function estimates for each VOC. Here, $t_{init}$ is the time point at which 0.2% of all confirmed cases were infected with a specific VOC, k is the growth rate and $F_{max}$ is the maximum distribution. $T_{50}$ represents the date at which the respective VOC constitutes 50% of the infections for the first time according to the growth function. The transmissibility factor $\varepsilon$ describes the relative increase in transmissibility of an VOC in comparison to wildtype.

| VOC | $t_{init}$ | k [days$^{-1}$] | $F_{max}$ | Transmissibility factor $\varepsilon$ | $t_{50}$ |
|---|---|---|---|---|---|
| **Alpha** | 2020-12-03 | 0.072 | 0.92 | 1.35 [1, 2] | 2021-03-02 |
| **Delta** | 2021-05-06 | 0.13 | 0.99 | 1.97 [3] | 2021-06-23 |
| **Omicron BA.1** | 2021-12-01 | 0.21 | 0.99 | 3.19 [a] | 2021-12-31 |
| **Omicron BA.2** | 2021-12-01 | 0.0689 | 0.99 | 4.79 [4] | 2022-03-01 |
| **Omicron BA.4/BA.5** | 2022-04-17 | 0.122 | 0.99 | 8.47 [b] | 2022-06-07 |

[a]fraction $\varepsilon_{Delta}*k_{BA.1}/k_{Delta}$, [b]fraction $\varepsilon_{BA.2}*k_{BA.4/5}/k_{BA.2}$

**Supplementary Table 2:** Changes in the effective reproduction number (Rt) due to NPIs and changepoints estimated by previously developed model (Dings et al. 2022). The median Rt provides an estimate for the population virus transmission rate in Germany averaged for all federal states.

| Date of CP | NPI/Explanation for change in Rt | Median Rt | Inter-state variability [%CV] |
|---|---|---|---|
| **28 Dec 2020** | | 1.14 | 15.2 |
| **7 Jan 2021** | Lockdown intensifications in force on 11 January | 0.77 | 13.8 |
| **22 Jan 2021** | Reopening of schools, 19 January: expansion of federal lockdown until 14 February | 0.85 | - |
| **28 Jan 2021** | Travel restrictions from countries with high incidence of VOC Alpha at 30 January | 0.69 | 35.4 |
| **09 Feb 2021** | 11 Feb: Federal government expands lockdown until 7 March; only some restrictions are lifted | 1.01 | 4.4 |
| **08 Mar 2021** | Lifting of several restrictions by the German federal government | 1.10 | 5.8 |
| **28 Mar 2021** | Easter: decrease of detected cases due to reduced testing during the holidays | 0.55 | - |
| **04 Apr 2021** | Easter Sunday: Increase of cases after easter holidays | 1.26 | - |
| **11 Apr 2021** | | 0.801 | 12.6 |
| **28 Apr 2021** | “Bundesnotbremse” beginning 23 Apr: contact restrictions in areas with weekly incidence rates >100/100.000 inhabitants | 0.602 | 12.7 |
| **16 May 2021** | 09 May: Vaccinated and recovered individuals have less restriction than others | 0.469 | 23.9 |
| **30 Jun 2021** | End of “Bundesnotbremse” | 1.24 | 6.8 |
| **10 Aug 2021** | Changes of infection protection measures decided by federal states | 1.45 | - |
| **18 Aug 2021** | 23 Aug: nationwide application of 3G rule (for access to public spaces, individuals need to be either vaccinated, recovered or tested) | 1.43 | 39.7 |
| **1 Sep 2021** | | 1.1 | 11.5 |
| **4 Oct 2021** | | 1.5 | 8.8 |
| **25 Oct 2021** | 11 October: end of free of charge SARS-CoV-2 tests | 1.65 | 16.2 |
| **18 Nov 2021** | Changes in infection protection law decided | 1.34 | 20.3 |
| **29 Nov 2021** | Changes in infection protection law come into force on 24 Nov | 1.05 | 24.0 |

| | | | |
|---|---|---|---|
| **16 Dec 2021** | Number of performed PCR tests dropped considerably during the Christmas holidays | 0.753 | 50.3 |
| **30 Dec 2021** | Increase of cases after Christmas holidays | 1.39 | - |
| **04 Jan 2022** | 7 Jan: Individuals need to be vaccinated or recovered to visit restaurants; quarantine is shortened for infected individuals | 0.76 | 27.5 |
| **24 Jan 2022** | | 0.613 | 21.6 |
| **07 Feb 2022** | | 0.476 | 24.5 |
| **27 Feb 2022** | | 0.594 | 19.1 |
| **13 Mar 2022** | | 0.527 | 15.7 |
| **23 Mar 2022** | 19 Mar: End of emergency infection protection law | 0.361 | 22.5 |
| **16 Apr 2022** | Easter Sunday on 17 Apr: Increase of cases during easter holidays | 0.612 | 22.2 |
| **21 Apr 2022** | | 0.365 | 18.6 |
| **26 May 2022** | | 0.462 | 30.6 |
| **21 Jun 2022** | | 0.322 | 18.1 |
| **19 Jul 2022** | | 0.209 | 49.1 |

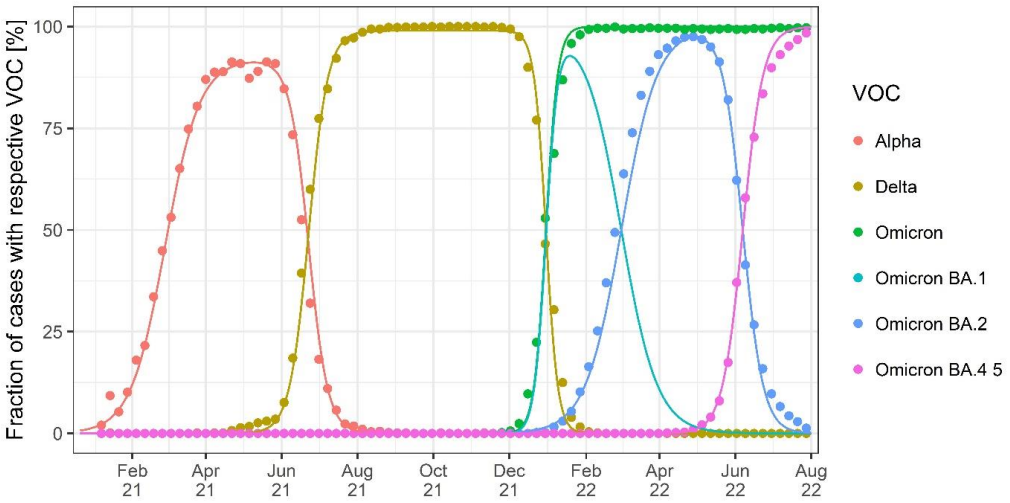


**Supplementary Figure 1:** Spreading of variants of concern (VOCs) in Germany. Points represent the observed fraction of new cases with the respective VOC. Lines represent the fraction predicted using the growth function.

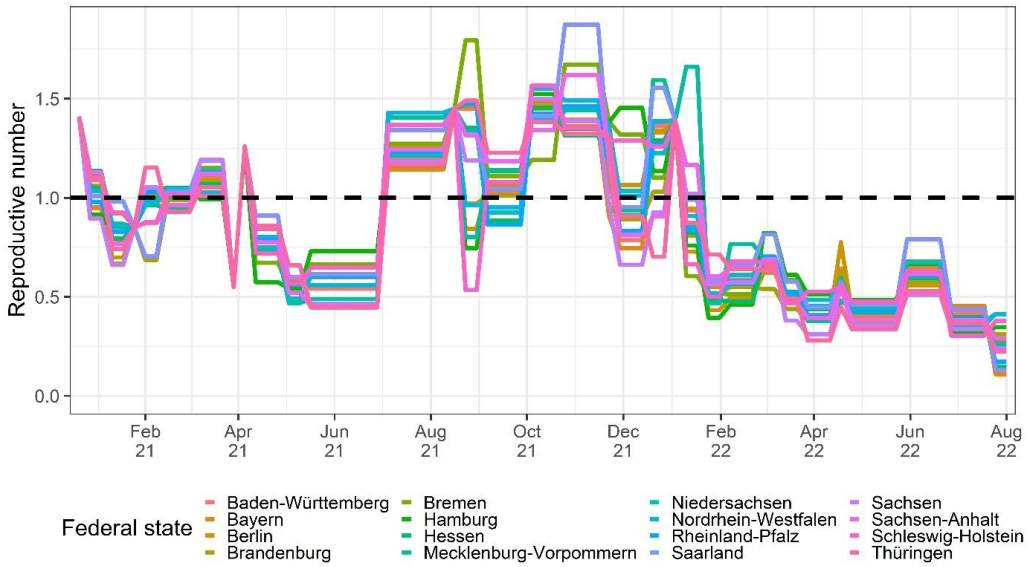


**Supplementary Figure 2:** Residual changes estimated for reproductive number between changepoints including inter-state variability without the impact of vaccinations, NPIs and VOCs.

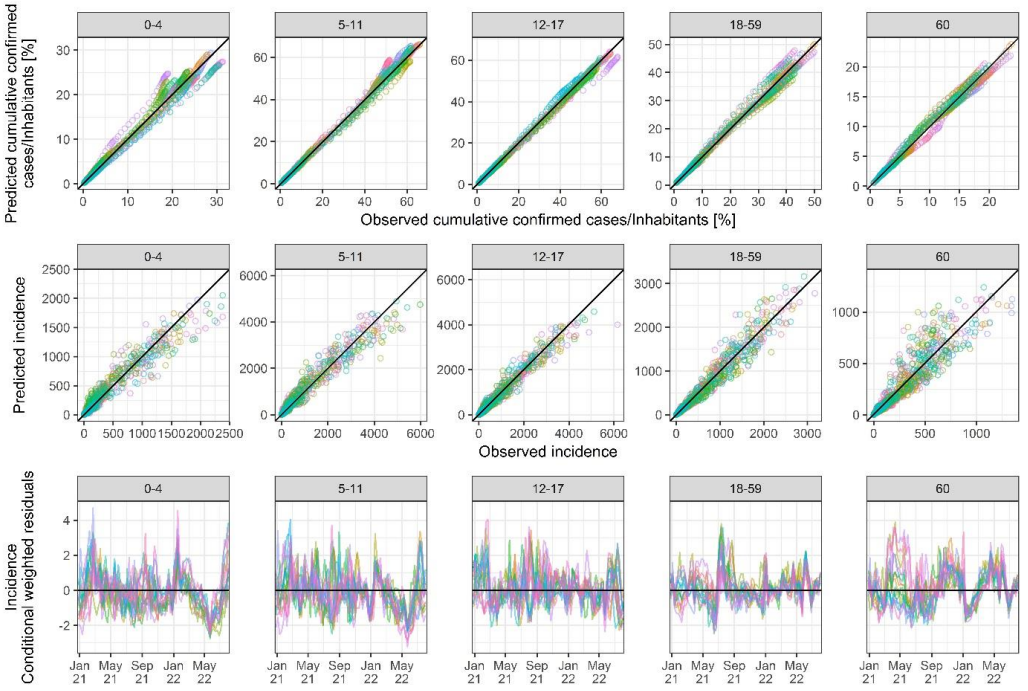


**Supplementary Figure 3:** Goodness-of-fit plots stratified by age group. Each color represents one German federal state.

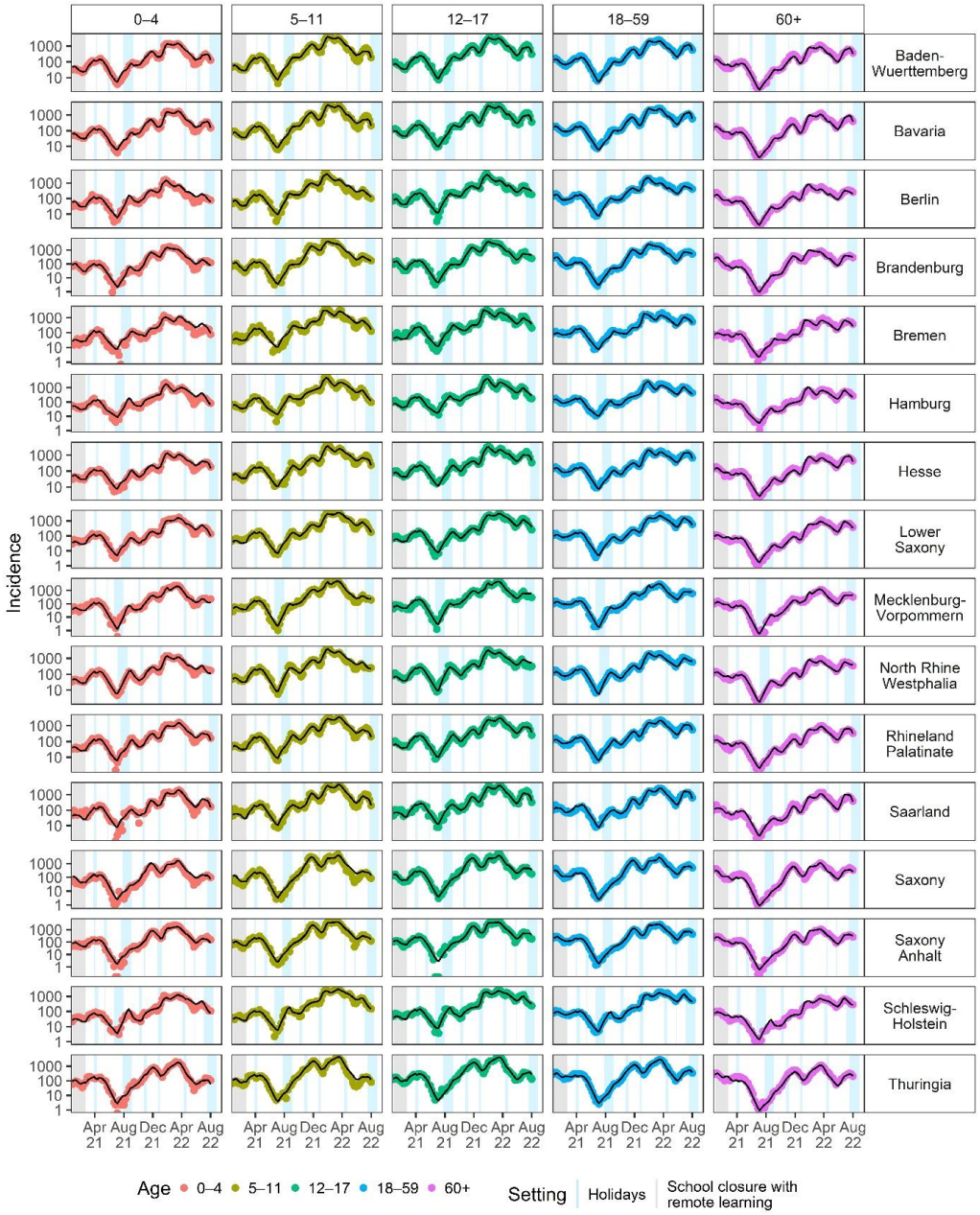


**Supplementary Figure 4:** Weekly incidence per 100,000 inhabitants stratified by federal state and age group. Points represent observations. Lines represent model predictions. Grey shaded areas indicate school closure with remote learning. Blue shaded areas indicate school holidays. While areas represent open schools.

**References**

1. Dings C, Götz KM, Och K, et al (2022) Model-Based Analysis of SARS-CoV-2 Infections, Hospitalization and Outcome in Germany, the Federal States and Districts. Viruses 14(10):2114. https://doi.org/10.3390/v14102114

2. Graham MS, Sudre CH, May A, et al (2021) Changes in symptomatology, reinfection, and transmissibility associated with the SARS-CoV-2 variant B.1.1.7: an ecological study. Lancet Public Heal 6(5):e335–e345. https://doi.org/10.1016/S2468-2667(21)00055-4

3. Campbell F, Archer B, Laurenson-Schafer H, et al (2021) Increased transmissibility and global spread of SARS-CoV-2 variants of concern as at June 2021. Eurosurveillance 26(24). https://doi.org/10.2807/1560-7917.ES.2021.26.24.2100509

4. Chen J, Wei G-W (2022) Omicron BA.2 (B.1.1.529.2): High Potential for Becoming the Next Dominant Variant. J Phys Chem Lett 13(17):3840–3849. https://doi.org/10.1021/acs.jpclett.2c00469

# B Publications

## *B1 Original Publications*

**Alternative treatment regimens with the PCSK9 inhibitors alirocumab and evolocumab: a pharmacokinetic and pharmacodynamic modeling approach.**
Nina Scherer, Christiane Dings, Michael Böhm, Ulrich Laufs, Thorsten Lehr.
*J Clin Pharmacol* **2017**; 57(7):846-54. DOI: 10.1002/jcph.866

**The impact and correction of analysis delay and variability in storage temperature on the assessment of HbA1c from dried blood spots - an IMI DIRECT Study.**
Nina Scherer, Azra Kurbasic, Christiane Dings, Andrea Mari, Valerie Nock, Anita M. Hennige, Robert W. Koivula, Markku Laakso, Maritta Siloaho, Tim J. McDonald, Imre Pavo, Giuseppe N. Giordano, Tue H. Hansen, Femke Rutters, Jacqueline M. Dekker, Bernd Jablonka, Hartmut Ruetten, Ewan R. Pearson, Paul W. Franks and Thorsten Lehr.
*Int J Proteom Bioinform* **2019**; 4(1):7-13.

**Pharmacometric modeling of the impact of azelastine nasal spray on SARS-CoV-2 viral load and related symptoms in COVID-19 patients.**
Christiane Dings, Peter Meiser, Frank Holzer, Michael Flegel, Dominik Selzer, Eszter Nagy, Ralph Mösges, Jens Peter Klussmann and Thorsten Lehr.
*Pharmaceutics* **2022**; 14(10):2059. DOI: 10.3390/pharmaceutics14102059

**Model-based analysis of SARS-CoV-2 infections, hospitalization and outcome in Germany, the federal states and districts.**
Christiane Dings, Katharina Martha Götz, Katharina Och, Iryna Sihinevich, Quirin Werthner, Sigrun Smola, Marc Bliem, Felix Mahfoud, Thomas Volk, Sascha Kreuer, Jürgen Rissland, Dominik Selzer and Thorsten Lehr.
*Viruses* **2022**; 14(10):2114. DOI: 10.3390/v14102114

**Significant impact of time-of-day variation on metformin pharmacokinetics.**
Denise Türk, Nina Scherer, Dominik Selzer, Christiane Dings, Nina Hanke, Robert Dallmann, Matthias Schwab, Peter Timmins, Valerie Nock and Thorsten Lehr.
*Diabetologia* **2023**; 6(66):1024–1034. DOI: 10.1007/s00125-023-05898-4

**Motivations for Adolescent COVID-19 Vaccination: A Comparative Study of Adolescent and Caregiver Perspectives in Germany.**
Tobias Rothoeft, Folke Brinkmann, Christoph Maier, Dominik Selzer, Christiane Dings,

Anna Kuehn, Eva Möhler, Hanna Grote, Alexandra Nonnenmacher, Markus Wenning, Michael Zemlin, Ulf Richter, Thorsten Lehr and Thomas Lücke.
*Children* **2023**; 10, 1890. DOI: 10.3390/children10121890

**Effect of vaccinations and school restrictions on the spread of COVID-19 in different age groups in Germany.**
Christiane Dings, Dominik Selzer, Nicola Luigi Bragazzi, Eva Möhler, Markus Wenning, Thomas Gehrke, Ulf Richter, Alexandra Nonnenmacher, Folke Brinkmann, Tobias Rothoeft, Michael Zemlin, Thomas Lücke and Thorsten Lehr.
*Infectious Disease Modelling* **2024**; 9(4):1250-1264. DOI: 10.1016/j.idm.2024.07.004

*B2 Conference Abstracts*

**Pharmacokinetic/pharmacodynamic modeling of acetylsalicylic acid and its major metabolite salicylic acid.**
Christiane Dings, Thorsten Lehr.
*25th Population Approach Group Europe (PAGE) meeting*, 2016, Lisbon, Portugal.

**Pharmacokinetic and Pharmacodynamic Modeling of Alirocumab and Evolocumab, two fully human monoclonal antibodies targeting PCSK9.**
Nina Scherer, Christiane Dings, Michael Böhm, Ulrich Laufs and Thorsten Lehr.
*25th Population Approach Group Europe (PAGE) meeting*, 2016, Lisbon, Portugal.

**Mathematical modeling of glucose, insulin and c-peptide during the OGTT in pre-diabetic subjects: a DIRECT study.**
Christiane Dings, Nina Scherer, Jan Freijer, Valerie Nock, Thorsten Lehr.
*26th Population Approach Group Europe (PAGE) meeting*, 2017, Budapest, Hungary.

**A population pharmacokinetic (PK) model of metformin regarding immediate and extended release formulations under fasted and fed conditions.**
Nina Scherer, Christiane Dings, Jan Freijer, Valerie Nock, Thorsten Lehr.
*26th Population Approach Group Europe (PAGE) meeting*, 2017, Budapest, Hungary.

**Mathematical modelling of glucose tolerance tests describing glucose, insulin and C-peptide levels in different cohorts: an IMI DIRECT study.**
Christiane Dings, Nina Scherer, Valerie Nock, Anita Hennige, Ewan Pearson, Paul W. Franks, Thorsten Lehr, for the IMI-DIRECT consortium.
*54th European Association for the Study of Diabetes (EASD) meeting*, 2018, Berlin, Germany.

**Quantification of individual disease progression in type 2 diabetes patients using a semi-mechanistic model: an IMI DIRECT study.**
Nina Scherer, Christiane Dings, Valerie Nock, Anita Hennige, Ewan Pearson, Paul W. Franks, Thorsten Lehr, for the IMI-DIRECT consortium.
*54th European Association for the Study of Diabetes (EASD) meeting*, 2018, Berlin, Germany.

**Mathematical modeling of the oral glucose tolerance test in pre-diabetic patients: An IMI DIRECT study**
Christiane Dings, Nina Scherer, Iryna Sihinevich, Valerie Nock, Anita M. Hennige, Ewan R. Pearson, Paul W. Franks and Thorsten Lehr for the IMI DIRECT consortium.
*28th Population Approach Group Europe (PAGE) meeting*, 2019, Stockholm, Sweden.

**Mathematical Modeling of Glucose Homeostasis in Morbidly Obese Diabetic Patients Undergoing Roux-en-Y Gastric Bypass Surgery: An IMI DIRECT Study**
Iryna Sihinevich, Christiane Dings, Nina Scherer, Valerie Nock, Anita M. Hennige, Violeta Raverdy, Francois Pattou and Thorsten Lehr for the IMI DIRECT consortium.
*28th Population Approach Group Europe (PAGE) meeting*, 2019, Stockholm, Sweden.

*B3 Book Chapters*

Jan-Georg Wojtyniak, Christiane Dings and Thorsten Lehr. **"Kardiologie"** in **Pharmakogenetik und Therapeutisches Drug Monitoring: Diagnostische Bausteine für die individualisierte Therapie**
Hanns-Georg Klein and Ekkehard Haen.
*Berlin, Boston: De Gruyter*, 2018. https://doi.org/10.1515/9783110352900

# DANKSAGUNG

Ich möchte mich von Herzen bei all denen bedanken, die mich während meiner Promotion immer wieder motiviert und unterstützt haben. Dabei gilt mein Dank an erster Stelle Prof. Dr. Thorsten Lehr dafür, dass er mir die Möglichkeit gegeben hat, meine Doktorarbeit in seiner Arbeitsgruppe zu erstellen. Dank seiner ansteckenden Begeisterung für die Pharmakometrie und seiner fortwährenden Unterstützung über so viele Jahre konnte ich diese Arbeit abschließen.

Des weiteren möchte ich mich bei Prof. Dr. Marc Schneider bedanken, für die Übernahme des Zweitgutachtens und die interessanten Diskussionen während meines Projektes.

Mein besonderer Dank gilt allen Kolleg*innen des Arbeitskreises der Klinischen Pharmazie für ihre Unterstützung, insbesondere Hannah Britz, Nina Scherer, Iryna Sihinevich, Katharina Götz, Katharina Och, Dr. Laura Fuhr, Dr. Dominik Selzer and Dr. Nicola Luigi Bragazzi für die Unterstützung, für die anregenden Diskussionen und Gespräche in einigen Kaffeepausen (virtuellen und vor Ort).

Vielen Dank an das Graduiertenprogramm PharMetrX, vor allem Prof. Dr. Charlotte Kloft und Prof. Dr. Wilhelm Huisinga für die Möglichkeit ein breites Wissen im Bereich der Modellierung zu erlangen, sowie meinen Mitstudent*innen im PharMetrX Programm für die lehrreiche Zeit. Mein weiterer Dank gilt den Co-Autor*innen meiner Manuskripte für ihre Unterstützung, ohne die diese Arbeit nicht zustande gekommen wäre.

Abschließend danke ich meinen Freunden und meiner Familie für ihre Unterstützung, tags und nachts, allen von meinen Eltern, Anne und Manfred, die mich in allen Lebenslagen stets unterstützt und ermutigt haben. Meiner Oma Hildegard für ein immer offenes Ohr und ganz viel Witz, wenn wir in meinen Schreibpausen telefoniert haben. Ég þakka ykkur, Katrine og Jón Ingi, fyrir að útvega herbergi með fallegu útsýni til að skrifa langt í burtu frá öllum truflunum.